LASZLO, C.A. Ph.D.

Electrical Engineering

ABSTRACT

In this work the electrical responses of the ear to sound stimulation are studied experimentally and by mathematical models. The comparison of the experimental data with the mathematical formulation of the dynamic processes is achieved by computer simulation of models of the mechano-electrical conversion process in the haircells. Using this method we clarified the relation between microscopic events and macroscopic electrical potentials measured in the cochlea. In particular we show that:

the assumption of a one-to-one relationship between the cochlear potentials and the behaviour of a single cochlear transducer is not valid;

the restrictive assumption of linearity of the transduction process over a very wide intensity range is not necessary;

and the paradoxical behaviour of the cochlear potentials in response to the stimulation of the efferent cochlear pathways is explicable in the terms of known physiological mechanisms.

MEASUREMENT, MODELLING AND SIMULATION

OF THE

COCHLEAR POTENTIALS

Measurement, Modelling and Simulation of the Cochlear Potentials

by

C. A. Laszlo

A thesis submitted to the Faculty of
Graduate Studies and Research
in partial fulfillment of the requirements
for the degree of

Doctor of Philosophy

Department of Electrical Engineering
McGill University
Montreal, Canada

July, 1968.

ACKNOWLEDGEMENTS

I wish to express my appreciation to Drs. J. H. Milsum and R. P. Gannon for guiding my efforts in this inter-disciplinary endeavour. Dr. Milsum directed my theoretical work in the engineering sciences and Dr. Gannon gave his time and knowledge to provide the experimental material.

I must also record my gratitude to Mr. D. H. Moscovitch for the many useful suggestions, to Mr. C. Granja for technical assistance in the experiments and to Mr. Siew-Soong Tso who prepared the cochleograms.

I am greatly indebted to the staff of the Research Laboratories, Otolaryngological Institute of McGill University whose collaboration made the experimental work and the preparation of this thesis possible; the assistance given by Mr. L. S. Deutsch and Mr. P. Milojevic of the McGill Computing Center made my task much easier.

Finally, I thank my wife, Doreen, for being an experimental assistant, data analyst, keypuncher, typist and proofreader while being a patient, encouraging and cheerful companion.

C. A. Laszlo.

TABLE OF CONTENTS

ABBREVIATIONS

AMD - amplitude of maximum displacement

AP - total nerve action potential

CM - cochlear microphonic potential

EP - endocochlear potential

MRF - maximum response frequency

SP - summating potential

SPL - sound pressure level

CHAPTER 1

INTRODUCTION

In this work the electrical responses of the ear to sound stimulation are studied experimentally and by mathematical models. The experimental work is approached with the philosophy of 'process identification' familiar from system theory, and the synthesis inherent in the formulation of system models of the various parts of the peripheral auditory apparatus is based on evaluation of physiological facts from a system analysis viewpoint.

The understanding of phenomena associated with the cochlear potentials is of great importance for two reasons, first because in the living ear only a few system performance parameters can be measured due to experimental difficulties, and secondly because these potentials are manifestations of the sensory processes in the ear.

In explanation of the first reason, performance parameters can be classified as subjective or objective. Phenomena associated with the sensation of hearing (loudness, pitch, masking, etc.) are considered to be subjective system parameters. In themselves, these seldom can be used as a measure of the physiological system performance because the underlying mechanical, neural and biochemical events are not

well understood. Objective performance parameters are those which can be observed physiologically and expressed in terms of physical quantities.

Such physical quantities representing the performance of the sound stimulated ear can be evaluated in terms of:

(a) the acoustic input impedance of the ear as measured at the eardrum;

(b) the motion of the ossicles and the transmission characteristics of the middle ear;

(c) the motion of the basilar membrane;

(d) the electrophysiological response of the cochlea;

(e) the neural pulse pattern of the acoustic nerve;

(f) the excitation pattern of the cortical and subcortical brain structures.

In any given experiment a suitable parameter for measurement must be selected, the choice of which is governed by practical and theoretical considerations. The parameter in question must be easily measurable, must yield reproducible measurements and exhibit small subject-to-subject variations.

Measurability is a very important factor in choosing an auditory system parameter for an experiment. In auditory work the acoustic input impedance is measured with relative ease. However, while ossicular motion can be recorded with capacitive probes, the surgical procedures and the measuring

apparatus necessarily exclude the measurement of other factors of interest. On the other hand the motion of the basilar membrane is very difficult to observe because the surgical procedure is by necessity destructive. As regards the neural pulse pattern, this cannot as of yet be observed with sufficient detail, due to the fact that present micro-electrode observations are restricted to only a very small percentage of the total number of nerve fibers in any one preparation. Gross electrodes, on the other hand, record a spatio-temporal summation of the pattern in which details are not distinguishable. On the cortical level similar measurement problems exist compounded by our sketchy knowledge of the anatomy of the nervous pathways.

Consider finally the cochlear potentials as a measure of the behaviour of the auditory system. These potentials are relatively easily determined experimentally, even in humans, and therefore are universally utilized in metabolic, pharmacological and other physiological research related to the cochlea and in the study of the communication channel characteristics of the auditory system.

We turn now to the second reason for the significance of the cochlear potentials, namely that they are closely related to the sensory processes of the auditory system. It is generally believed that the cochlear potentials are

generated by a mechano-electrical conversion process in the sensory cells and that they are manifestations of the mechanism initiating the activation of the sensory nerve fibers.

The description of sensory process in terms of mathematical models requires a part physiological and part mathematical view. In this work the comparison of experimental data with the mathematical formulation of the dynamic processes is achieved by computer simulation of models of the middle ear, the basilar membrane and the mechano-electrical conversion process in the haircells. Using this method we are able to clarify the relation between microscopic events and macroscopic electrical potentials measured in the cochlea and to establish the general constraints which determine the behaviour of the cochlear potentials from the physical point of view. In particular we show that:

> the assumption of a one-to-one relationship between the cochlear potentials and the behaviour of a single cochlear transducer is not valid;
>
> the restrictive assumption of linearity of the transduction process over a very wide intensity range is not necessary;
>
> and the paradoxical behaviour of the cochlear potentials in response to the stimulation of the efferent cochlear pathways is explicable in the terms of known physiological mechanisms.

A reasonably detailed account of the anatomy and the functional physiology of the mechano-acoustical part of the auditory system is given in Chapter 2. However, this chapter by no means comprises a complete summary of all related physiological knowledge, but is restricted to areas directly relevant to this work.

In Chapter 3 the electrophysiology of the cochlea is discussed in considerable detail, with particular attention given to the cochlear microphonic and summating potentials. An attempt is made to summarize diverse experimental results in a systematic fashion in preparation for later 'process identification' studies.

The physiology and functional characteristics of the cochlear transducer are treated in Chapter 4, followed by a detailed analysis of the generation of the cochlear potential in Chapter 5. The existing theories of the generation and distribution of the cochlear potentials are re-examined and some basic assumptions are shown to be unnecessary. Also, a new concept is introduced, namely, a possible mechanism of interaction between neighbouring sensory cells.

In Chapter 6 we report on experimental work designed to provide quinea-pig cochlear-potential data in a form suitable for system evaluation in the engineering sense. Towards this

end the cochlear potentials were measured as a function of frequency and stimulus intensity at various points of the cochlea. In this chapter a complete description of the experimental techniques and instrumentation is given followed by the presentation and discussion of the results.

Models of the mechano-acoustical part of the guinea-pig ear are discussed in Chapter 7. From previous work the transfer functions of the guinea-pig middle ear and cochlea are given. The computer simulation of the basilar membrane motion is accomplished by the convolution technique and by state variable methods. It is shown, however, that in this case the convolution technique is too time consuming and therefore the models are reformulated in terms of state variables. The solutions of the state equations of the model of the guinea-pig ear are also presented with details of the problems of actual computer implementation.

Chapter 8 deals with the modelling of the cochlear potential generators. The latter are considered as distinct potential sources whose behaviour along the cochlea is a function of anatomical position and of the auditory stimulus. The modelling of the individual cochlear transducer involves the specification of the mechanical-to-electrical 'conversion law' and the analysis of electrical filtering effects arising from membrane capacitances. The potential distribution in the fluid of the cochlea is also considered.

In Chapter 9 the results of the computer simulation of the cochlear potentials are presented. Utilizing the models derived in Chapters 7 and 8 we first investigate the linearity of the mechano-electrical conversion process in the cochlear transducer. Then frequency responses of the various cochlear potentials are established and the potential magnitudes are related to the input intensity. Finally, the efferent input to the individual cochlear transducer is considered.

The work is summarized in Chapter 10 where the implications of the experimental work and the computer simulation of the cochlear potentials are also discussed.

CHAPTER 2

PHYSIOLOGICAL BASIS

In order to place subsequent developments in the proper context, the treatment of the subjects of Chapters 2 and 3 are admittedly somewhat general and are intended to be descriptive. There are three areas fundamental to this work as a whole, and they are treated in considerable detail, namely the dynamics of the middle ear and the motion of the basilar membrane (Chapter 2), and the electrophysiology of the inner ear (Chapter 3).

This Chapter describes the anatomy and functional physiology of the outer, middle, and inner ear. Our main interest is the behaviour of the ear of the guinea pig, but not all relevant measurements were carried out on this animal. Therefore, it was necessary to examine data gathered from other mammals, including man. Fortunately, it was found that there are great anatomical and physiological similarities between the auditory apparatus of the various animals, thus permitting careful generalizations in regard to function.

Fig. 2.1 is the information flow diagram of the ear. The outer ear receives the sound pressure variations and conducts these to the eardrum. The eardrum serves as a boundary between the outer and middle ears, with the middle ear

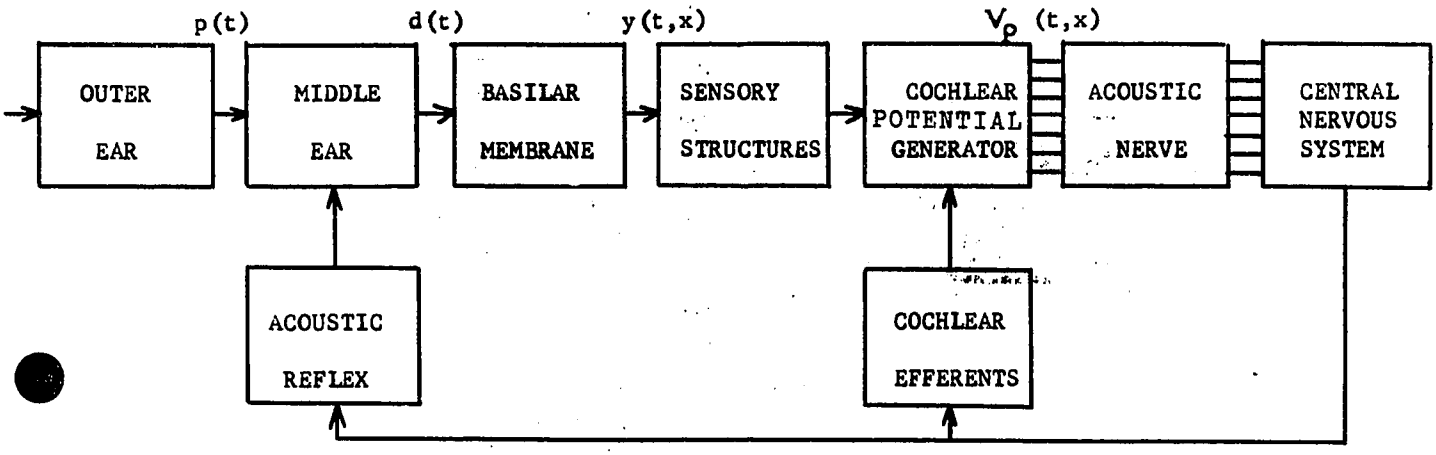

p(t) = Sound Pressure Level at the eardrum
d(t) = volume displacement of the stapes
y(t,x) = displacement of the cochlear partition 'x' distance from the stapes
$V_p(t,x)$ = cochlear potential measured 'x' distance from the stapes

FIG.2.1 INFORMATION FLOW DIAGRAM OF THE AUDITORY SYSTEM

transmitting to the inner ear the motion of the eardrum induced by the pressure variation. In the inner ear some mechanical selection of the frequency components first takes place, followed by electromechanical conversion of the vibrating energy. Then in the final transduction stage, the axons of the acoustic nerve are stimulated to transmit towards higher nervous centers in terms of action potentials the information received by the ear.

2.1. The outer ear

The outwardly visible ear flap (pinna) and the ear canal (external auditory meatus) form the outer ear. The pinna plays a role in the localization of sounds and it also modifies the frequency response characteristics of the outer ear as a whole (1). The external auditory meatus is essentially an open ended pipe. The length of this pipe is about 2.5 centimeters for man and less than 1 centimeter for the guinea pig. At the inner end, the ear canal is terminated by the flexible eardrum (tympanic membrane). Due to its shape and size the ear canal serves as a resonator whose resonant frequency is in the frequency region of the highest sensitivity of hearing. The maximum pressure amplification of 5-10 db is achieved by the meatus in the frequency range of 2000-5000 Hz (2). The constancy of the elastic properties of the eardrum is

of prime importance for hearing. The meatus also keeps the temperature and the humidity of the eardrum relatively constant and independent of the environment.

2.2. The middle ear

At the eardrum the incident acoustic pressure variations are changed into mechanical vibrations. In the middle ear the vibrations are transmitted towards the inner ear by the ossicular chain consisting of three small coupled bones. These bones are called descriptively the hammer (malleus), the anvil (incus) and the stirrup (stapes) (Fig. 2.2). The mode of vibration of the chain as a whole has been recently described by Guinan and Peake (3) who showed that at frequencies below 3 kHz the ossicles move as a rigid body. At frequencies above 3 kHz the stapes and incus movements lag behind the malleus displacement. The displacement amplitude is linearly related to sound pressure up to 130 SPL. The eardrum vibrates somewhat like a stretchable, funnel-shaped piston at low frequencies above 2400 Hz (4). The hammer is partially embedded in the eardrum and it is coupled to the incus by a joint whose rigidity is a function of frequency. The stapes appears exactly like a small stirrup with a footplate which fits into one of the entrances of the inner ear, namely the oval window.

The motion of the ossicles, up to a frequency of approximately 200 Hz, is determined by suspending ligaments. Above this frequency the ossicles vibrate about their center of gravity which roughly coincides with the axis fixed by the ligaments. Vibrations are transmitted to the cochlea by the movement of the footplate of the stapes, whose motion is very complex but is best described either in terms of pressure generated at the oval window or as the volume displacement of the fluids of the inner ear.

The primary function of the ossicles is considered to be impedance matching. The middle ear couples the low acoustic impedance of the air at the eardrum to the high acoustic impedance of the fluid filled cochlea. To minimize transmission loss, impedance matching is necessary. The required pressure transformation is effected partly by the difference in area of the eardrum and the footplate of the stapes and partially by a lever action of the ossicular chain. In cats, for example, the effective area ratio is approximately 24 and the lever ratio is between 2.5(7) and 2.0 (3).

The secondary roles of the middle ear are twofold. First, the delicate structures of the inner ear must be protected against the effects of high intensity sound. To achieve this the mode of motion of the ossicles changes in the presence of potentially harmful sound pressures by

increasing the effective attenuation. In this regard, two small, reflexly activated muscles which are attached to the malleus and the stapes respectively are thought to play an important role. Also, in order to eliminate unwanted interference, the arrangement of the ossicles is such that bone conducted vibrations have the least effect (8). Secondly, it appears that the middle ear and the reflexly activated muscles attached to the ossicles play a role in the differentiation of several simultaneous sound stimuli (9,10). Chewing and talking can also produce middle ear muscle contractions thereby changing the transmission properties of the middle ear and producing a selective effect.

The middle ear of the guinea pig is structurally somewhat simpler than the human ear, but the two are essentially similar. The most important anatomical difference between the human and the guinea-pig middle ear is that the latter is enclosed, together with the cochlea, in an air filled cavity, the bulla. This anatomical arrangement has important experimental implications, because depending on whether the bulla is kept intact or opened during the surgical procedure, the transmission characteristics of the middle ear change.

2.3. The inner ear (11)

The cochlea of the guinea pig is a snail-shaped bony capsule of about four complete turns while the human cochlea

is a similarly shaped cavity of two and three-quarter turns in the temporal bone. Their lengths are 18 and 35 mm respectively. The largest cross-sectional area of this cavity is at the basal end where the oval and the round windows are located. The cochlea is divided into three longitudinal channels, the scala vestibuli, the scala media (cochlear duct), and the scala tympani (Fig. 2.3), by the partitioning membranes called the basilar and Reissner's membranes. The scala tympani and scala vestibuli communicate through a small opening (helicotrema) at the apical end of the cochlea. These two scalae are filled with fluid called perilymph while the cochlear duct is filled with another fluid called endolymph. These fluid compartments are respectively common with corresponding compartments of the other vestibular receptors.

The sensory elements are enclosed in the cochlear duct (Fig. 2.3). The tectorial membrane partially overlaps the elastic basilar membrane on which the sensory elements of the cochlea and their supporting structures lie. These sensory structures are composed of arrays of inner and outer haircells, radial and spiral nerve fibers and associated nerve endings, the whole complex being called the organ of Corti.

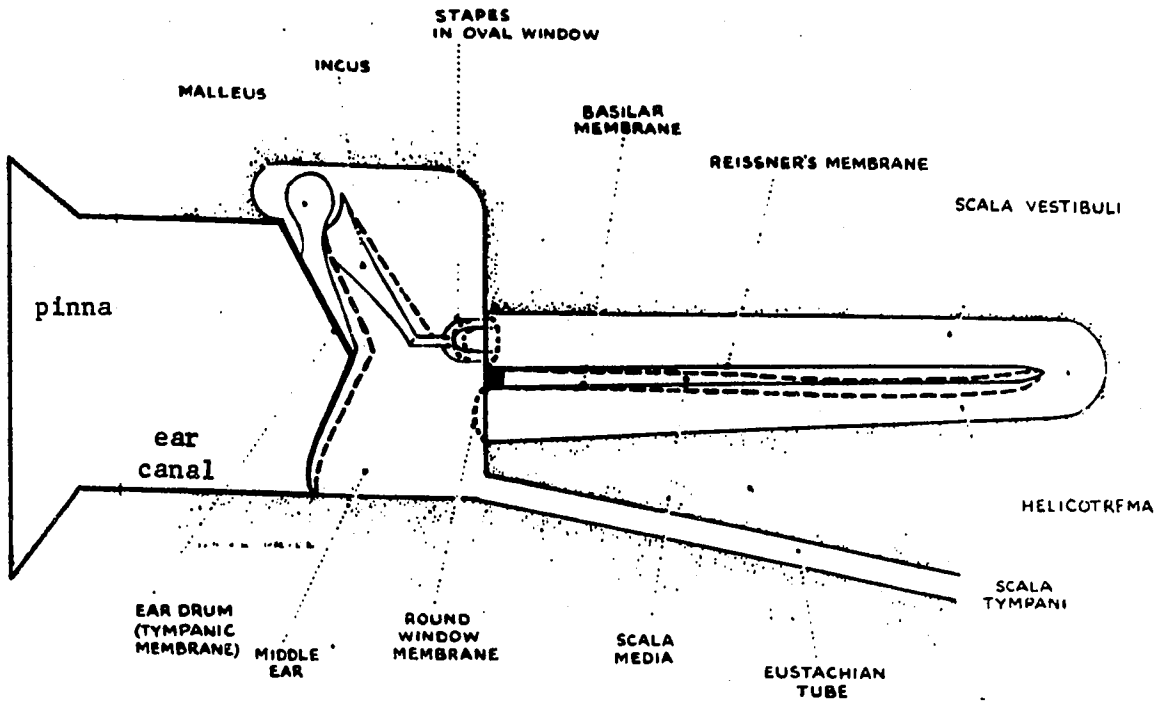

Fig.2.2 Schematic diagram of the ear.(From Burns[5])

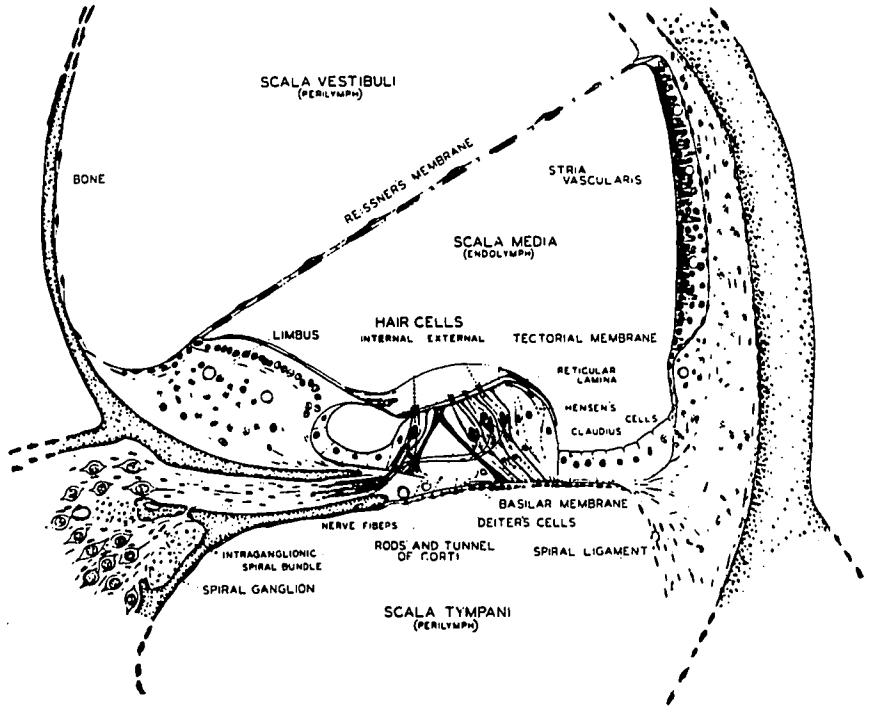

Fig.2.3. Cross section of the cochlea. Scala vestibuli and scala tympani are incompletely shown.(From Davis et al.[6])

The electro-mechanical conversion of the original sound energy takes place in the haircells. Each of these cells contains 60-70 hair-like protrusions (cilia) which extend into the scala media and are attached to the tectorial membrane. The body of the haircell is surrounded by supporting cell structures which are in turn firmly connected to the basilar membrane. Each haircell is innervated by afferent and efferent nerve fibers which pass through the spiral lamina and leave the cochlea as parts of the auditory nerve. The number of haircells depends on the species, being about 10000 for the guinea pig and 40000 for the human. The auditory nerve contains approximately the same number of fibers.

The stimulation of the haircells is the result of the movement of the basilar membrane. The result of this movement in the organ of Corti is that the tectorial membrane slides with respect to the former, and the shearing action created bends the cilia. This bending initiates neural excitation, by some process as yet unknown, but one which is also common to the semi-circular canal and otolithic transduction.

The motion of the basilar membrane is very complex, and since models of this motion will be examined in a later chapter, we now turn to an examination of the mechanical properties of the cochlea.

2.3.1. Mechanical properties of the cochlear partition

Almost all the basic measurements of the various physical parameters of the structures of the inner ear were first done by Bekesy. The following paragraphs outline his work and results.

The cochlear partition is not under tension and consequently it is not a stretched membrane (12). The behaviour of the basilar membrane in this respect is similar to unstrained skin's. Also, the elasticity of the cochlear partition increases by a factor of 100 from the basal end of the cochlea where it is fixed to the apical end where it is relatively loose (12,13). The elasticity of the cochlear partition also varies in the transverse direction at any cross section of the cochlea. The damping of the cochlear partition has been determined in a series of experiments comprising direct observation of the motion of the cochlear partition when the oval window is subjected to a loud click (14).

The viscosity of the perilymph (.0197 cgs units) has been also measured by Bekesy (15). From density measurements of the fluid (1.034 g/cm^3 at $37^{\circ}C$) he also concluded that the velocity of sound waves in the perilymph is approximately the same as in water (1400 mm/msec).

2.3.2. Motion of the cochlear partition

Due to the extremely small amplitudes of the mechanical movements (Fig. 2.4) it is very difficult to measure the displacement of the cochlear partition as a function of displacement of the stapes (16). This was achieved, however, by Bekesy utilizing stroboscopic illumination and microscopic silver crystals to make the membrane movements visible. Recently Johnstone and Boyle also succeeded in measuring the displacement of the cochlear partition by using the Mössbauer technique (17).

By using a sinusoidal displacement input at the stapes, Bekesy obtained the so-called tuning curves of the cochlea (Fig. 2.5). These curves represent the amplitude and phase responses of the basilar membrane for various points as a function of frequency. They were obtained for a constant displacement amplitude at the stapes and were given by Bekesy in the normalized form shown. Fig. 2.6 shows similar data for the guinea pig. If under the same experimental conditions the whole length of the cochlear partition is observed, the maximum response at any given frequency (MRF) can be mapped in terms of distance from the stapes (Fig. 2.7).

Due to the changing dimensions and the varying mechanical properties along the cochlear partition the amplitude of maximum displacement (AMD) of the cochlear partition is also

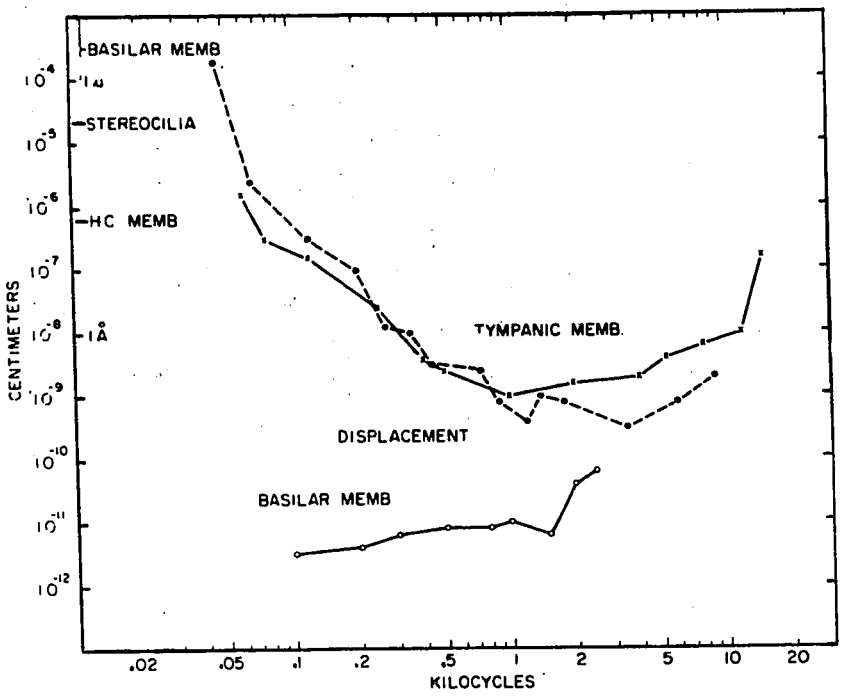

Fig.2.4 The amplitude of movement of the basilar and tympanic membranes at the threshold of hearing. The upper solid and dashed curves represent the tympanic membrane displacement calculated by Lawrence using different data. The lower solid line is the amplitude of movement of the basilar membrane at the threshold of hearing.(From Lawrence[18])

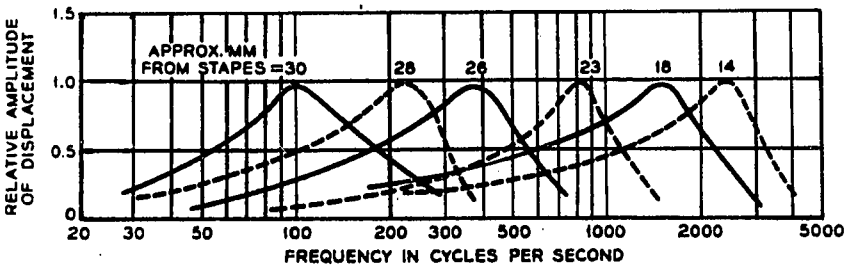

Fig.2.5a Normalized amplitude of the displacement of the cochlear partition as a function of frequency for various points along the cochlea. The input amplitude is constant.(After Bekesy[16] and Flanagan[19]).

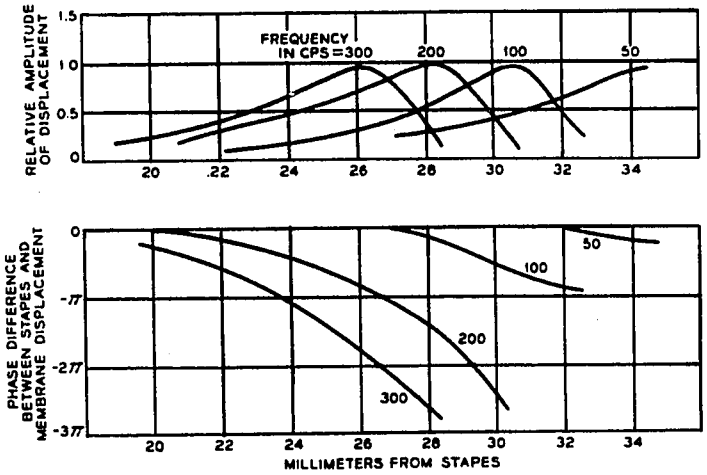

Fig.2.5b Normalized amplitude and phase of the cochlear partition displacement as a function of distance along the cochlea for various sinusoidal inputs.(After Bekesy[16] and Flanagan[19])

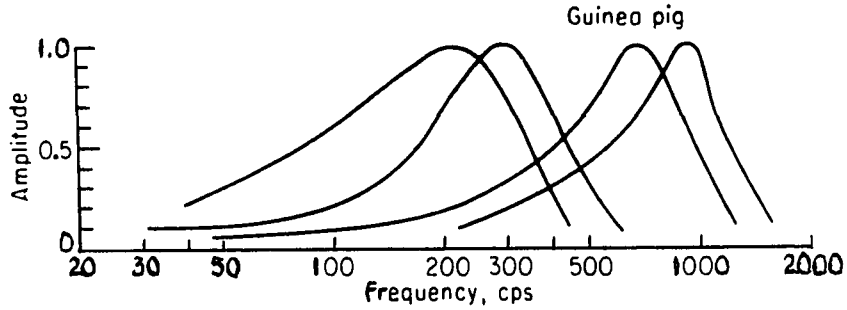

Fig.2.6 Mechanical tuning curves of the cochlear partition of the guinea pig measured at four different positions along the cochlea.(From Bekesy[20])

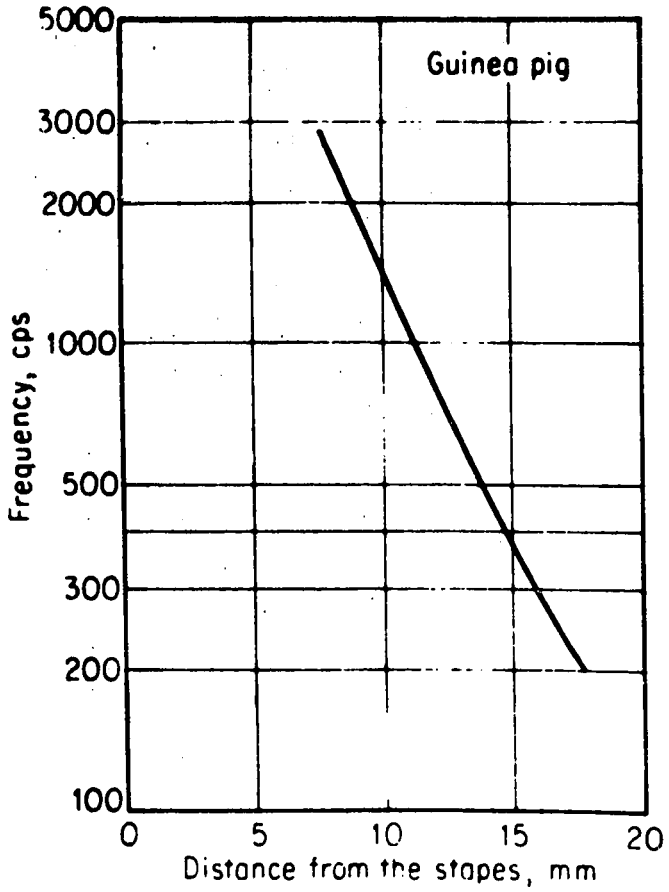

Fig.2.7 Frequency localization along the cochlea of the guinea pig.(From Bekesy[20])

a function of the distance from the stapes. The ratio of volume displacement of the stapes to peak displacement of the basilar membrane is shown in Fig.2.8.

It is to be noted that no reference is made by Bekesy to the absolute values of the sound intensities used. This is unfortunate and it is probably due to the tremendous experimental difficulties Bekesy faced when doing these measurements. Although the sound pressure level was not explicitly measured it was within physiological limits. In order to satisfy himself that the system is linear within these limits (up to 140 db SPL), Bekesy measured the amplitude of vibration of the stapes with the results shown in Fig.2.9. The indicated area represents the physiologically permissible region of amplitudes(21). In all subsequent work we will assume that the displacement of the cochlear partition is linear as a function of stapes displacement.

In regard to the actual time domain phenomena, Bekesy observed that a sudden displacement of the stapes results in a pseudo-travelling wave of displacement along the cochlear partition. Sinusoidal excitation shows a similar pattern of displacement (Fig.2.10).

Based on Bekesy's work the following conclusions can be drawn regarding the dynamic behaviour of the cochlea. Pressure waves generated by the stapes in the fluid reach

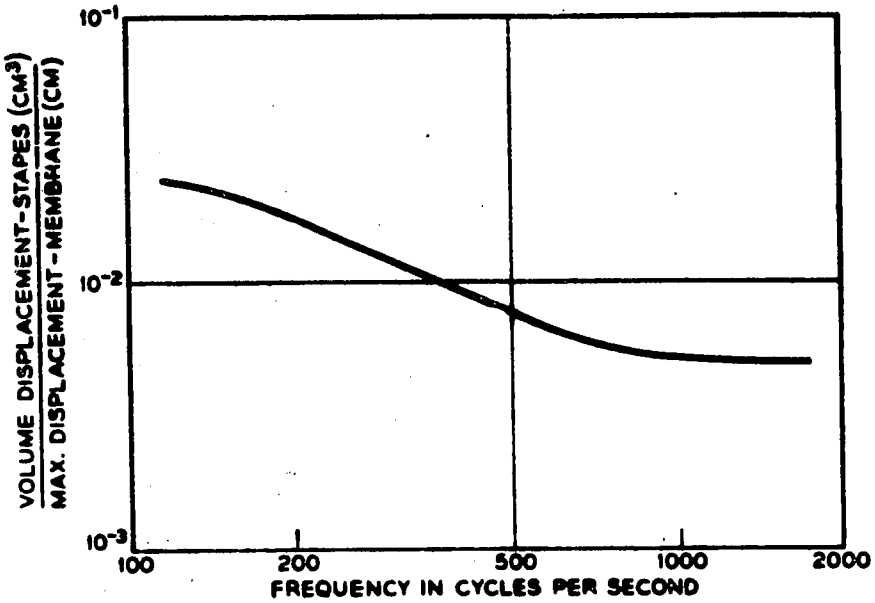

Fig.2.8 Ratio of volume displacement of stapes to peak displacement of the cochlear partition. Data obtained from human cochleas.(From Flanagan[19] and Bekesy[16])

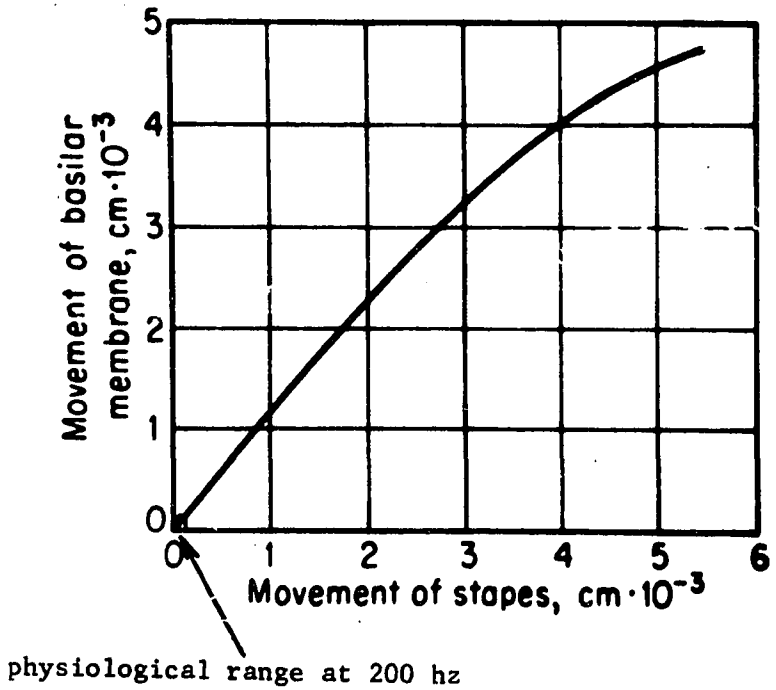

Fig.2.9 Amplitude of vibrations of the basilar membrane as a function of the amplitude of vibrations of the stapes.(From Bekesy[16])

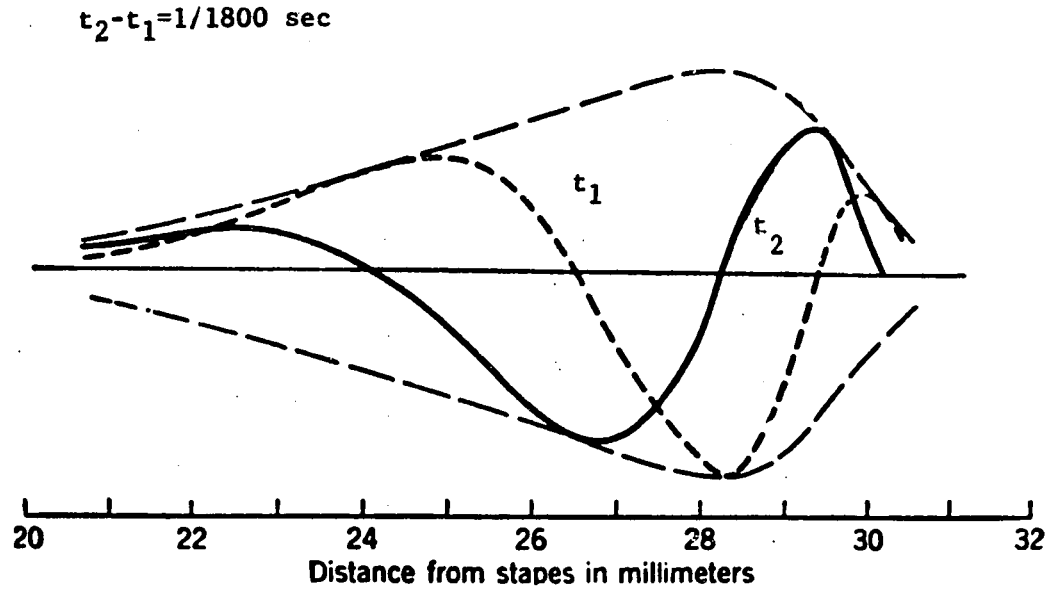

Fig.2.10 Pseudo-travelling wave on the cochlear partition at two instants.(From Bekesy[16])

the apical end of the cochlea almost instantaneously (in 25 microseconds). Due to differences in scalae cross-sections, flow around the helicotrema, and the energy absorbing effect of the round window, the phase and magnitude of the pressure on the two sides of the cochlear partition will be different. This net pressure difference will set the cochlear duct into motion but the response of any one point will be a function of the pertinent local parameters, specifically of the elasticity, mass, friction and coupling of the elements of the membranes. Since these physical characteristics change along the cochlea, the partition sustains a pseudo-travelling wave. This wave cannot be classified as a true travelling wave since the energy transfer is not between subsequent membrane elements. Evidence indicates that the energy necessary to sustain this motion of the membrane is transmitted to it by the fluid.

CHAPTER 3

ELECTROPHYSIOLOGY OF THE COCHLEA

Cochlear potentials exist which are closely related to the sensory processes of the cochlea. These potentials can be observed either by differential electrodes placed in the scala tympani and scala vestibuli (Fig.3.1) or by an electrode placed on the round window. The potentials thus recorded are classified as the endocochlear potential (EP), the cochlear microphonic potential (CM), the summating potential (SP), and the total nerve action potential (AP).

The endocochlear potential is observable in the unstimulated ear as a dc potential and according to Schmidt and Fernandez (22) it has a value between 6 mV and 100 mV, the actual value depending on the species. The same investigators also observed that there was no apparent connection between the size of the endocochlear potential and the measured cochlear microphonic potential, contradicting a hypothesis of Davis (see Section 5.1.1) who postulated a causal relationship between them. Although much effort has been spent on the investigation of the EP, there is still no conclusive evidence for the functional importance of this potential.

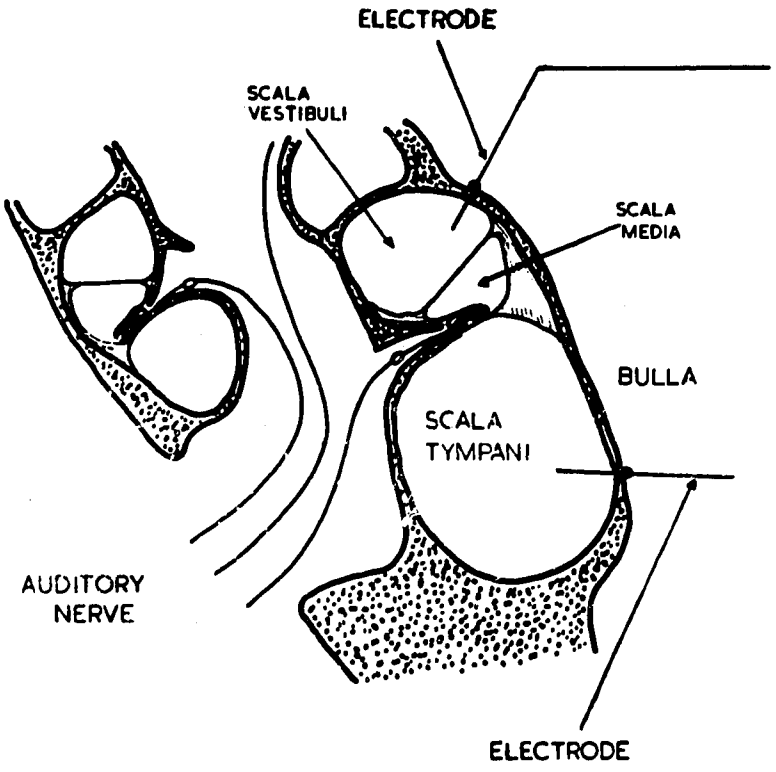

Fig.3.1 Differential electrodes in the first turn of the guinea-pig cochlea.(From Burns5)

The action potential may be looked upon as the spatio-temporal summation of the electrical activity in the fibres of the acoustic nerve. The AP has the general waveform shown in Fig.3.2b, as recorded at some point along the cochlea.

3.1. The cochlear microphonic potential (CM)

When the ear is stimulated by sound the cochlear microphonic potential (CM) is observable as an ac potential between two electrodes placed in the scala tympani and scala vestibuli respectively (Fig.3.2a). Although the CM is also observable between either scalae and a reference electrode, or between the round window and a neck electrode, only differential electrodes placed in opposition on two sides of the basilar membrane will record pure CM without other potentials, especially the AP, complicating the waveform. The cochlear microphonic potential is a function of many factors. Symbolically this functional relationship may be written as

$$CM = fn(f, x, SPL, I_{pol}, OCB, \alpha_1, \alpha_2, \ldots, \alpha_n) \qquad (3.1)$$

where

CM = magnitude and phase of the cochlear microphonic potential

f = frequency of the stimulus

SPL = sound pressure level at the eardrum

x = distance from the stapes

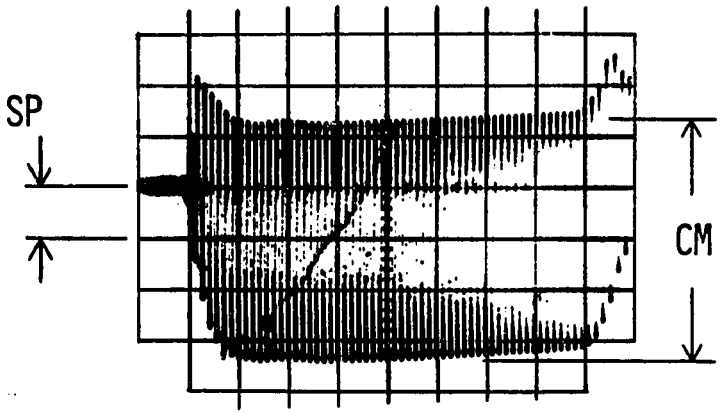

(a) cochlear microphonic (CM) and summating potentials (SP)

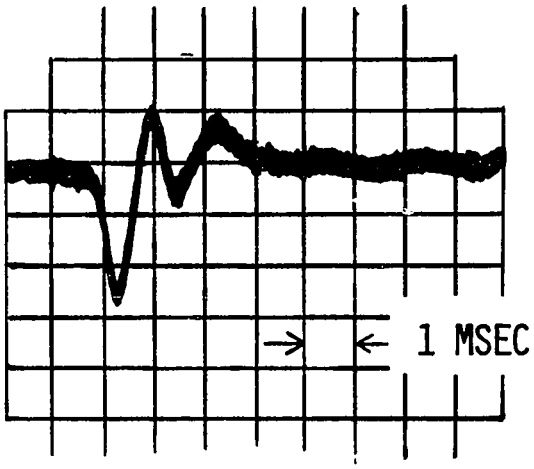

(b) action potential (AP)

Fig.3.2 The cochlear microphonic and action potential responses for a 7000 Hz tone burst. (D.H.Moscovitch[23],unpublished data)

I_{pol} = polarizing current through the organ of Corti

OCB = olivocochlear bundle stimulation

$\alpha_1, \alpha_2, \ldots, \alpha_n$ = other physiological and chemical factors

Observations of the CM as a function of frequency were published by Tasaki et al (24) who used differential electrodes in two or more turns of the cochlea of the guinea pig. One electrode pair was also implanted very close to the beginning of the cochlea and was used as a reference for Turn-1 measurements. The outputs of the second, third and fourth turns were compared with the output of the first turn, thus providing relative amplitude and phase curves as a function of frequency (Fig.3.3). The absolute amplitude and phase were not established since the sound pressures corresponding to a constant Turn-1 CM potential were not measured due to experimental difficulties. This unfortunately resulted in the somewhat misleading curves of Fig.3.3 which indicate that the cochlear microphonic potential transfer characteristics are essentially those of a low pass filter. This is in contradiction with the expected characteristics as predicted by other observations and studies.

In particular, the tuning characteristics of the cochlea as observed by Bekesy (16) and his evidence that the CM is proportional to the displacement of the cochlear partition (25)

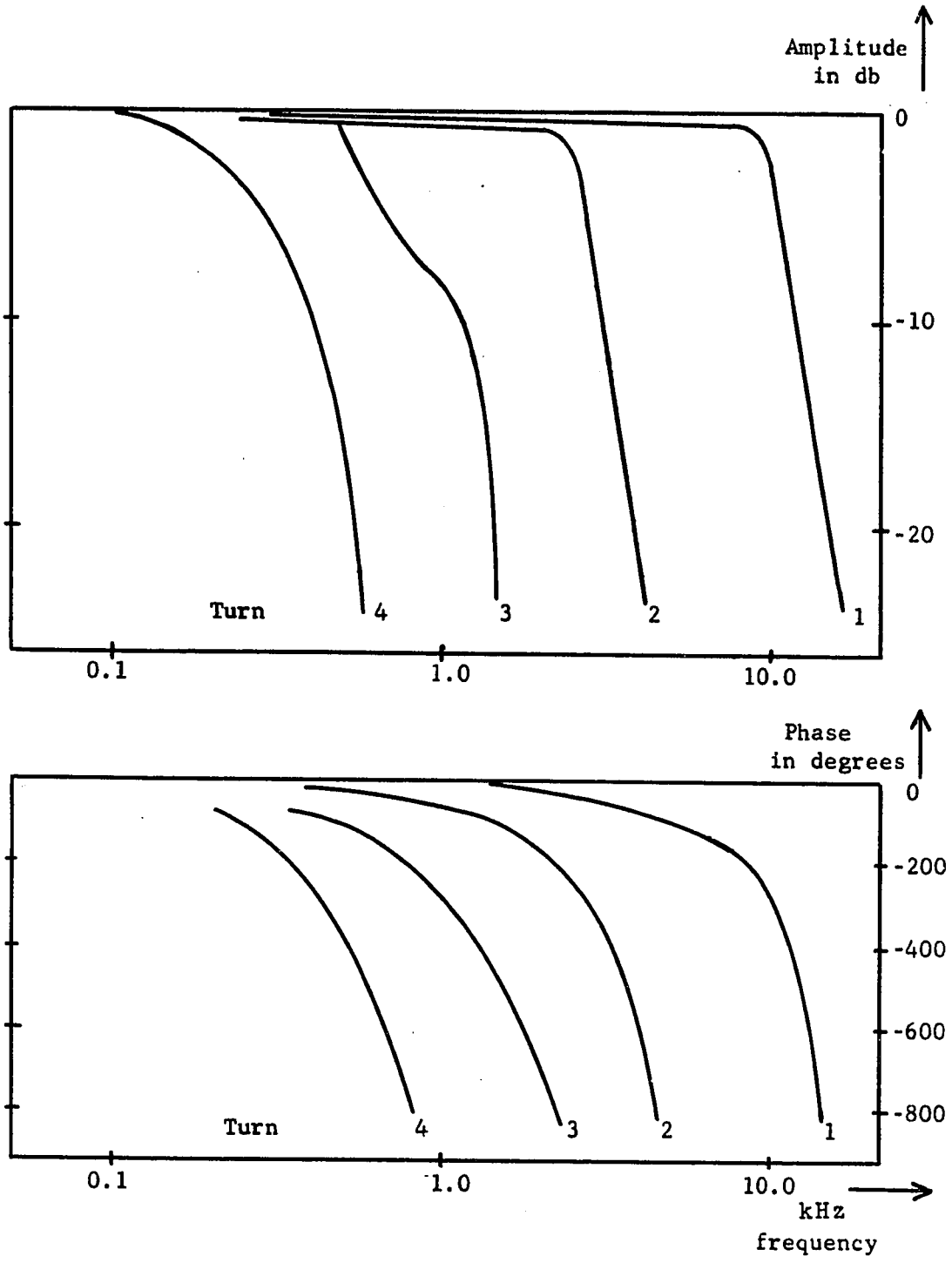

Fig.3.3 Normalized cochlear microphonic amplitude and phase curves, replotted from Tasaki's data (Tasaki[24]).

would indicate that the CM vs frequency plot is somewhat similar to the mechanical tuning curves. The amplitude results of Tasaki, Davis and Legouix (24), however, do not show the expected frequency response characteristics. Zwislocki (26), and more recently Laszlo (21), analysed this problem and found that the sole reason for the discrepancies is that Tasaki and his co-workers used the round window CM potential as the constant reference.

Tonndorf (27) improved on some of Tasaki's techniques; the results are shown in Fig.3.4. He attempted to control the sound pressure level in front of the eardrum for various frequencies and for electrode pairs placed in various turns of the cochlea. However, Tonndorf did not measure the sound pressure level at the eardrum, but instead, calibrated the acoustic source used in his experiments in a 1 cc acoustic coupler. The voltage corresponding to a constant SPL in the coupler was applied to the sound source during the experiment.

It is now apparent (see Chapter 6) that neither of these observations is sufficiently accurate because the techniques do not ensure constant SPL and consequently the results must be treated with caution.

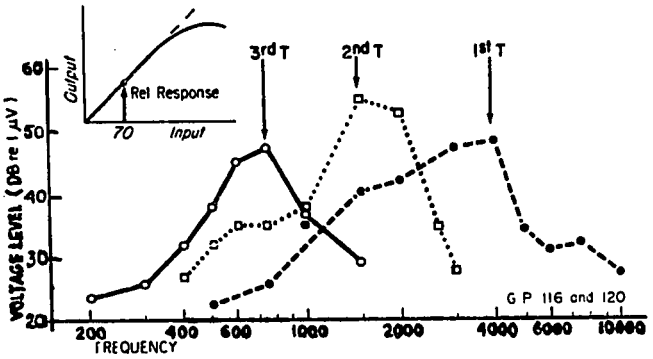

Fig.3.4 Relative responses as a function of frequency at an input level of 70 db, measured by Turn-1, Turn-2 and Turn-3 electrodes. The acoustic driver was calibrated by measuring the necessary voltage to keep the sound pressure level constant in an acoustic coupler. The voltage thus measured was used to drive the acoustic driver when placed in the ear of the guinea pig.(From Tonndorf[27])

Tasaki et al also published data on the changes of the CM as a function of SPL and the variation of this relationship with electrode position (24). It can be seen from their results (Fig.3.5) that the voltage of the CM is a linear function of the SPL for a wide range of sound intensities and frequencies. The CM is unique among the other cochlear potentials in that it reproduces the stimulating frequency waveform with great fidelity. Although the low frequency waveforms become distorted when the CM vs SPL relationship becomes non-linear, for high frequencies a sinusoidal waveform is reproduced up to the point of overloading of the ear and beyond, with little distortion. It is also notable that the CM appears to have no measurable threshold, the lower limit being imposed on the observations by noise arising from physiological sources and from the instrumentation.

It is quite difficult to describe the variation of the CM with electrode position at constant frequency and SPL because only a few data points are available (24). Also, Turn-2 and Turn-3 data were not taken from the same animals and since the true SPL in front of the eardrum was not measured the absolute values of the published data do not allow direct comparisons. This is not to say, of course, that the functional relationships are not accurately shown by Fig.3.5 but that these experimental results must be considered as relative with respect to some unknown SPL.

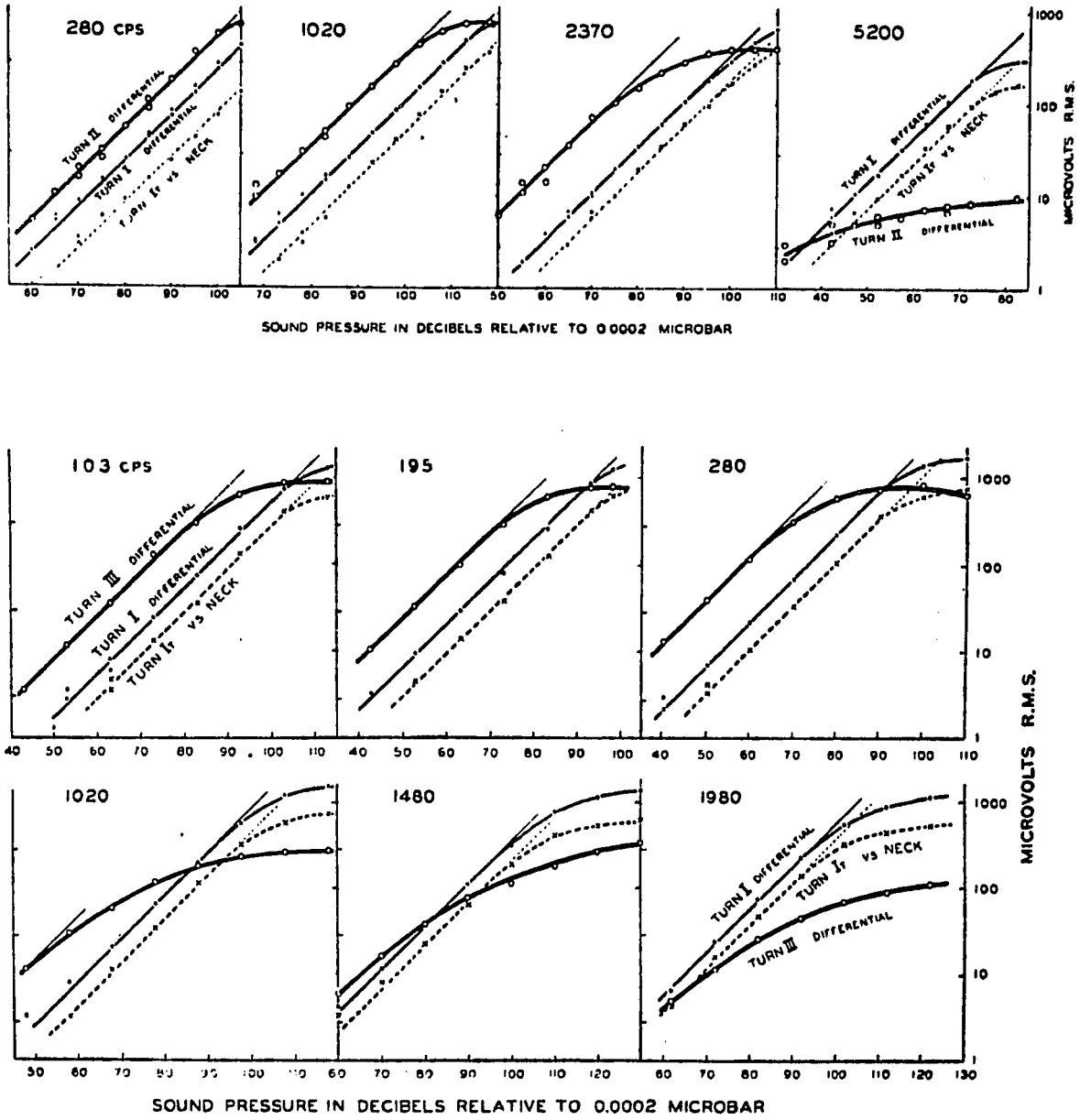

Fig.3.5 The cochlear microphonic potential (CM) as a function of sound pressure level recorded in Turn 1, Turn 2 and Turn 3 of the guinea pig. The broken line shows the CM measured between the scala tympani and the neck. Measurements were from oscillograms.(From Tasaki[24])

The CM potential may be modified temporarily and reversibly by externally applied polarizing currents. Tasaki and Fernandez (28) found that if the scala vestibuli is made positive with respect to the scala tympani the CM potential is depressed (Fig.3.6). Furthermore, they observed the relationship between the strength of the current and the CM potential amplitude for fixed input sound intensity and frequency (Fig.3.7). These investigators concluded that the dc polarizing current does not spread from one turn to the next and that the electrical attenuation of the cochlea is 6 db/mm along the cochlear partition.

Observations indicate that the activity of haircells can be modified by central stimulation of the olivo-cochlear bundle (OCB) in the brainstem and that this modification is reflected in CM potential changes. In particular, it was found that stimulation of the crossed olivo-cochlear fibres results in the augmentation of the cochlear microphonic potential observed with gross electrodes (29,30). In a more recent study Sohmer (31) evaluates the effect of OCB stimulation on the CM for different auditory inputs. By varying the frequency and intensity of the sound stimulus, Sohmer established the functional relationships shown in Figs.3.8,3.9 and 3.10. Unfortunately in his experiments the location of the CM electrode was not varied but was kept on the round window.

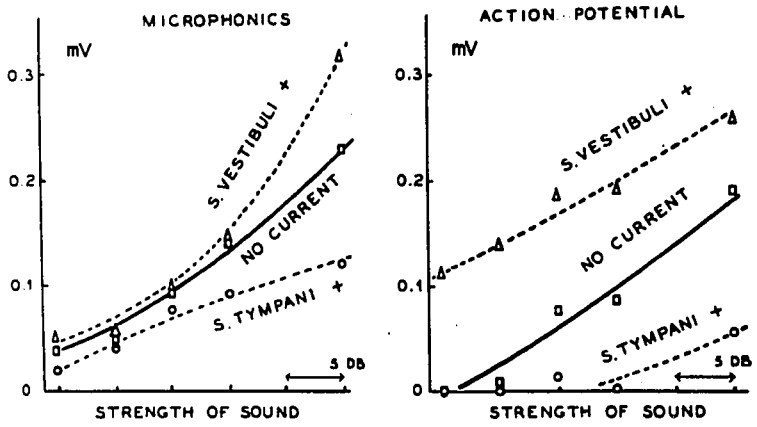

Fig.3.6 Effect of dc applied in Turn 1 upon cochlear microphonics and on action potentials recorded in Turn 1. Sound stimulus: 8000 Hz tone pips. Strength of current: 150 microamps.(From Tasaki[28])

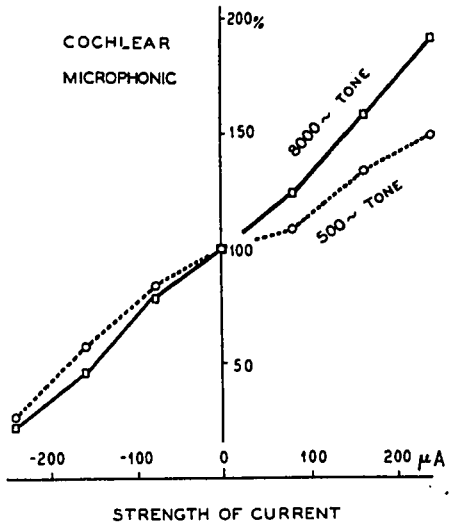

Fig.3.7 Effect of dc upon cochlear microphonic potentials induced by sinusoidal stimuli. Current was applied in Turn 1 and responses were recorded from same turn. Size of CM: 0.42 mV for 8000 Hz; 1.1 mV for 500 Hz. Direction of current: positive from scala vestibuli to scala tympani.(From Tasaki[28])

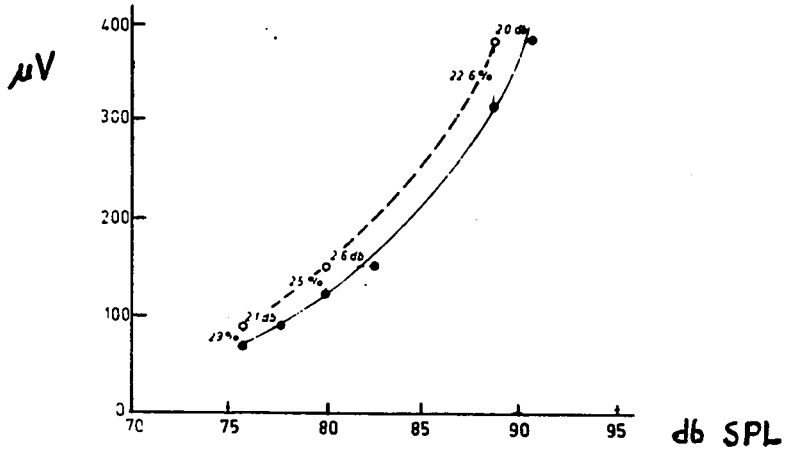

Fig.3.8 Typical cochlear microphonic input-output curve before (continuous line) and during (broken line) olivo-cochlear bundle (OCB) stimulation.(From Sohmer31)

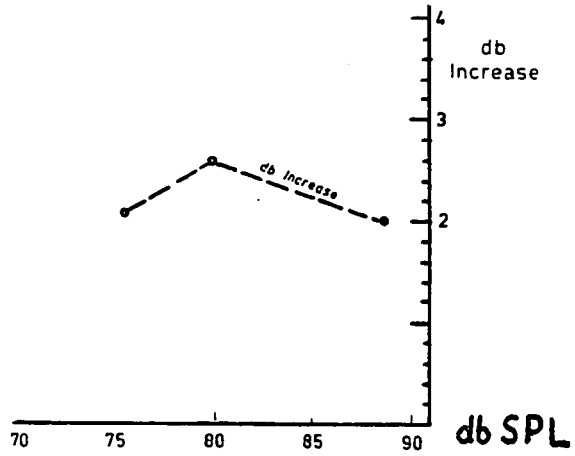

Fig.3.9 Typical cochlear microphonic augmentation in response to pure tone stimuli of increasing intensity during olivo-cochlear bundle stimulation.(From Sohmer31)

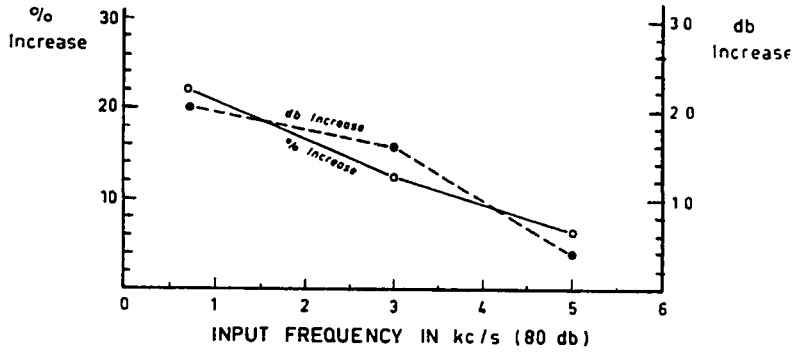

Fig.3.10 Typical cochlear microphonic augmentation in response to constant intensity tone pips of different frequencies during olivo-cochlear bundle stimulation.(From Sohmer31)

The evidence of Fex (32) shows that the OCB stimulation acts on the haircell in a direct efferent fashion. If this is so, then the centrifugally-controlled efferent outflow will have a direct effect on the CM potential augmentation.

3.2. The summating potential

Observations of the cochlear potentials produced in response to transient stimulation indicate the presence of a dc potential which was given the name "summating potential"(SP) by Davis and his co-workers (33). While stimulating the ear with high frequency tone bursts, the summating potential appears as a shift in the base line of the oscilloscope trace on which the cochlear microphonics is superimposed (Fig.3.2a). This shift may be negative or positive, the polarity depending on the location of the electrodes, frequency of the tone burst, anoxia, sound intensity, hydrostatic pressure distribution in the cochlea and centrally controlled efferent action.

Although many studies have been made on the SP it is difficult to give a consistent description of its behaviour, the main reason for this being the great variability between preparations and the unpredictable individual changes during experiments. These changes reflect the fact that the SP is a sensitive function of the general physiological state of the experimental animal, the surgical processes, drugs and

the characteristics of the sound stimulus (34). The general functional relationship may be stated as

$$SP = fn(f,x,SPL,V_{pol},OCB,\alpha_1,\alpha_2,\ldots,\alpha_n) \qquad (3.2)$$

where

SP = magnitude and polarity of the summating potential

f = frequency of stimulus

x = distance from the stapes

SPL = sound pressure level at the eardrum

V_{pol} = polarizing current through the organ of Corti

$\alpha_1,\alpha_2,\ldots,\alpha_n$ = other physiological and biochemical factors

To describe the SP as a function of frequency Davis et al (34) placed differential electrodes (Fig.3.1) into the cochlea at different positions along the basilar membrane and measured the magnitude of the SP and CM simultaneously for various frequencies. From these observations two semiquantitative observations emerged:

(1) the SP/CM ratio increases as the frequency increases and

(2) the SP has very small negative or even positive values for frequencies below 3000 Hz.

In similar experiments Konishi and Yasuno (35) placed dc electrodes in various turns of the guinea pig cochlea at known distances from the round window and used sinusoidal

stimuli of known frequency to obtain the results shown in Fig.3.11. Although their quantitative data are the best available, the observations were taken under conditions which make it difficult to compare the behaviour of the SP with the behaviour of the CM.

In particular, the measurements were not taken with differential electrodes although two electrodes were used, one in the scala vestibuli, the other in the scala tympani or the neck muscles. Thus, common mode potentials representing relatively remote events will be picked up by the electrodes. This is the reason they observed SP responses in the fourth turn for 8 kHz stimulus frequency. (It would be interesting to know the size of the CM they observed simultaneously!) Furthermore, although it is mentioned in the paper that stimulus intensity was measured in front of the eardrum with a probe microphone, the exact arrangement was not specified. Consequently, it is difficult to judge the accuracy and reliability of their SPL measuring method.

The behaviour of the SP as a function of the electrode position in the cross-sectional plane of the cochlea and the electrode placement along the basilar membrane is also of primary interest. According to Davis (34) the SP is best observed between scala media and neck reference

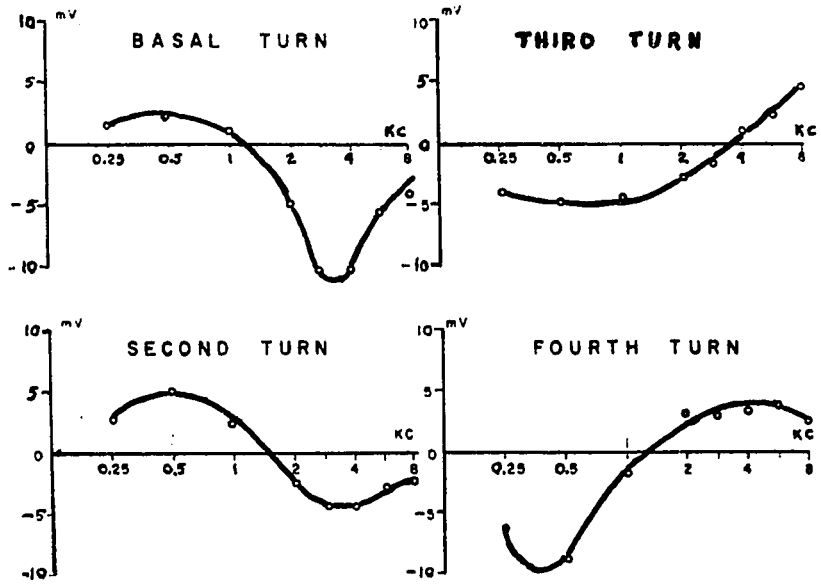

Fig.3.11 The summating potential as a function of frequency in different turns of the cochlea. The electrode arrangement is unbalanced; one micro-electrode was inserted into scala media through the stria vascularis, the other into the scala tympani. The measurements in each turn were made in one animal.(From Konishi35)

electrode or a scala tympani reference electrode. When an exploring electrode is advanced into the scala media from the spiral ligament, large increases in the size of the SP and the CM are observable. The spatial distribution of the SP is different, however, from the distribution of the CM, probably because the SP and CM have different frequency components and consequently the electrical impedances for the two potentials are different. On the basis of experiments using exploring electrodes Davis, and later Konishi (35) confirmed that the SP is generated in the same haircell region as the CM.

Observation of the distribution of the magnitude of the SP along the basilar membrane shows that the SP, like the CM, is a function of location. However, this function is not the same one for the CM and the SP, according to Davis (34), who found that the distribution of the magnitudes of the two potentials is quite different. It appears that the negative SP is related to the "eddy region" of the mechanical pseudo-travelling wave sustained on the basilar membrane and so the SP is more closely associated with the MRF than the CM. This association is a function of location along the cochlea since the ratio of the SP and CM is larger at the higher MRF points, moreover, the absolute value of the negative SP also increases as the MRF increases. Unfortunately,

from the available sources in the literature (34,35), a detailed description of the spatial distribution of the SP cannot be given, because the actual data have never been published.

The complex functional relationship between the magnitude of the SP and the SPL of a sinusoidal stimulus is governed by the stimulus frequency and the location of the measuring electrodes. Observations are made difficult by the fact that the magnitude and polarity of the SP are altered by static pressure changes which arise from middle ear muscle contractions and mechanical injury due to surgery. It is difficult to obtain consistent and reproducible measurements and consequently, published data are often qualitative and incomplete.

Fig.3.12 shows the SP vs SPL function for various frequencies as measured in the basal turn of the cochlea of a guinea pig (35). In Fig.3.13 the SP^- vs SPL and the CM vs SPL functions are compared showing that at least for the given location and stimulating frequency, the SP will increase monotonically in the entire intensity range and the CM attains a maximum around 100 db SPL (36).

Investigations of the effect of the polarizing current on the SP generated by continuous tones have only been partially successful because experiments yield inconsistent

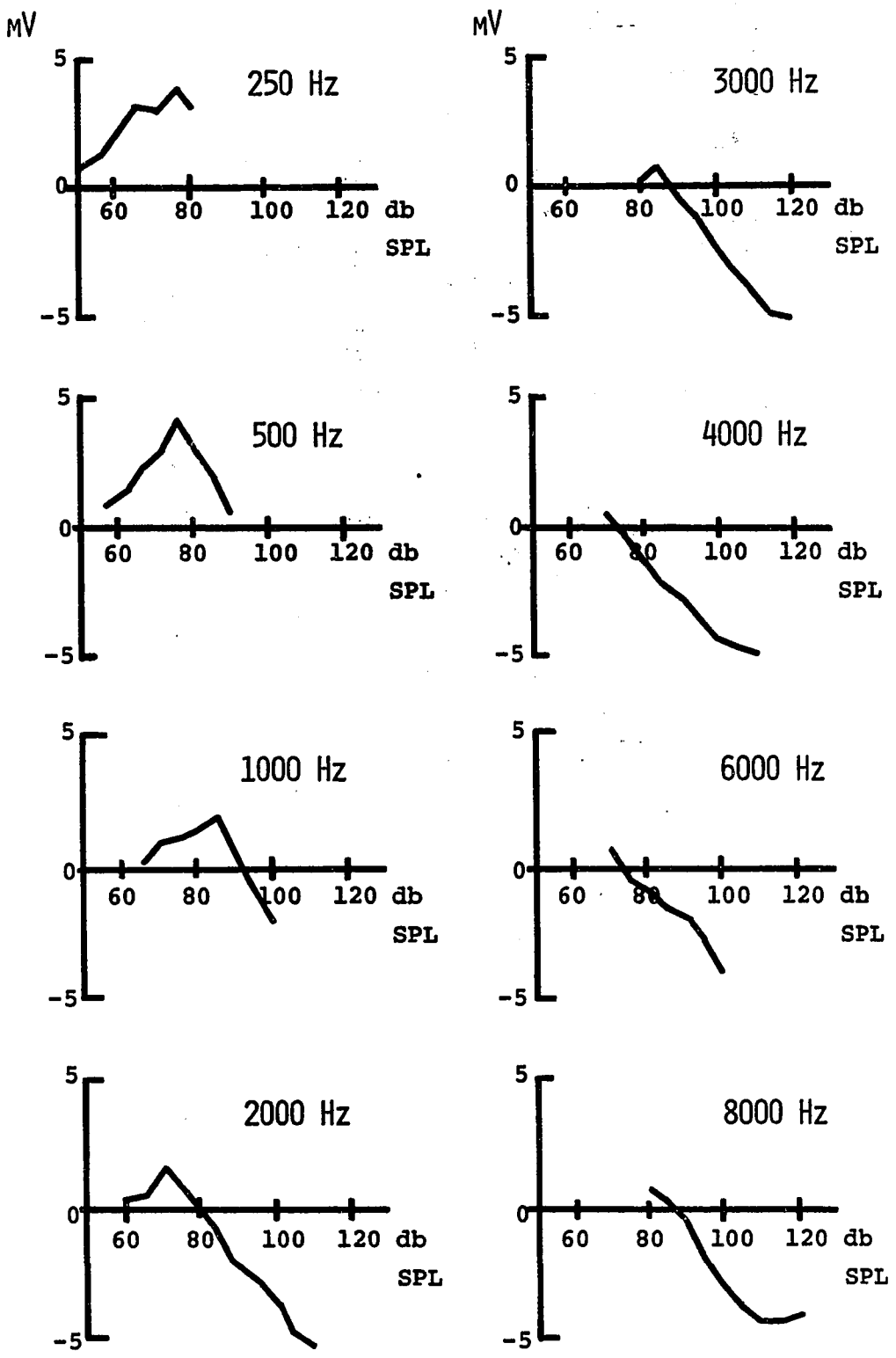

FIG.3.12 THE SUMMATING POTENTIAL AS A FUNCTION OF INTENSITY IN TURN 1. STIMULI: CONTINUOUS SINEWAVES. THE ELECTRODE ARRANGEMENT IS UNBALANCED; ONE MICROELECTRODE WAS INSERTED INTO SCALA MEDIA THROUGH THE STRIA VASCULARIS, THE OTHER INTO THE SCALA TYMPANI. THE DATA WAS OBTAINED FROM A SINGLE ANIMAL.(FROM KONISHI[35])

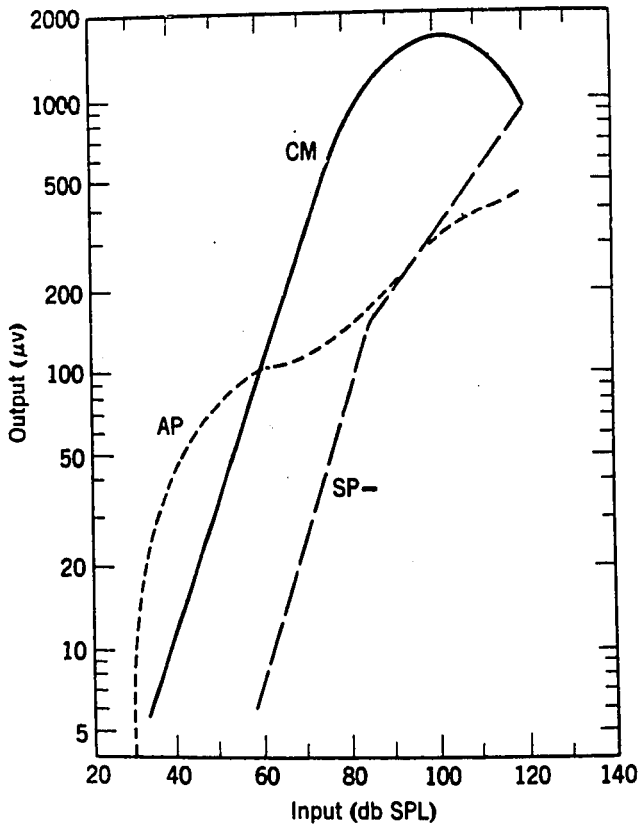

Fig.3.13 The cochlear microphonic potential (CM), the negative summating potential (SP) and the action potential (AP) measured in Turn 1 of the guinea-pig ear stimulated by 7000 Hz tone bursts with 1 msec rise time. Differential electrodes were used. The curves for CM and SP^- represent the median values of about thirty experiments and the AP curve represents one particular experiment selected as typical.(From Davis[36])

results (35). It has been observed, however, that in many cases both the CM and SP increase when the polarizing current flows from the scala vestibuli to the scala tympani and both potentials decrease for reverse current direction. Reversing the current often also changes the SP polarity from negative to positive. Other data indicate that the SP vs SPL and CM vs SPL functions shift along the SPL axis, the amount of shift being proportional to the intensity and direction of the applied current.

There is no quantitative data on the effect of olivocochlear bundle stimulation on the SP. By observing sound and OCB stimulation evoked dc potentials Fex (32) demonstrated that when the sound stimulus gives rise to a positive SP there is little interaction between the efferent activity and the activity evoked by sound; the potentials simply summate. On the other hand, if the sound gives rise to negative SP, the OCB stimulation has little effect and the sound evoked dc activity (the negative SP) seems to occlude the efferent system evoked activity.

At this point it would be logical to discuss the function and generation of the cochlear potentials. However, this topic is so closely related to the physiology of the organ of Corti and in particular, the haircell, that the discussion of the function and generation of the CM and SP will be deferred to Chapter 5 while the properties of the cochlear transducer will be appraised first.

CHAPTER 4

ON THE COCHLEAR TRANSDUCER

From a functional point of view, the haircells are the last link in the chain of mechano-acoustical components of the ear and may be classified as specialized mechano-receptors. The haircells are the transducers in which the mechanical energy originating in the input sound is finally transformed into electrical and/or chemical events of the nervous system.

The method by which the mechanical motion of the basilar membrane acts on the haircell is not known. Bekesy stated that since shearing forces are present between the top of the haircells and the tectorial membranes, these forces will bend the hairs (cilia) extending from the top of the haircell thus transmitting energy to it (37). Recently it was found that these hairs do not buckle when subjected to shearing forces. Thus, it has been suggested by Hawkins (38) and Engstrom et al (39) that the hairs act as microlevers, passively transmitting energy to the hairbearing end of the haircell.

Although the exact mechanism of energy transfer from the surrounding structure to the haircell is in doubt, the observation of the cochlear potentials (CM) indicates that

deformation of the organ of Corti, and thus the haircell, results in the generation of proportional electric potentials (25,40). The actual site of the generation of the CM and SP seems to be located somewhere between the top of the haircell and the tectorial membrane. As indicated by Bekesy's evidence (25) the potential generator is probably an active 'device' and since the excitatory mechanical movements are extremely small it is probably on the molecular scale (18).

Although the details of the mechanism by which the acoustic nerve fibers are excited are not known, it is generally accepted that the CM and SP represent a generator potential which is responsible for initiating neural discharge (11,41).

4.1. The structure and anatomy of the sensory structures of the ear

The microscopic structure of the organ of Corti has been the subject of investigations for over a hundred years. The early work of Corti (42), Hensen (43), Retzius (44), Held (45) and others has been followed by the more recent efforts of Duvall (46), Engstrom (39,47,48,49), Flock (50), Hawkins (38) and Wersall (51). In current research an effort is being made to systematically investigate the

submicroscopic structural patterns of the haircells and surrounding structures (52,47).

In the sections which follow, all references are to the guinea-pig cochlea except where otherwise explicitly stated.

4.1.1. Haircell arrangement and the organ of Corti

Haircells are classified according to their anatomical location on the organ of Corti as outer haircells (OHC) and inner haircells (IHC). Microscopically, the two types of haircells are different since two distinct cell shapes, haircell orientations and connecting nerve-endings are distinguishable (Fig.4.1).

The haircells are arranged in three rows of OHCs and one row of IHCs with the tunnel of Corti dividing the two types of cells. The schema of the arrangement is shown in Fig. 4.2 and 4.3. The plan view of the top of the organ of Corti shows a very regular grouping of the haircells (Fig.4.4). According to Schuknecht (53) a count of the population density in 9 different regions of the cat's cochlea revealed uniform haircell distribution. In particular, the average number of cells was found to be 416 OHC/mm and 120 IHC/mm. A similar counting of haircells of the guinea pig by us showed that in this animal there are about 340 OHC/mm and 90 IHC/mm.

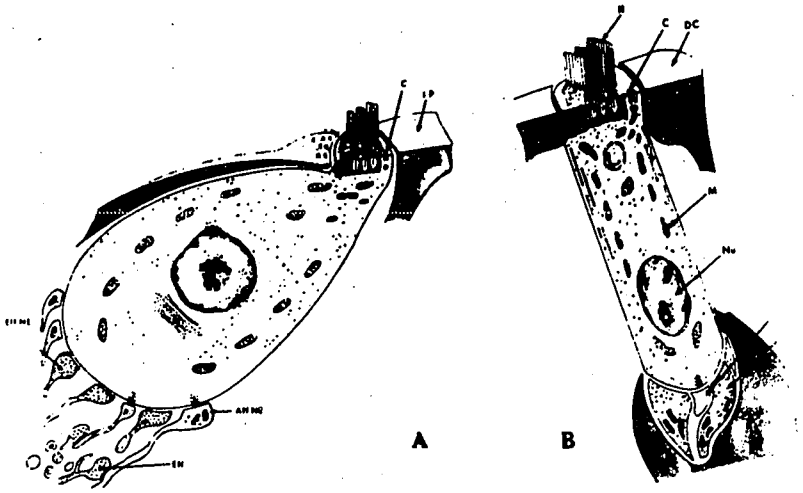

Fig.4.1 Schematic drawing of an inner (A) hair cell and an outer (B) haircell. C-centriole. Aff.NE-afferent nerve ending. Eff.NE-efferent nerve ending. IP-inner pillar. DC-Deiters cell. M-mitochondrion, Nu-nucleus.(From Wersall[51])

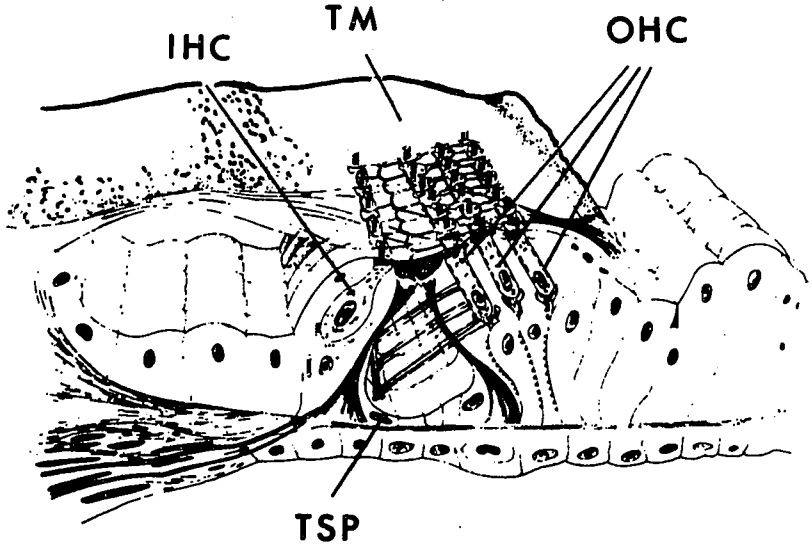

Fig.4.2 Schematic survey of the structure of the organ of Corti in mammal. OHC-outer hair cells. IHC-inner hair cells. TM-tectorial membrane. TSP-tunnel spiral fibers. (From Wersall[51])

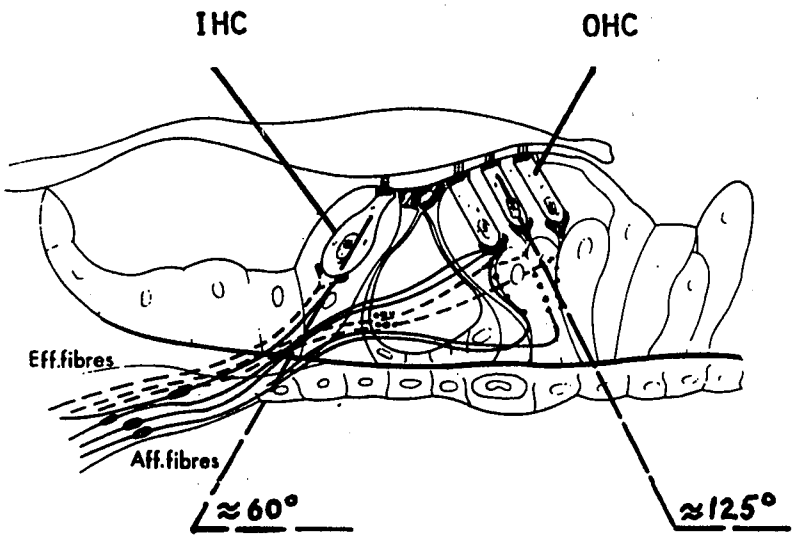

Fig.4.3 Schematic section through the organ of Corti with afferent and efferent nerve fibers. Note the different orientation of the IHCs and OHCs with respect to the basilar membrane.(From Wersall51)

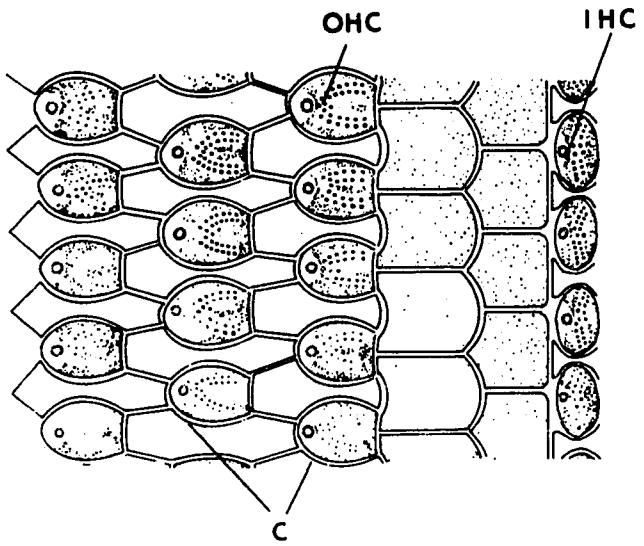

Fig.4.4 Schematic drawing of the organ of Corti seen from the surface with outer hair cells (OHC) and inner hair cells (IHC). The centrioles (C) of inner and outer hair cells are facing toward the stria vascularis.(From Wersall51)

Although the regular grouping of the haircells is observable all along the cochlea, the size of cells and their relation to the width of the basilar membrane changes as a function of distance from the stapes. This was investigated quantitatively by Hawkins (38) who found that the upper diameter of the OHC is approximately constant at 7.5-8.0 microns throughout the cochlea. The length of the OHC is about 25 microns in all three rows in the first turn, while in the fourth turn it changes from 45 microns in the first row to 65 microns in the third row. Hawkins also notes that only about a third of the total width of the basilar membrane is taken up by the IHCs and OHCs, the rest being occupied by supporting cells.

The cross-sectional view of the organ of Corti shows the different spatial orientation of the haircell bodies and their relation to the surrounding supporting cells (Fig.4.3). It is important to note that the geometric relationship between the surrounding structures and the haircells is different for the OHCs and the IHCs. Consequently, the orientation of the hairs with respect to the haircell body and possibly the reticular and tectorial membranes is not the same for the two types of cells (Fig.4.1). It is rather difficult, however, to ascertain the exact orientation of these structures in vivo, since the preparation of histological specimens invariably introduces distortions of the critical areas.

4.1.2. The sensory hairs of the OHC and IHC

According to Wersall (51), the hairs (or cilia) of the OHCs form a bundle consisting of 3 rows shaped like a 'W' pointing always towards the stria vascularis. On the other hand, the hair bundle of the IHCs is arranged in four or five rows shaped like the 'wings of a bird' (Fig.4.5). The number of hairs per haircell has been investigated for a number of mammals, including man (45,54,55). For the guinea pig Engstrom et al (39) found that in the basal and middle turns each OHC bears about 115 hairs, while on the IHCs only 35-40 hairs per cell were observed. It is noteworthy that while on the vestibular and other haircells both stereo and kinocilia are present, on cochlear haircells only stereocilia are observable. Each haircell, however, contains on the hairbearing cell surface, a structure called the basal body, which may be analogous in function to the kinocilia of other sensory cells. Structures similar to the basal body in other sensory cells have been observed to be capable of responding to minute amounts of energy and may represent the ultimate 'sensor' of the ear (Fig. 4.6b).

The cross-sectional view of the hairs and neighbouring structures under a phase-contrast microscope allowed Engstrom and his co-workers (39) to conclude that the hairs

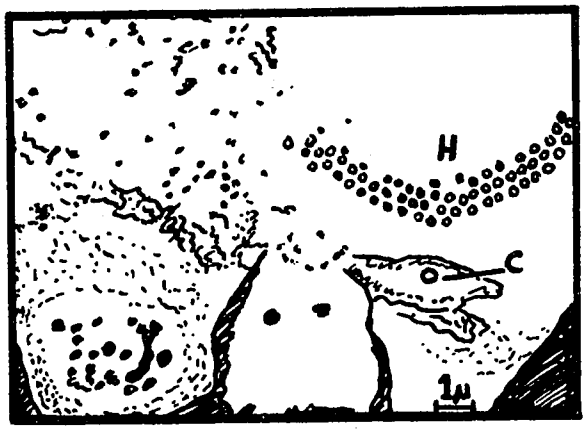

Top of inner hair cells of the organ of Corti with sensory hairs- H and centriole-C

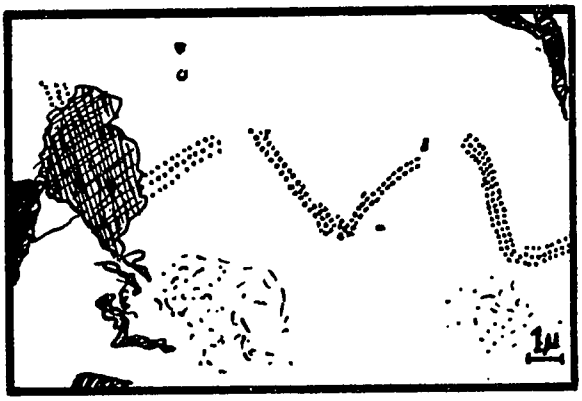

Section through a row of hair bundles from outer hair cells in the organ of Corti

Fig.4.5 Hair Bundle Arrangements.(After Wersall[51])

of the OHC are not continuous with the tectorial membrane. There is no evidence to show that the tops of the hairs of the IHCs are in direct contact with the tectorial membrane when the structure is at rest.

From the works of Engstrom et al (39), Hawkins (38) and Iurato (55) we can also learn the general shape and size of the cochlear stereocilia (Fig.4.6a). The individual hairs are always somewhat club-shaped and appear to be narrowest just above the cell surface proper. The mechanical rigidity of the cochlear stereocilia appears to be high and when mechanically displaced, slight bending of the hairs is seen under microscopic observation before they snap.

4.2. Mechanical dynamics of the haircells

It is rather unfortunate that it is not possible to draw any definite conclusions regarding the mechanical dynamics of the organ of Corti from available physiological data. At best one can hypothesize on the basis of the little which is known of the dynamic properties of the haircells.

The several possible means by which the hairs may receive some form of mechanical deformation from their environment are now discussed.

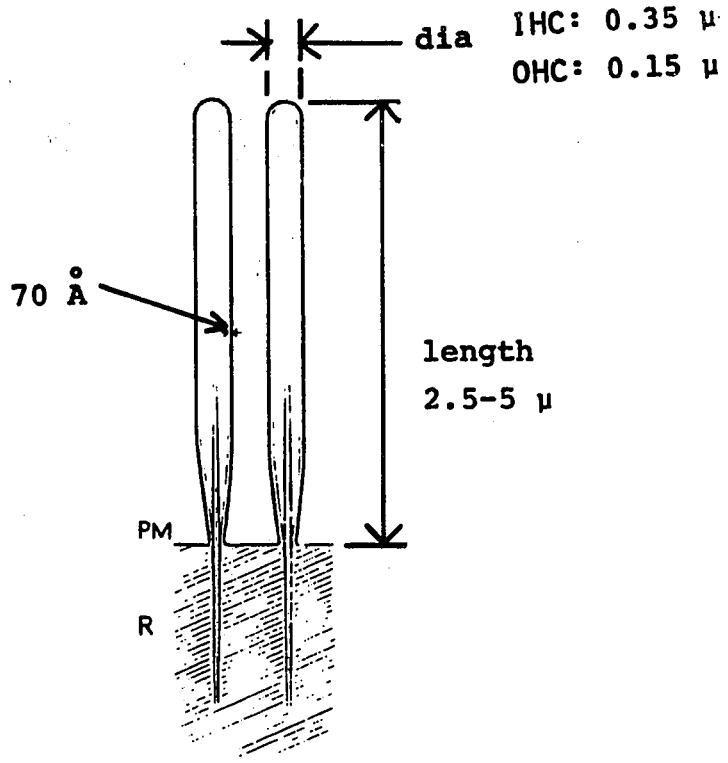

Fig.4.6a Schematic drawing of cochlear stereocilia. PM is the plasma membrane, R the rootlet. The small arrows indicate the two outer membranes of the hair.(From Engstrom39)

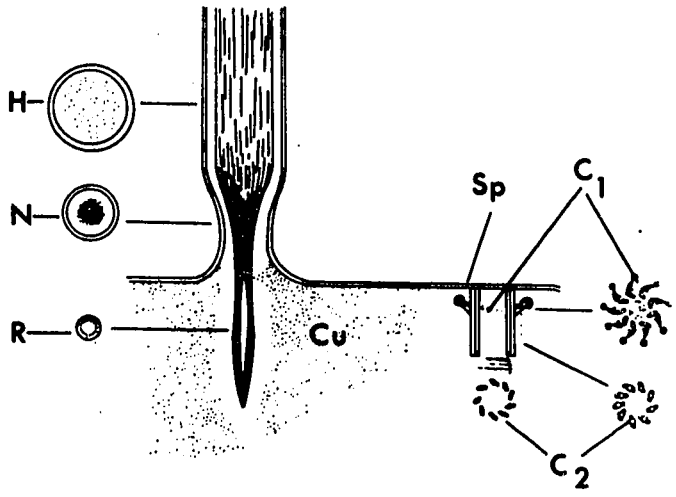

Fig.4.6b Schematic drawing of structure of hairs and centriole on top of the hair cell in the organ of Corti. H-hair. N-neck of hair. R-rootlet. Cu-cuticle. C_1-centriole 1. C_2-centriole 2. Sp-spikes.(From Wersäll51)

4.2.1. Hair bending as a mechanical stimulus for the haircell

The first and perhaps most obvious possibility of mechanical stimulation of the hairs is bending since the relative motion of the tectorial and basilar membranes will result in a shearing motion between them (37). This hypothesis is very attractive because it is simple, structurally feasible and it can be shown that it satisfies many experimental phenomena. There are some assumptions inherent in this bending theory which should be kept in mind. Firstly, it is tacitly assumed that the tectorial membrane is rigid, but this may not be so. Secondly, parallel motion of the two membranes is not necessarily permissible, because the hairs cannot withstand pull and so complex motion is required on the part of the tectorial membrane. Thirdly, most hairs do not seem to touch the tectorial membrane (39) and thus they cannot be bent by the motion as supposed.

We would like to add a possible corollary to the original bending theory. It may be possible that the hairs of the haircells are not directly stimulated by the relative motion of the two membranes, but are set in motion by the fluid streaming between the tectorial and basilar membranes. This would explain why most hairs do not touch the tectorial membrane and may also be an explanation of the particular pattern hairs form on the haircells (see Fig.4.5).

4.2.2. Pressure as a mechanical stimulus for the haircell

An alternate mechanism proposed for the mechanical stimulation of the haircell is pressure acting on the hairs and/or cell body (56,57,58). It is imagined that the displacement of the membranes changes their relative positions in some manner and this results in the change of pressure exerted on the hair, haircell and supporting cell complex. At first glance this hypothesis appears to be perfectly feasible, since almost any type of movement with rigid or viscous membranes will produce some sort of deformation of the cochlear structures producing pressure changes on the hairs or cell body. One must consider, however, that pull on the hairs is not possible and that the hairs are very rigid, possibly permitting little deformation. Although it is conceivable that the pressure is transmitted to the cell body through the hair (39,38), according to Bekesy (59), experimental evidence indicates that shearing forces are the primary factor in stimulating the haircells.

4.2.3. Is the assumption of mechanical stimulation of the haircell necessary?

There is also a possibility that the haircells are not stimulated in a direct fashion by mechanical movement at all. Naftalin (60) proposes an alternate mechanism according to

which the mechanical-to-electrical transduction takes place through the special chemical properties of the tectorial membranes. The charge distribution of the tectorial membrane suggests a biased semiconductor arrangement somewhat in the same fashion as suggested by Wei (61).

It is also conceivable that the movement of the membranes only serves to establish contact between the top of the hairs and the tectorial membrane. This means that depending on the particular displacement patterns established on the basilar membrane, certain hairs would touch the tectorial membrane, while others would not. Thus, a pattern of conducting pathways may be established which would pass through the cells associated with the hairs and so ultimately give rise to the auditory nerve fiber discharge.

4.3. Innervation of haircells

The innervation of the inner and outer haircells differs although both appear to receive afferent and efferent fibers as shown in a schematic form in Fig.4.3. The IHC is innervated by the afferent radial fibers and efferent fibers from the Intraganglionic Spiral Bundle. It is also possible that some efferent innervation is due to fibers running in the Inner Spiral Bundle. The OHC receives its afferent innervation from spiral fibers running in the basal direction while its efferent innervation appears to pass through the

Intraganglionic Spiral Bundle and possibly form the Tunnel Spiral Bundle as well (Fig.4.7). As indicated on the diagram the radial fibers characteristically innervate one or two haircells and each haircell is innervated by one or two neurons. The spiral fibers, on the other hand, innervate several haircells along their paths in the cochlea. The efferent fibers may be said to belong to one of two classes according to their origin which may be in either the uncrossed or the crossed olivo-cochlear bundle.

The nerve endings adjoining the haircells not only differ from afferent to efferent but also from OHC to IHC. Furthermore, the nerve endings change as a function of the distance of the haircells from the stapes. The small afferent nerve endings are in close contact with their respective sensory cells and contain characteristic microstructures such as mitochondria, neurofibrils and granules. The numerous efferent nerve endings on the IHC are small and irregularly shaped. On the OHC the efferent nerve endings are large and also numerous (Fig.4.1).

In the basal turn all sensory cells are provided with many large efferent and a small number of afferent endings. The number of efferent nerve endings diminishes as the distance from the stapes increases and only the first row of OHCs retains efferent endings all the way to the apex of the cochlea.

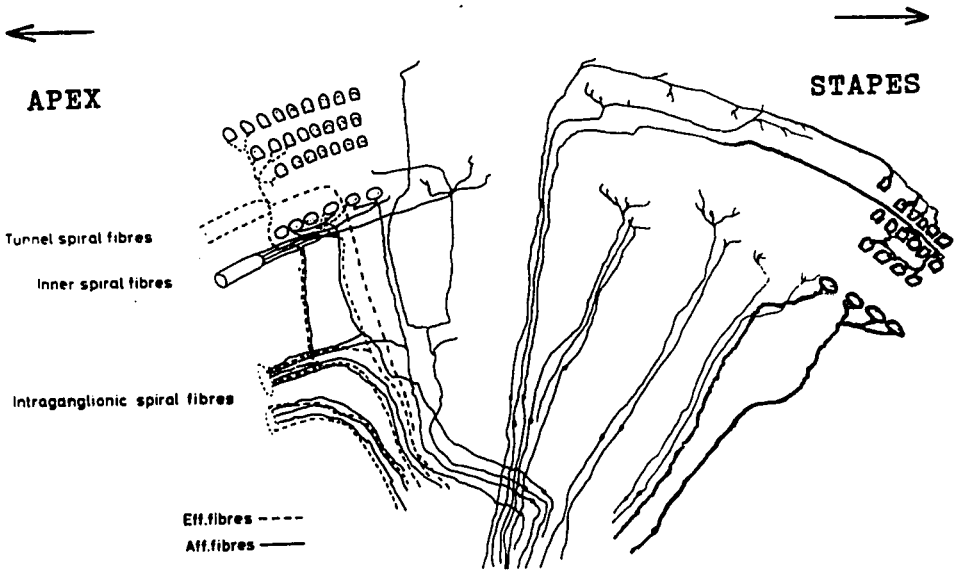

Fig.4.7 Schematic survey of part of a basal coil in the organ of Corti showing the distribution of afferent and efferent nerve fibers.(From Wersall[51])

CHAPTER 5

THE GENERATION AND DISTRIBUTION OF THE COCHLEAR POTENTIALS

Present theories of the generation of cochlear potentials are greatly limited by the lack of experimental evidence. Historically, a number of concepts have been introduced such as the piezoelectric microphone analogy (62), the resistance microphone theory (62) and the movement controlled 'two-state' voltage generator (63). Other theories are mainly modications or extensions of these main hypotheses. With the notable exception of Johnstone (64) linearity of the movement-potential relationship is generally assumed in both experimental and theoretical work, although this is not justified for the single transducer by the available evidence.

There is also very little known about the distribution of potentials in the cochlea due to an individual haircell. In most works it is assumed that the gross electrodes used pick up potentials from a small segment of the cochlea only and within that segment all potential generators are in phase.

In this chapter we will examine theories of the generation and distribution of the cochlear potentials. It will be shown that the linearity assumption renders many of the existing hypotheses untenable and that the 'in-phase' assumption is artificial and restrictive.

5.1 Theories and models of the generation of the cochlear potentials

5.1.1. The variable resistance theory

Davis' comprehensive description of the sensory mechanism in the cochlea was mentioned briefly in connection with the functional description of the haircells. Now we will examine his theory in greater detail with emphasis placed on the concepts related to the generator potential.

The theory advanced by Davis (62) considers the cochlear transduction process to be somewhat similar to the action of a resistance microphone. It is supposed that the mechanical distortion of the haircell which arises from the motion of the basilar membrane results in the change of ohmic resistance of some active part of the haircell. This resistance is a part of a circuit which consists of tissue resistances and biological batteries located in the stria vascularis and the haircell itself (Fig.5.1). The changes in mechanically induced ohmic resistances are assumed to be linear over 3 or 4 decades and, given constant voltage sources in the circuit, will produce linear current changes through the haircell. This in turn will produce voltage changes across the haircell resistance and this voltage change will be the generator potential which by some action on the nerve junction on the haircell initiates the firing of the nerve fiber.

Davis explicitly assumes that the cochlear transducer is linear over a 60-80 db range. We will now examine the validity of this assumption by using circuit analysis and physiological considerations.

From Fig.5.1. we may draw the equivalent electrical circuit of Davis' concept (Fig.5.2). Then

$$V_2 = i_2 \times R_2 = \frac{V}{R + R_2} R_2$$

$$= \frac{R_2}{R + R_2} V$$

$$= \frac{1}{1 + \frac{R}{R_2}} V \qquad (5.1)$$

where

$R = R_1 + R_3$ = the sum of the resistances of the stria vascularis, the scala media, the tectorial membrane and the paths from the haircell to the scala tympani and the stria vascularis.

Let

$$\frac{R_2}{R} = x \qquad (5.2)$$

so that

$$V_2 = \frac{1}{1 + \frac{1}{x}} = \frac{x}{1 + x} V \qquad (5.3)$$

where 'x' is not known experimentally and it may be greater or smaller than 1, but of course it cannot be negative.

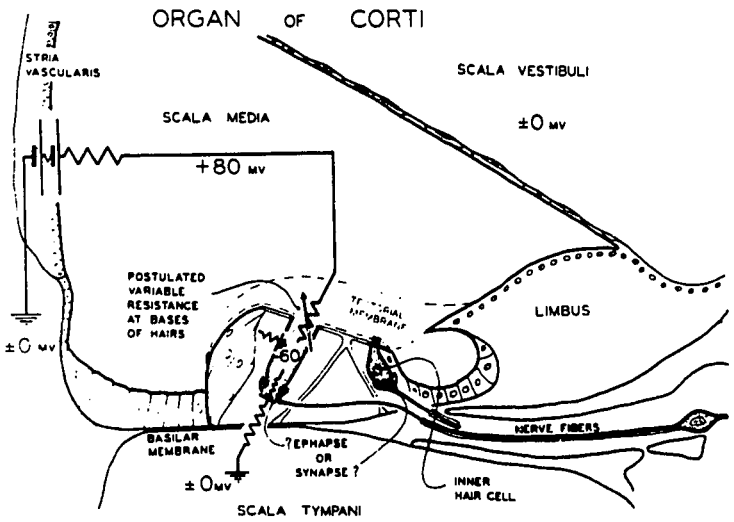

Fig.5.1 'Resistance microphone' theory of cochlear excitation with the primary 'battery' in the haircell and an accessory battery in the stria vascularis.(From Davis62)

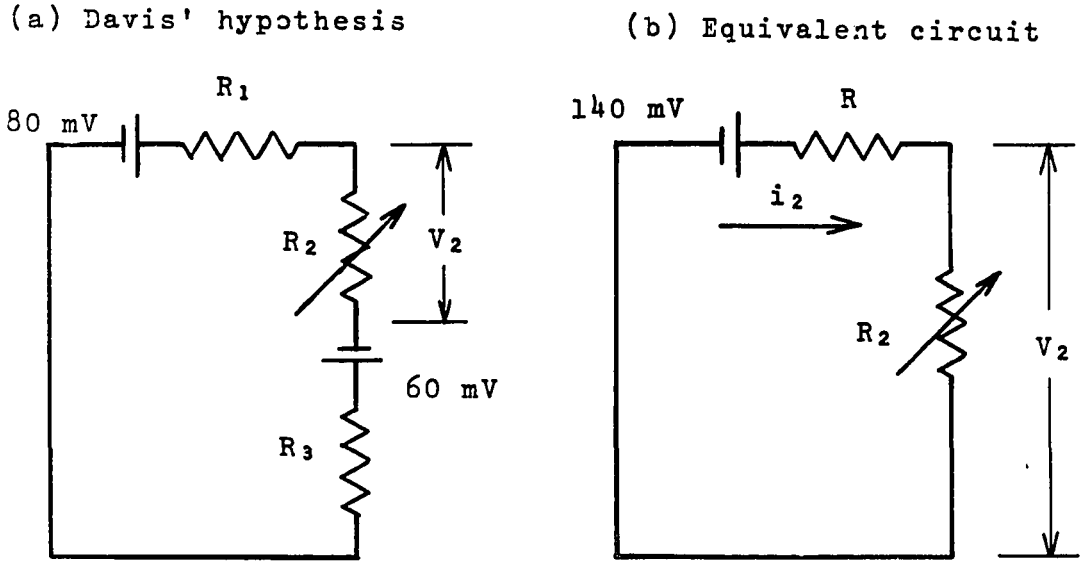

Fig.5.2 The 'resistance microphone' concept R_1 = resistance of the stria vascularis, scala media and the tectorial membrane. R_2 = variable resistance (HC), R_3 = resistance from the HC to scala tympani and stria vascularis.

A simple analysis of the function

$$\frac{x}{1 + x} \tag{5.4}$$

may be carried out to determine regions of approximate linearity. Differentiating we get

$$\frac{d}{dx}\left(\frac{x}{1 + x}\right) = \frac{1}{(1 + x)^2} \tag{5.5}$$

The original function and its derivative are plotted in Fig.5.3. From this it may be shown that if 10% deviation from linearity is considered acceptable and a 60 db range of linearity is specified, then 'x' must be either less than .053 or greater than 2.117.

Let us now suppose that 'x' is less than 0.053. This means that R_2 has the lowest value when there is no stimulus and increases as the stimulus intensity is increased. Judging from data collected by Johnstone (65) R is approximately equal to 40 kohms. Thus, in the linear range the maximum R_2 must be

$$R_2 = 0.053 \times 4 \times 10^4 = 2.1 \text{ kohms.}$$

For the linear range the lowest value would be 2.1 ohms and since the range of haircell output extends well over the linear 60 db, the resting R_2 would probably be much smaller than 1 ohm.

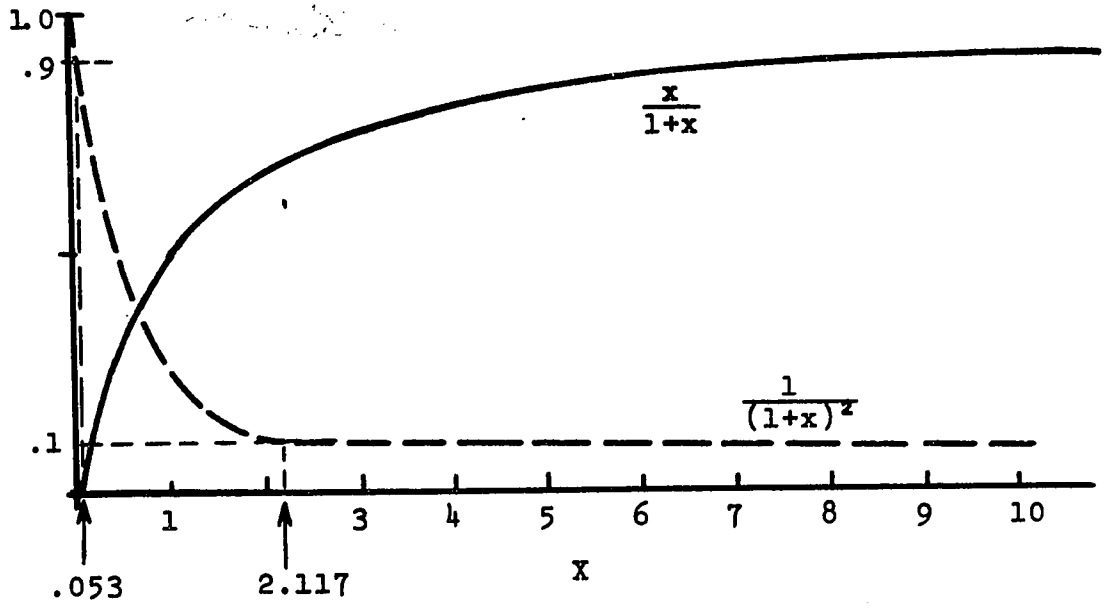

Fig.5.3 The function $\frac{x}{1+x}$ and its derivative.

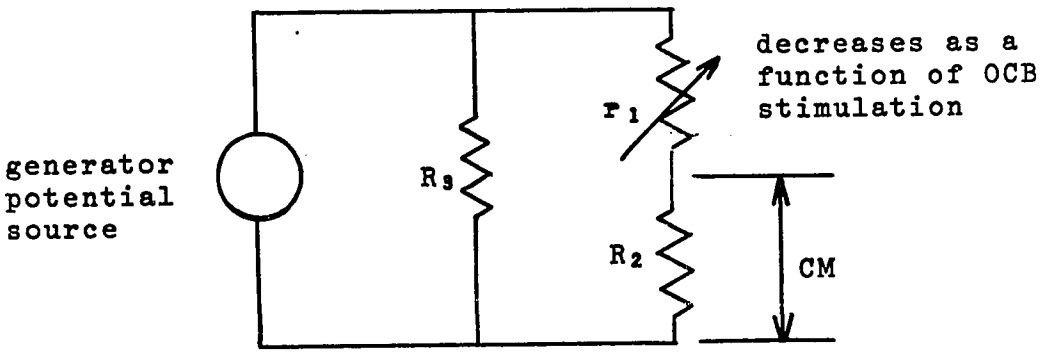

Fig.5.4 Haircell equivalent circuit.(After Sohmer[31])

The next step is to determine the current requirements in the circuit of Fig.5.2b. Since $R_2 = 0.053 \times R$ the current will be essentially determined by R and it will be in the neighbourhood of

$$\frac{0.14}{4 \times 10^4} = 3.5\ \mu A.$$

At first glance it appears to be quite conceivable that such a resting current flows through the individual haircell. Consider, however, that there are about 10000, or more, haircells in the guinea pig cochlea and thus the total current would be 35 mA which is quite large. Such a current implies a large power consumption: 49 watts for the assumed R = 40 kohms. This power consumption is inconceivably large, being approximately three times that of the whole brain or perhaps 60% of the Basal Metabolic Rate of the human body. In reality the cochlear metabolic energy consumption must be small since the cochlear microphonic potential will be present for an appreciable length of time after death in which condition only small energies are available due to lack of oxygen. To our knowledge a current of this magnitude was never observed in the cochlea.

Let us now suppose that 'x' is greater than 2.117. Since in this case the value of R_2 will be <u>largest</u> when there is no stimulus; the resting current is expected to be

small. Numerically, the lowest R_2 in the linear range would be

$$R_2 = 2.117 \times 40000 = 84.8 \simeq 85 \text{ kohms.}$$

Assuming the 60 db linearity range again, the largest R_2 will be 85 Mohms or larger which is consistent with the estimate of Johnstone (65) who puts the individual haircell resistance in the neighbourhood of 50 Mohms. For such large values the resting current would certainly be small, but the thermal noise generated by such a large resistance would be extremely high.

The question of thermal noise requires further attention. In the first case ($x = 0.053$) the resistance of the circuit will be about 40 kohms. Now thermal noise is always generated in a resistor (66) and for a metallic resistor the mean-square-value of noise is expressed by

$$v_R^2 = 4 \times k \times T \times R \times \Delta f \qquad (5.6)$$

where

k = Boltzman constant = 1.38×10^{-23} joule/deg K
T = absolute temperature
R = resistance in ohms
Δf = bandwidth

Taking a bandwidth of 15 kHz which is certainly valid in the basal turn and animal temperature as 37 deg C = 310 deg K, we have

$$v_R^2 = 4 \times 1.5 \times 10^4 \times 3.1 \times 10^2 \times 1.38 \times 10^{-23} = 2.57 \times 10^{-16}$$

Thus for 40 kohms

$$\text{ave } v_R^2 = 10.3 \times 10^{-12}$$

$$\sqrt{(\text{ave } v_R^2)} = 3.21 \times 10^{-6} \text{ V} = 3.21 \text{ μV} \qquad (5.7)$$

This noise voltage must be compared to the expected generator voltage which at threshold must be in the neighbourhood of

$$v_{gen} = R_2 \times i = 1 \times 3.5 \times 10^{-6} \text{V} = 3.5 \text{ μV}$$

The signal-to-noise ratio would then be approximately 1. This is consistent with the concept of a physical threshold in the mechano-electrical conversion process in the haircell. We can also see that in the second case ($x > 2.117$) the noise voltage would be

$$\text{ave } v_R^2 = 8.5 \times 10^8 \times 2.57 \times 10^{-16} \text{ V} = 21.8 \times 10^{-8} \text{ V}$$

$$\sqrt{(\text{ave } v_R^2)} = 4.67 \times 10^{-4} \text{ V} = 467 \text{ μV} \qquad (5.8)$$

which is unacceptably high, because the signal-to-noise ratio would be much less than 1.

In summary, the concept of a simple resistance modulator circuit as a haircell model must be re-examined from the point of view of circuit analysis since linearity considerations limit the acceptable resistance values to very small and very large values. When R_2 is small the resting current is large, and has never been observed experimentally; when R_2 is assumed to be large noise considerations make the hypothesis questionable in its present form. In Chapter 9 we will show

that there is no need to assume linearity of the mechanical movement-to-cochlear microphonic potential generator. Then, of course, Davis' hypothesis is eminently reasonable and plausible since it is the assumption of linearity which creates inconsistencies in the theory.

5.1.2. A movement controlled voltage generator

An alternative to Davis' model is an arrangement in which the mechano-electrical transducer is a movement controlled voltage generator. Such a model was suggested by Tasaki (63) who assumed that the hair bearing end of the haircell shows large variations in potential in response to mechanical stimuli. This potential represents one of two possible stable chemical states of the membrane but it is not of the "all-or-none" type. The action of many haircells then gives rise to macroscopically observable potentials in the form of the CM and the SP.

The origins of the above hypothesis lie in the nerve membrane theory proposed by Tasaki. According to this theory the nerve membrane is very unstable and sensitive to pressure changes because of a molecular construction which has two stable chemical states. To explain the sensitivity of the membranes to minute chemical and mechanical changes, it is necessary to presume that the membrane is on the verge of

transition from one stable state to the other. Thus any small stimulation triggers the transition giving rise to the haircell generator potential. The conditions necessary to maintain the haircell membrane in such an unstable state are supposed to be created by the endolymphatic potential and the existence of high potassium concentration in the endolymph.

5.1.3. A modified variable resistance model

Sohmer (31) presents a haircell model (Fig.5.4) in the context of his explanation of AP depression and CM augmentation as a result of OCB stimulation. According to Sohmer, part of the current generated by the generator potential source flows through resistances R_2 and r_1. R_2 is the resistance across which the CM is measured and r_1 is an 'OCB-controlled' resistance representing an electrical pathway passing through the afferent nerve endings adjoining the haircell. It is supposed that the OCB stimulation changes this resistance, thereby increasing the current through R_2 and consequently a CM increase results. Although this model was inspired by Davis' concepts of the generation of the receptor potential, it does not include the series resistances necessary to complete the circuit. Turning again to circuit analysis concepts it is possible to express all sources and resistances 'looking into' R_2 (or R_2 and r_1 in series) in terms of a resistance and an ideal voltage source connected

in series, but not in parallel as R_3. With this modification the circuit becomes essentially the same as that discussed in connection with Davis' hypothesis and of course, the same comments apply.

5.1.4. A non-linear cochlear potential generator model

Consideration of the properties of the summating potential led Johnstone and Johnstone (64) to extend Davis' variable resistance theory of the cochlear potential generation. Their model includes the mechanical movement-to-resistance change transfer characteristics as an essential part. Based on those observations of Bekesy which indicate that the mechanical stimulation of the haircells is due to shearing action between the basilar and tectorial membranes, the Johnstones derive a mathematical relationship for the generated cochlear potentials (CM and SP) as a function of the angle between the haircell's body and cilia. The model is shown in Fig.5.5a. and, using the notation shown, the haircell body-to-cilia angle (ϕ) as a function of angular displacement of the basilar membrane (α) can be derived by trigonometry as

$$\phi = \operatorname{arcot}\left(\frac{K}{h_0}\,\alpha + \cot\,\phi_0\right) \qquad (5.9)$$

This relation is plotted in Fig.5.5b and it can be seen immediately that ϕ will vary asymetrically for a symmetric α variation as a function of the 'bias angle' (ϕ_0). ϕ_0 will be

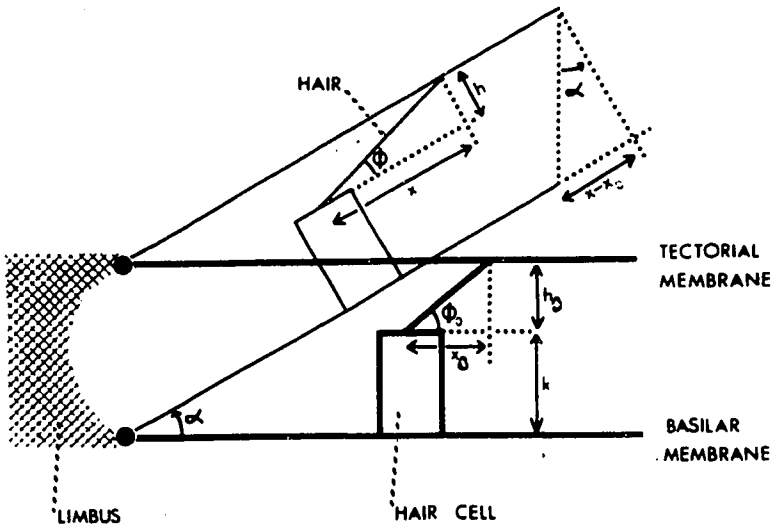

Fig.5.5a Diagrammatic representation of movement of the cochlear partition. The angular movement (α) of the basilar membrane, the hair cell angle ϕ, and the distance h_0 are greatly exaggerated.(From Johnstone[64])

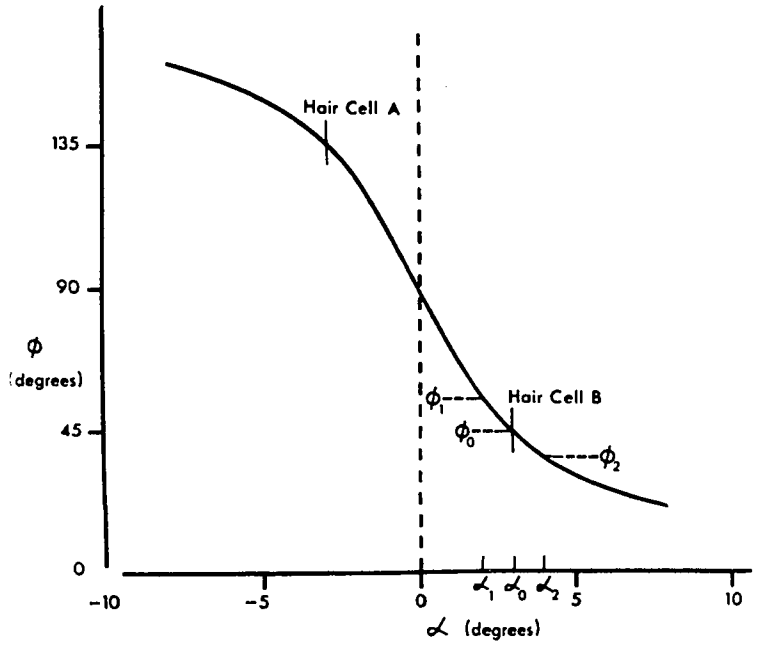

Fig.5.5b Theoretical relationship between basilar-membrane movement (angle α) and hair angle (ϕ). The marks on the curve indicate the positions of the Y axis for two arbitrary hair angles. Hair cell A:$\phi_0=135^\circ$. Hair cell B: $\phi_0=45^\circ$. An asymmetrical variation $\phi_1-\phi_0-\phi_2$ arises from the symmetrical variation $\alpha_1-\alpha_0-\alpha_2$.(From Johnstone[64])

present because of the resting angle between haircell body and cilia and it will be different for the IHC and the OHC (see Fig.4.1). This fact is used by the authors to explain the generation of the SP^- and SP^+ by assuming after Davis (11) that the SP^- is generated by the outer and the SP^+ by the inner haircells.

The model accounts for a number of experimentally observable facts, such as potential changes in the cochlea due to static pressure changes in the various scalae, the generation of harmonics in the observed CM and the magnitude variations of both the CM and the SP as a function of the SPL of the stimulus. Nevertheless, the theory may be criticized in that the SP as measured by gross electrodes is not a localized potential since it is picked up from distant points of the cochlea as well (see Section 5.3). Thus, similarity between responses predicted by the model and as measured by the authors at <u>one</u> point in the basal turn to a specific stimulus (4.5 kHz tone pip) may be coincidental. This model, however, is very valuable because it formulates mathematically the relation between the basilar membrane and the cochlear potentials. The theory also shows how a relatively simple non-linear mechanism may account for many diverse physiological phenomena.

5.2. Interaction between haircells

Davis' considerations are limited to a single receptor cell and its 'circuit'. Since there are many receptors in close proximity and since there is no knowledge of insulated pathways for each haircell, interaction between individual haircells, or the circuits representing them, must be considered. In Fig.5.6 a network representing the haircells and a possible interconnection scheme is shown. Considering only a neighbouring pair of haircell circuits, it is possible to derive the effect a change in R_2 will have on the voltage across R_2' when R_2' remains constant. Using the notation of Fig.5.6 and considering R_5 to be negligibly small, the circuit equations may be written down:

$$a_{11}i_1 + a_{12}i_2 + a_{13}i_3 = b_1$$

$$a_{21}i_1 + a_{22}i_2 + a_{23}i_3 = 0$$

$$a_{31}i_1 + a_{32}i_2 + a_{33}i_3 = 0$$

where

$$a_{11} = R_1 + R_3 + R_2$$
$$a_{12} = -R_1$$
$$a_{13} = R_3 + R_2$$
$$a_{21} = -R_1$$
$$a_{22} = 2R_1 + R_4$$
$$a_{23} = -R_4$$
$$a_{31} = -R_3 - R_2$$
$$a_{32} = -R_4$$
$$a_{33} = 2R_3 + R_4 + R_2 + R_2'$$
$$b_1 = V_E + V_{HC}$$

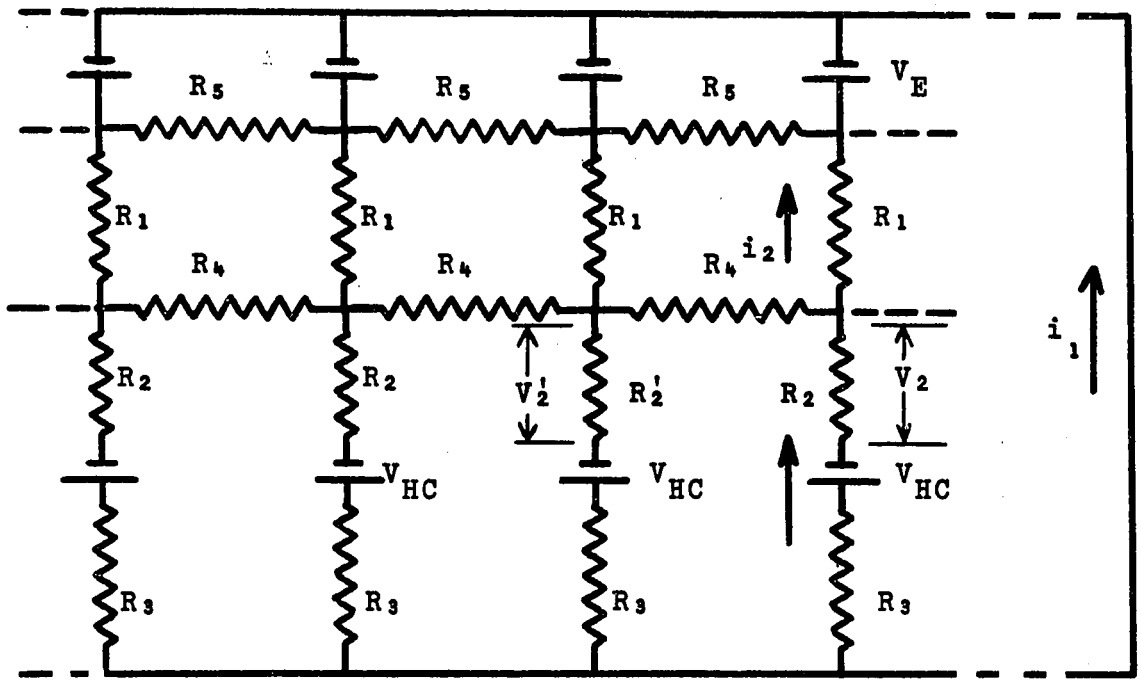

Fig.5.6 Interaction between haircells. The haircells are represented by the circuit of Davis' 'resistance microphone' model (see Figs.5.1 and 5.2). The network represents a segment of the organ of Corti; R_4 is the resistance between neighbouring haircells. Haircell 'interaction' arises from the circuit properties of this network. This interaction may be 'inhibitory' or 'excitatory', depending on the values of the various resistances.

Let us denote the voltage across R_2 and R_2' by V_2 and V_2' respectively. Then

$$V_2 = R_2(i_1 - i_3)$$

$$V_2' = R_2'(i_3)$$

What we would like to know is what change will be observable on V_2 as V_2' is changed. In particular is it possible to observe an increase in V_2 as a result of a decrease in V_2' ? To answer this question we must investigate the ratio

$$\frac{DV_2}{DV_2'} \quad \text{where} \quad D = \frac{d}{dR_2'}$$

and determine whether it can become negative or not for certain combinations of resistance values. After differentiation and manipulation we find that

$$\frac{DV_2}{DV_2'} = \frac{a_{22}a_{13}A_{13} - a_{23}A_{23} + a_{23}a_{32}A_{33} + (a_{21}a_{32}-a_{31}a_{22})A_{33}}{a_{13}A_{13} - a_{23}A_{23} + 2R_3 + R_4 + R_2}$$

that is, a function determined by all the R terms except R_2'. This expression may be positive or negative depending on the relative values of R_1, R_2, R_3, and R_4, but our present knowledge does not allow even an approximate calculation. The interesting and important feature of this analysis is that it implies that neighbouring haircells may interact in an excitatory or an inhibitory fashion. If the DV_2/DV_2' ratio is positive, this implies that the CM generated in one haircell is accompanied by a CM generated in the same sense in

the neighbouring haircells. Thus, the cochlear microphonic potential spreads in an 'excitatory' fashion. On the other hand if the ratio is negative it implies that a potential increase across one haircell is accompanied by a decrease of potential across its neighbours and hence an 'inhibitory' effect is produced.

5.3. Recording electrodes and the distribution of the cochlear potentials

In Chapter 3 we described the previously reported properties of the cochlear potentials (CM, SP and AP) as recorded by differential electrodes. However, since the relationship between the gross recording electrodes and the cochlear potential generators is of central importance in our work, further examination of the physical and physiological factors is warranted.

Fig.5.7 is a simplified illustration showing both the transverse and the longitudinal cross section of the cochlea with the differential electrodes (see also Fig.3.1). The electrodes are immersed in perilymph and are separated from the source of the CM by several layers of membranes. According to Bekesy (67), the membranes are good insulators while the endolymph and the perilymph are relatively good conductors; conductivity = 0.02 mho/cm. It was also observed by Bekesy that the potentials on two sides of an insulating

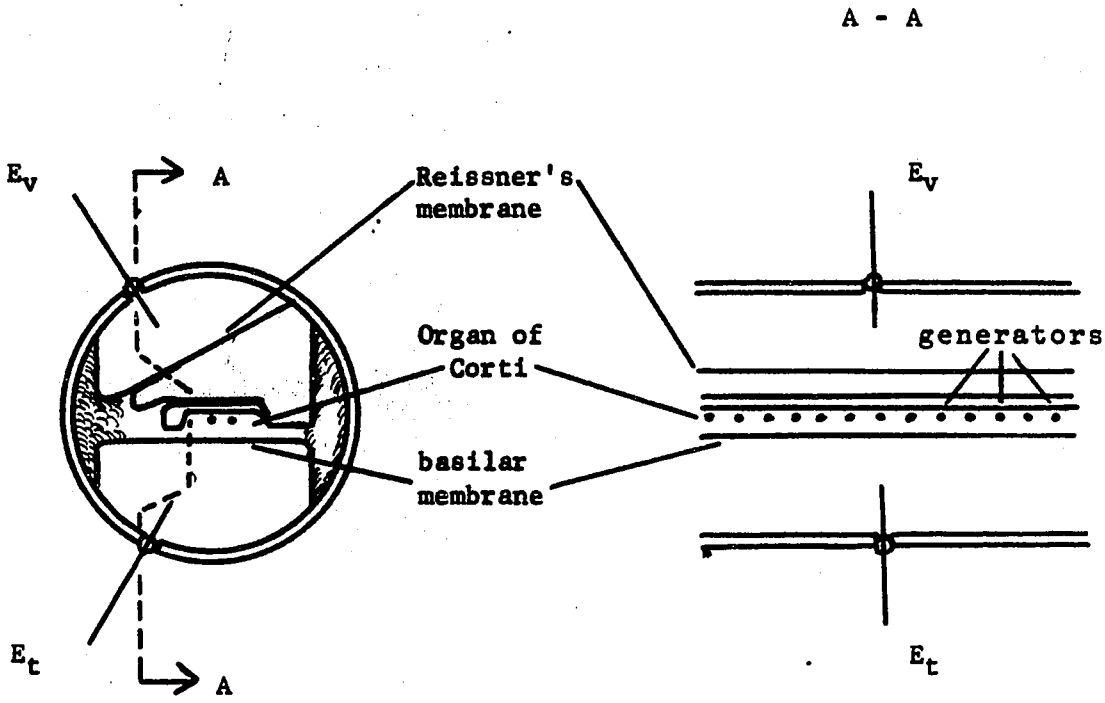

E_v = electrode in scala vestibuli
E_t = electrode in scala tympani

Fig.5.7 Cross-sections of the cochlea with differential electrodes. The points marked as 'generators' correspond to the physiological source of the CM. The exact location of this source is not known.

sheet representing Reissner's membrane in a model have different spatial distribution, i.e., "any local disturbance inside the endolymph is spread out over practically the whole length of the cochlea in the perilymph..."(67). Bekesy also calls attention to the fact that the impedances around the cochlear potential generator are very complex (68). Thus, it is possible to observe different distributions for different frequencies and dc.

In spite of the foregoing considerations it appears to be generally assumed in cochlear electrophysiological, pharmacological and auditory behavioural work that potentials picked up from differential or even round window electrodes originate from a segment of the basilar membrane all of whose elements move in phase. This assumption being made, usually only implicitly, the measurements of cochlear potentials with gross electrodes are taken to represent events on the individual haircell level.

Because of its great importance, we will first examine the origins of the assumption that the CM, and in general the cochlear potentials, are recorded from a small group of in-phase sources. Tasaki et al. present several independent pieces of evidence that the CM potentials recorded by differential electrodes originate within a few millimeters of the recording site (24,28). In the first paper the

authors show phase curves of the CM as recorded by two pairs of electrodes approximately 1 mm apart and note that at certain frequencies the phase shift between the corresponding two phase curves is 90°. As additional supporting evidence, on p. 508 of (24) two markedly different amplitude curves, which were recorded at the round window and in Turn 1 respectively with electrode separation of about 2 mm are shown. A different kind of evidence is given by Tasaki and his co-workers in (28). They showed, by selectively suppressing the haircells of the cochlea (KCl injection), that differential electrodes pick up voltages only from that turn of the cochlea in which they are implanted. Also, when dc current was passed through Reissner's and the basilar membrane, the observed polarizing effect suppressing or enhancing the CM depending on the polarity, was restricted to a one turn segment of the cochlea.

Simmons and Beatty arrived at a conclusion similar to those of Tasaki's group (69) by correlating the physiological findings with psychoacoustic observations. Using chronically implanted electrodes and measuring sensory hearing loss they showed that damage caused by high frequency intense sound to the organ of Corti is also reflected in changes of the round window cochlear microphonic potential. They concluded that "the CM measured at the RW does not reflect cochlear changes more apically located than a very few millimeters" (69).

Although none of these authors states the following assumption explicitly, their observations and conclusions have been taken by many workers to mean implicitly that the cochlear microphonics can be assumed to be recorded from a segment of the cochlea small enough so that the generators can be considered to be in phase. As the preceding two paragraphs indicate, experimental evidence does not warrant such a conclusion. In particular, the "few millimeters" close to the round window will cover a 10 kHz range of MRFs and for any of these frequencies a characteristic pseudo-travelling wave will exist on the basilar membrane segment in question. Thus, the generators will not be in phase and macroscopic observation will reflect not only the summation of the individual responses, but possible cancellation effects due to phase differences between the outputs of the cochlear generators located varying distances from the round window.

The work of Whitfield and Ross (70) is very significant. These authors investigated the effect of abandoning the tacit assumption that the source of the cochlear potentials, as observed by gross electrodes, is a set of in-phase generators. Their conclusion is that as a result of considering the generators out-of-phase, interference effects must be taken into account.

By assuming a non-linear voltage generator which is distributed along the basilar membrane, Whitfield and Ross were capable of explaining, albeit qualitatively, a great number of the experimentally observed properties of the cochlear potentials. They assume that the cochlear electrodes will pick up a weighted and low pass filtered average of the output of the individual generators. Then, although the individual generator output may be quite distorted, the summated response will be nearly sinusoidal and will correspond to the amazingly undistorted CM waveform. It is also easy to see that due to the assumed non-linearity of the individual generators a dc shift is possible corresponding to the SP as observed experimentally. The time delay inherent in the movement of the pseudo-travelling wave down the basilar membrane will produce various interference patterns with respect to the electrode and it is quite possible that these patterns explain many of the peculiarities of the CM and the SP. The authors did not develop their theory in quantitative detail, but only investigated the possibilities of their basic idea through some very rudimentary models.

CHAPTER 6

EXPERIMENTAL DETERMINATION OF THE COCHLEAR POTENTIALS

This chapter reports on the experimental work designed to provide guinea-pig cochlear potential data in a form suitable to effect a comparison with simulated cochlear potentials to be obtained from model studies. Since frequency domain analysis seems to be the 'natural' choice in the case of the ear, it was decided that data suitable for the construction of appropriate Bode diagrams would be collected. In particular, we measured the cochlear microphonic amplitude and phase in various turns of the cochlea as a function of frequency at pre-selected constant sound pressure levels at the eardrum. The summating potential was measured under similar conditions in various turns of the cochlea using very carefully balanced electrodes. Also, many of the experiments were repeated several times using different SPLs.

6.1. The design of new experiments

As we have seen in Chapter 3, frequency domain observations related to the cochlear potentials are available but closer examination reveals that many of the published experimental results are not suitable for system

analysis, modelling and simulation. In particular we note that it is not possible to utilize published time domain observations of the CM for our purposes. Pestalloza and Davis (71) used 7 kHz tone bursts of 2.5-3.0 msec duration as the acoustical input and Teas et al. (72,73) employed slow acoustic transients lasting 0.5 to 1.0 msec to stimulate the ear. The exact acoustic waveforms of these transients are again unknown, since the waveform was recorded with an earphone in an acoustic coupler. In order to compare experimental results with model simulation results it is necessary to have data which were obtained with a known input signal.

For recording the cochlear potentials from the guinea pig we use the differential electrode arrangement developed by Tasaki and his co-workers (24). Typically, two pairs of electrodes are implanted, one pair always in Turn 1 and the second pair in either Turn 2 or Turn 3. The potentials picked up by these electrodes contain either the CM alone or the CM, SP and AP, depending on the acoustic input to the ear. For measurement of the cochlear microphonic potential amplitude and phase with respect to the input sound pressure at the eardrum, the acoustic stimulus used is a continuous sinewave. For measurement of the magnitude and sign of the summating potential, trapezoidal tone bursts

of known duration and leading and trailing slopes are used. This latter type of stimulus is also the best for measurement of the AP.

To measure the acoustic input amplitude and phase, an acoustic probe is implanted immediately in front of the eardrum (see Section 6.3). When the input in an uninterrupted sinusoidal signal, this probe measures the SPL continuously and directly. However, when the input is a tone burst, the SPL is established by using a continuous tone of the same frequency and of peak amplitude equal to the maximum amplitude of the tone burst.

In a typical experiment, the CM amplitude and phase are measured in two turns of the cochlea using continuous sinewaves with 27 different frequencies (Table 6.1) at 50, 60, 70 and 80 db SPL. If the condition of the animal permits, the SP is measured next, using tone bursts of the same frequencies and intensities as used for the CM measurements. Although it is attempted to measure all the relevant parameters on one animal in every experiment, this is often impossible. Thus, while a full experiment may run as long as 8 hours without significant changes in the electrical signal of the cochlea the animal more often dies before the measurements are completed. In some exceptional cases the animal has been maintained long enough so that

two sets of CM measurements could be made and the changes due to the deterioration of the animal's general physiological state could be observed.

Table 6.1

List of frequencies used for CM and SP measurements in establishing the frequency response

kHz	kHz	kHz
.1	1.2	4.0
.2	1.4	5.0
.3	1.6	6.0
.4	1.8	7.0
.5	2.0	8.0
.6	2.2	9.0
.7	2.4	10.0
.8	2.6	
.9	2.8	
1.0	3.0	

6.2. Instrumentation and measuring techniques

The instrumentation for the experiments described in this chapter can be divided into two parts, the stimulus generating system and the measuring/recording system. The stimulus generating system is required to supply continuous and gated sinusoidal waveforms of any frequency in the audio range with controlled amplitude and phase. The measuring/recording system is designed for the on-line observation and permanent recording of the low level physiological signals originating in the auditory apparatus of the experimental animal.

6.2.1. The generation and control of the acoustic stimulus

The acoustic input to the experimental animal's ear is generated by the system shown in Fig.6.1. The Acoustic Pulse Generator *[1] produces sinusoidal bursts of controlled envelope shape. The audio frequency sinewaves originate in the Digital Oscillator (hp Model 4204A) which may be connected to bypass the Acoustic Pulse Generator to give ungated continuous output. The Digital Timing Unit* controls the length and repetition rate of the tone bursts and also

---

[1] Use of * indicates that the instrument has been designed (or modified) and built in the OTL Research Laboratories.

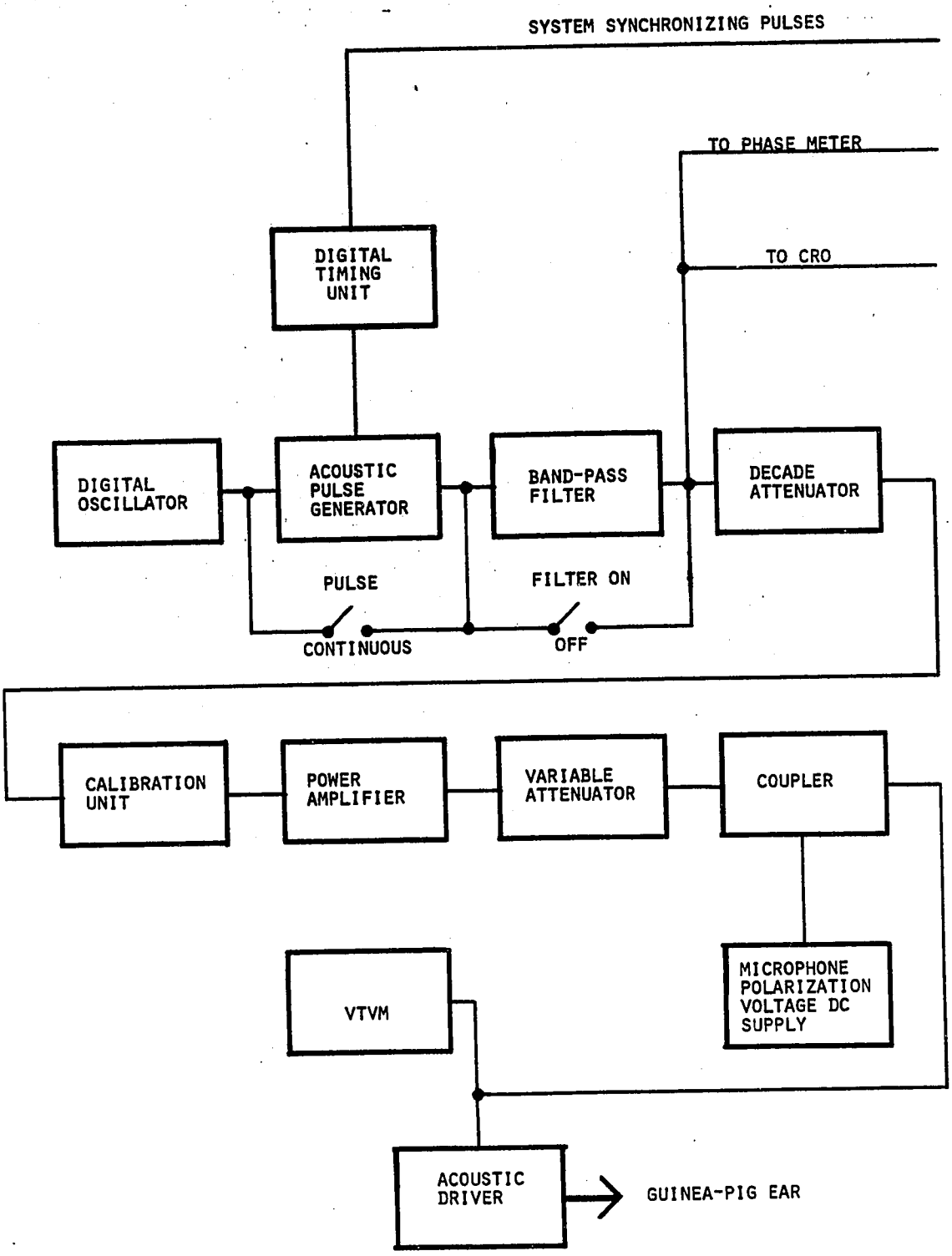

FIG.6.1. BLOCK DIAGRAM OF THE INSTRUMENTATION SYSTEM GENERATING AND CONTROLLING

produces the synchronizing signals used to trigger the oscilloscopes, timers and cameras. Switching transients in the system are eliminated by ensuring that gate operations occur only during waveform zero-crossing.

The Calibration Unit* is employed in presetting the gain of the frequency channels used so that the measured SPL is constant in front of the eardrum. Once this unit is set up for a given experiment the Decade Attenuators can be used to change the SPL by the same amount for all frequencies of interest. The output of the Power Amplifier (McIntosh 75, 70 V output) is coupled to the output of the High Impedance DC Supply* which provides the polarization voltage for the Acoustic Driver. The Acoustic Driver* consists of a Bruel and Kjaer 1" Condenser Microphone (Model 4132) mounted in a special low volume coupler which was designed to eliminate resonances in the acoustic system (Fig.6.2). For sound pressures in excess of 100 db SPL a University Model PA-HF Driver Unit is connected into the system. The VTVM is used to monitor the voltage which is necessary to achieve the desired SPLs at the eardrum. From these voltage measurements information can be derived regarding the performance and sensitivity of the middle ear.

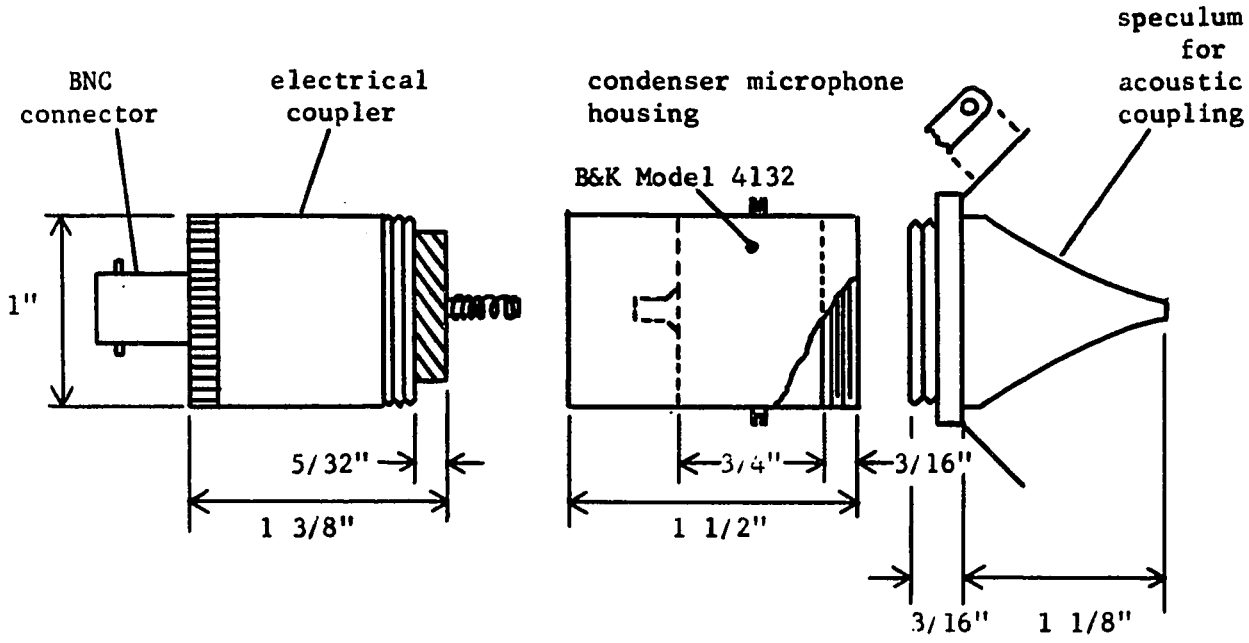

Fig.6.2 Acoustic driver unit, featuring a condenser microphone sound source and a closed acoustical system.

6.2.2. Measuring and recording instrumentation

Fig.6.3 shows the block diagram of the measuring system. The preamplifiers* are similar to those used by Tasaki (24) and are characterized by their low input noise (2 microvolts rms). These preamplifiers include a remote balancing arrangement which compensates for any slight misbalance of the electrodes. Further amplification of the signals is achieved by Modified* Grass Model 6 Amplifiers. Two hp Model 122A Oscilloscopes are used for direct observation of the responses and for photography with a Grass Kimograph Camera. The input to the oscilloscopes is controlled by attenuators and customarily the stimulus and the responses are displayed on four traces. The Narrow Band Frequency Analyzer (Bruel and Kjaer Model 2107) can be connected to any of the channels and used as a tunable audio-frequency voltmeter permitting direct reading of the continuous sinewave rms, average or peak levels at improved signal-to-noise ratios.

Accurate time measurements are made using a technique described by Laszlo and Gannon (74). This method uses the two channel Variable Delay Pulse Generator (Tektronix 160 Series) in order to place two movable time-markers on the oscilloscope trace. The 'distance' between the markers is measured in time units by the Electronic Timer (CMC Model 226B)

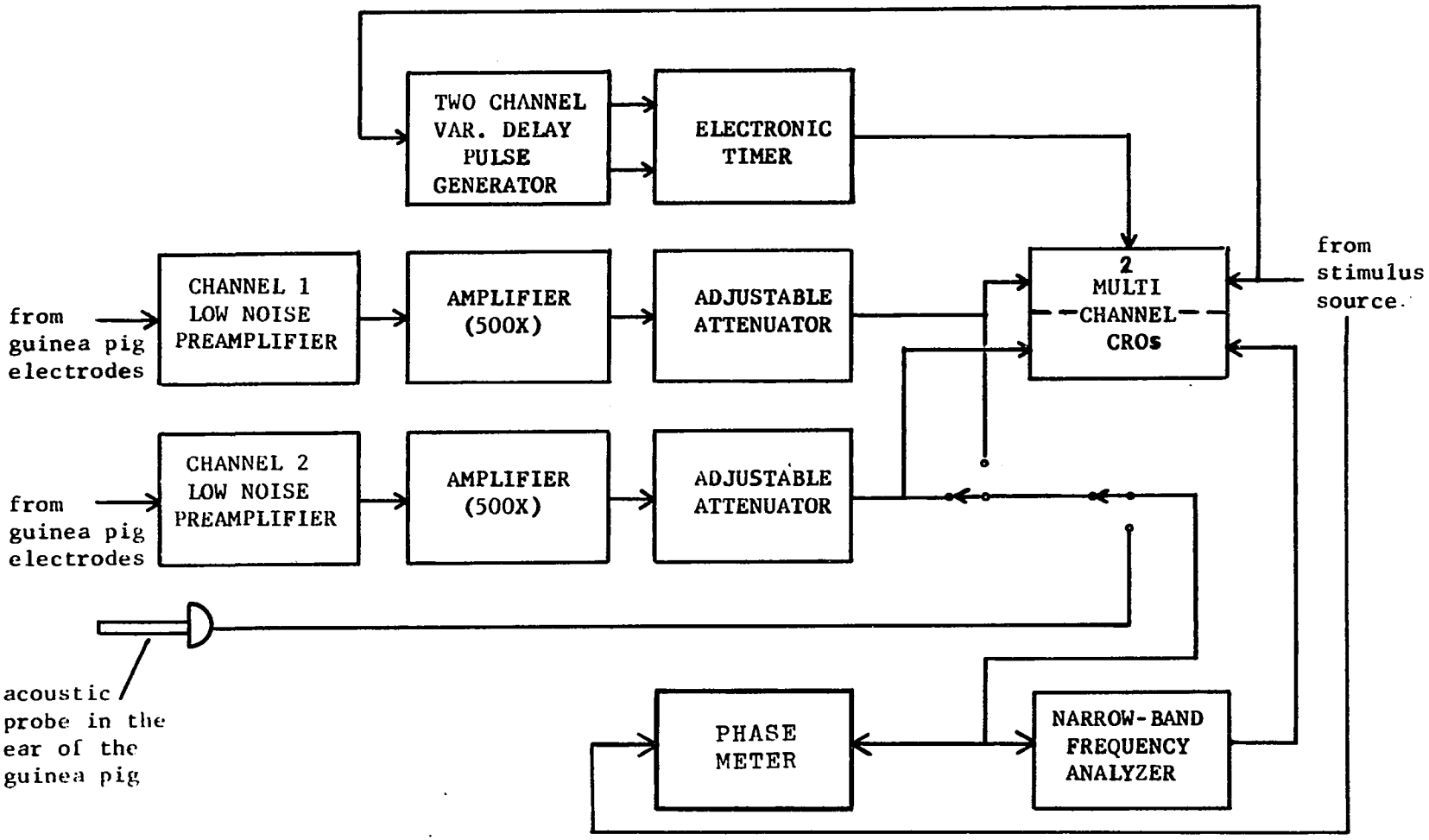

Fig.6.3 Block diagram of the measuring instrumentation.

and since the stimulus frequency is known this time datum can be reinterpreted in terms of phase. Phase measurements, however, are more expeditiously made by utilizing the Phase Meter (Phazor 210B) which will extract the phase information from extremely noisy signals.

The Acoustic Probe (Fig.6.4) has been developed by Dr. R.P. Gannon, Mr. D.H. Moscovitch and the author and is used with a 1/4" Bruel and Kjaer Model 4134 Condenser Microphone.

6.2.3. Calibration procedure

The calibration of the instrumentation is performed by measuring the amplitude and phase responses of the entire measuring and recording system. Neither the amplitude nor the phase calibration of the electronic instrumentation creates any problems. To calibrate the system a known sine or square wave input is applied to the preamplifiers and the necessary amplitude and time (phase) measurements are made on the oscilloscopes and other recording devices.

However, difficulties arise in the phase calibration of the acoustic probe, because in commercially available couplers the phase pattern is complicated and unknown although the rms sound pressure level is constant. Unless special attention is given to accurate phase calibration

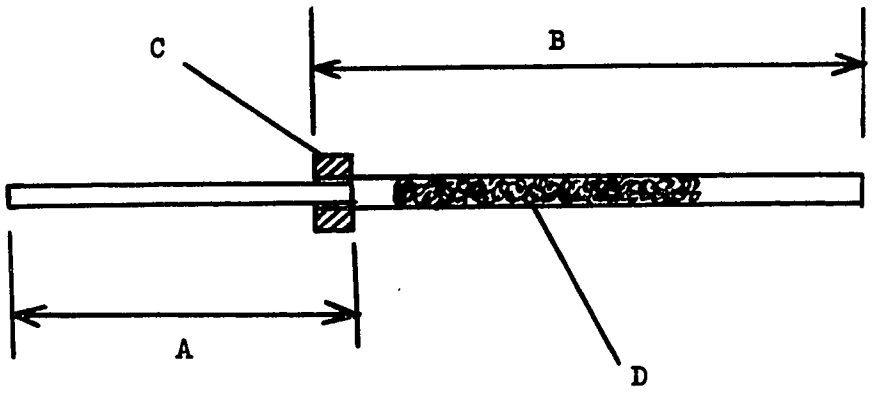

A - 15 mm, steel tubing 1 mm OD

B - 28-30 mm, PE 100 polyethylene tubing

C - ring made of PE 240 polyethylene tubing

D - approximately 15 mm long steel wool tuft for acoustic damping. Exact length is determined experimentally by adding small tufts of steel wool until all resonance peaks are eliminated.

Fig.6.4 The acoustic probe

then, as in the past, accurate representation of the eardrum-to-CM transfer characteristics remains impossible. Therefore, the phase calibration of the acoustic probes is carried out in a coupler designed by Dr.E.Shaw of the Applied Physics Section of the National Research Council. The calibration setup is shown in Fig.6.5. The design of the coupler ensures that only plane waves reach the end of the cavity where the probe and the control microphone are inserted. Since the probe tip is very close to and is exactly in front of the control microphone and since the two microphone-amplifier 'chains' are exactly the same, the phase difference recorded by the phase meter is entirely due to the probe tube. Typical calibration results are shown in Fig.6.6.

6.2.4. On the significance of accurate sound pressure measurement

In the foregoing we have repeatedly stated that the acoustic driver cannot be pre-calibrated in an acoustic coupler and then used in the ear on the assumption that the sound pressures generated will be equal. To prove this point quantitatively we compared the SPL measured in front of the eardrum and the SPLs measured in both a 2 cc and 1/2 cc acoustic coupler while keeping the voltage across the driver constant.

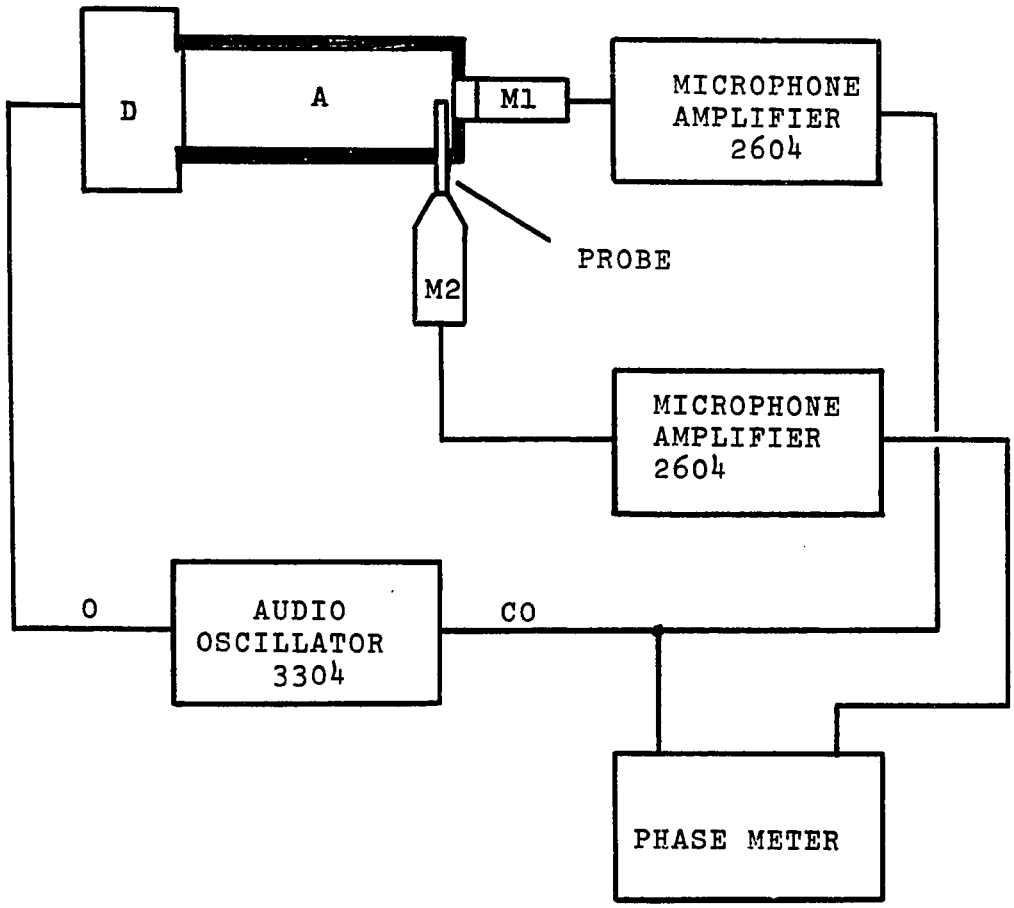

M1 - Control Microphone (B and K 4134)
M2 - Probe Microphone (B and K 4134)
A - Acoustic Coupler
D - Acoustic Driver
O - Output
CO - Compressor Output

Fig.6.5 Probe calibration instrumentation.

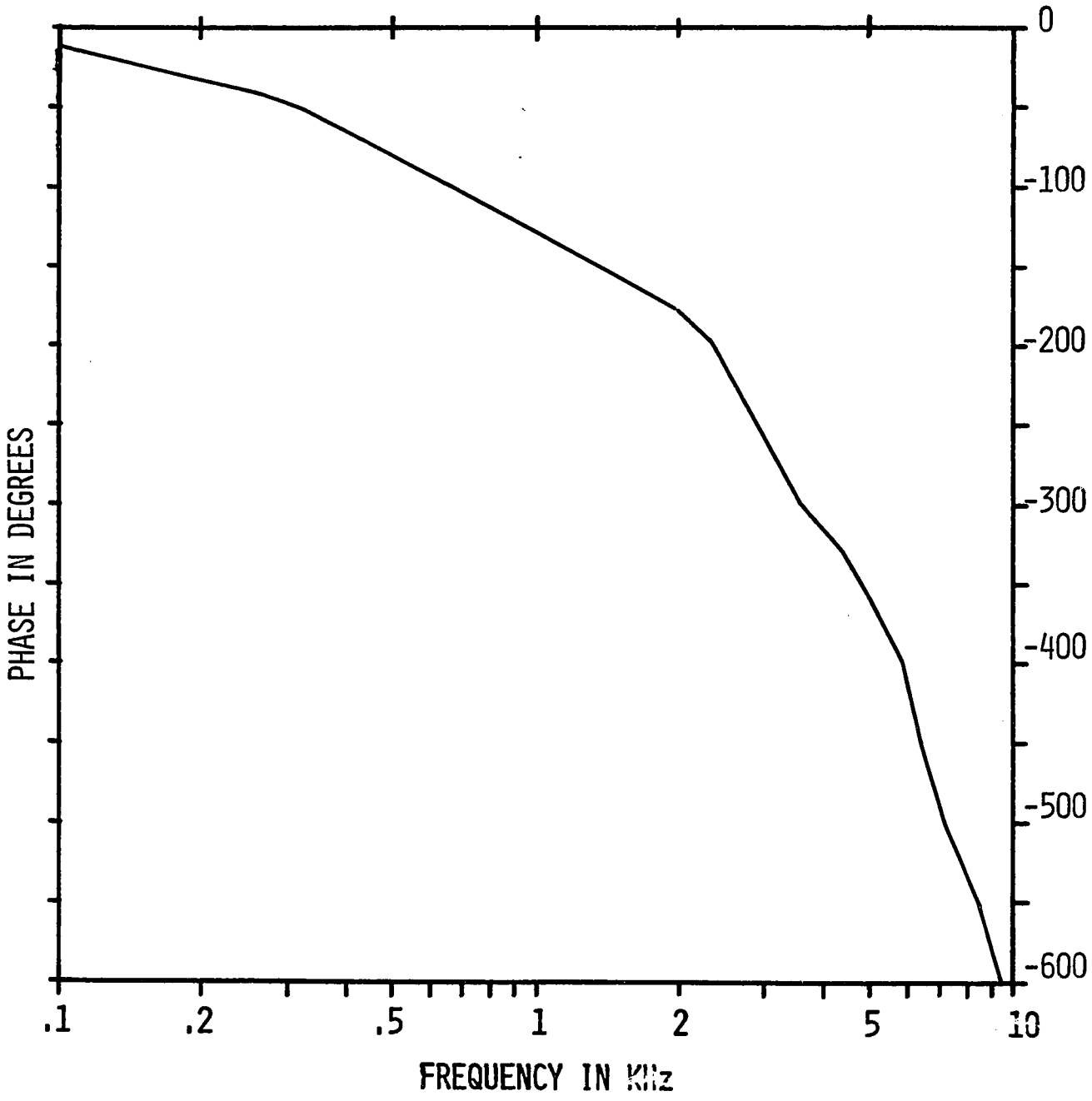

Fig.6.6 Typical phase calibration curve for the probe shown in Fig.6.5.

The experiment started with a normal guinea-pig preparation for CM and SP measurements. The SPL was monitored in front of the eardrum in the standard fashion with an implanted acoustic probe and the acoustic driver voltages necessary to maintain a constant SPL at all 27 frequencies (Table 6.1) were also measured. Next, the Driver Unit and the acoustic probe were removed from the animal and were introduced into a coupler mounted on a Sound Level Meter[1] (Fig.6.7). Then the same voltages were applied to the acoustic driver as when it was in the guinea-pig's ear, and the SPL was measured simultaneously with the Sound Level Meter and the acoustic probe. The results of Fig.6.8 show that the voltages across the driver which produce a constant SPL in the guinea-pig's ear produce SPLs varying over 30-35 db in the coupler. The reverse is also true, namely that when the voltage necessary to maintain the coupler SPL constant is applied to the Acoustic Driver while in the ear, the SPL will vary over a similar range, but in the opposite direction than shown.

Clearly, precalibration of the acoustic driver in a coupler is an inaccurate method and the input SPL (and phase) must always be determined by direct measurement in front of the eardrum.

---

[1] Bruel and Kjaer Type 2203

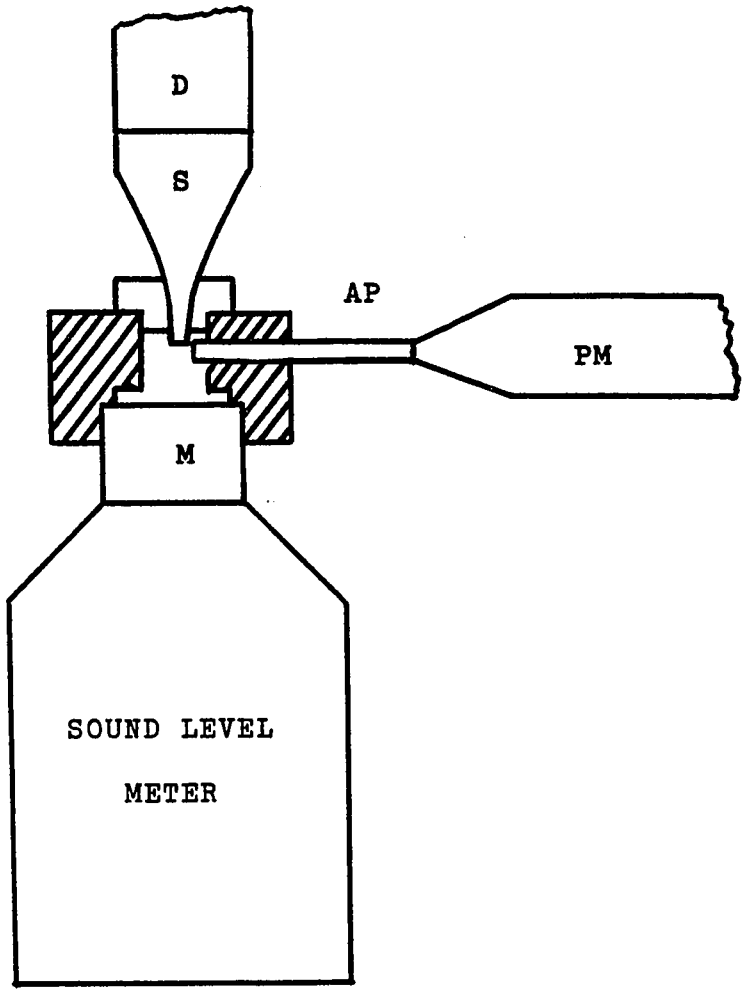

D - acoustic driver
S - speculum
AP - acoustic probe
M - 1" condenser microphone
PM - 1/2" probe microphone

Fig.6.7 Measurement of sound pressure level in a coupler to determine the accuracy of the coupler calibration of the acoustic driver.

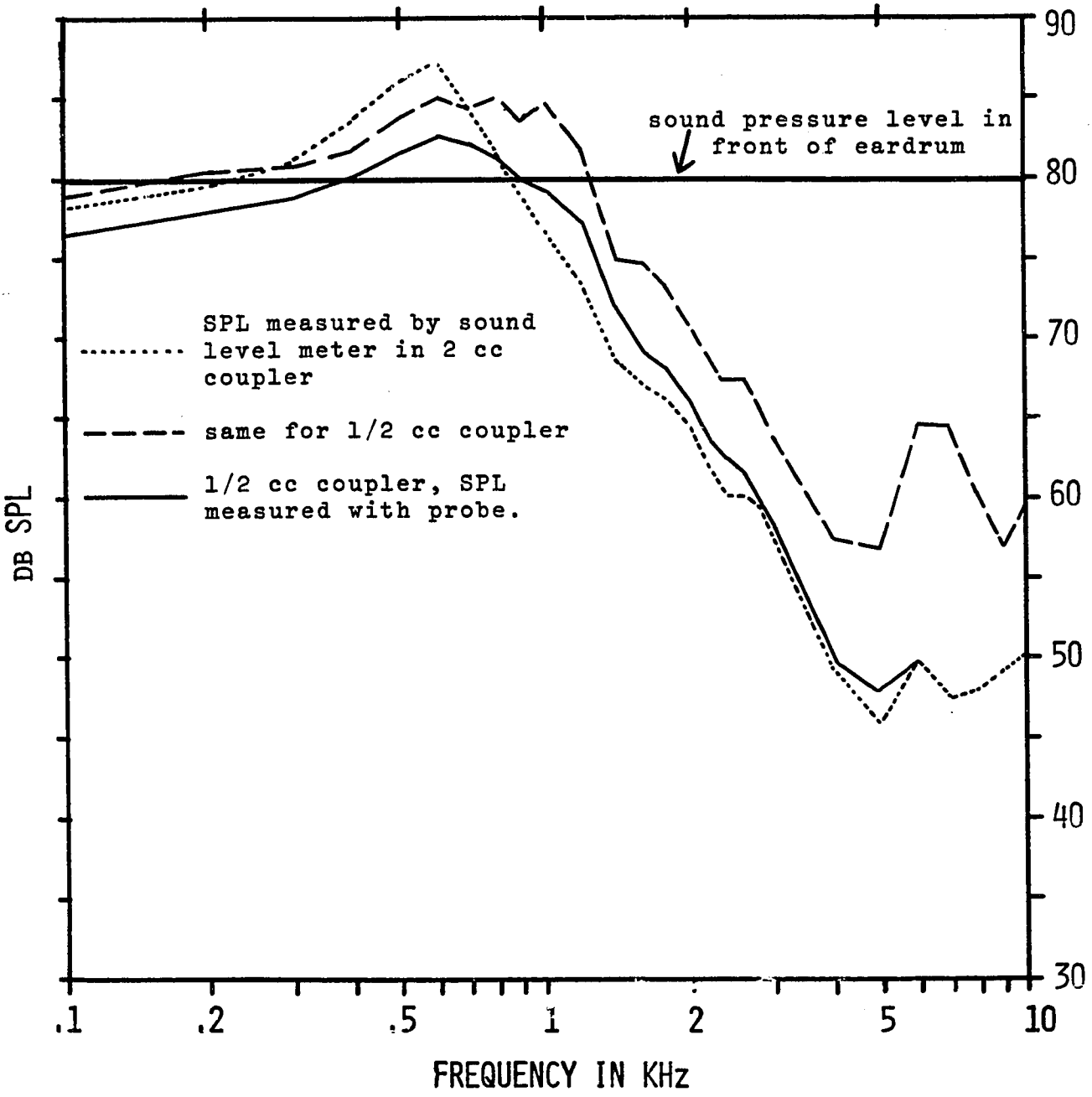

Fig.6.8 Comparison of the sound pressure levels (SPL) measured in front of the eardrum and in 1/2 cc and 2 cc acoustic couplers while keeping the voltage across the driver constant.at the value which gives constant SPL in front of the eardrum.

6.3. Surgical Procedure[1]

For this study guinea pigs weighing between 250 and 300 gms were anaesthetised with Dial (CIBA). The right bulla was exposed via a ventro-lateral approach and the bony wall of the bulla itself was opened widely so as to expose the ventral half of the tympanic ring. Then a hole was drilled through the wall of the bulla, just external to the tympanic ring, by using a small dental burr with cutting teeth perpendicular to the axis of rotation. To ensure that the diameter of the hole be the same as the outside diameter of the acoustic probe, a dummy probe was used to ensure a snug fit. Finally, the skin lining of the external canal was incised and pushed away from the hole so as not to interfere with the later insertion of the probe tube. On completing this stage of the operation the tympanic membrane was very carefully checked under forty-times magnification to ensure that no damage had occurred.

Next, the holes for the intracochlear electrodes were drilled in the appropriate turns and a conical plastic speculum, specially modified to screw onto the transducer, was sewn into the external canal. Attention was once more centered on the bulla and the acoustic probe tube to be used

---

[1]This section is based on a description by Dr.R.P. Gannon.

in the experiment for the measurement of the SPL was inserted in the hole prepared for it. Then intracochlear electrodes made from nicrome steel wire were inserted into the holes and laid against the edge of the opening in the bulla. After ensuring by visual inspection through the tympanic membrane that the tip of the probe was in a correct position immediately external to but not touching the ear-drum, the probe and electrodes were cemented into position with dental cement. To ensure a complete seal a thin mix of cement was run around the probe at the point of entrance to the hole drilled in the bulla and a slightly thicker mix of cement was run around the electrodes and the probe for mechanical support. Thus, after the cement had set both the electrodes and the probe were securely fastened to the bulla. Finally, a visual inspection was made once more to ensure that the probe tip as seen through the tympanic membrane was in the correct position.

A tracheotomy was performed in most cases in order to secure a completely free airway and to reduce the respiratory noise but artificial respiration was not found necessary. Whenever exceptionally quiet conditions were desired Flaxedil (Poulenc Ltée, 0.5 mg/kg) was injected to paralize the animal and a specially modified respirator was used to maintain the airflow.

6.4. The amplitude and phase of the cochlear microphonic potential as a function of frequency, SPL and electrode position

6.4.1. The amplitude of the cochlear microphonic potential

Due to variations between peak amplitudes and the corresponding frequencies observed in the three turns of the cochlea the individual results must be normalized before any comparisons are made. This normalization is always carried out with respect to both the peak amplitude measured and the corresponding frequency, that is, both are adjusted to be 1.0. Figs.6.9 to 6.12 show the resulting averaged and normalized CM curves together with the minimum and maximum curves in order to indicate the ranges of experimental variability.

In Fig.6.13 the normalized curves are reinterpreted into absolute terms. The actual average peak amplitudes and the corresponding average frequencies and their lower and upper limits are also plotted.(Fig.6.14).

The general feature of the curves shown in Figs.6.9 to 6.12 is the 'tuning-curve' shape similar to the cochlear partition displacement curves measured by Bekesy (Figs.2.5 and 2.6). It is also notable that the peak amplitude in Turn 1 (electrode location MRF ≈ 7000 Hz) never appears at frequencies higher than 2000 Hz, and usually at only half this value. This is in full agreement with model studies

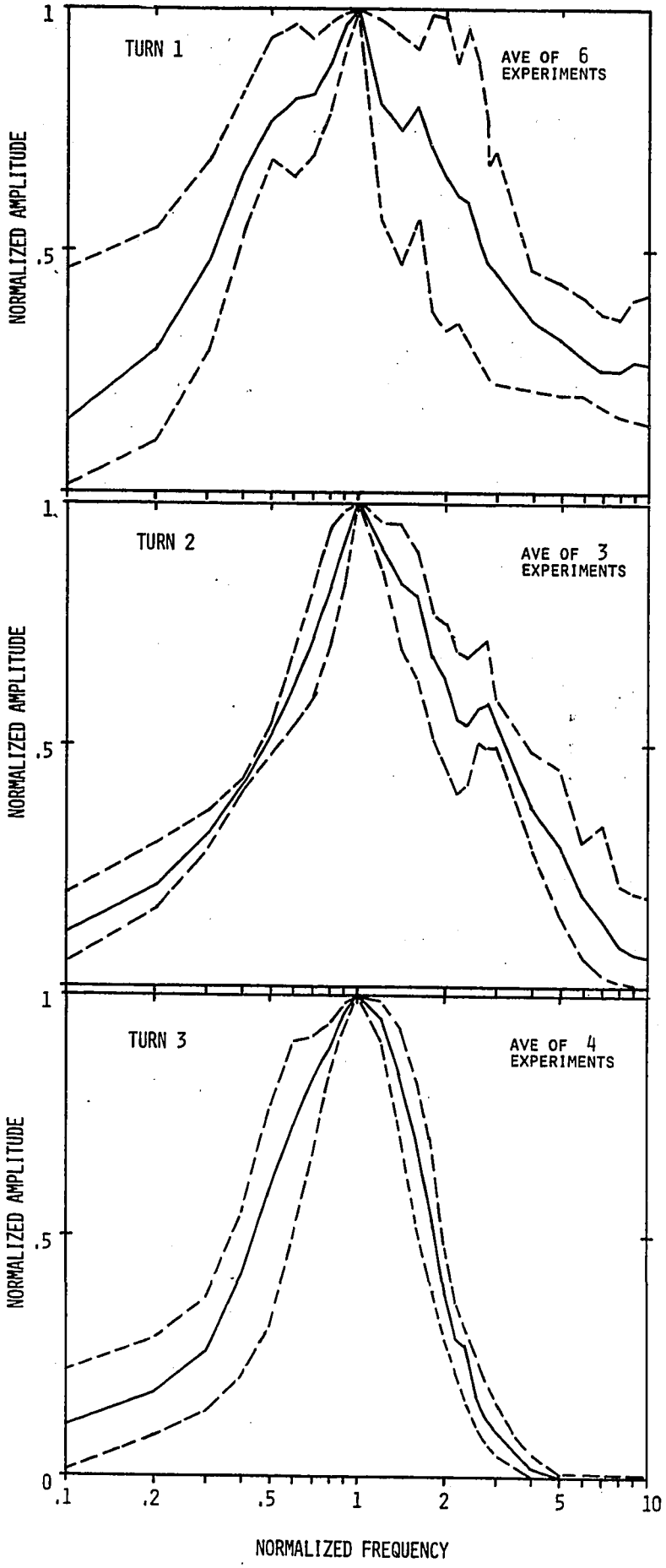

FIG.6.9 NORMALIZED AMPLITUDE OF THE COCHLEAR MICROPHONIC POTENTIAL AS A FUNCTION OF NORMALIZED FREQUENCY. DOTTED LINES REPRESENT MAXIMUM AND MINIMUM VALUES RESPECTIVELY.

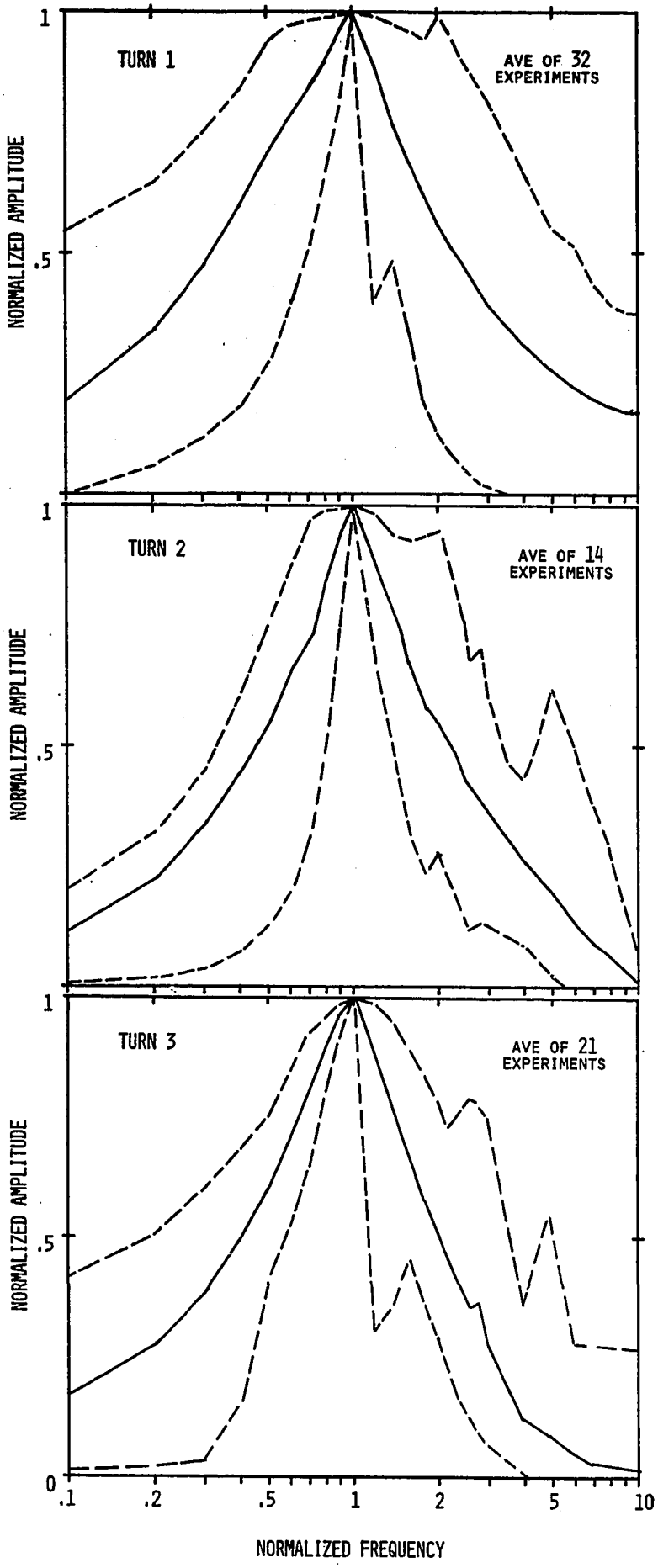
TURN 1
AVE OF 32 EXPERIMENTS
TURN 2
AVE OF 14 EXPERIMENTS
TURN 3
AVE OF 21 EXPERIMENTS
NORMALIZED AMPLITUDE
NORMALIZED AMPLITUDE
NORMALIZED AMPLITUDE
1
.5
1
.5
1
.5
0
.1
.2
.5
1
2
5
10
NORMALIZED FREQUENCY

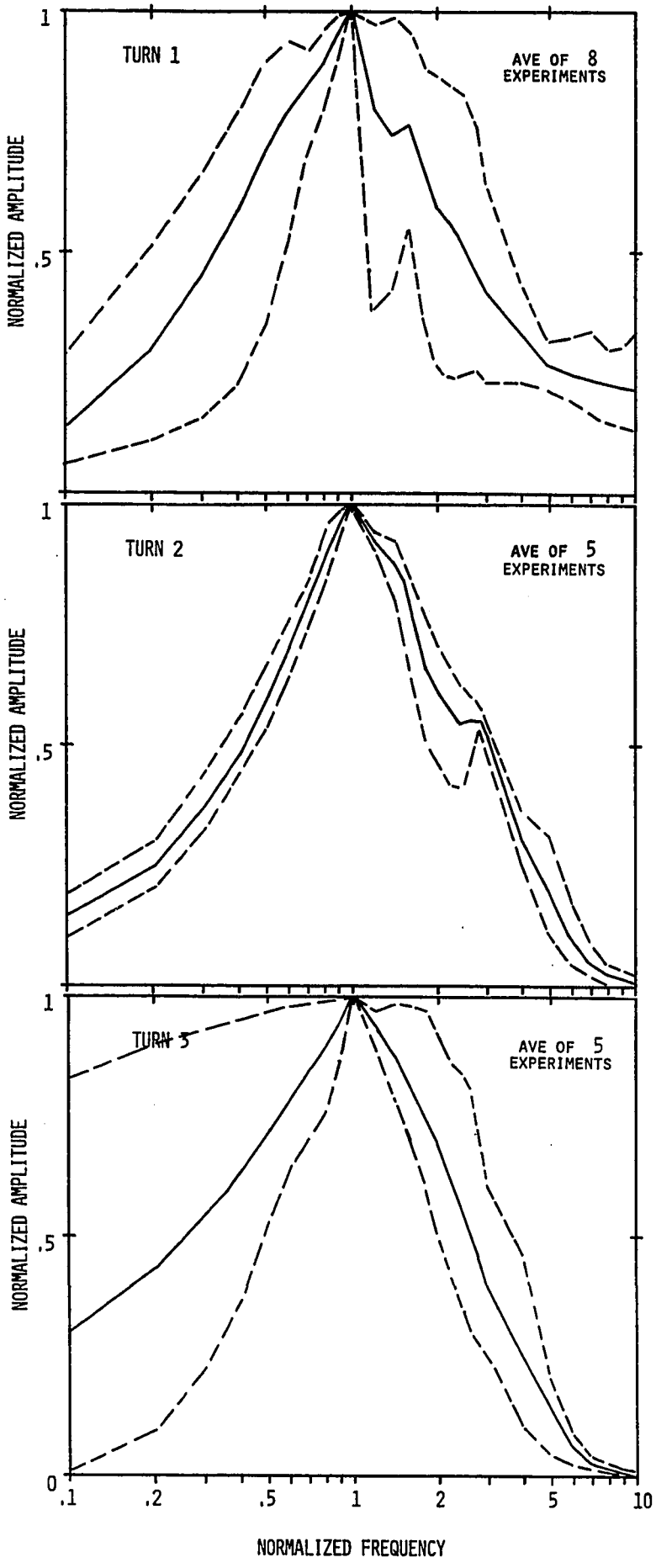
TURN 1
AVE OF 8 EXPERIMENTS
TURN 2
AVE OF 5 EXPERIMENTS
TURN 3
AVE OF 5 EXPERIMENTS
NORMALIZED AMPLITUDE
1
.5
0
.1
.2
.5
1
2
5
10
NORMALIZED FREQUENCY

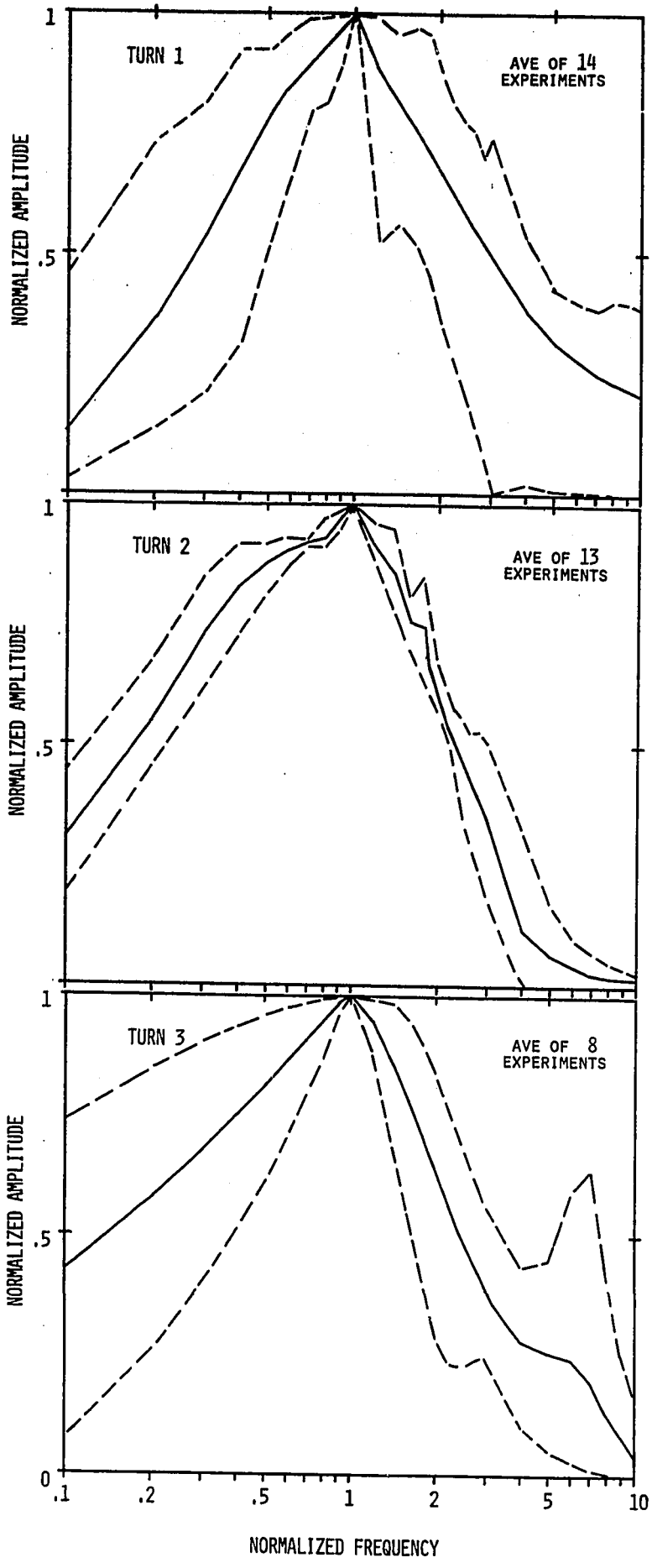
TURN 1
AVE OF 14 EXPERIMENTS
TURN 2
AVE OF 13 EXPERIMENTS
TURN 3
AVE OF 8 EXPERIMENTS
NORMALIZED AMPLITUDE
NORMALIZED AMPLITUDE
NORMALIZED AMPLITUDE
1
.5
0
1
.5
1
.5
.1
.2
.5
1
2
5
10
NORMALIZED FREQUENCY

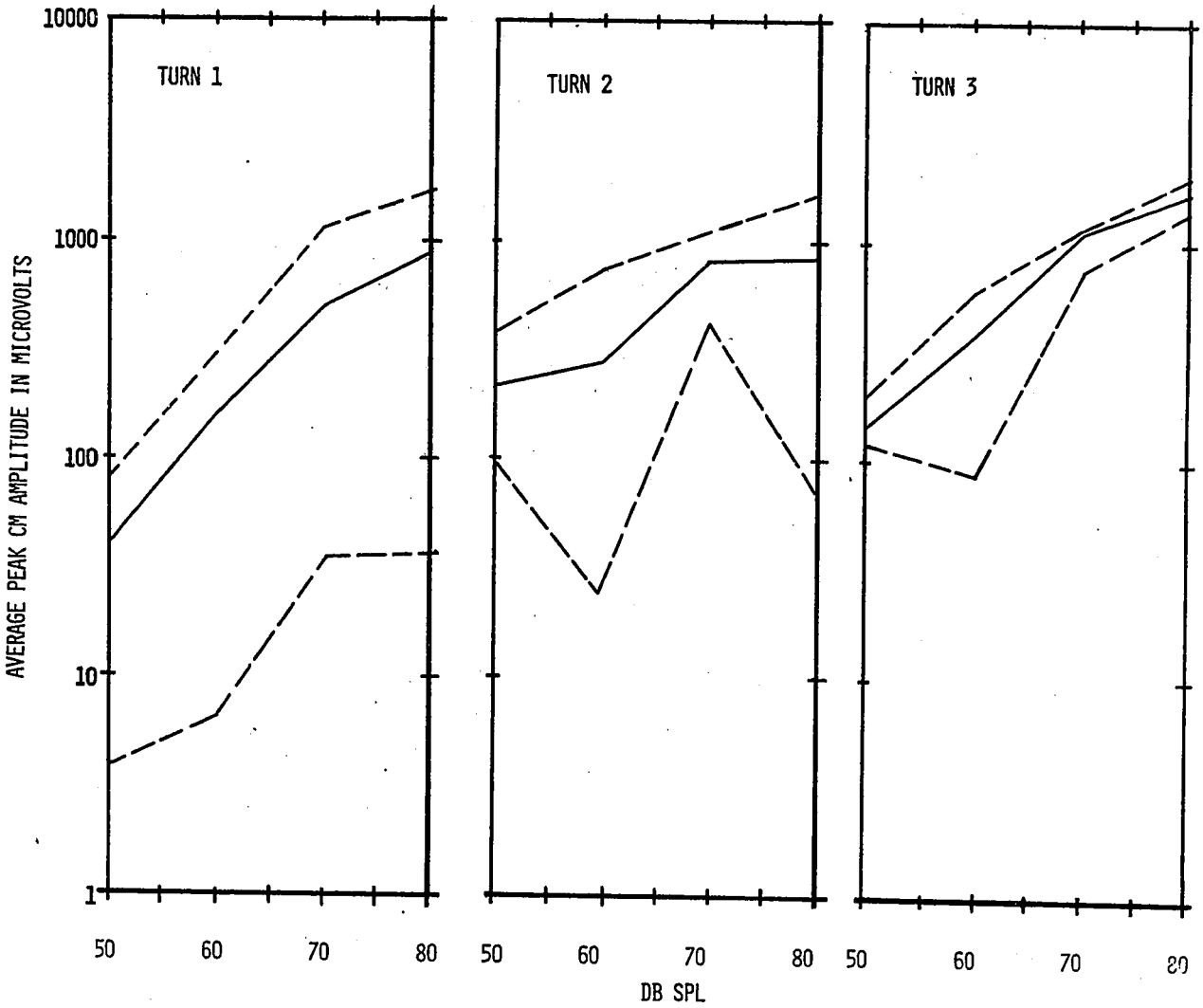

FIG.6.13 AVERAGE PEAK COCHLEAR MICROPHONIC POTENTIAL AMPLITUDES AS FUNCTIONS OF SOUND PRESSURE LEVEL.

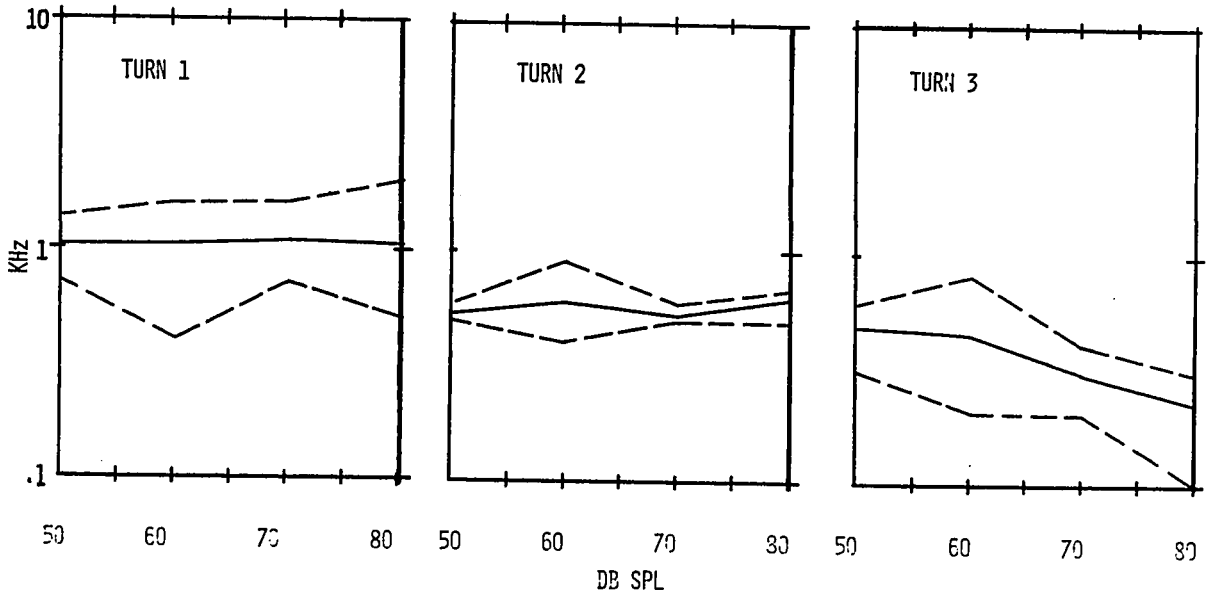

FIG.6.14 FREQUENCY OF PEAK COCHLEAR MICROPHONIC POTENTIAL AMPLITUDES AS A FUNCTION OF SOUND PRESSURE LEVEL.

(Chapter 7) which indicate similar behaviour for the combined middle ear and basilar membrane response. Turn 2 (electrode MRF ≃ 2000 Hz) and Turn 3 (electrode MRF ≃ 700 Hz) results are also consistent in this respect.

Bekesy has observed that the position of maximum displacement of the basilar membrane changes as a function of sound intensity (14) because the pattern of vibration is displaced towards the apex of the cochlea. When the frequencies corresponding to the maximum CMs measured are plotted as a function of SPL, Fig.6.14, then Turn-3 data show this phenomenon quite clearly, although Turn-1 and Turn-2 average results are not consistent. Individual measurements, however, do show this movement of the vibration pattern for all three turns of the cochlea (see for example Figs.6.23-6.26).

The average normalized amplitude curves also show that as we take our measurements of the CM for Turn 1 to Turn 3 the curves become progressively narrower, at least at 50 and 60 db SPL. Also, if we compare the curves recorded at different SPLs from the same turn it can be seen that for Turn 2 and Turn 3 the curves become broader as the SPL increases, but for Turn 1 the changes are not consistent.

6.4.2. The phase of the cochlear microphonic potential

Since phase data recorded from individual experiments show that the phase response varies little with the SPL (Figs.6.15 to 6.17), average CM phase responses as a function of frequency for 60 db SPL (Fig.6.18) are representative of the CM phase for sound pressure levels up to 80 db. The repetition of the phase measurements at different sound pressure levels in all experiments is thus unnecessary, which is fortunate since the combined CM amplitude and phase measuring procedure is so time consuming that measurements of the summating potential cannot be taken before the animal's physiological condition deteriorates.

The most notable feature of the phase curves shown is that the phase response recorded from Turn-1 electrodes is relatively 'flat' while Turn-2 and Turn-3 responses display steeply increasing phase lag. This we interpret to be the result of the interference between the outputs of the individual CM generators; specifically, in Turn 1 where the interference is the greatest the phase change is relatively small, whereas in Turn 2 and Turn 3 where large numbers of haircells are excited in phase the gross CM phase clearly reflects the travelling wave characteristics of the mechanical motion of the basilar membrane.

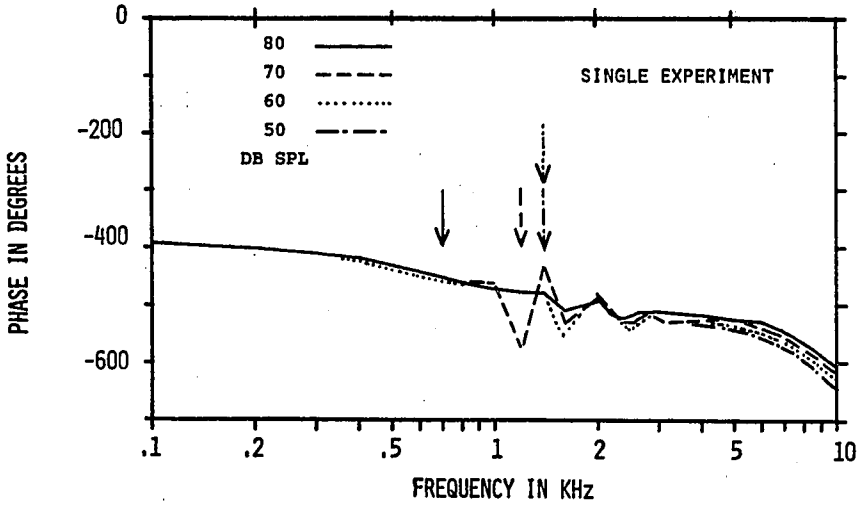

FIG.6.15 COCHLEAR MICROPHONIC PHASE MEASURED IN TURN 1. THE ARROWS INDICATE THE FREQUENCY AT WHICH THE AMPLITUDE RESPONSE MAXIMUM APPEARS AT THE DIFFERENT SOUND PRESSURE LEVELS.

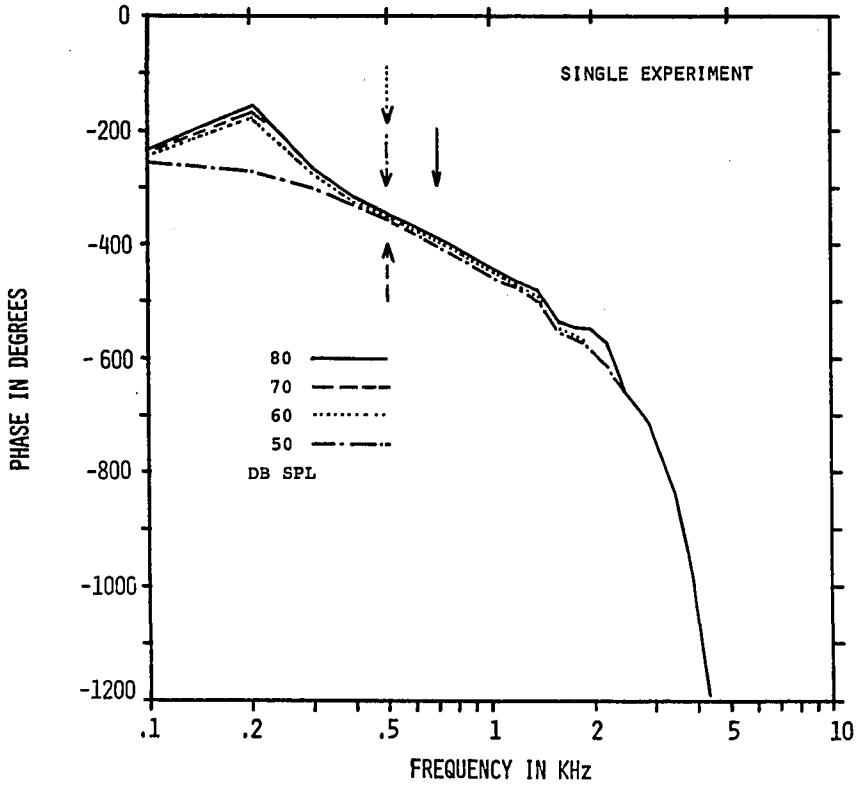

FIG.6.16 COCHLEAR MICROPHONIC PHASE MEASURED IN TURN 2. THE ARROWS INDICATE THE FREQUENCY AT WHICH THE AMPLITUDE RESPONSE MAXIMUM APPEARS AT THE DIFFERENT SOUND PRESSURE LEVELS.

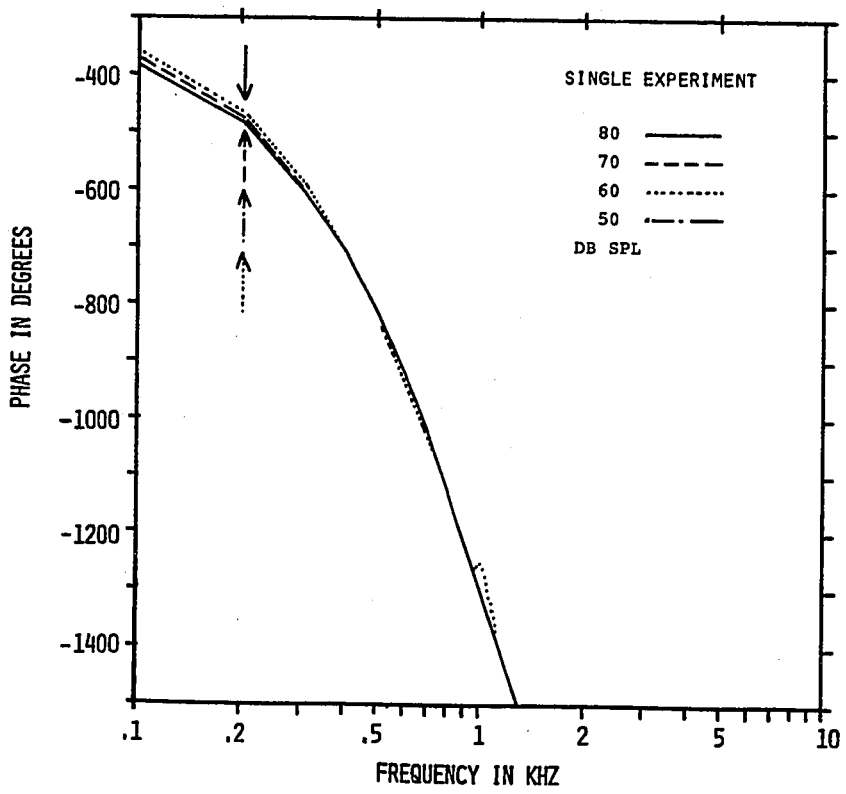

FIG.6.17 COCHLEAR MICROPHONIC PHASE MEASURED IN TURN 3. THE ARROWS INDICATE THE FREQUENCY AT WHICH THE AMPLITUDE RESPONSE MAXIMUM APPEARS AT THE DIFFERENT SOUND PRESSURE LEVELS.

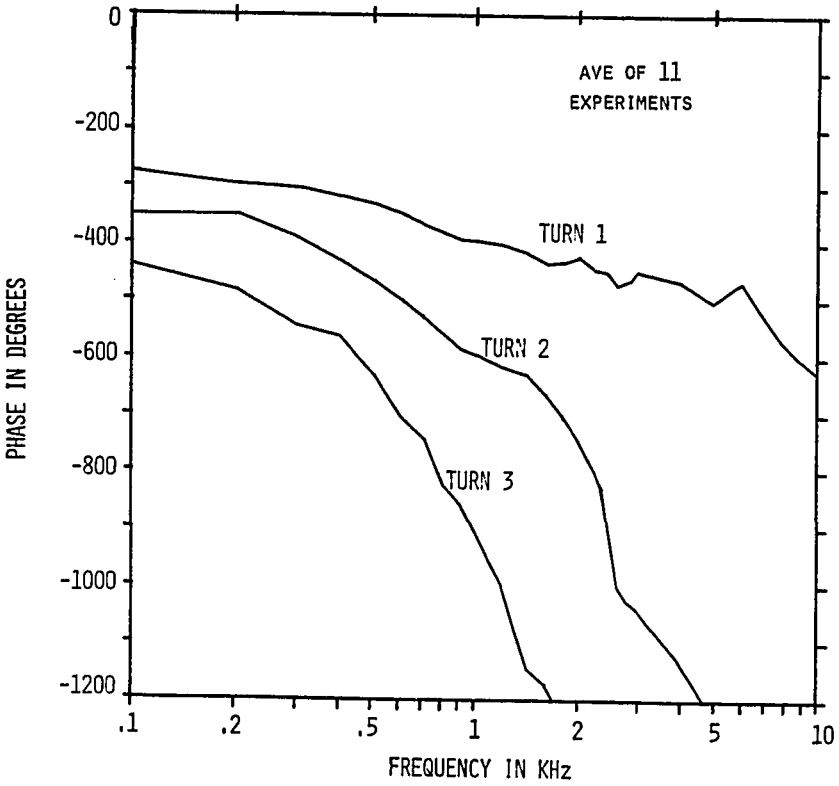

FIG.6.18 AVERAGE COCHLEAR MICROPHONIC PHASE AT 60 DB SPL MEASURED IN TURN 1, TURN 2, AND TURN 3 OF THE COCHLEA.

We have mentioned previously that Bekesy found a change in the basilar membrane displacement pattern as a function of sound intensity. His description of this observation can be used to describe the phase response curves of Figs.6.15 to 6.17 as well: "It appears that with increasing amplitude the phase difference between the stapes and the point of measurement steadily decreases..." (14). Although Bekesy observed the phase shift of the basilar membrane response pattern only at SPLs above the threshold of feeling in normal hearing, the phase response curves already show phase shift at moderate SPLs. It is interesting to note that the significant phase shifts appear in Turn 1 for high, in Turn 2 for medium and in Turn 3 for low frequency sounds.

6.4.3. The effect of middle ear infection on the frequency response curves

In some experiments traces of middle ear infection were found during surgery. While most of these preparations were discarded some of them were used to find the amplitude and phase response changes which may be expected due to the diseased middle ear. In Fig.6.19 the CM amplitude and phase curves are shown for an ear in which there were signs of past middle ear infection. The irregularities between 1000 and 2000 Hz are observable on both the amplitude and the phase curves. In some other experiments the amplitude

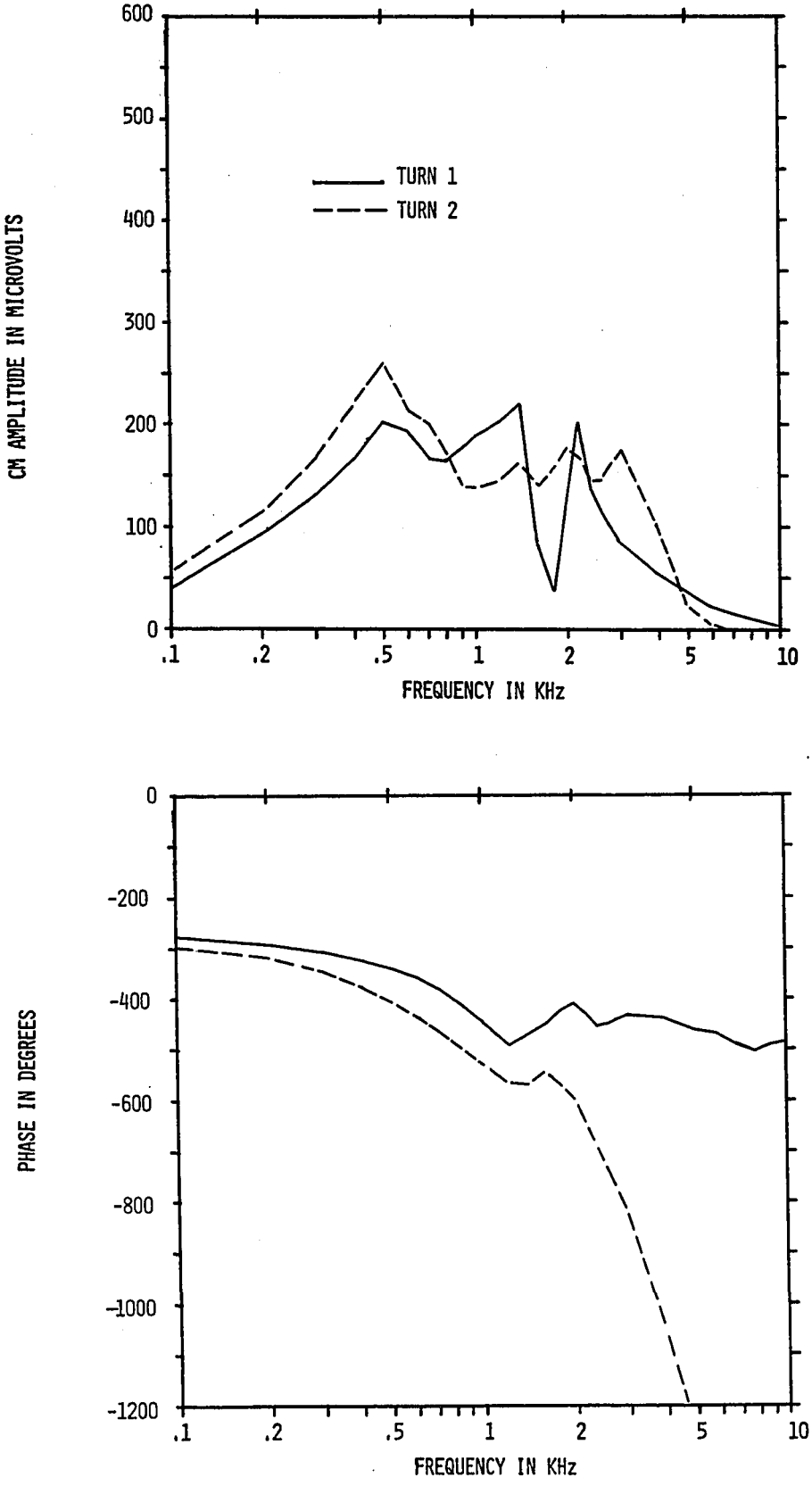

FIG.6.19 THE EFFECT OF MIDDLE EAR INFECTION ON THE AMPLITUDE AND PHASE RESPONSES MEASURED IN TURN 1 AND TURN 2 AT 70 DB SPL.

irregularities were found to be more pronounced, but unfortunately no phase observations were made in those cases.

6.4.4. Notes on high frequency CM potentials measured in the third turn of the cochlea

It is well known from experimental practice that unbalanced differential electrodes will record common mode signals originating at relatively remote locations. It is not known, however, how much CM potential is due to remote 'pickup' by well balanced electrodes. This is of particular interest for Turn-3 electrodes because measurable high frequency CM potentials appear across these when the sound pressure levels are over 80 db SPL although for high frequencies Turn-3 basilar membrane displacements are very small.

To investigate the remote electrical 'pickup' of high frequency CM by third turn electrodes we selected pairs of guinea pigs, one of which was injected with an ototoxic drug (neomycin) some weeks previously, while the other was not. Cochlear damage was assessed post-operatively with the help of 'cochleograms' which were obtained by microscopic examination of the upper surface of the organ of Corti (Fig.6.20). The cochleogram of the cochlea of the injected animal shows complete destruction of haircells in the first turn, while the other cochleogram shows an essentially normal cochlea although some damage is apparent.

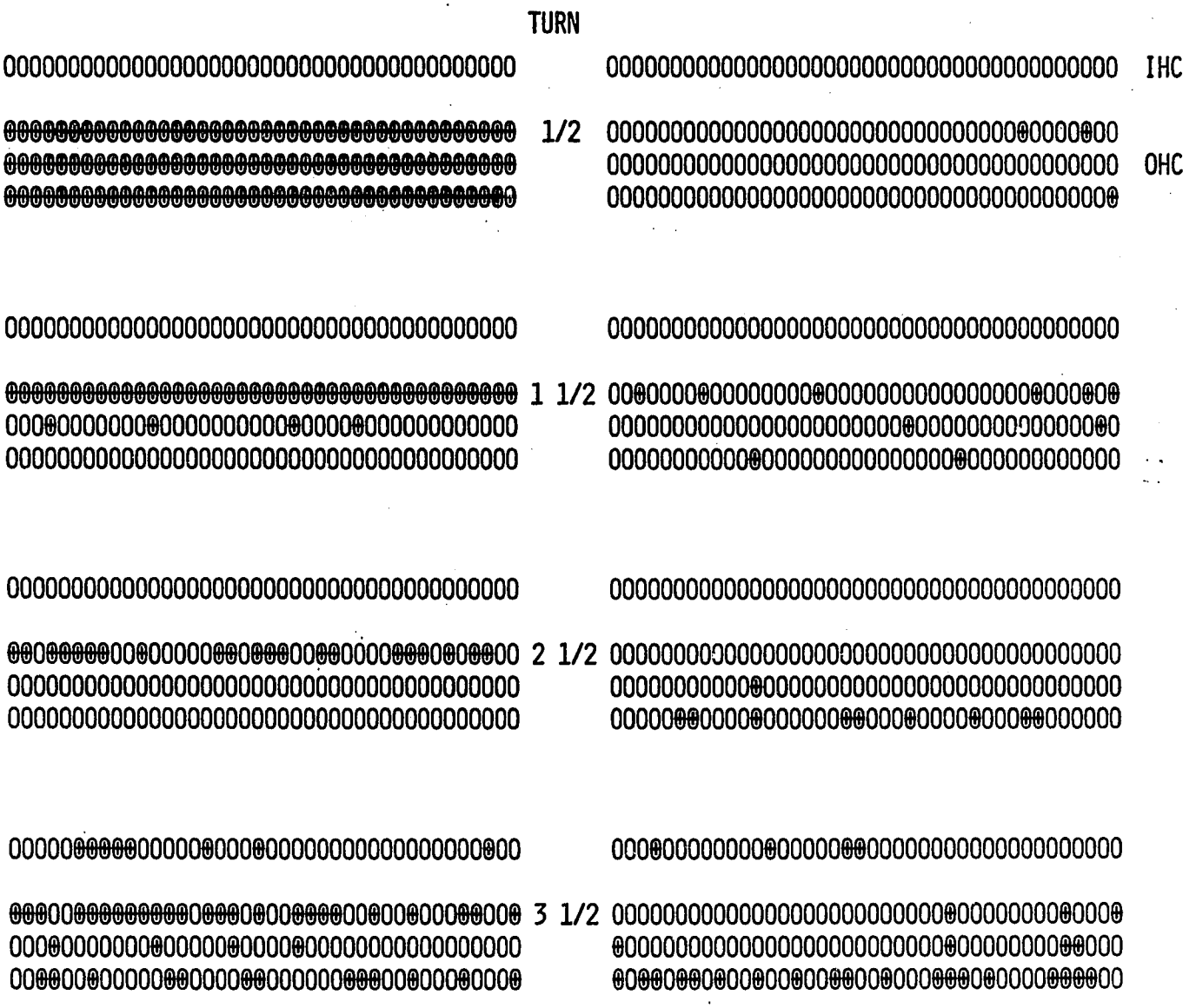

(A) NEOMYCIN INJECTED COCHLEA

(B) NORMAL COCHLEA

A comparison of the CM measurements taken at 80 db SPL shows that the third turn voltages at low frequencies are essentially the same for both animals (Fig.6.21). In the cochlea damaged in the first turn or so, however, there is no response in the third turn to stimulus frequencies higher than 1200 Hz, while the response from the same turn of the normal animal extends to 10000 Hz and beyond. The first turn responses are also very different. The damaged cochlea shows very small CM potentials at any frequency while the response of the normal animal is about average.

These observations indicate that third turn responses observed for frequencies above 2 kHz are probably remote electrical events picked up from the first and second turns.

6.5. The summating potential as a function of electrode location, SPL and frequency

The measurement of the summating potential is much more difficult than that of the cochlear microphonic potential. It is difficult to record consistent data because variations in the physiological state of the animal and spontaneous muscle activity can cause drastic changes in the SP values measured from moment to moment and even greater changes from one experimental preparation to another. Also, even slight imbalance of the differential electrodes seems to change the frequency response pattern of the summating potential, especially in Turns 2 and 3.

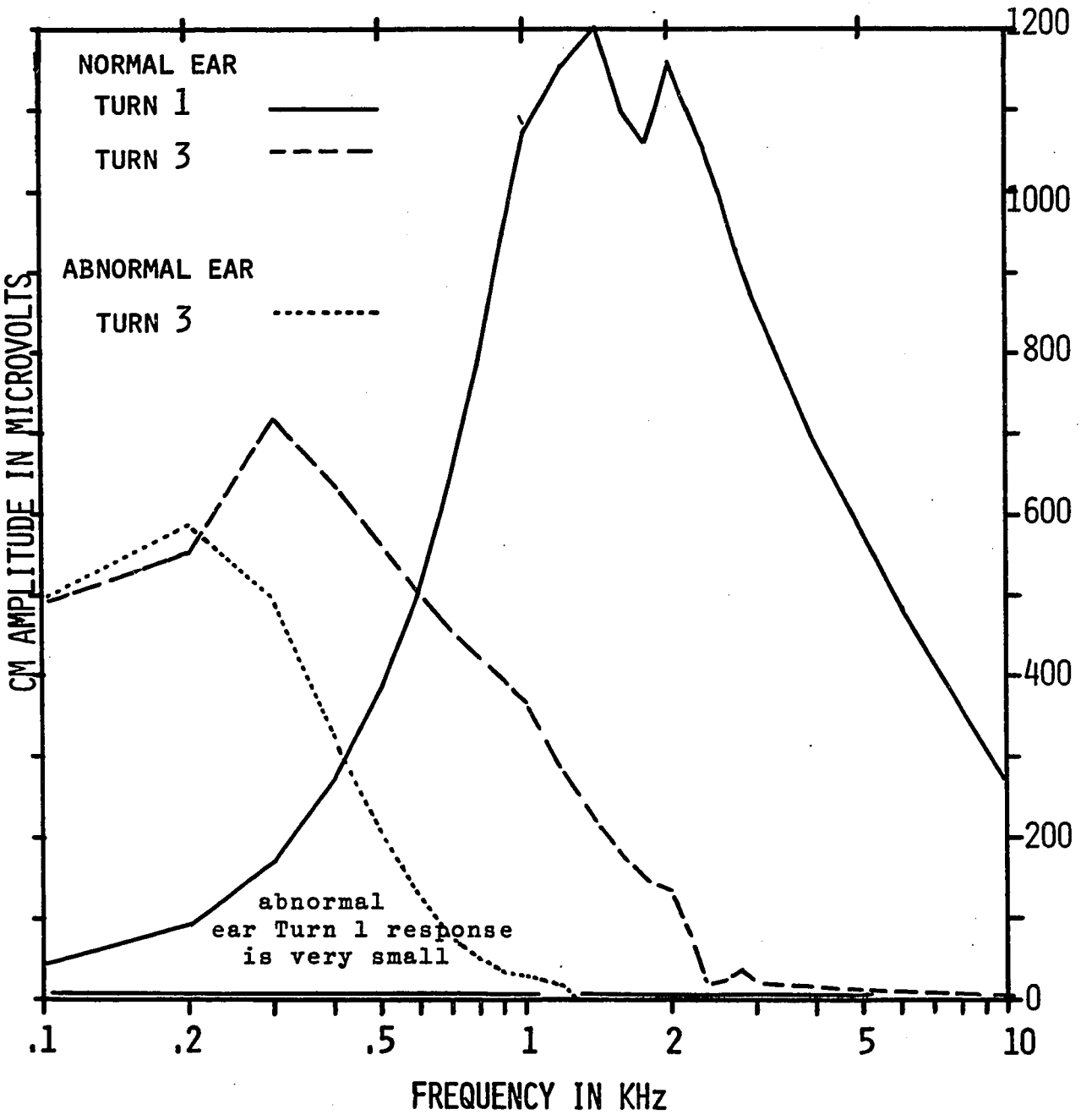

Fig.6.21 Comparison of the cochlear microphonic potential amplitude measured in Turn 1 and Turn 3 in normal and neomycin-damaged cochlea. The sound pressure level = 80 db.

The evaluation of the summating potential also causes difficulties. Thus to obtain the SP it is necessary to use tone burst stimuli of several msec duration, then to photograph the resulting cochlear potential waveform (see Fig.3.2) and measure the waveform shifts with respect to the base line on the enlarged film. At any given frequency and SPL only a small number of waveforms can be photographed, usually three non-consecutive responses 6-10 seconds apart. Often all three of these responses are similar, but sometimes the consecutive photographs seem to bear no relationship to each other.

The calculation of average SP values is possible only for Turn 1 (Fig.6.22) because the responses recorded for this turn show much greater consistency than potentials obtained from either Turn 2 or Turn 3.

Some preparations have shown excellent stability and good balancing of the electrodes was also possible. In such experiments the measurements were repeatedly reproducible, and hence the results are probably more representative of the physiological processes producing the SP than the SP averaged over a widely scattered set of data points.

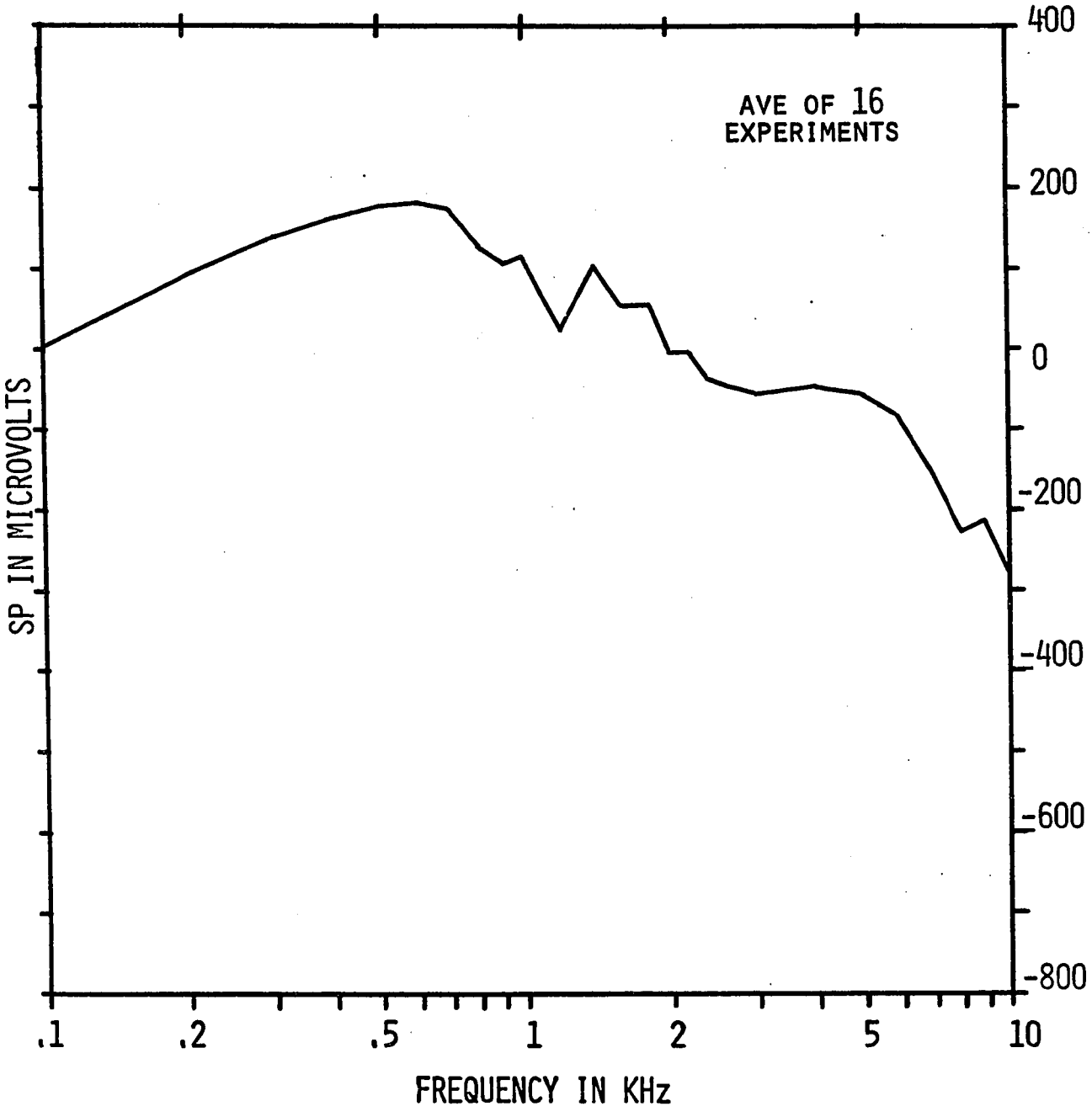

Fig.6.22 Average summating potential measured in Turn 1 at 80 db SPL.

In Figs.6.23 to 6.26 the summating potentials measured in individual experiments as a function of frequency, electrode location and sound pressure level are shown. The cochlear microphonic response data are also included, because the relation between the CM and SP frequency response curves will be important if the SP is a distortion product of the CM.

The SP vs frequency curves show, in general, the great sensitivity and variability of the SP. It is also noticable that the SP is a non-linear function of the sound intensity everywhere in the frequency range covered. The most interesting feature of the SP plot, however, is that there appears to be a correlation between the location of the peak of the CM responses and the sign of the SP. This can be quite clearly seen in Turns 2 and 3 but in Turn 1 SP negativity seems to be correlated with the Turn 1 MRFs (3-10 kHz).

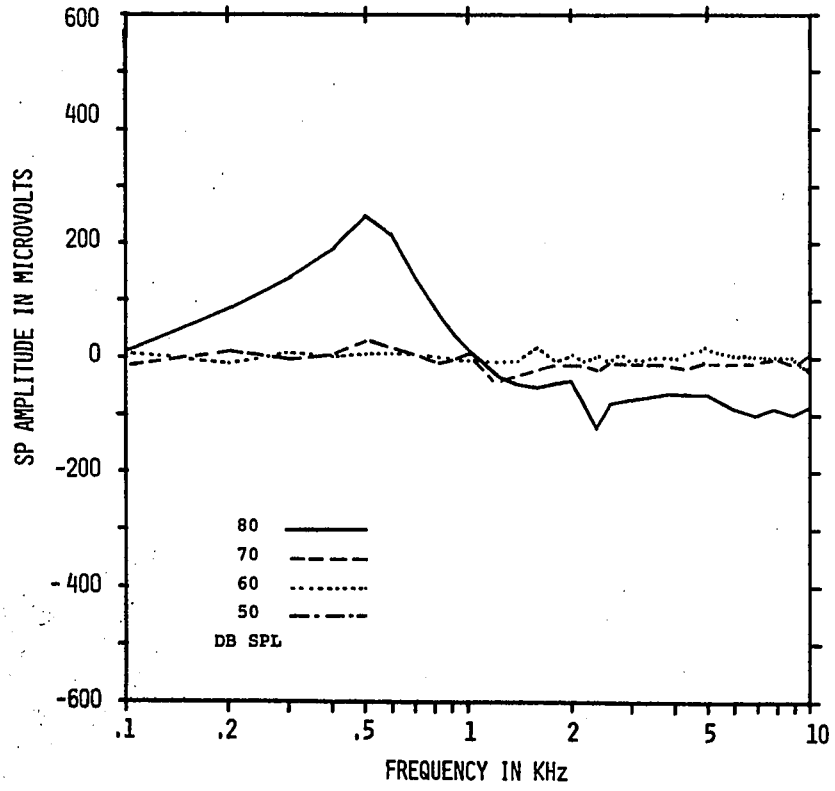

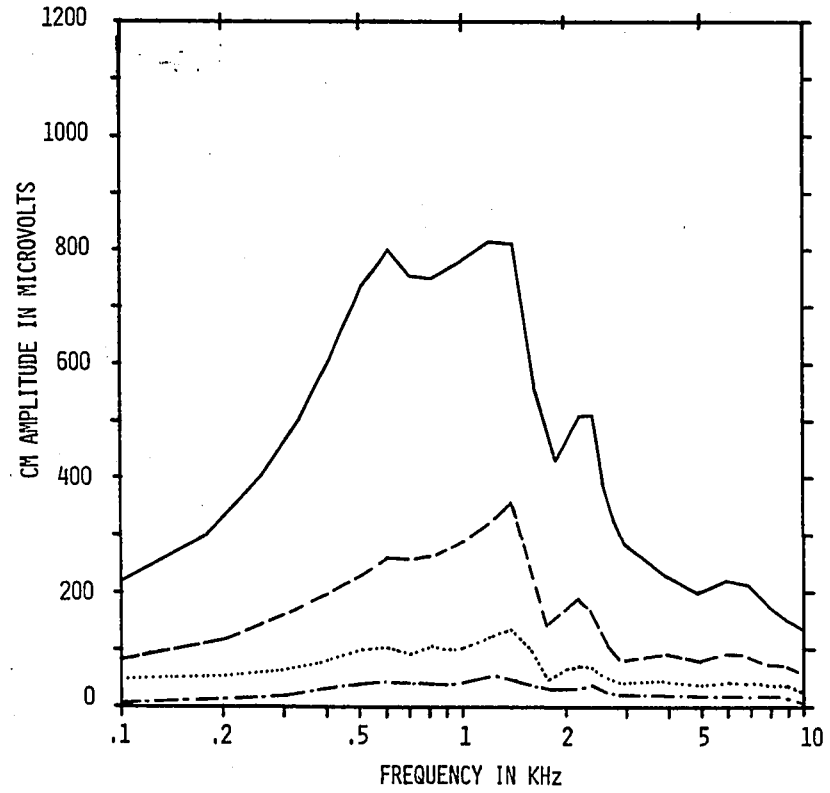

FIG.6.23 THE SUMMATING POTENTIAL AND THE COCHLEAR MICROPHONIC POTENTIAL MEASURED IN TURN 1 AT 50, 60, 70 AND 80 DB SPLs. SINGLE EXPERIMENT: GP 31/67.

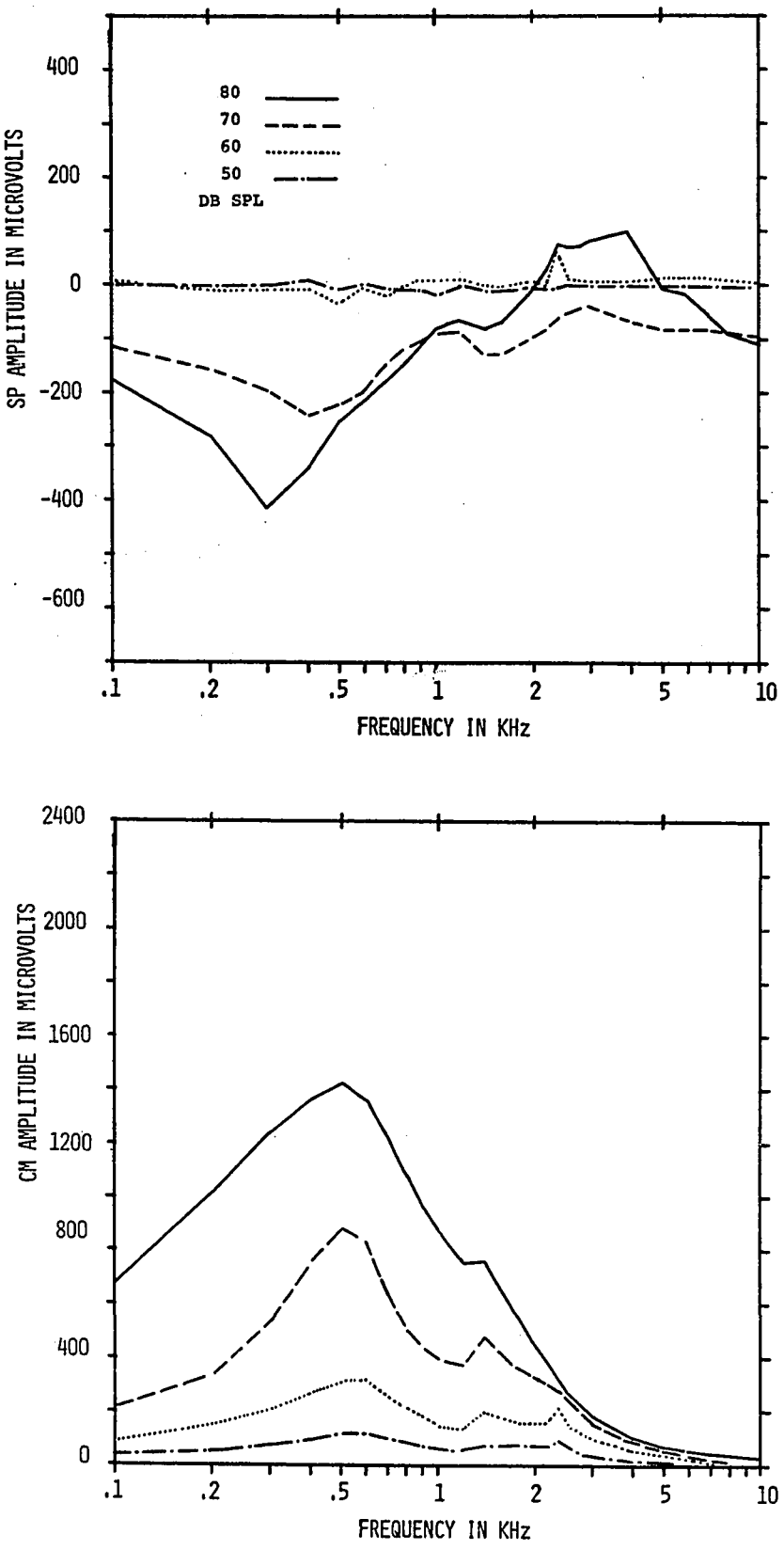

FIG.6.24 THE SUMMATING POTENTIAL AND THE COCHLEAR MICROPHONIC POTENTIAL MEASURED IN TURN 2 AT 50, 60, 70 AND 80 DB SPLs. SINGLE EXPERIMENT: GP 31/67.

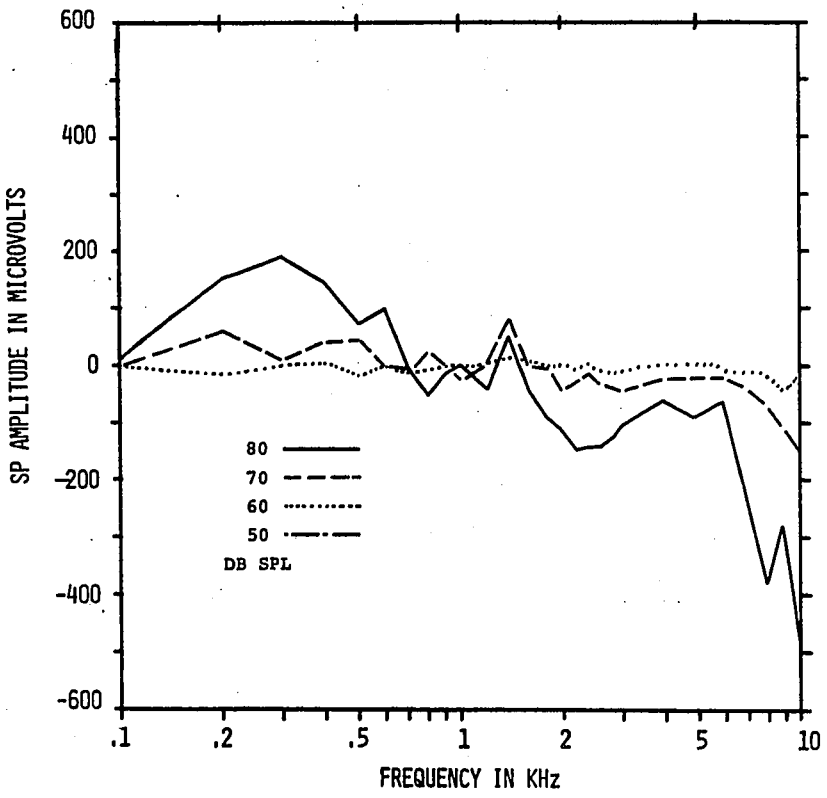

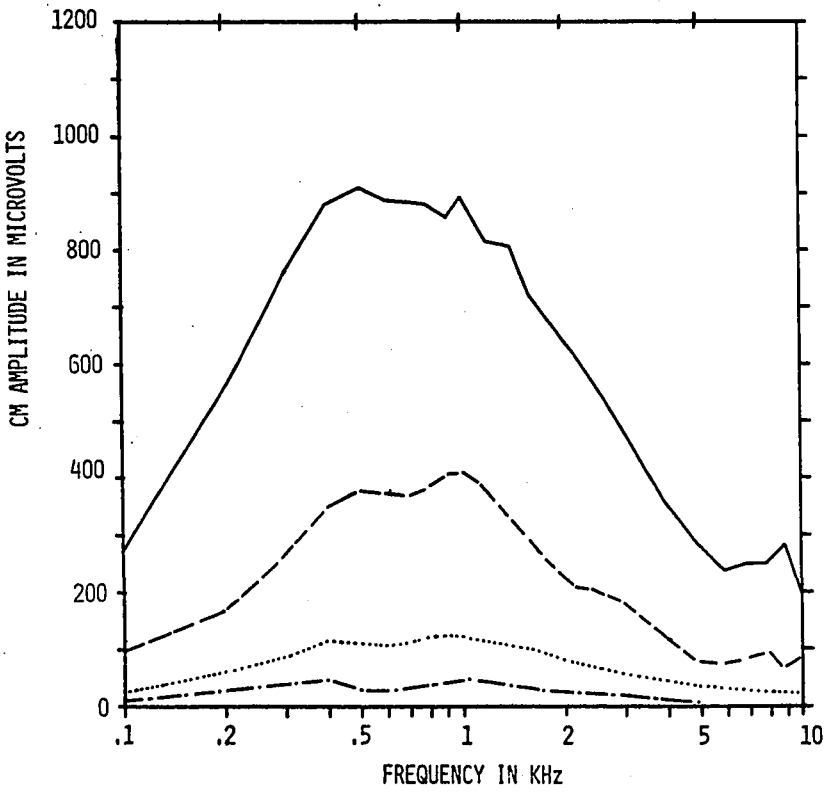

FIG.6.25 THE SUMMATING POTENTIAL AND THE COCHLEAR MICROPHONIC POTENTIAL MEASURED IN TURN 1 AT 50, 60, 70 AND 80 DB SPLs. SINGLE EXPERIMENT: GP 51/67.

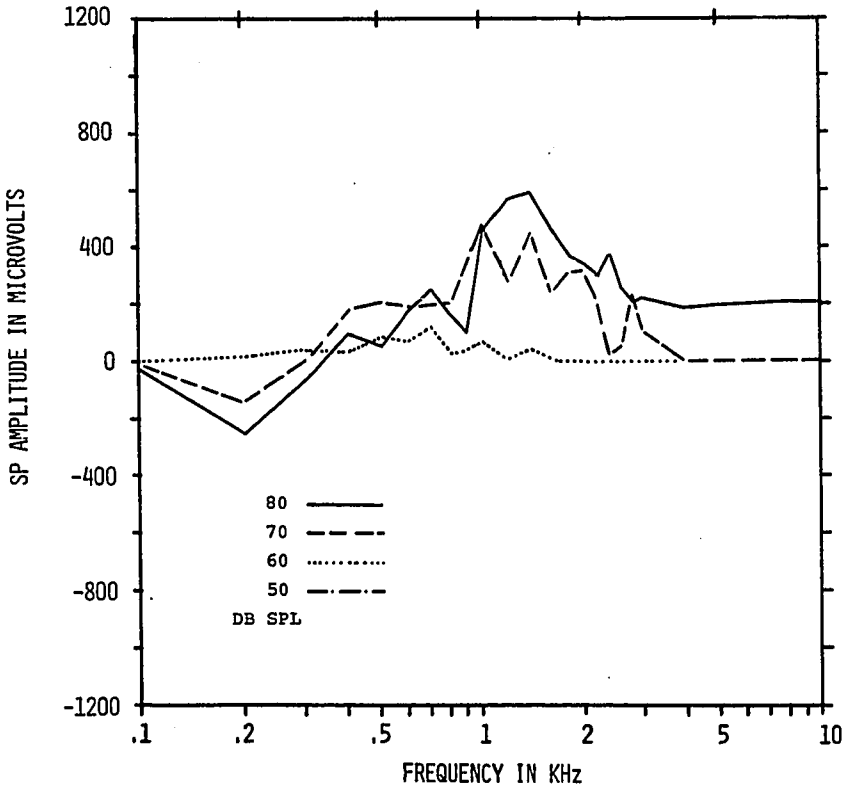

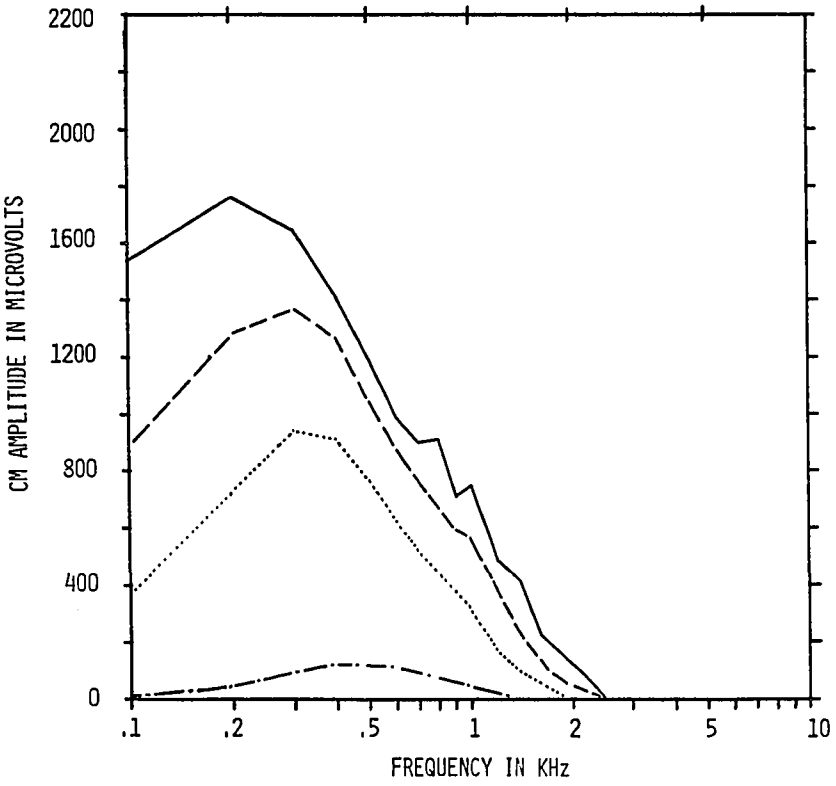

FIG.6.26 THE SUMMATING POTENTIAL AND THE COCHLEAR MICROPHONIC POTENTIAL MEASURED IN TURN 3 AT 50, 60, 70 AND 80 DB SPLs. SINGLE EXPERIMENT: GP 51/87.

CHAPTER 7

MATHEMATICAL MODELS OF THE GUINEA-PIG EAR

The subjects of this chapter are the modelling of the dynamic behaviour of the mechano-acoustical part of the auditory system of the guinea pig and the solutions of the resulting differential equations in the time domain. In this work the model for the guinea-pig middle ear and cochlea reported previously by Laszlo (21) will be used. Since in (21) the author carefully examines the various conditions and criteria related to the modelling of the mechano-acoustical components of the ear and gives the details of the mathematical derivation, only a brief summary of these topics and the final formulae are therefore now presented.

The simulation of the model is accomplished by using either the convolution technique or the state variable method. It is shown that because of limitations on computer core memory size and computation time, in this case the state variable method is preferable.

7.1. A model of the mechano-acoustical part of the guinea-pig ear

As we have indicated in Chapter 2, two transfer functions of the guinea-pig middle ear must be considered, one corresponding to the bulla closed and the other to the bulla open.

In determining the middle ear transfer functions use is made of the evidence of Möller (75) stating that the transfer functions may be estimated entirely from the acoustic impedance data measured in the plane of the eardrum and of the acoustic impedance data of Zwislocki (76). Based on their results and on other considerations a satisfactorily simplified form of the guinea-pig middle ear transfer function was shown to be

$$M(s) = \frac{a^2 + b^2}{(s + a)^2 + b^2} \qquad (7.1)$$

The values of the parameters 'a' and 'b' are given in Table 7.1. The frequency response diagrams for both the bulla closed and bulla open cases are shown in Fig.7.1.

The model of the guinea-pig cochlear partition was developed by paralleling Flanagan's treatment of the human basilar membrane (19,77,78,79). From basilar membrane displacement amplitude and phase data it is possible to deduce a general transfer function form containing appropriate parameters. These parameters enable us to adjust the form of the general equation to fit any particular response at various points along the basilar membrane:

$$P(s) = c_1 \times c_2 \frac{s}{s + \gamma} \left[\frac{\beta^2}{(s + \alpha)^2 + \beta^2}\right]^2 \times \exp(-sT) \qquad (7.2)$$

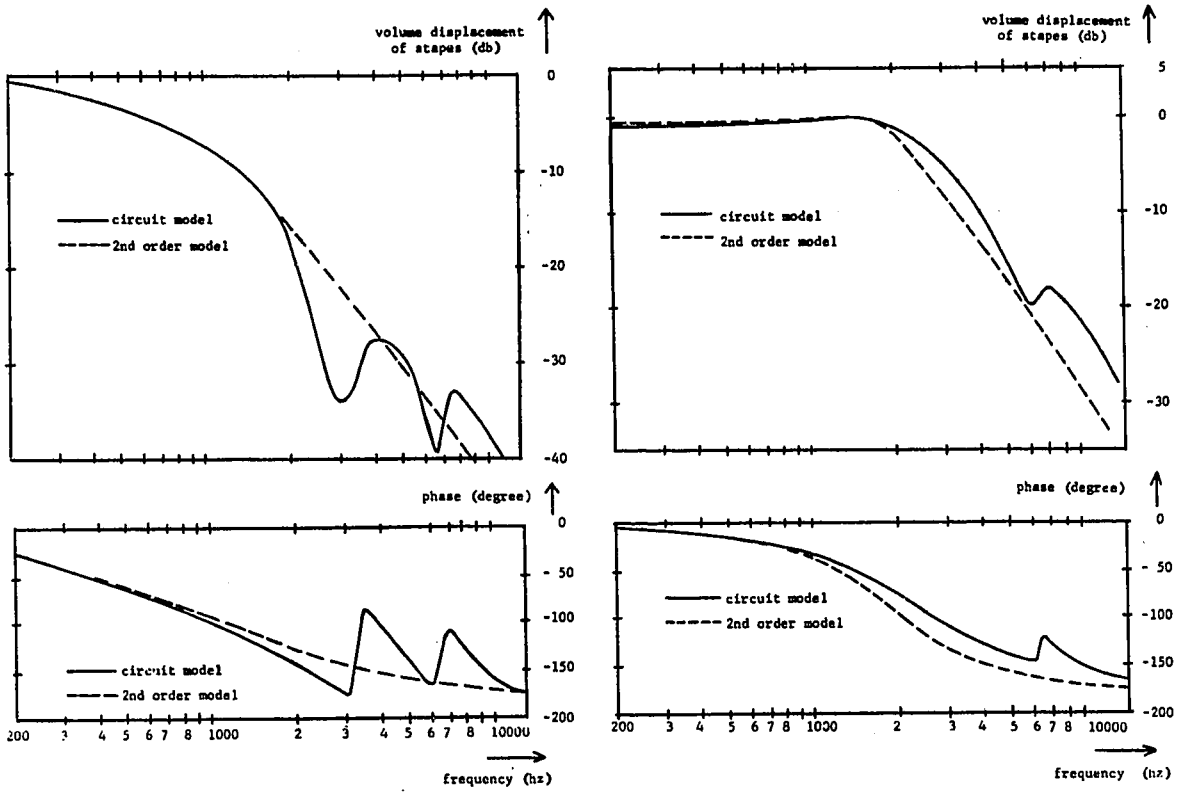

(A) BULLA OPEN

(B) BULLA CLOSED

FIG.7.1 FREQUENCY RESPONSE OF THE GUINEA PIG MIDDLE EAR MODEL. INPUT IS IN TERMS OF SOUND PRESSURE, OUTPUT IN TERMS OF VOLUME DISPLACEMENT. 'CIRCUIT MODEL' REFERS TO ZWISLOCKI'S ELECTRICAL ANALOG MODEL OF THE MIDDLE EAR OF THE GUINEA PIG (76).

where

$P(s)$ = basilar membrane displacement

β = maximum response frequency of a given point on the basilar membrane. The value of β is determined for a point along the cochlea by the distance of the point from the stapes.

α, γ = parameters dependent on β

c_1, c_2 = amplitude factors

$\exp(-sT)$ = delay term which brings the phase response of the model into agreement with the phase measured experimentally.

Of the above parameters β determines the location of the maximum of the magnitude of $P(s)$, whereas α and γ ensure proper absolute tuning curve bandwidth. The delay term is physically due to the time taken for the pseudo-travelling wave to traverse the distance between the stapes and a point on the basilar membrane. The values of these constants were determined by the author (21) and are given in Table 7.1.

Using these constants, the normalized frequency plot of $P(z)$, $z = \frac{s}{\beta}$ is shown in Fig.7.2. c_1 and c_2 were determined by Flanagan as:

$$c_1 = \frac{10^{-7}}{(0.66) \times (2\pi \times 1000)^r} \qquad (7.3a)$$

$$c_2 = K\left[\frac{2\pi q\beta}{\beta + 2\pi q}\right]^r \qquad K = 2^r, \beta \leq 2\pi q \qquad K = 1, \beta > 2\pi q \qquad (7.3b)$$

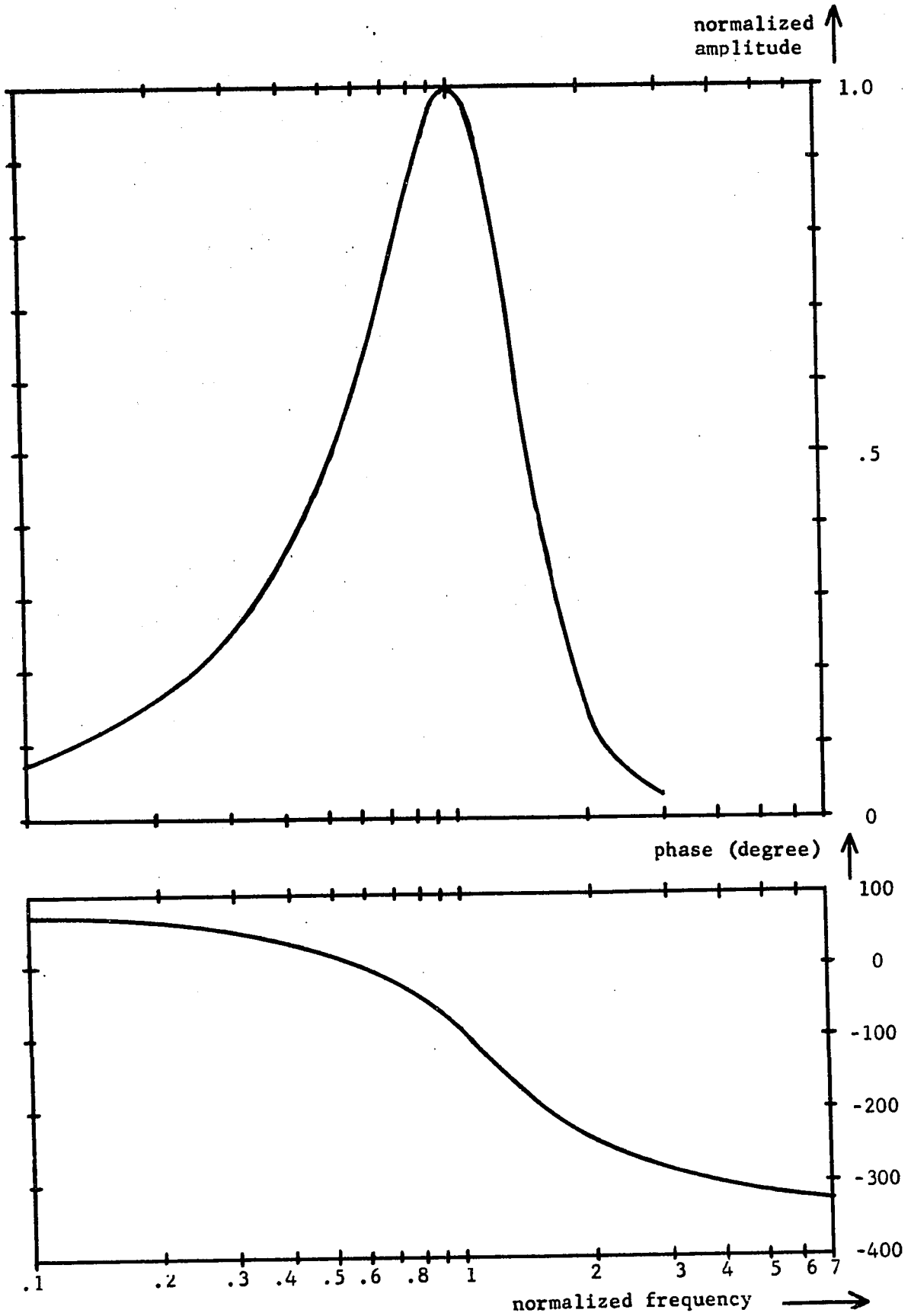

Fig.7.2 Frequency response of the model of the cochlear partition.

where r = 0.8 and q = 1000 for the human ear. In the absence of corresponding data for the guinea-pig ear, the same values are used in our model.

The combination of the appropriate models for the middle ear and cochlea yields a complete model of the mechanical system of the guinea-pig peripheral auditory apparatus. The overall transfer function is

$$H_m = c_1 \times c_2 \frac{a^2 + b^2}{(s+b)^2 + b^2} \frac{s}{(s+\gamma)} \left[\frac{\beta^2}{(s+\alpha)^2 + \beta^2}\right]^2 \exp(-sT) \qquad (7.4)$$

with the values of the parameters given in the Table below:

Table 7.1

	m = o Bulla open	m = c Bulla closed
c_1 c_2	as given on page 132	
a	$2\pi \times 900$	$2\pi \times 950$
b	0	$2\pi \times 1645$
α	0.5β	
γ	2.0β	
T	$2\pi \times 0.2085/\beta$	

Bode plots for some values of β are shown in Fig.7.3. To obtain the impulse response of the above transfer function, the Inverse Laplace Transform of the expression for H_m was found.

$$h_m(t) = c_1 c_2 \Big[C\exp(-\gamma x) + E +$$

$$+ \frac{1}{2\beta^3} \{D_0 - \alpha D_1 + (\alpha^2+\beta^2)D_2 - (\alpha^3+3\alpha\beta^2)D_3\} \exp(-\alpha x) \sin(\beta x) +$$

$$+ D_3 \exp(-\alpha x) \cos(\beta x) +$$

$$+ \frac{1}{2\beta^3} \{\beta^2 D_1 - 2\alpha\beta^2 D_2 + (3\alpha^2\beta^2 - \beta^4)D_3\} x \exp(-\alpha x) \sin(\beta x) -$$

$$- \frac{1}{2\beta^2} \{D_0 - \alpha D_1 + (\alpha^2-\beta^2)D_2 - (\alpha^3 - 3\alpha\beta^2)D_3\} x \exp(-\alpha x) \cos(\beta x) \Big] \qquad (7.5)$$

where

$x = t - T$

t = time variable

$T = 2\pi 0.2085/\beta$

For the <u>bulla closed</u> case $h_m(t) = h_c(t)$

$$E = \frac{1}{gA_c} \left(\left\{ \frac{B_c}{A_c} - f \right\}^2 + g^2 \right)^{1/2} \exp(-fx) \sin(gx+\psi)$$

$$\psi = \tan^{-1} \left(\frac{g}{(B_c/A_c) - f} \right) \qquad (7.6)$$

$$C = C_c, \; D_0 = D_{c0}, \; \ldots \text{ etc}$$

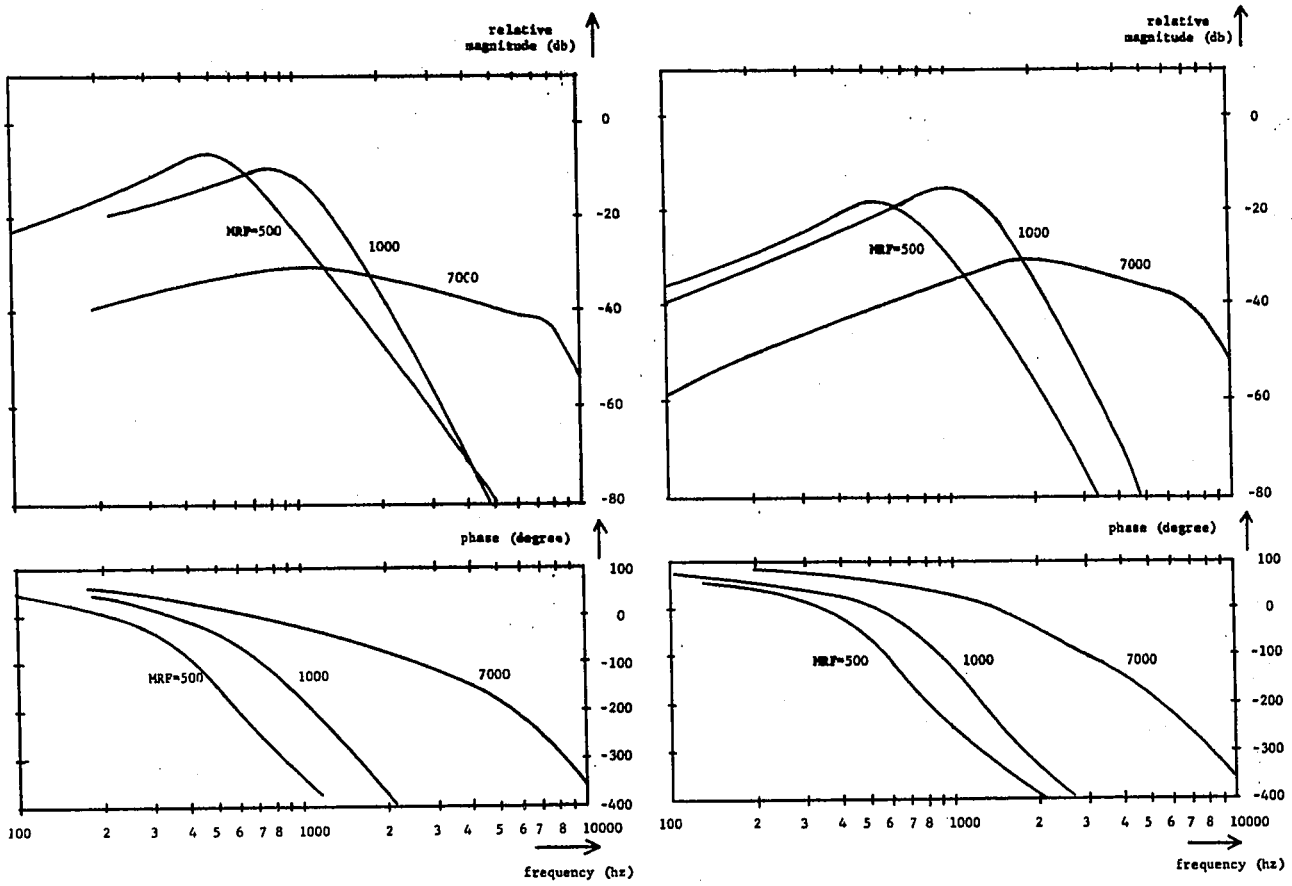

(A) BULLA OPEN

(B) BULLA CLOSED

FIG.7.3 FREQUENCY RESPONSE OF THE MECHANICAL SYSTEM OF THE GUINEA PIG EAR.

For the bulla open case $h_m(t) = h_o(t)$

$$E = \left((B_o - d \times A_o)x - A_o\right) \exp(-xd) \qquad (7.7)$$

$$C = C_o, \; D_0 = D_{o_0} \text{ etc.}$$

The values of the constants are given in Appendix 1.

7.2. Computer simulation of the basilar membrane motion by the convolution method

To simulate the basilar membrane motion the expressions for $h_o(t)$ and $h_c(t)$ can be used to calculate the response of the model in the time domain by solving the convolution integral:

$$y(\lambda) = \int_o^\infty h(x) \times i(\lambda - x) \times dx \qquad (7.8)$$

where $i(t)$ is a time function representing the input stimulus to the ear, and it is defined analytically or by a set of data points. The convolution integral is best solved by digital methods and FORTRAN IV programs were written to calculate and plot $y(\lambda)$ for any arbitrary $i(t)$. Using these programs we found that while the convolution technique is straightforward and simple, its use in this case is impractical, because it is very time consuming and costly.

To illustrate this point consider that the waveforms are sampled at 200 points for good resolution and accuracy in integration. The 'reflection, multiplication and advance' phase of the calculation will take 14000 multiplications, while the integration step requires 60000 multiplications. Since 180 points are necessary for the distributed cochlear potential model to be described in Chapter 9, 13.32 million multiplications are necessary for one simulation run involving only one waveform. Using an optimistic multiplication time of 20 microseconds, the time required for such a run is 266.4 seconds. This, plus the other necessary calculations in a given run add up to about 8 minutes of computer time per waveform simulated for a given electrode location. Thus, for a run involving the 27 'standard' frequencies (see Chapter 9), approximately 3.5 hours of computer time would be necessary.

Another limitation arises due to the available computer memory size. In the example above the memory requirements are about 30000 computer words or about 120000 bytes. Such a memory is seldom available, necessitating the use of disc or tape for auxiliary data storage. The additional time involved in data transfer increases the necessary computer time further to approximately 4 hours.

7.3. State variable formulation of the guinea-pig ear model

Instead of calculating the impulse response and solving the convolution integral it is possible to reformulate the guinea-pig ear model for simulation, expressing it in terms of state variables. From a purely mathematical viewpoint, the state variable method comprises the use of various techniques of algebra in solving problems of system analysis and design. The state variable technique is not only amenable to computation, but it also aids conceptual thinking about complex problems. Furthermore, it provides a unified approach to linear and non-linear problems which are treated in an unrelated fashion by other methods.

7.3.1. Scaled state equations for linear systems

The concept of state is fundamental and it may be said that the state of the system contains all the relevant information concerning the past history of the system necessary to determine its behaviour in response to any prescribed input form.

The properties of systems whose behaviour is described by the notion of state can clearly be defined and mathematically these properties are expressed as a set of state equations

$$y(t,t_0) = g\{x(t_0),v(t,t_0)\}$$

$$x(t) = f\{x(t_0),v(t,t_0)\} \qquad (7.9)$$

where

f and g are single valued functions and

t_0 = 'zero' time

t = time, $t > t_0$

These equations simply state that in the time interval t_0 to t both the output (y) and the state (x) of a continuous deterministic system are single valued functions of the state at time t_0 and the input (v) during the interval t_0 to t.

If the system can be described by a set of linear ordinary differential equations with constant coefficients, the state equations may be written as

$$\dot{\underline{x}}(t) = \underline{A}(t) \times \underline{x}(t) + \underline{B}(t) \times v(t)$$

$$y(t) = \underline{C}(t) \times \underline{x}(t) + \underline{D}(t) \times v(t) \qquad (7.10)$$

where

$\underline{x}(t)$ are the state variables $(x_1,x_2,\ldots,x_n)$,

$\underline{A}(t)$ is the essential matrix,

$\underline{B}(t)$, $\underline{C}(t)$, $\underline{D}(t)$ are coupling matrices and

$v(t)$ is the input function (scalar).

A general simulation diagram for these equations is shown in Fig.7.4.

For an nth order single input-single output, linear and constant coefficient system the differential equation can be written as

$$(p^n+a_{n-1}p^{n-1}+\ldots+a_1p+a_0)y = (b_np^n+b_{n-1}p^{n-1}+\ldots+b_1p+b_0)v \tag{7.11}$$

where

$$p = \frac{d}{dt} .$$

The simulation diagram is shown in Fig.7.5. Note that on the simulation diagram a normalizing or scaling constant is included. The role of this constant in the computer implementation of the state variable solution is very important and will be discussed in detail at the appropriate point in this chapter. Eq.(7.11) may be expressed in terms of 'n' first order differential equations in which the variables are the 'x_i' shown in Fig.7.5. Since these variables satisfy the necessary consistency criteria (80) x_i's are chosen as state variables. After appropriate substitutions and rearrangement the state equations may be expressen in the form of Eqs.(7.10):

$$\begin{bmatrix} \dot{x}_1 \\ \dot{x}_2 \\ \dot{x}_3 \\ . \\ . \\ \dot{x}_{n-1} \\ \dot{x}_n \end{bmatrix} = \begin{bmatrix} 0 & 1/k & 0 \ldots\ldots 0 \\ 0 & 0 & 1/k \ldots\ldots 0 \\ 0 & 0 & 0 \ldots\ldots 0 \\ . & . & . \quad . \\ . & . & . \quad . \\ . & . & . \quad 1/k \\ -k^{n-1}a_0 & -k^{n-2}a_1 & \ldots\ldots\ldots a_{n-1} \end{bmatrix} \begin{bmatrix} x_1 \\ x_2 \\ x_3 \\ \\ \\ x_{n-1} \\ x_n \end{bmatrix} + \begin{bmatrix} B_1/k \\ B_2/k \\ B_3/k \\ \\ \\ B_{n-1}/k \\ B_n/k \end{bmatrix} \times v \tag{7.12}$$

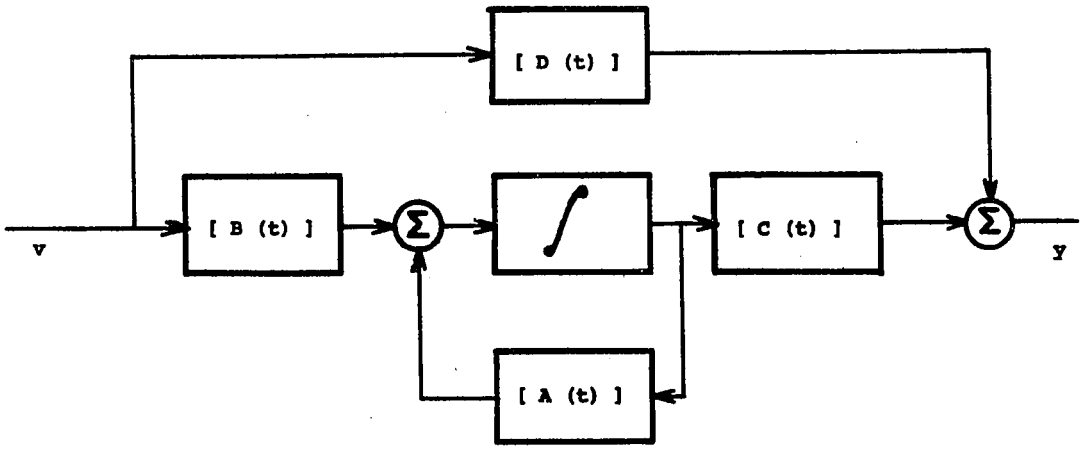

FIG.7.4 GENERAL SIMULATION DIAGRAM FOR THE STATE EQUATION.

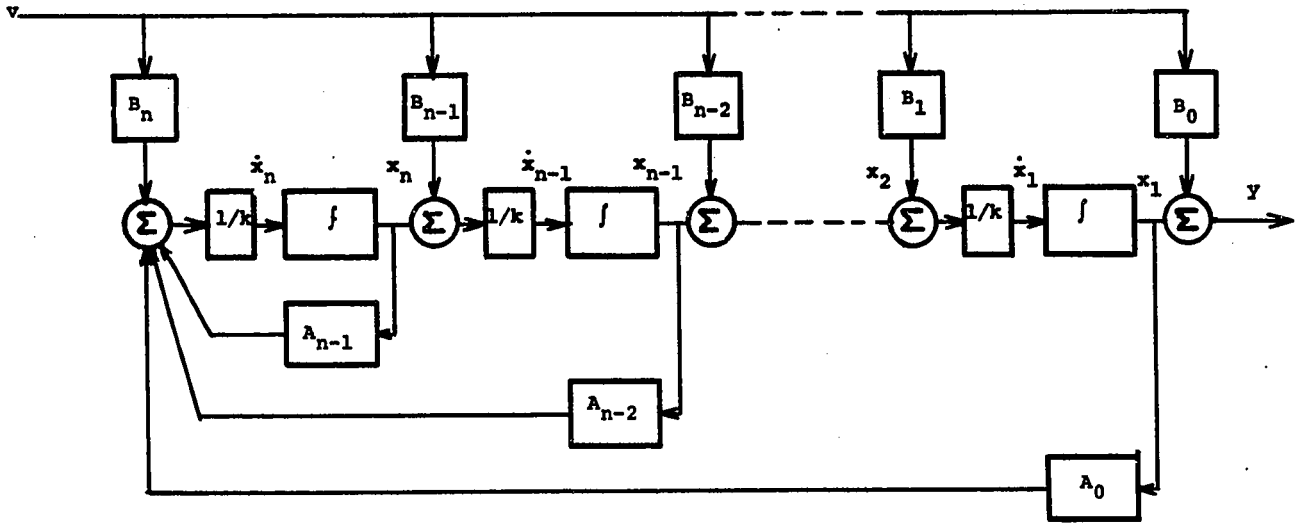

FIG.7.5 SIMULATION DIAGRAM WITH SCALING FACTOR

The matrix $\underline{B}$ can also be expressed in terms of the original differential equation coefficients:

$$\begin{bmatrix} B_0 \\ B_1 \\ B_2 \\ B_3 \\ \cdot \\ \cdot \\ \cdot \\ B_i \end{bmatrix} = \begin{bmatrix} b_n \\ kb_{n-1} - ka_{n-1}B_0 \\ k^2b_{n-2} - k^2a_{n-2}B_0 - ka_{n-1}B_1 \\ k^3b_{n-3} - k^2a_{n-3}B_0 - k^2a_{n-2}B_1 - ka_{n-1}B_2 \\ \\ \\ \\ k^ib_{n-i} - k^ia_{n-i}B_0 - k^{i-1}a_{n-i+1}B_1 - \cdots - ka_{n-1}B_{i-1} \end{bmatrix} \qquad (7.13)$$

Also

$$\underline{C} = \begin{bmatrix} 1 & 0 & 0 \cdots\cdots 0 \end{bmatrix}$$

$$\underline{D} = \begin{bmatrix} B_0 \end{bmatrix} = b_n \qquad (7.14)$$

7.3.2. State equations of the guinea-pig ear model

The displacement transfer function of the basilar membrane of the guinea pig is given by Eq.(7.4). To simplify calculations c_1 and c_2 will be disregarded, to be resupplied at the end of the numerical calculations. The time-delay term is also disregarded in the following considerations and

when the actual computer calculations are carried out the time-delay is reintroduced by defining a relative time variable t_{rel}:

$$t_{rel} = t - T$$

where

t = real time

T = time delay as determined by Table 7.1. Note that T is a function of β.

$t_{rel}(t,\beta)$ is then the time variable used in the calculation of the displacement of the basilar membrane at a given distance from the stapes, which is characterized by the parameter β, and at a given time.

Eq.(7.4) may be rewritten as

$$\frac{b_7s^7 + b_6s^6 + b_5s^5 + b_4s^4 + b_3s^3 + b_2s^2 + b_1s + b_0}{s^7 + a_6s^6 + a_5s^5 + a_4s^4 + a_3s^3 + a_2s^2 + a_1s + a_0} \qquad (7.15)$$

and the coefficients are easily determined (Table 7.2). Thus, the state equation matrices for the guinea-pig ear model are:

$\underline{A}_m$ = Eq.(7.12) with values supplied by table 7.2.

$$\underline{B}_m = \begin{bmatrix} 0 \\ 0 \\ 0 \\ 0 \\ 0 \\ k^6 b_1 \\ -k a_6 B_6 \end{bmatrix} \qquad \text{also } \underline{B}'_m = (1/k)\underline{B} \tag{7.16}$$

$$\underline{C}_m = \begin{bmatrix} 1 & 0 & 0 & 0 & 0 & 0 & 0 \end{bmatrix} \tag{7.17}$$

$$\underline{D}_m = \begin{bmatrix} 0 \end{bmatrix}$$

Table 7.2

Bulla open $f = a$ $g = a^2$	Bulla closed $f = a$ $g = a^2 + b^2$

Coefficient	value
a_6	$2f + \gamma + 4\alpha$
a_5	$g\gamma + 2f\gamma + 4\alpha(2f+\gamma) + 6\alpha^2 + 2\beta$
a_4	$g\gamma + 4\alpha(g+2f\gamma) + (2f+\gamma)(6\alpha^2+2\beta^2) + 4\alpha^3 + 4\beta^2\alpha$
a_3	$4\alpha f\gamma+(g+2f\gamma)(6\alpha^2+2\beta^2)+(2f+\gamma)(4\alpha^3+4\alpha\beta^2)+(\alpha^2+\beta^2)^2$
a_2	$g\gamma+(6\alpha^2+2\beta^2)+(g+2f\gamma)(4\alpha^3+4\alpha\beta^2)+(2f+\gamma)(\alpha^2+\beta^2)^2$
a_1	$g\gamma(4\alpha^3+4\alpha\beta^2) + (g+2f\gamma)(\alpha^2+\beta^2)^2$
a_0	$g\gamma(\alpha^2+\beta^2)^2$
b_1	$g\beta^4$
b_i	$0,\ i \neq 1$

7.4. Computer simulation of the basilar membrane motion by the state variable method

The solution of the state equations (7.10) is given by

$$\underline{x}(t) = \underline{\phi}(t-\lambda)\, x(\lambda) + \int_{\lambda}^{t} \underline{\phi}(t-\zeta)\, \underline{B}\, v(\zeta)\, d\zeta \tag{7.19}$$

$$y(t) = \underline{C}\, \underline{x}(t) \tag{7.20}$$

where

$$\underline{\phi}(t-\lambda) = e^{\underline{A}(t-\lambda)}$$

Let T be the sampling period and then

$$t = (n + 1)T$$

$$\lambda = nT \tag{7.21}$$

By substituting (7.21) into (7.19) and using Simpson's Rule it may be shown that

$$\underline{x}\{(n+1)T\} =$$

$$\exp(\underline{A}T)\{\underline{x}(nT) + (T/6)\underline{B}v(nT)\} + (2/3)T \exp(\underline{A}T/2)\, \underline{B}v\{(n+1/2)T\} +$$

$$+ (T/6)\underline{B}v\{(n+1)T\} \tag{7.22}$$

Thus, from Eqs.(7.20) and (7.22) by using the state variables given at time nT and the input given at times nT, (n + 1/2)T,

and $(n + 1)T$ the output of the system,

$$y\{(n + 1)T\} = \underline{C}\ \underline{x}\{(n + 1)T\},$$

at time $(n + 1)T$ can be calculated. It is necessary, however, to find the state transition matrix $\phi = \exp(\underline{A}T)$ first. To evaluate ϕ we use a method of Liou (81), who approximates the state transition matrix with a matrix series:

$$\underline{\phi} = \exp(\underline{A}T) \simeq \sum_{r=0}^{R} \frac{\underline{A}^r T^r}{r!} \qquad (7.23)$$

If appropriate error bounds are specified, it is possible to calculate ϕ to any desired accuracy by evaluating the necessary number of terms in the series.

The actual implementation of the above scheme is made difficult by the fact that the values of the coefficients of the matrix $\underline{A}$ are very large (see Table 7.3). Since the rate of convergence of the matrix series depends on the norm of the matrix, this means that the series convergence will be very slow. Appropriate scaling will speed up the series convergence and this is in fact why we have included the scale factor 'k' in our formulation of the general state equations.

One definition of the norm of the matrix $\underline{A}$ is

$$||A|| = (1/k)\{(m-1) + \sum_{i=0}^{m-1} k^{m-i}|a_i|\} \qquad (7.24)$$

where

m = order of original differential equation.

This expression may be minimized with respect to 'k':

$$\frac{d||A||}{dk} = -\frac{m-1}{k^2} + \sum_{i=0}^{m-1} (m-i-1)k^{(m-i-2)}|a_i| = 0$$

$$\sum_{i=0}^{m-1} (m-i-1)k^{m-i}|a_i| - (m-1) = 0 \qquad (7.25)$$

The foregoing polynomial may be solved for 'k' and the resulting values substituted back into Eq.(7.24). The 'k' value giving the smallest $||A||$ is used as the scaling factor in subsequent calculations.

Table 7.3

Approximate values of the coefficients of the guinea-pig ear mathematical model

differential equation coefficients	coefficients of unscaled A and B matrices	value
a_0	A_{71}	10^{28}
a_1	A_{72}	10^{25}
a_2	A_{73}	10^{21}
a_3	A_{74}	10^{17}
a_4	A_{75}	10^{13}
a_5	A_{76}	10^{9}
a_6	A_{77}	10^{5}
	B_{61}	10^{24}
	B_{71}	10^{29}

CHAPTER 8

MODELLING OF THE COCHLEAR POTENTIAL GENERATORS

Although there have been many hypotheses and theories regarding the mechanism of the generation of the cochlear potentials, in the more restricted system analysis sense only few true modelling efforts have been made. The work of Johnstone (64) has already been mentioned briefly in Chapter 5 and will be elaborated in greater detail in Section 8.3.2. Also, from second turn cochlear microphonic measurements Matsuoka et al. (82) calculated the impedance values of the simplest series and parallel equivalent circuits fitting their data. Another approach was taken by the author (21) who attempted to find a 'gross' mathematical model of the cochlear microphonic potential. As we will see in a review of this latter work, the attempt has been only partially successful but it has quite clearly shown that a gross or lumped model is inadequate. This fact is also suggested by the fundamental work of Whitfield (70) whose work has also been reviewed in Chapter 5.

In the present work we do not restrict our considerations to the cochlear microphonic potential alone and furthermore, our approach is quite different from those of the past. First of all we look upon the cochlear potential

generators as distinct, distributed sources along the basilar membrane. Secondly, we consider the individual haircell, its mechanical and electrical characteristics and its microscopic contribution to the macroscopically observable potentials. Thirdly, we pay attention to the circumstances of recording and the relations of the electrode and the haircells.

8.1. 'Gross' model of the cochlear microphonic potential

In the author's previous work (21) the basic consideration was that, in general, the complex frequency domain equation for the cochlear microphonic potential could be written

$$V_{cm}(s,x) = W(x) \times A_f(x) \times P(s) \qquad (8.1)$$

where

$W(x)$ = weighting factor

$A_f(x)$ = amplitude factor

$P(s)$ = transfer function of the mechanical part of the auditory system

V_{cm} = cochlear microphonic potential

x = distance from the stapes.

The problem is of course to find functions $W(x)$ and $A_f(x)$ and towards this end a straightforward approach was taken. Since the generation of the cochlear microphonic potential depends on the displacement of the cochlear partition, we can find the transfer characteristics of a 'CM model' by

subtracting the appropriate displacement curves of the partition from the corresponding electrical tuning curves. When this procedure is carried out it is found that the mechanical and electrical tuning curves fall closely together on normalized plots; consequently, the results involve small differences (Fig.8.1) and hence must be treated with caution.

At first glance little regularity or general trend can be observed in Fig.8.1. This should hardly be surprising, however, because the CM is not due to a single potential source. It is a distribution of 'generators' at the level of the haircells which gives rise to the cochlear microphonic potential as measured. Due to the distributed character of the CM potential sources, the gross CM must be dependent not only on the movement of the basilar membrane at the point of observation, but also on the behaviour of neighbouring points. In view of this, we accepted the fact that every point along the cochlear partition has a characteristic curve, like those shown in Fig.8.1, associated with it. We also proposed that as a first approximation we may take

$$W(x) = \text{constant} \qquad (8.2)$$

since this is tacitly assumed in experimental work and a more accurate description of W(x) is not possible from the available data.

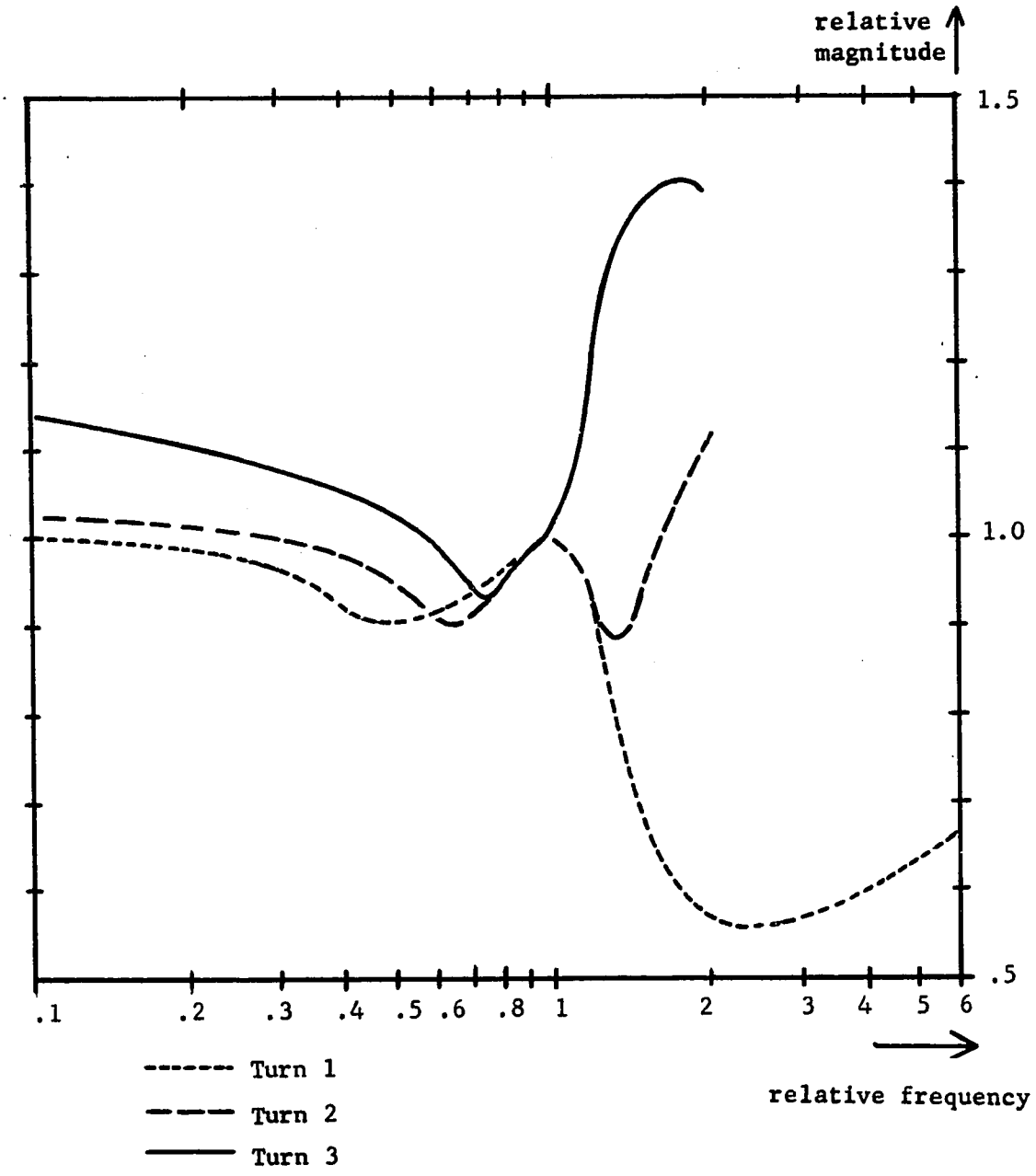

Fig.8.1 Relative differences between the electrical and mechanical tuning curves of the guinea pig ear.

The amplitude factor $A_f(x)$ is similar to $W(x)$ in that it is also a function of the location along the cochlear partition. Physiologically the amplitude factor probably represents another manifestation of the process of the generation of the cochlear microphonic potential. Using a curve fitting procedure a purely mathematical representation of the amplitude factor was derived in the form of a weighting function

$$A_f(x) = c_8p^8+c_7p^7+c_6p^6+c_5p^5+c_4p^4+c_3p^3+c_2p^2+c_1p+c_0 \qquad (8.3)$$

where all c's are functions of 'x' and 'p' is the sound pressure.

Although this attempt to model at least one of the cochlear potentials met with only limited success, nevertheless, this early work produced some important results. Firstly, it showed that the cochlear microphonic response amplitude as a function of frequency is closely related to the mechanical tuning curves of the cochlea. Secondly, the proposed transfer functions provided explicit expressions of heretofore tacitly assumed transfer characteristics. Thirdly, it became apparent that since the potential generators are distributed, the appropriate model to investigate would be a distributed one. Last, but not least, in the experimental phase of the early work old measurement techniques were

improved upon and new ones introduced, with particular relevance to the measurement of the sound pressure level of the stimulus and the CM phase (see Chapter 6).

8.2. Modelling of the potential distribution in the cochlea

In Section 5.3 we have already discussed some aspects of the distribution of the potentials generated by the individual haircells. It was pointed out that we are not justified in assuming that the potentials measured by gross electrodes bear a one-to-one relationship to the potentials generated by an individual haircell. Instead, we have to take into account the phase differences arising from the delays with which the mechanical pseudo-travelling wave excites the various groups of haircells and also the various attenuating impedances which lie between the source cell and the recording electrodes. In this section this latter aspect of cochlear potential recording will be investigated with the aim of finding the appropriate functional relationship describing the contribution of a single potential generator to the measured 'macroscopic' potential.

The functional relationship may be stated formally

$$V_{ei} = f(x_e, x_i, h) \times V_i \qquad (8.4)$$

where

V_{ei} = the potential measured by the electrode due to the ith haircell;

x_e = location of the electrode;

x_i = location of the haircell;

h = electrode distance from the basilar membrane;

V_i = potential generated by the individual haircell.

It follows that

$$V_e = \sum_{i=1}^{n} V_{ei} \qquad (8.5)$$

where

V_e = total cochlear potential recorded by the electrode;

n = total number of haircells.

Our aim is to find $f(x_e, x_i, h)$.

8.2.1. The cochlear potentials and electrostatic considerations

The individual haircell generator may be considered electrically as a dipole located in a non-homogenous media and we assume that its potential is recorded by differential electrodes (Fig.8.2). It is obvious that due to the insulating properties of the membrane separating the two poles of the dipole, the contribution of the positive and negative pole will prevail on the scala vestibuli and the scala tympani side respectively. It would thus be easy to

write down the exact relationships, using the expression for the electric potential,

$$V = \int_{r_1}^{r_2} K(r) \frac{V_i}{r^2} \, dr \qquad (8.6)$$

if only we could describe K(r), which represents the electrical insulating properties of the membranes. Experimental data is lacking, however, and we are forced to turn to macroscopic measurements of the overall cochlear impedances.

8.2.2. The attenuation of the cochlear potentials and the electric impedance of the cochlea

The fundamental work in what may be called the 'electroanatomy' of the cochlea is due to Bekesy (83). Through a series of experiments he showed, that

(a) the bony wall of the cochlea is a good insulator;

(b) the main grounding pathway of the cochlea is through the acoustic nerve to the brain;

(c) considerable cross-conduction exists between the the different turns of the cochlea.

Furthermore, by introducing a pair of electrodes at one point in the cochlea and applying a known voltage across them while exploring the voltage distribution with another pair, Bekesy also measured the electrical attenuation along the cochlea as a function of distance (Fig.8.3).

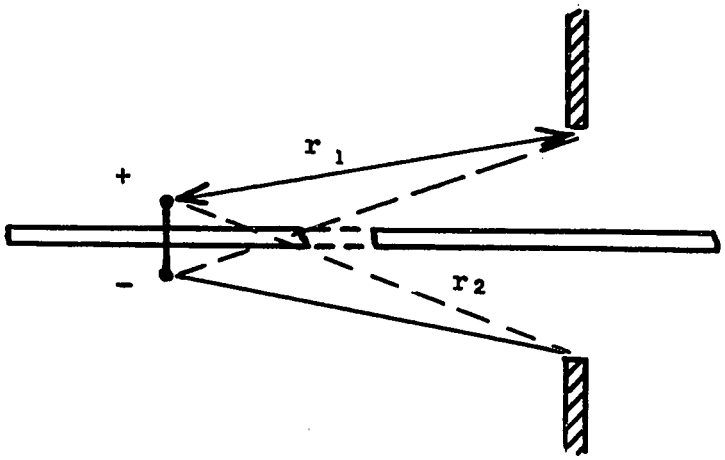

Fig.8.2 The cochlear potential generator as a dipole.

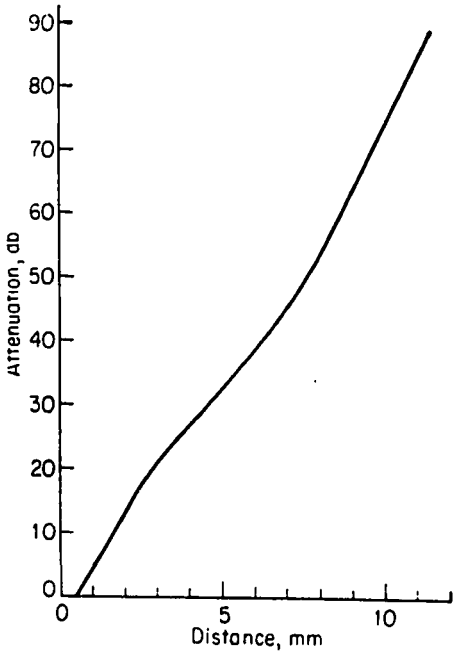

Fig.8.3 Electrical attenuation along the cochlea as a function of distance.(From Bekesy[83])

Using potentiometric arrangements Bekesy also measured what he termed as "...the coarse pattern of the electrical resistance in the cochlea" of the guinea pig. More recent determination of intracochlear impedances are due to Misrahy et al. (84), Mizukoshi et al. (85) and Johnstone et al.(65). Unfortunately these investigators did not 'map' the cochlear impedances as a function of distance but restricted their measurements to only a few electrode positions. Misrahy established that shunting impedances exist between the scala media and the scala vestibuli, because "...under all conditions examined, the potential difference between scala vestibuli and scala tympani was smaller than between scala media and scala tympani." The work of Johnstone's group gives us some idea of the significance of the various pathways. In particular, by placing electrodes in the various scalae and on the neck of the experimental animal, they were able to estimate the resistance values attributable to six pathways:

(a) blood vessels inside the cochlea to the outside of the bulla = 1.6 kohm;

(b) blood vessels inside the cochlea to scala tympani = 0.6 kohm;

(c) blood vessels inside the cochlea to scala vestibuli = 0.8 kohm;

(d) blood vessels inside the cochlea via the stria vascularis to scala media = 13 kohm;

(e) scala media direct to scala tympani (organ of Corti) = 24 kohm;

(f) scala media direct to scala vestibuli (Reissner's membrane) = 46 kohm.

8.2.3. Calculation of the potential distribution factor

As we have seen in the foregoing paragraphs the cochlear resistance distribution data is incomplete. Thus, while we have attempted to use resistance values obtained by Bekesy to describe the attenuation pattern, we nevertheless found that the results are not consistent due either to the inaccuracy and/or the insufficiency of the data. Thus we turn to the attenuation data of Bekesy (Fig.8.3) and assume that the cochlear potential due to a single generator is attenuated as a function of the distance between it and the electrode, regardless of the absolute positions of generator and electrode along the cochlea. From Fig.8.4 we may write

$$f(x_e, x_i, h) = A^q$$

$$q = \sqrt{h^2 + (x_e - x_i)^2} \qquad (8.7)$$

where

A = attenuation per unit distance.

In Chapter 9, it will be shown that the value of 'A' is not critical, i.e., relatively significant changes in 'A' will not affect the observed cochlear potentials to a great extent.

Since, as described in Chapter 4, the haircell distribution is fairly uniform throughout the cochlea we will also assume that the cochlear potential generators form a regular and uniform pattern throughout the cochlea.

8.3. Modelling of the single cochlear transducer (haircell)

The available physiological and anatomical facts related to the haircell and the transduction process (see Chapter 4) allow us to draw up the information flow diagram of the cochlear mechano-electrical transducer mechanism (Fig.8.5). This information flow diagram does not differentiate between IHCs and OHCs and ignores possible electrical interaction effects between haircells, due of course to complete absence of any significant qualitative data on which to base a more refined model. In the following we will consider only parts of the complete process as shown in Fig.8.5. In particular we will attempt to describe the conversion law, model the effects of the electrical environment of the haircell and consider the effect of inherent noise in the transduction process.

8.3.1. Mechanical dynamics and the conversion law

In Chapters 4 and 5 the physiology of the haircell and the theories related to haircell excitation were discussed. At this point the actual nature of the haircell transducer

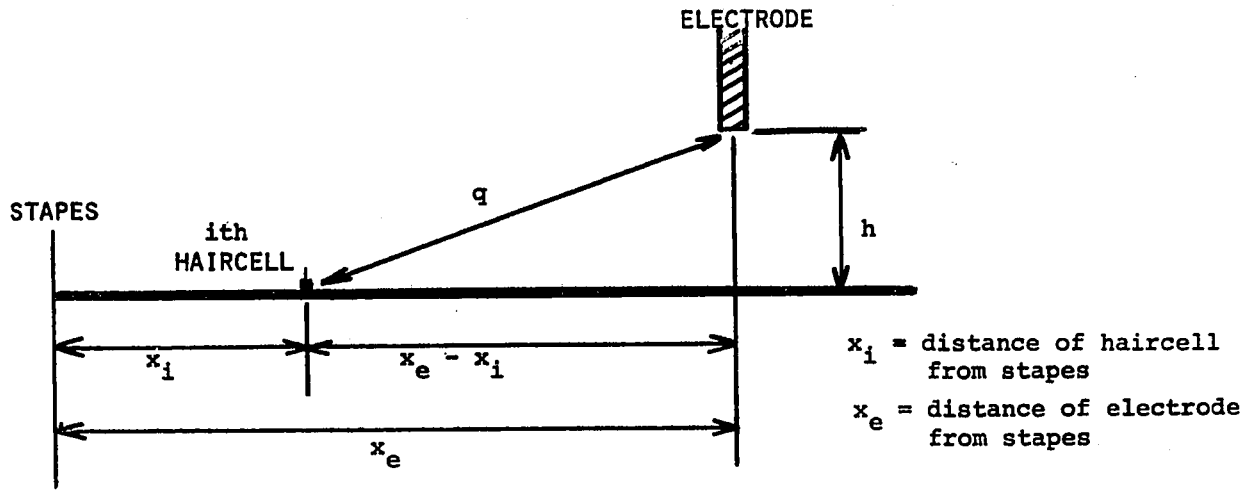

FIG.8.4 RELATIVE POSITIONS OF HAIRCELL AND ELECTRODE.

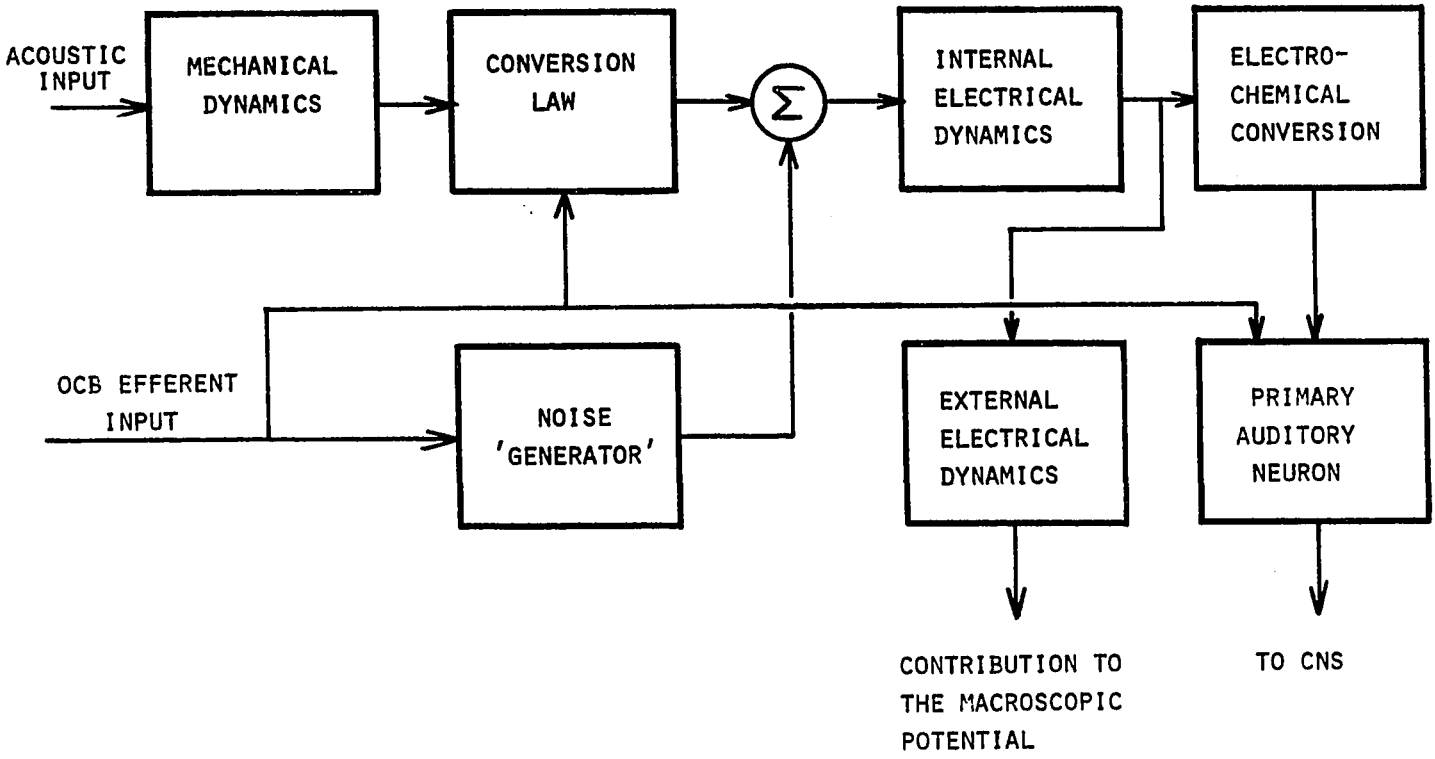

mechanism is of no interest to us. What is important, however, is the functional nature of the mechano-electrical conversion, that is, the relation between mechanical displacement and the generated potential.

As is the case with other aspects of the transduction and potential generating mechanism very little is known about the details of the transduction process. Much of the evidence is indirect in the sense that it was derived from cochlear potential studies when the cochlear potentials measured were gross potentials. Consequently, assumptions had to be made in regard to the movement of the basilar membrane and the nature of the individual haircell transducer as well to explain the observed effects. In any case there is no experimental data connecting displacement of a point with the output of one individual haircell.

One of the main benefits derivable from an attempted modelling of the cochlear potentials is that it will give an opportunity to investigate the various mechano-electrical conversion schemes. Thus, in the next chapter we will simulate the various physiologically plausible conversion schemes and correlate the resulting cochlear potentials with experimentally observable facts. The following aspects of the transduction process will be considered and modelled:

(1) linearity;

(2) nature of possible non-linearities;

(3) gain.

Although it is presently accepted that the transduction process is essentially linear over a large operational range, the validity of this assumption must now be questioned. Until very recently the SP was not considered to be a distortion product, but a cochlear potential with independent source and function. This interpretation is no longer accepted, however, and there are indications that the SP is indeed a result of non-linear processes in the transducing mechanism(86).

The non-linearity must almost certainly include a limiting function of some sort because the range of intensities handled by the system has finite limits, although very large. It is probable, however, that at relatively low levels the behaviour of the conversion process is essentially linear. If there is a linear portion of the operating characteristics of the transducer the slope of this curve will determine the gain of the conversion process. It has been suspected in the past that there is such a gain but no details are available (87). The gain factor therefore should be taken as unity, at least as a first approximation.

8.3.2. Formulation of the 'conversion law'

T.F. Weiss (88) suggested in 1963 that a sigmoid type transducer function is necessary to explain some properties of first order auditory neuron model behaviour. Interestingly, Johnstone et al. (64) derived an arcot function relationship between the displacement of the basilar membrane and the potential generator mechanism from purely geometrical considerations (see Section 5.1.4). In Johnstone's model it is assumed that the potential generating process is governed by the haircell-to-basilar membrane deflection angle (Fig.5.5). For the resting angle (ϕ_0) Johnstone and co-workers assume that $\phi_0 = 60^\circ$ for the IHC and $\phi_0 = 130^\circ$ for the OHC with the implication that this is the angle between the basilar membrane and the hairs. A search of the literature did not yield any data whatsoever relating the angle of the hair to the cell body or the basilar membrane. Neither could we determine this angle from histological material available at the OTL Research Laboratories using light microscopy. Clearly, it is necessary to prepare special histological material with the measurement of the aforementioned angular relationships in mind. This task, however, is beyond the scope of this work.

A reason for the choice of the ϕ_0(IHC) = 60° and ϕ_0(OHC) = 130° is that for these values the positive potential produced by the IHC will be greater than the negative potential produced by one OHC at low SPLs of the input. Although this is consistent with experimental data (35,64), if the modelling of this low level SP^+ is desired then ϕ_0 must be chosen for the IHC so that the IHC will produce at least three times the positive potential generated by the OHC because there are three times as many OHCs as IHCs. Thus, it appears that the selection of the ϕ_0s has been arbitrary or possibly they were suggested by the angles the cell bodies make with the basilar membrane (Fig.4.3).

To find a more realistic criterion for the choice of the resting angle we may turn to psychoacoustic observations which show that the sensitivity of the hearing process is greatest for low intensity sounds (89). Thus, one would expect that the individual cochlear transducer is also the most sensitive for low intensity sounds. Inspection of the transfer characteristics suggested by Johnstone shows that this condition exists for ϕ_0 = 0 rather than for ϕ_0 = 60° or ϕ_0 = 130°. For these latter resting angles the input SPL vs the ac potential output plot shows relatively low sensitivity for small amplitudes and the highest sensitivity to a small range of large amplitudes with a rapid onset of

complete saturation (Fig.8.6). Although for $\phi_0 = 0$ the sensitivity is the greatest for small amplitudes, for this resting angle the Johnstone model will not produce an SP type dc shift of a sinusoidal input waveform as it does for $\phi_0 \neq 0$. The reason for this is, of course, that for $\phi_0 = 0$ the transfer characteristics are perfectly symmetrical.

The model we propose for the representation of the transducer characteristics retains Johnstone's concept that the mechanical movement produces a change in the hair-to-haircell angle and that it is this angle which determines the potential generated by the transducer. We will, however, incorporate appropriate modifications in our model to satisfy the sensitivity and assymmetric considerations discussed in the previous paragraphs. Accordingly, the transducer transfer characteristics are described by

$$V = K_1 \operatorname{arcot}\{f(\alpha)\} \qquad f(\alpha) \geq 0$$

$$V = 0.5K_1 \operatorname{arcot}\{2f(\alpha)\} \qquad f(\alpha) < 0$$

$$\alpha = g(D)$$

where

V = potential output

α = basilar membrane deflection angle

D = basilar membrane displacement

K_1 = constant

The plot of this function is shown in Fig.8.7.

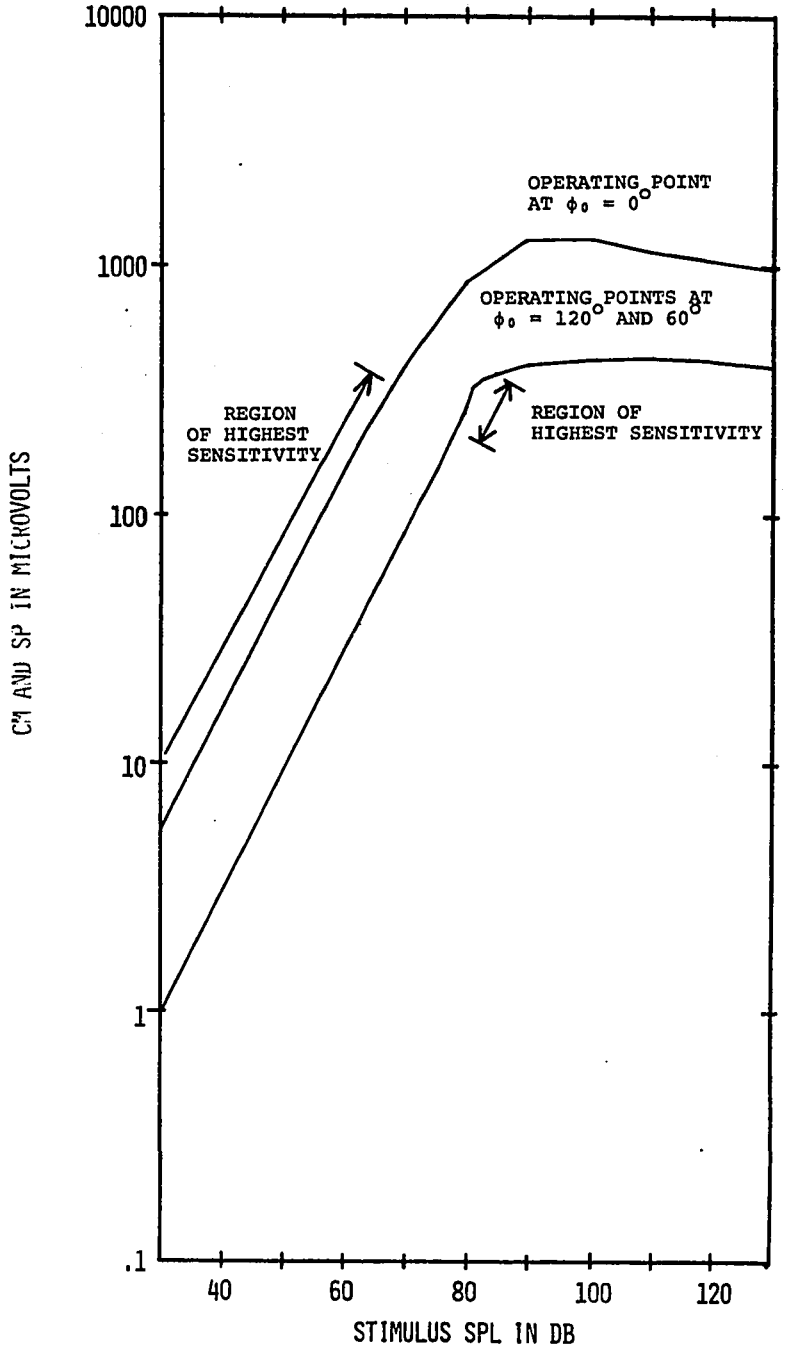

FIG.8.6 REGIONS OF HIGHEST SENSITIVITY FOR DIFFERENT OPERATING POINTS OF THE COCHLEAR TRANSDUCER MODEL PROPOSED BY JOHNSTONE (64).

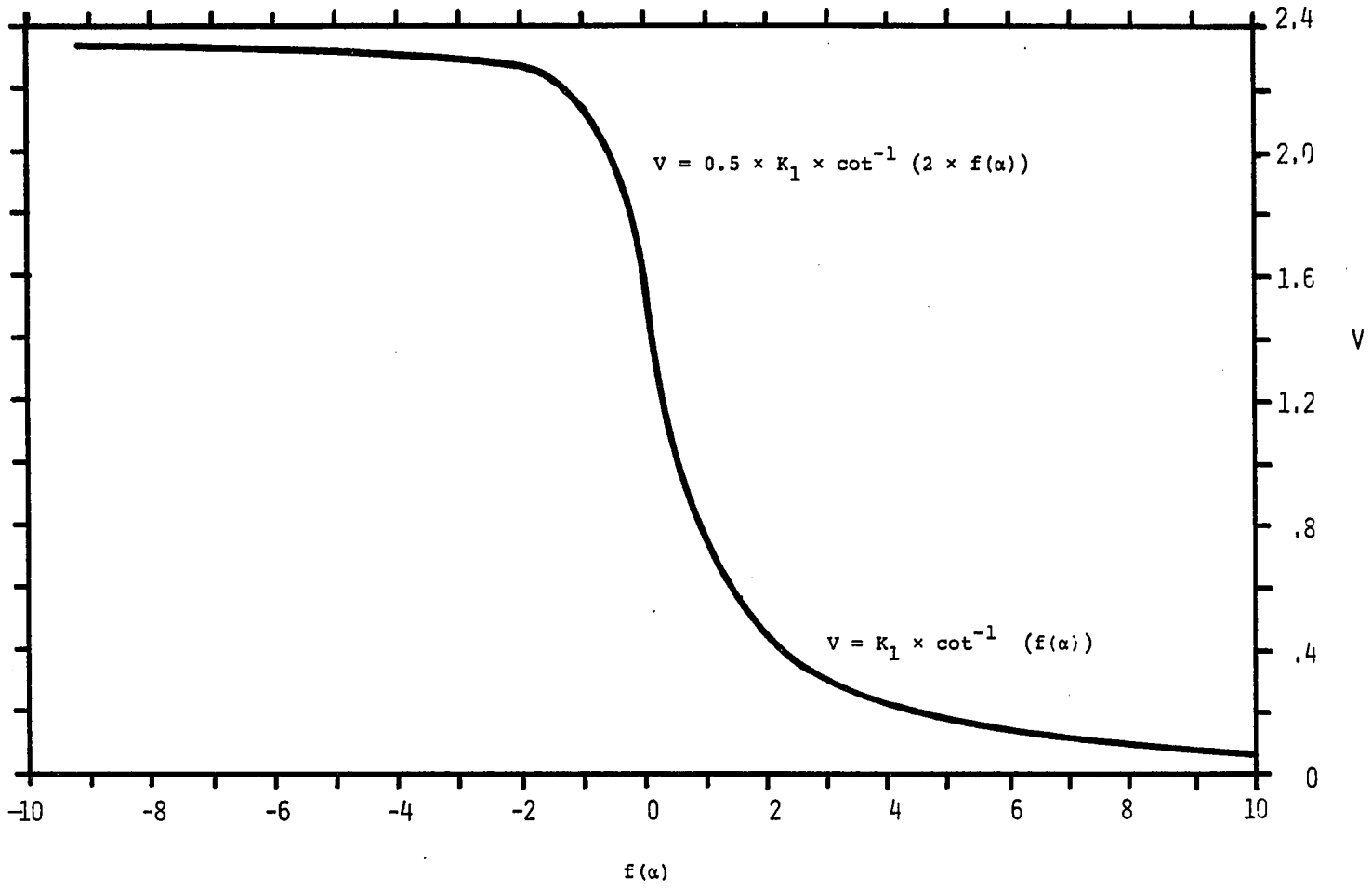

FIG.8.7 SIGMOID TYPE TRANSDUCER TRANSFER CHARACTERISTICS (CONVERSION LAW) SATISFYING THE SENSITIVITY AND ASYMMETRY CONSIDERATIONS DISCUSSED IN THE TEXT.

For $f(\alpha)$ we assume, after Johnstone, that

$$f(\alpha) = B \times \alpha$$

where 'B' is a constant, but find that it is difficult to establish theoretical guidlines for the selection of the value of 'B'. Heuristically one would estimate 'B' to be in the neighbourhood of 10^6 since this would give 'α' values large enough to introduce significant non-linearities at reasonable sound pressure levels (Fig.8.8)

To make use of this model it is necessary to determine $\alpha = g(D)$ which represents the functional relationship between the basilar membrane displacement (D) and the membrane deflection angle (α).

Knowing the displacement and the width of the basilar membrane and making the assumptions that the basilar membrane distension is triangular and the displacement is a linear function of the SPL, the angle (α) may be calculated (Fig.8.9):

$$\alpha = g(D) \simeq \frac{2D}{W}$$

The values of 'D' may be found from the basilar membrane displacement model given in Chapter 7. The maximum variation of 'D' as shown by the model is approximately 2 decades from one end of the cochlea to the other. However,

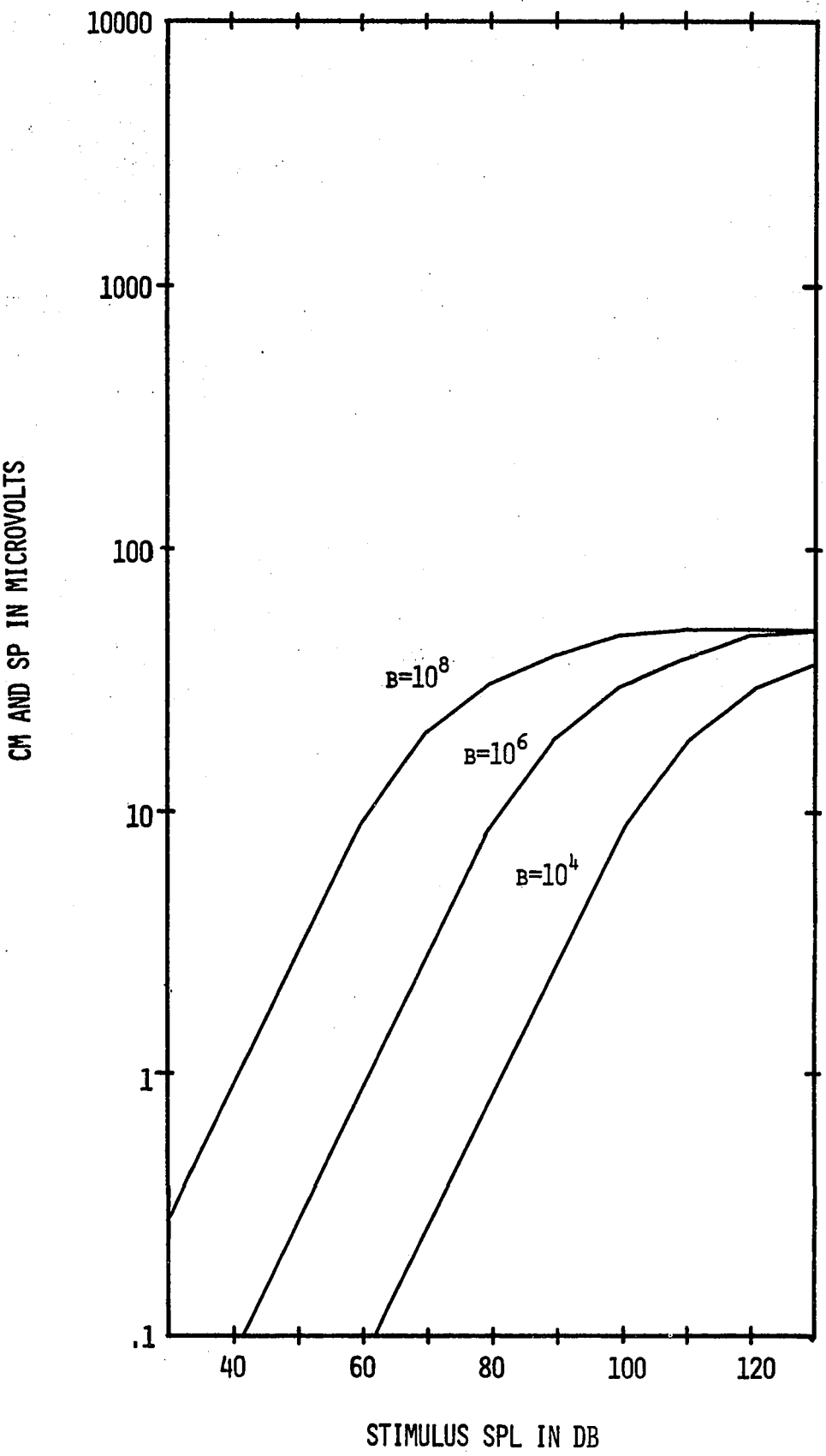
10000
1000
100
10
1
.1
CM AND SP IN MICROVOLTS
B=10^8
B=10^6
B=10^4
40
60
80
100
120
STIMULUS SPL IN DB

since 'W' also increases (90) when 'D' increases as we go farther away from the stapes the increase in 'α' would not be significant.

For illustrative purposes, the values of 'α' were calculated for two points, 3.5 and 18 mm from the stapes respectively, with 74 db SPL in front of the eardrum (Table 8.1). We see that even maximal values of 'α' are only fractions of a second of arc at this SPL.

Table 8.1

	distance = 3.5 mm		distance = 18.0 mm	
freq Hz	D mm	α radians	D mm	α radians
100	$.59\times10^{-8}$	$.68\times10^{-7}$	$.12\times10^{-6}$	$.50\times10^{-6}$
1000	$.27\times10^{-7}$	$.31\times10^{-6}$	$.43\times10^{-9}$	$.17\times10^{-9}$
10000	$.28\times10^{-8}$	$.32\times10^{-7}$	-	-

Note that one second of the arc = $.485\times10^{-5}$ radians

8.3.3. Alternative possibilities

We have shown in Section 5.1.1 that according to Davis' resistance-microphone model for the generation of the cochlear microphonic, the generated potential changes as the function $x/(1 + x)$. Inspecting Fig.5.3 we see that on the basis of the general criteria discussed previously (see Section 8.3.1) it is possible to propose a model which is simultaneously plausible on physiological and physical grounds and which is based on the resistance relationships.

In general we may state that

$$V = f(x) = \frac{x}{1 + x} \tag{8.9}$$

$$x = g(D) \tag{8.10}$$

where

V = potential generated by a single transducer (haircell),

x = (variable resistance) / (non-varying resistance) in the haircell 'circuit' (see Section 5.1.1),

D = displacement of the basilar membrane at a given point.

The relationship 'f' based on the $x/(1 + x)$ ratio is satisfactory but since 'x' can never be negative, we must find a functional relationship 'g' such that it will be applicable for positive and negative values of 'D'.

The simplest possible expression is linear:

$$x = g(D) = K_1(D + K_2), \qquad (8.11)$$

with the restriction that the term in brackets will not become very small for physiologically permissible values of 'D'. It may be argued that for large negative values the $V = x/(1 + x)$ relationship will not hold and instead some other characteristics will be applicable, but unfortunately we could only guess what this characteristic should be (Fig.8.10a - see dotted line).

To consider an alternative possibility, it is conceivable that 'x' will have some lower limit below which its value cannot go, implying that at some mechanical displacement the variable resistance will have a minimal value. When the displacement differs from this particular value 'x' will always be greater than the minimum. If we consider shearing forces to be the mechanical stimuli to the haircell, our hypothesis presents the picture of the hair of the haircell having one position where the modulating resistance is smallest so that when the hair is displaced from this position in any direction, the value of the modulating resistance increases. Functionally, the relationship may be expressed as

$$x = g(D) = |D + K_3| \qquad (8.12)$$

(1) basilar membrane at rest

(2) basilar membrane deflected ('D' is not to scale)

$$\tan \alpha \approx \alpha = \frac{2D}{w}$$

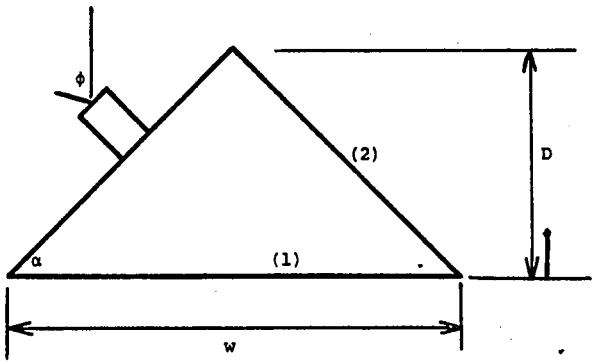

FIG.8.9 BASILAR MEMBRANE DISPLACEMENT (D) AND DISPLACEMENT ANGLE (α). 'w' IS THE WIDTH OF THE MEMBRANE AND 'ϕ' IS THE HAIR DEFLECTION ANGLE. SEE ALSO FIG.5.5.

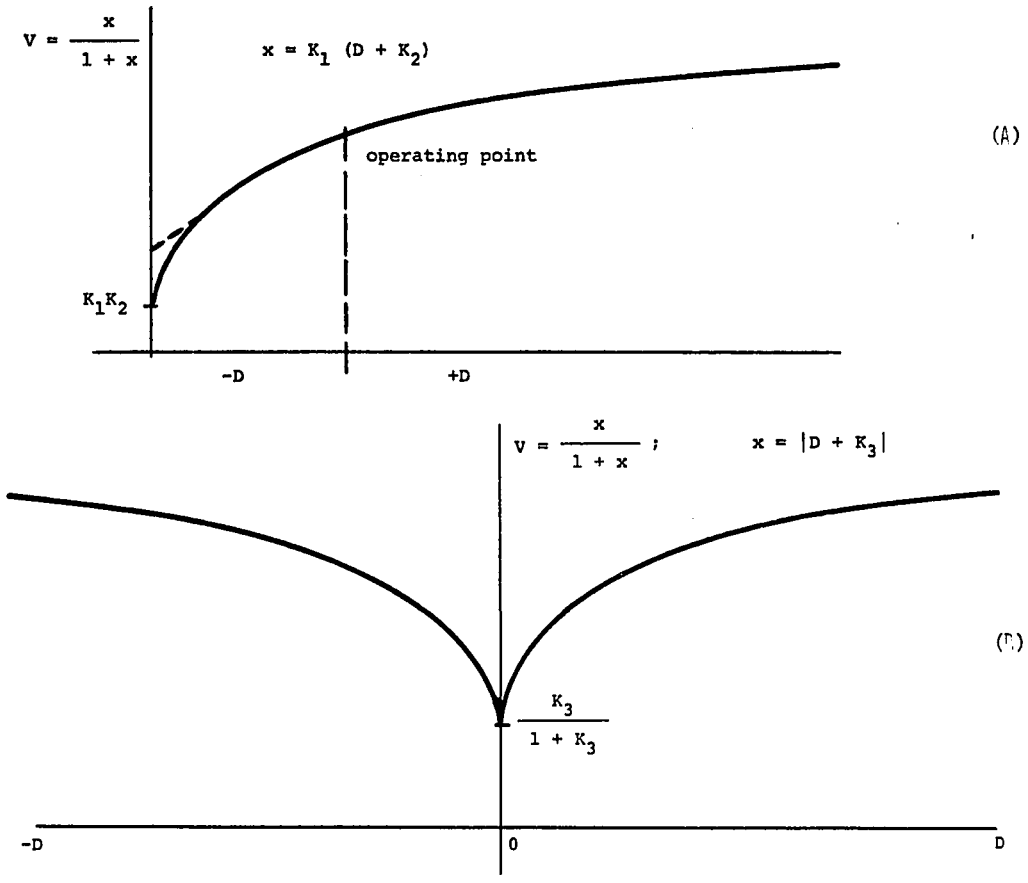

FIG.8.10 TWO HYPOTHETICAL COCHLEAR TRANSDUCER CHARACTERISTICS BASED ON DAVIS' 'RESISTANCE MICROPHONE' THEORY.

with V = f(x) as in Equation 8.9 and the plot of V vs D is shown in Fig.8.10b. Further discussion of the various formulations of the conversion law will be given in Chapter 9 within the context of the simulated cochlear potentials.

8.3.4. Internal electrical dynamics of the cochlear transducer

When describing the process of the haircell potential generation the resistances and capacitances associated with the haircell must be taken into account. The potentials observed by an electrode not actually inside the cell body will be greatly affected by the electrical filtering effects produced by the haircell body and surrounding membranes.

A greatly simplified picture of the haircell is shown in Fig.8.11 and its equivalent electrical circuit in Fig.8.12. The justification for using a lumped representation instead of a distributed one originates in the nerve membrane calculations of Cooley and Dodge (91). They found that it is permissible to 'lump' 500 micron long longitudinal segments while still retaining sufficient continuity in calculating field and propagation effects. Although the haircell may not be as uniform as a nerve axon, it is only 20-50 microns long and, therefore, the lumped representation of Fig.8.12 is considered to be permissible.

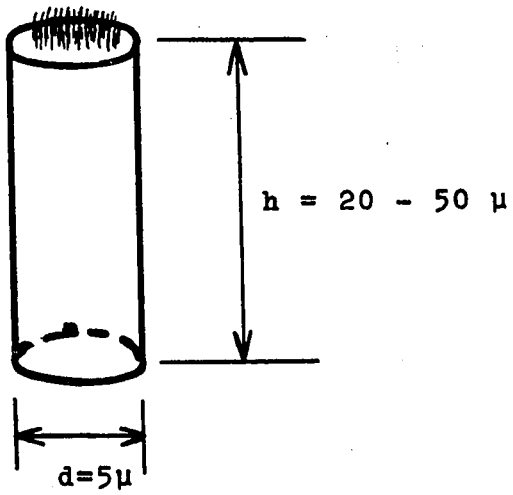

Fig.8.11 Simplified haircell geometry. (Numericel data from Spoendlin[92]).

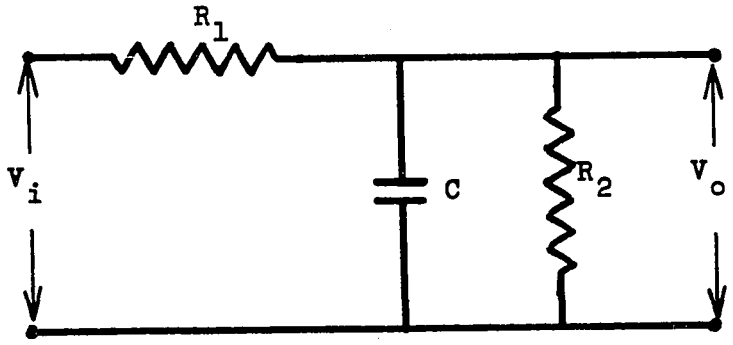

Fig.8.12 'Lumped' representation of the circuit properties of the haircell body and membranes.

First we calculate the minimum and maximum values of the haircell area corresponding to the change in haircell size from the base of the cochlea to its apex. Using data from Spoendlin (92):

$$A_{max} = 8.2 \times 10^{-6} \text{ cm}^2$$

$$A_{min} = 3.5 \times 10^{-6} \text{ cm}^2$$

Since data do not exist for the electrical properties of the haircell we are forced to take estimates from other neurophysiological data. After Cooley and Dodge (91) we also take the membrane capacitances to be 1 $\mu F/cm^2$. The membrane conductance is more difficult to estimate, since the conductance of the active or the inactive membranes varies greatly from cell to cell in the same tissues. These variations are even greater from tissue to tissue, but usually fall within the range of .1 to 1 $mmho/cm^2$ (93). Using these values we find the approximate values

$$C_{max} = 8.2 \times 10^{-12} \text{ F}$$

$$C_{min} = 3.5 \times 10^{-12} \text{ F}$$

$$R_{2_{max}} = 2.9 \times 10^{8} \text{ ohms}$$

$$R_{2_{min}} = 1.2 \times 10^{8} \text{ ohms}$$

The cell interior specific resistance is taken to be the same as the neuron axoplasm's (about 35 ohm-cm). Thus, the resistance of the cell interior will be

$$R_{1_{max}} = 4.5 \times 10^7 \text{ ohms}$$

$$R_{1_{min}} = 1.8 \times 10^7 \text{ ohms}$$

Now we are ready to calculate the characteristics of the circuit of Fig.8.12. The output voltage is represented by

$$V_0 = \frac{R_2}{(R_1 + R_2) + j\omega C R_1 R_2} V_i$$

and for 'minimal' and 'maximal' values the expressions are

$$\frac{.869}{1 + j\omega \times 5.5 \times 10^{-5}}$$

$$\frac{.865}{1 + j\omega \times 3.2 \times 10^{-4}}$$

respectively. Thus, interestingly, we find that for hair-cells in the basal turn (high frequency response region) the filter cutoff frequency is about 2.9 kHz and for haircells at the apex (low frequency response region) the cutoff frequency is about 500 Hz. However, before we attach any significance to these results we should remember that the preceeding calculations are not based on direct evidence and perhaps should not be taken too seriously.

8.3.5. External electrical dynamics

In order to draw conclusions regarding the external electrical dynamics of the haircell we would have to determine the details of the configuration of the electrical surroundings of one haircell (Fig.8.13), estimate the physical constants of the membranes and fluids and finally calculate the equivalent lumped network.

Unfortunately little information is available because only indirect data exist. Due to obvious experimental difficulties measurements yield results which are representative of a large segment of, or perhaps, the entire cochlea. These results are therefore more appropriately discussed in terms of the macroscopic potential distribution in the cochlea (Section 8.2). Due to the lack of specific information we will not attempt to describe further the configuration shown in Fig.8.13. As experimental evidence becomes available this may be done at a later date.

8.3.6. Noise

Cochlear potential waveforms displayed on an oscilloscope show that the electrical events of the cochlea as recorded by 'gross' electrodes are noisy. Since the noise due to the recording apparatus can be measured, it is easy to show that most of this noise is physiological in

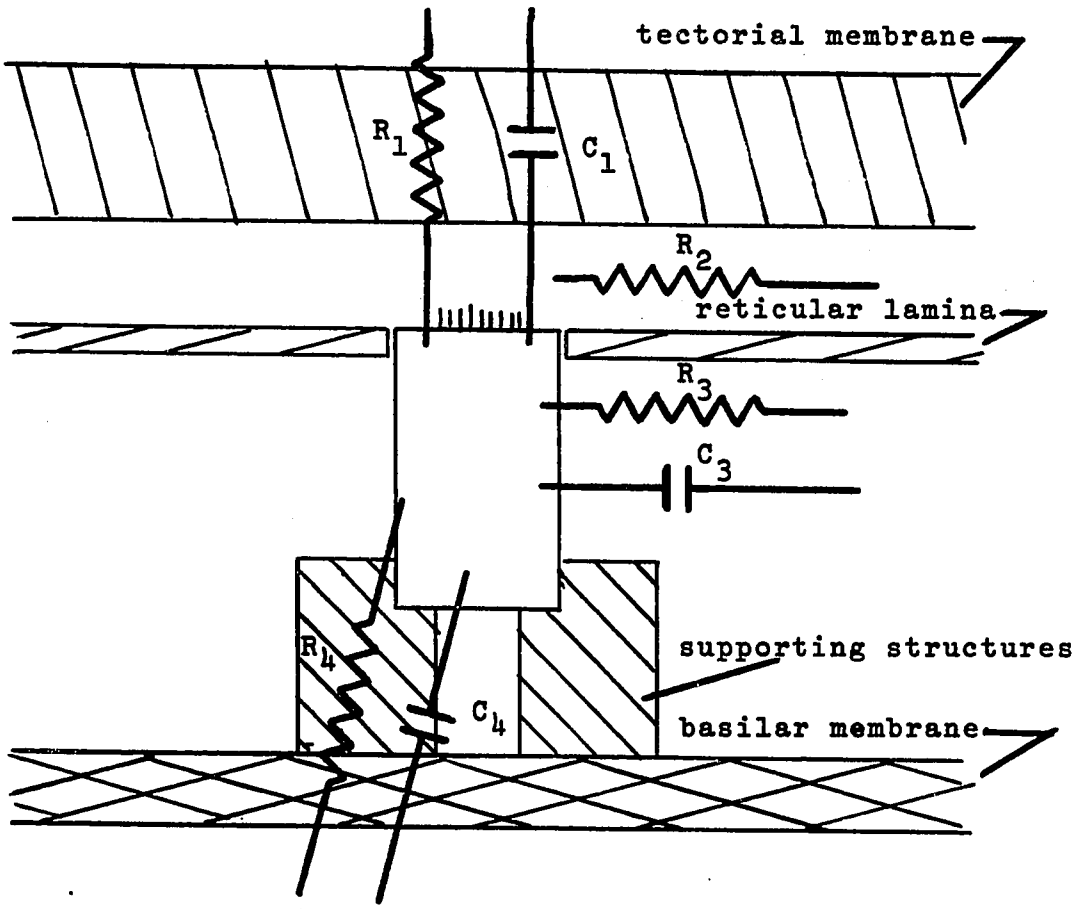

	resistance and capacitance:
R_1 and C_1	to scala media and scala vestibuli
R_2	along scala media
R_3 and C_3	between neighbouring haircells
R_4 and C_4	to scala tympani

Fig.8.13 The electrical surroundings of a haircell.

origin. Furthermore, since noise due to muscle contraction and breathing can be recognized and eliminated, it may be stated with some certainty that the ongoing physiological processes of the cochlea are inherently 'noisy' from the electrical point of view. This noise may have many origins: it may be noise associated with random events in metabolism, membrane permeability, etc.; it may originate in mechanical motions associated with haircell stimulation or in the generation of streaming potentials. The possibility that noise is an inherent property of the conversion process cannot be ruled out, however, and may have significance in the study of generator potential-nerve firing relationships.

Conceptually we may separate the observed noise into two components according to origin: one part being due to the transduction process and the second part being due to other physiological processes. Now, according to the Central Limit Theorem, the noise due to the sum of several thousand haircells will be very close to the Gaussian, regardless of the statistical distribution of the noise of the individual transducer. Thus, it can be seen that adding random noise to our model of the single transducer will not affect the characteristics of the CM or the SP. This is supported by the fact that we do not know of any

experimental observation where modification of the cochlear potentials was due to the noise generated in the cochlea, except of course, in determining the thresholds of the observable potentials.

The inclusion of a noise potential generator in our model does not meaningfully alter the simulation of the generation of the cochlear potentials, but it can significantly complicate their implementation on the computer. Therefore, noise is not included in our model of the single transducer.

CHAPTER 9

SIMULATION OF THE COCHLEAR POTENTIALS

In this chapter we present the results of digital computer simulations of the cochlear potentials, making use of the models of the various parts of the peripheral auditory system. Our investigations here consider the linearity of the potential generation process, the frequency response of the cochlear potentials for the different turns, the behaviour of the CM and SP as a function of sound pressure level and the effect of efferent input to the haircell.

9.1. Organization of the simulation model and the computer program

The model for the simulation of the cochlear potentials is shown in Fig.9.1. The middle ear model (ME) and the basilar membrane model (BM) have been derived in Chapter 7. The transducer mechanism (TD) will be represented by the model discussed in Section 8.3 or its modification as given in Section 9.3.3 and the potential distribution factors (PDF) are determined by the relations given in Section 8.2. As shown on the diagram the various processes which are part of the overall model share a common parameter 'x', which is the distance from the stapes measured along the cochlea. A

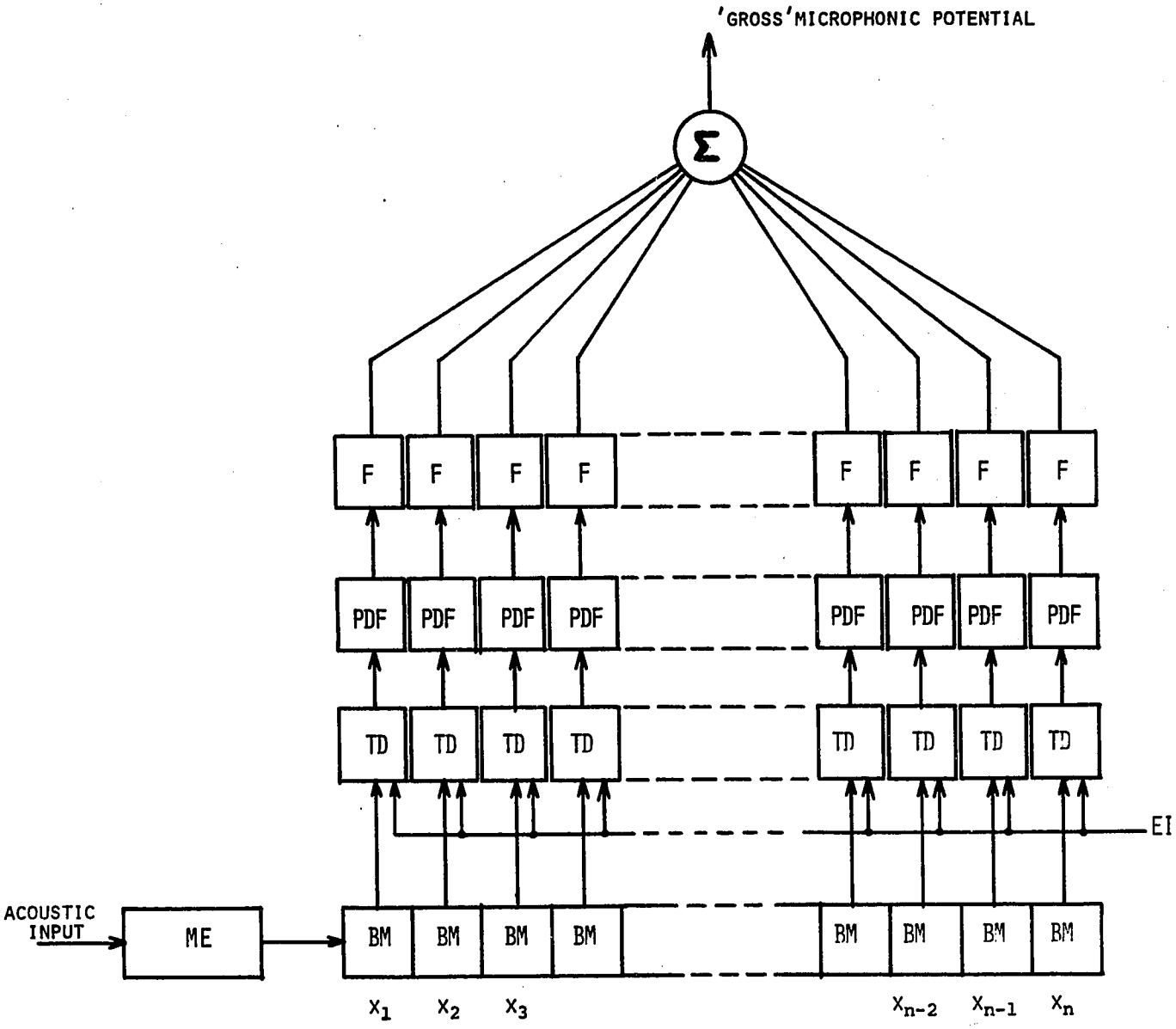

ME - MIDDLE EAR MODEL
BM - BASILAR MEMBRANE MODEL
TD - TRANSDUCER MECHANISM
PDF - POTENTIAL DISTRIBUTION FACTOR
F - FILTER
EI - EFFERENT INPUT
X_i - DISTANCE FROM THE STAPES, i=1,2,3,...n

FIG.9.1 SIMULATION MODEL

second parameter of great importance is the location of the electrode, but this parameter is incorporated into the potential distribution factors and is not shown explicitly in Fig.9.1.

For exactness, the output of every haircell along the basilar membrane should be calculated and summed but this is both impractical and unnecessary. In this respect the number of haircells to be considered is about 10000 and so 10000 calculations of the basilar membrane displacement and the transducer process output would be required. Timing analyses of the computer programs show that the calculations take approximately 10 msec per haircell per time step and so the total time per time step is 100 seconds. This is prohibitively long, since, for example, to determine the amplitude and phase of the model output in response to a sinusoidal input it is necessary to take about 20-30 time steps of appropriate size, needing over 30 minutes of computer time. Consequently, we decided to 'lump' the process with fewer discrete elements, by using 'segments' of the basilar membrane which may be considered to be moving in phase and by assuming that the haircells on that segment have identical outputs. If these simplifications can be shown to be permissible we may represent all the OHCs and IHCs within a segment by a single generator 'complex' containing 3 OHC

and 1 IHC models. It must be emphasized that since the phase shift along a 'segment' is small and since at this point no distinction is made between IHCs and OHCs this generator complex is representative of the individual haircell generator and differs from it only in a multiplying constant.

Consequently, the entire guinea-pig basilar membrane (length = 18 mm) is divided up into 180 segments, each 100 microns long. Thus, on each segment there are 10-12 rows of haircells, which seems to be a reasonably small number. To prove that these segments are not too large we took the 'worst-case' approach. Clearly, the phase shift along the basilar membrane will be the greatest for high frequencies and so we plotted the phase change over a segment as a function of distance along the basilar membrane for a 15 kHz input. Note that 15 kHz is 5 kHz higher than the highest frequency (10 kHz) considered either experimentally or in the simulation. In Fig.9.2. the curves for 15, 5, 1 and 0.1 kHz are given. The dotted parts of the curves indicate that the amplitudes dropped below 0.5% of the maximum amplitude and consequently, for the frequencies 15 and 5 kHz respectively, the contribution of haircells from these regions is negligible. Thus we see that even for the 'worst case' (15 kHz) the largest phase shift along a segment is 13 degrees and for the great majority of segments the phase shift is below 10 degrees.

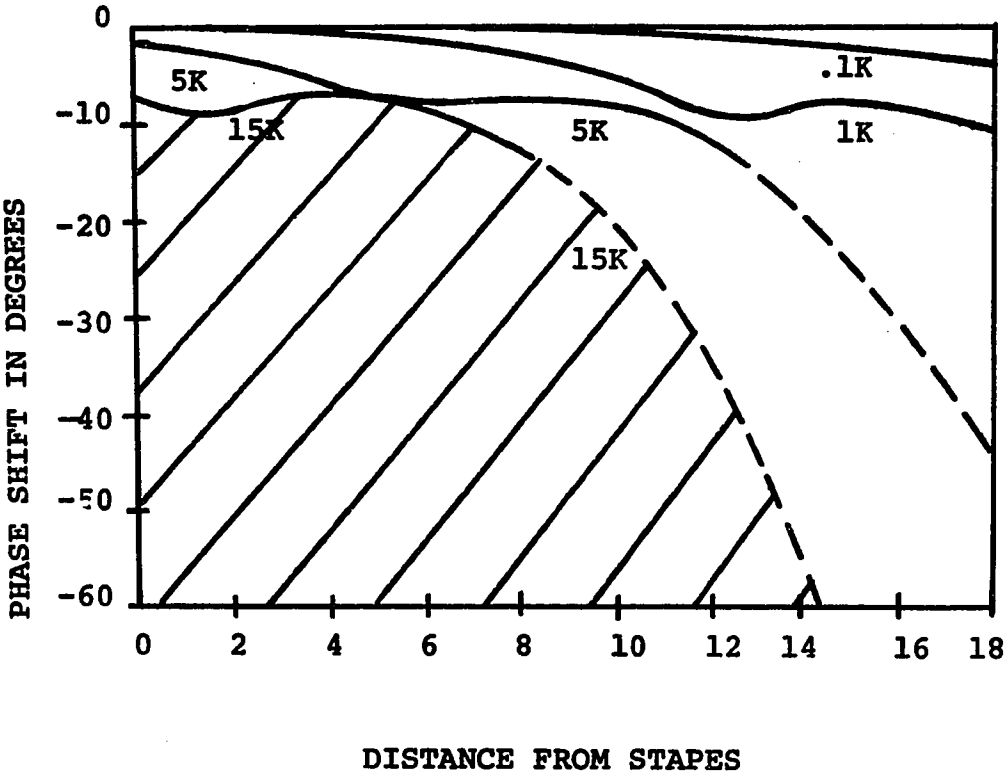

Fig.9.2 Plot of phase shift along a 100 micron segment of the basilar membrane as a function of location along the basilar membrane. The curves were drawn for input frequencies of 15, 5, 1 and .1 kHz. The dotted parts of the curves indicate that the amplitudes dropped below 0.5% of the maximum amplitude.

Such a phase shift will not cause significant cancellation effects over a segment and so the 100 micron segment length is acceptable.

In Sections 8.3.4 and 8.3.5 we discussed the electrical dynamics of the haircell and the surrounding structures and demonstrated a low-pass filter between the site of the generation of the cochlear potentials and the location of the electrode. Since the parameters of this filter cannot be specified due to the lack of relevant experimental data, we employ a simple digital filter of the form

$$V_o(t_m) = \sum_{i=-n}^{n} V_i\{(km + i)\Delta t\} \qquad (9.1)$$

where

V_o = output point

V_i = input samples

$1/\Delta t$ = initial sampling frequency

m = number of points the average is moved

$t_m = k(m \times \Delta t), \qquad k = 1,2,3,...$

The cutoff point of this filter is determined by the number of points used in the linear average (Fig.9.3). If the same cutoff point is chosen for all filters, it is not necessary to determine the filtered output of each transducer separately but for calculation purposes the filter may be considered to follow the summation.

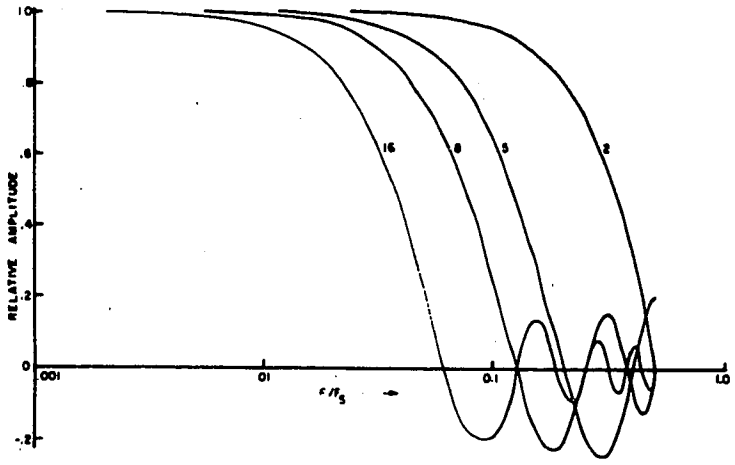

Fig.9.3a Frequency response curves for various moving linear averages. The numbers on the curves denote the number of points used in the averages.

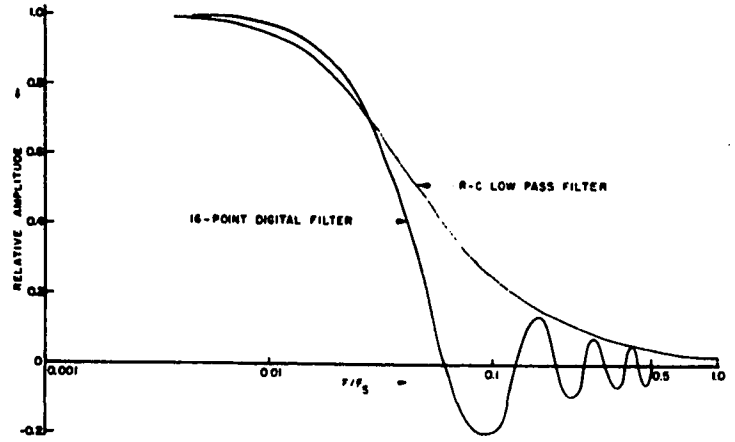

Fig.9.3b Comparison of a 16-point moving linear average with a low pass RC filter having the same 3-db point.(From Stauffer[94])

The simulation of the cochlear potentials is carried out on digital computers available at the McGill Computing Center (IBM 7044 and 360/50) and at the Otolaryngological Research Laboratories (LINC-8). Using the LINC-8 and the campus-wide RAX network which allows remote entry into the 360/50 system it is possible to run the simulation 'on-line'. The LINC-8 permits the use of such display devices as an oscilloscope and a digital plotter and the model's parameters can be modified instantaneously via an attached teletypewriter. Thus, the versatility of digital techniques is combined with the convenience found in analog computers. The flow diagram shown in Fig.9.4. presents the features of the simulation programs, of which a number of variations were written in FORTRAN.

9.2. Linearity of the transduction process and the waveform of the 'gross' CM

The evidence for the linearity of the transduction process is that for sinusoidal stimulation of the ear there is a remarkable lack of distortion in the CM even at high intensities. With reference to Fig.3.13 we may quote Davis' words to summarize the accepted ideas in this respect: "...Further increase in the intensity of the stimulus causes actual decrease in the electrical output. This relationship is most unusual for a mechanical system, and it is even more

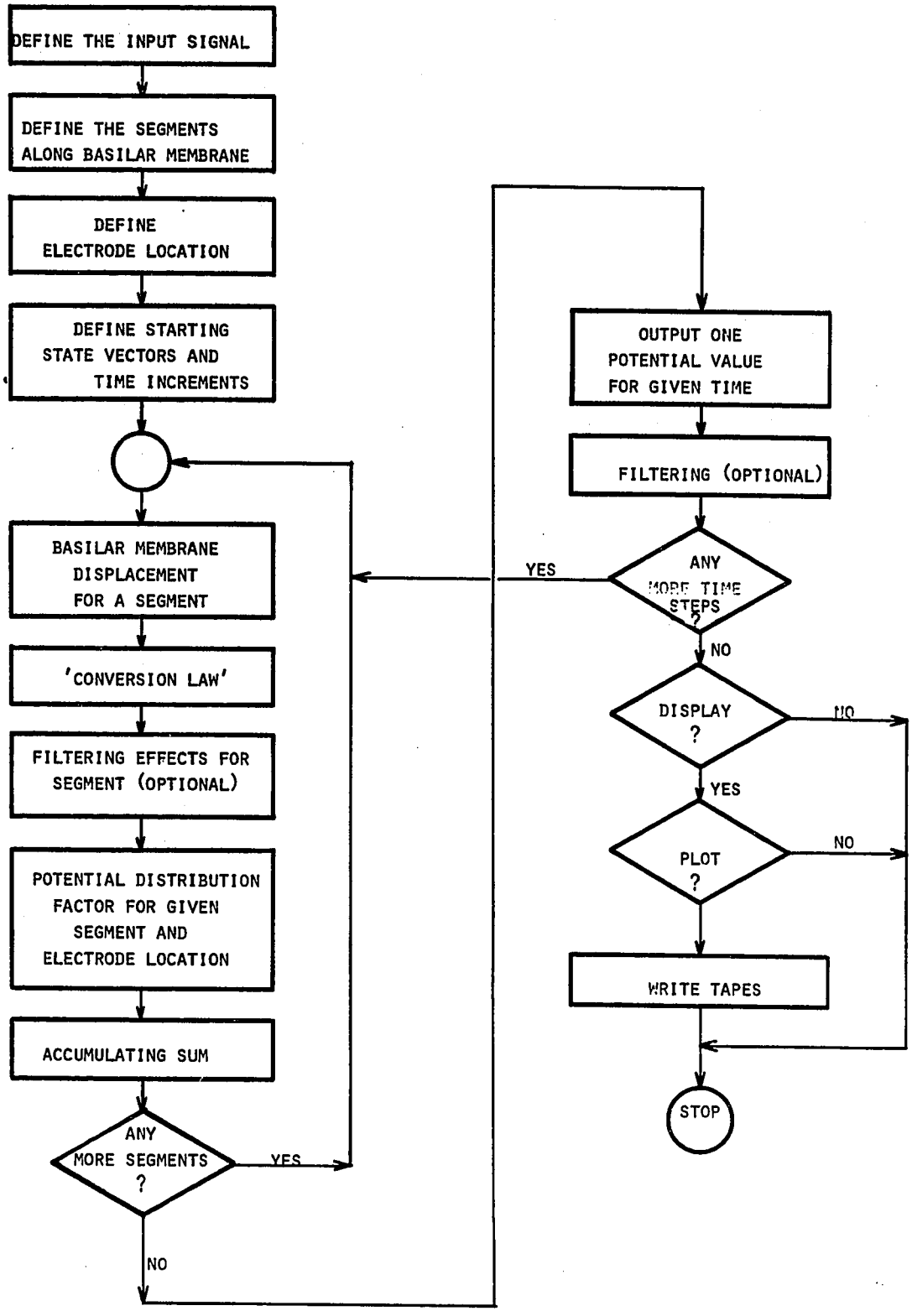
DEFINE THE INPUT SIGNAL
DEFINE THE SEGMENTS ALONG BASILAR MEMBRANE
DEFINE ELECTRODE LOCATION
DEFINE STARTING STATE VECTORS AND TIME INCREMENTS
BASILAR MEMBRANE DISPLACEMENT FOR A SEGMENT
'CONVERSION LAW'
FILTERING EFFECTS FOR SEGMENT (OPTIONAL)
POTENTIAL DISTRIBUTION FACTOR FOR GIVEN SEGMENT AND ELECTRODE LOCATION
ACCUMULATING SUM
ANY MORE SEGMENTS ?
YES
NO
OUTPUT ONE POTENTIAL VALUE FOR GIVEN TIME
FILTERING (OPTIONAL)
ANY MORE TIME STEPS ?
YES
NO
DISPLAY ?
NO
YES
PLOT ?
NO
WRITE TAPES
STOP

extraordinary that the limitation and finally the reduction in the amount of electrical output is accomplished without distortion of the waveform. The ear seems to have a true 'automatic gain control'." (95)

As we have discussed in Sections 5.1.2 and 5.3 the assumption regarding the linearity of the transduction process is both restrictive and unnecessary. In Sections 8.3.2 and 8.3.3 we have already presented some non-linear transduction functions and now we will show that such transduction functions are indeed compatible with physiological observations.

Our approach to this problem is very simple and straightforward. Using the conversion law given in Section 8.3.2 and the rest of the model as described in Section 9.1 we have simulated the potential output both for a single haircell 3.5 mm distant from the stapes, and also for the 'gross' CM potential recorded by an electrode at the same location. Fig.9.5 shows the output of the single haircell in response to a sinusoidal stimulus of varying intensity. This output is also sinusoidal, at low intensities, but at 80 db SPL the distortion becomes noticable and at 110 db the output is essentially a square wave. On the other hand Figs.9.6 and 9.7 show that although there is some distortion of the simulated 'gross'

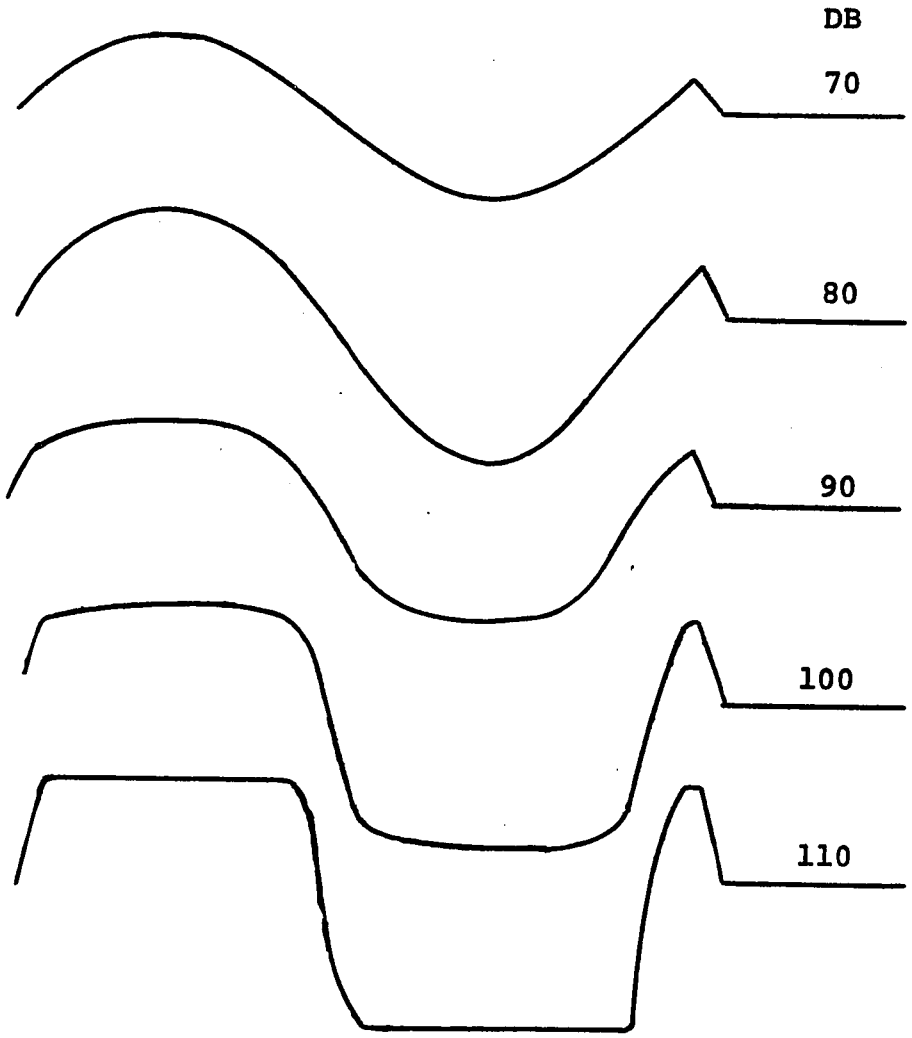

Fig.9.5 Waveforms of the cochlear potential generated by a single haircell as a function of sound pressure level. HC located at 3.5 mm; electrode at 3.5 mm; attenuation 6 db/mm. Stimulus: 7000 Hz sinewave.

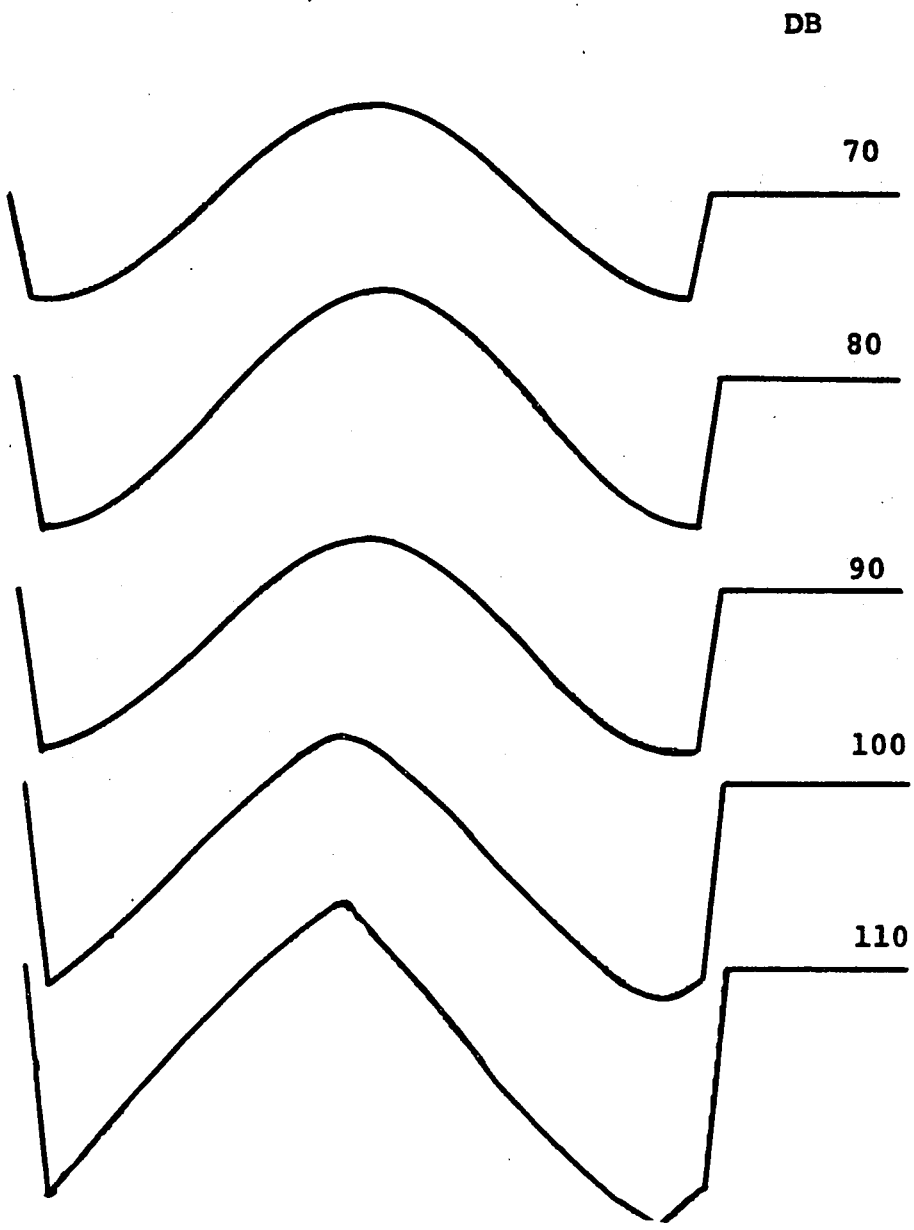

Fig.9.6 Waveforms of the 'gross' cochlear potential arising from 180 HCs distributed along the cochlea. The individual HCs produce the output shown in Fig.9.5. Electrode located at 3.5 mm; attenuation 6 db/mm. Stimulus: 7000 Hz sinewave.

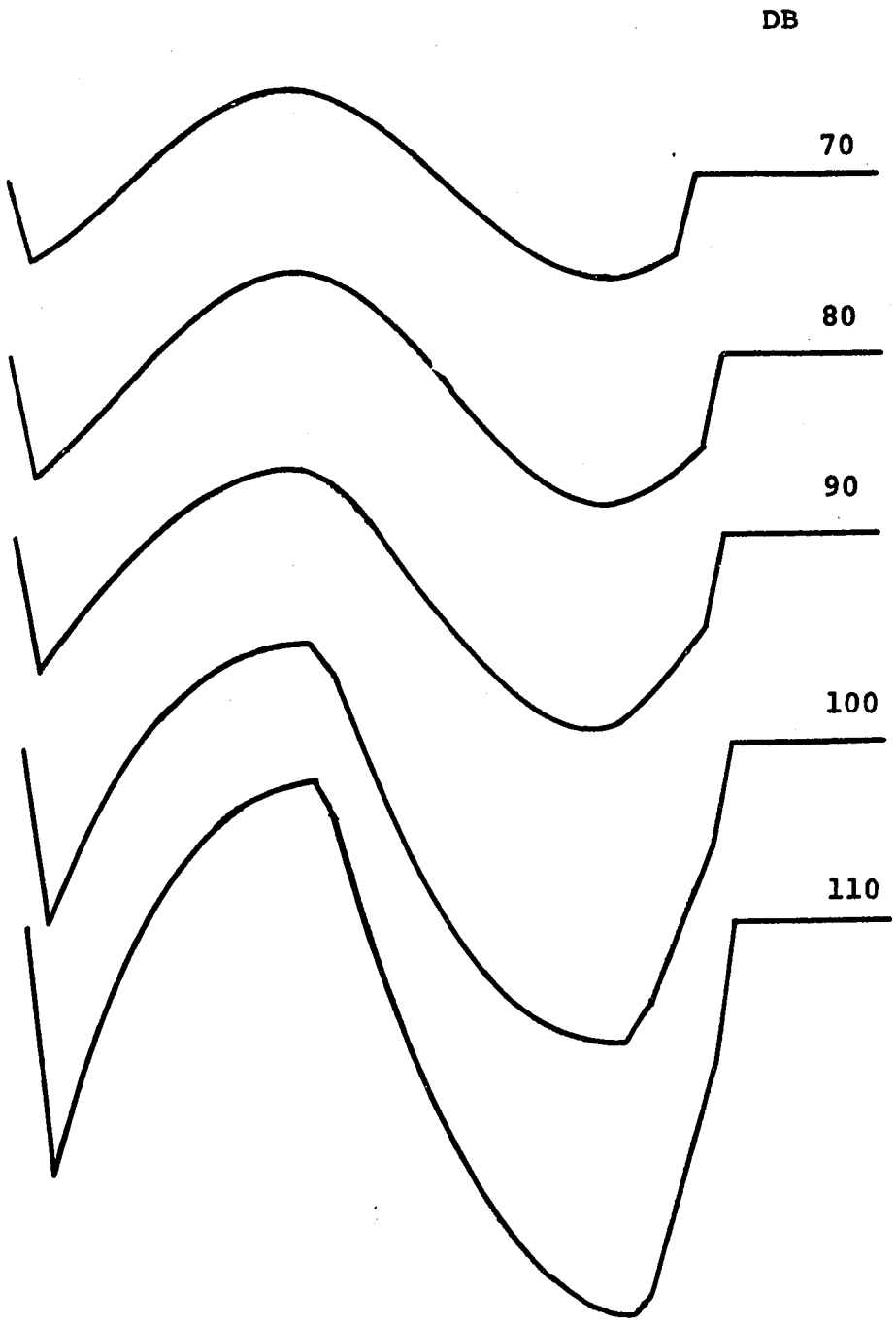

Fig.9.7 Waveforms of the 'gross' cochlear potential arising from 180 HCs distributed along the cochlea. The individual HCs produce the output shown in Fig.9.5. Electrode located at 3.5 mm; attenuation 0 db/mm. Stimulus: 7000 Hz sinewave.

potential arising from the distributed HCs all along the cochlea, nevertheless the waveforms resemble sinusoidal waves even at 110 db SPL. It must be emphasized that the model used here does not even include the filtering effects which exist in the real system due to membrane capacitances (see Sections 8.3.4 and 8.3.5). Our aim first is to prove that the distributed nature of the basilar membrane and the haircell potential generators can themselves account for the elimination of waveform distortion. In addition, filtering of the waveforms further reduces distortion (Fig.9.8) by eliminating higher harmonics. It is also notable that for an electrode located 8.7 mm from the stapes, the 'gross' potential is considerably more distorted (Fig.9.9). This is a well known physiological fact: namely, high intensity CM recorded in Turn 2 (8.7 mm) can show 'clipping' of the waveforms while the Turn-1 (3.5 mm) CM remains undistorted.

On the basis of the foregoing we can state that the physiological evidence cannot be used to justify a claim that the mechanical-to-electrical transduction process is linear. Furthermore, as discussed in Section 5.1.1, other considerations also place the concept of a linear transducer in doubt. The conclusion is, therefore, that the individual cochlear transducer output bears a non-linear relationship to the stimulus, but that the 'gross' potentials observed will be similar to the sinusoidal input waveform with the degree

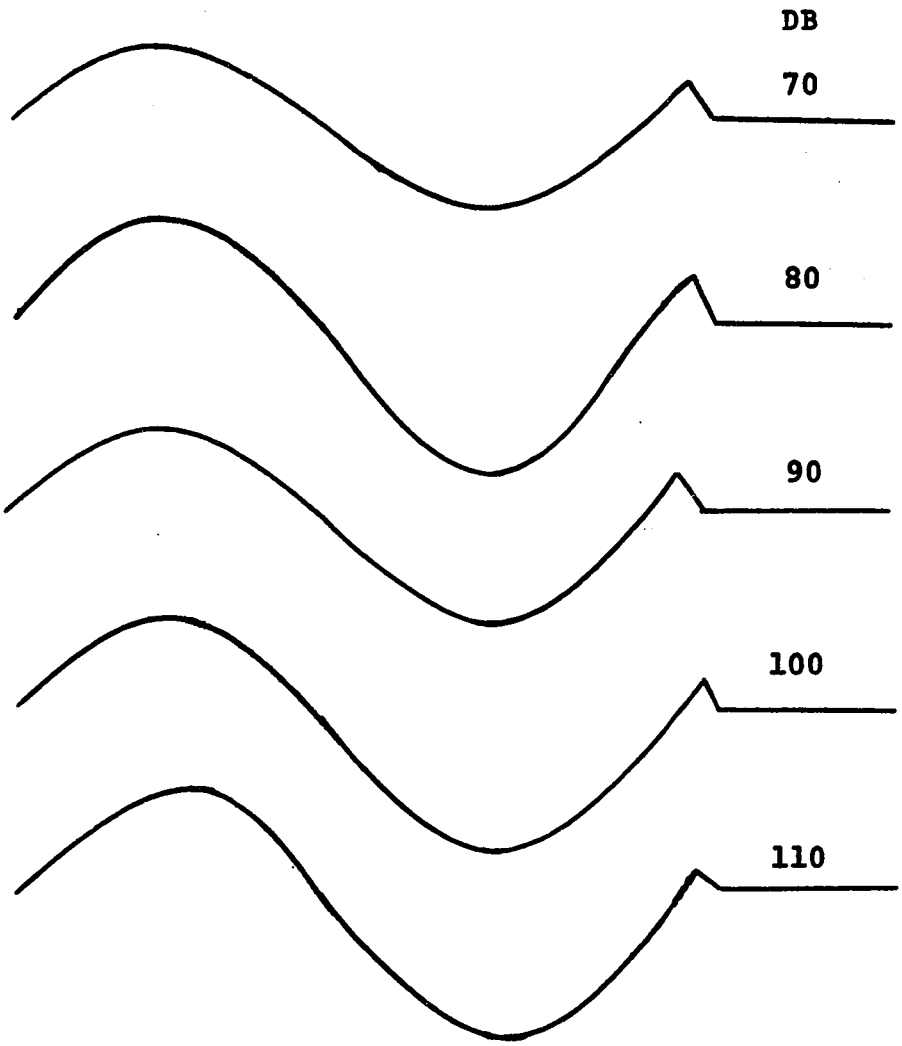

Fig.9.8a Waveforms of the filtered cochlear potential generated by a single haircell as a function of sound pressure level. HC located at 3.5 mm; electrode at 3.5 mm; attenuation 6 db/mm; 15 point linear average filter. Stimulus: 7000 Hz sinewave.

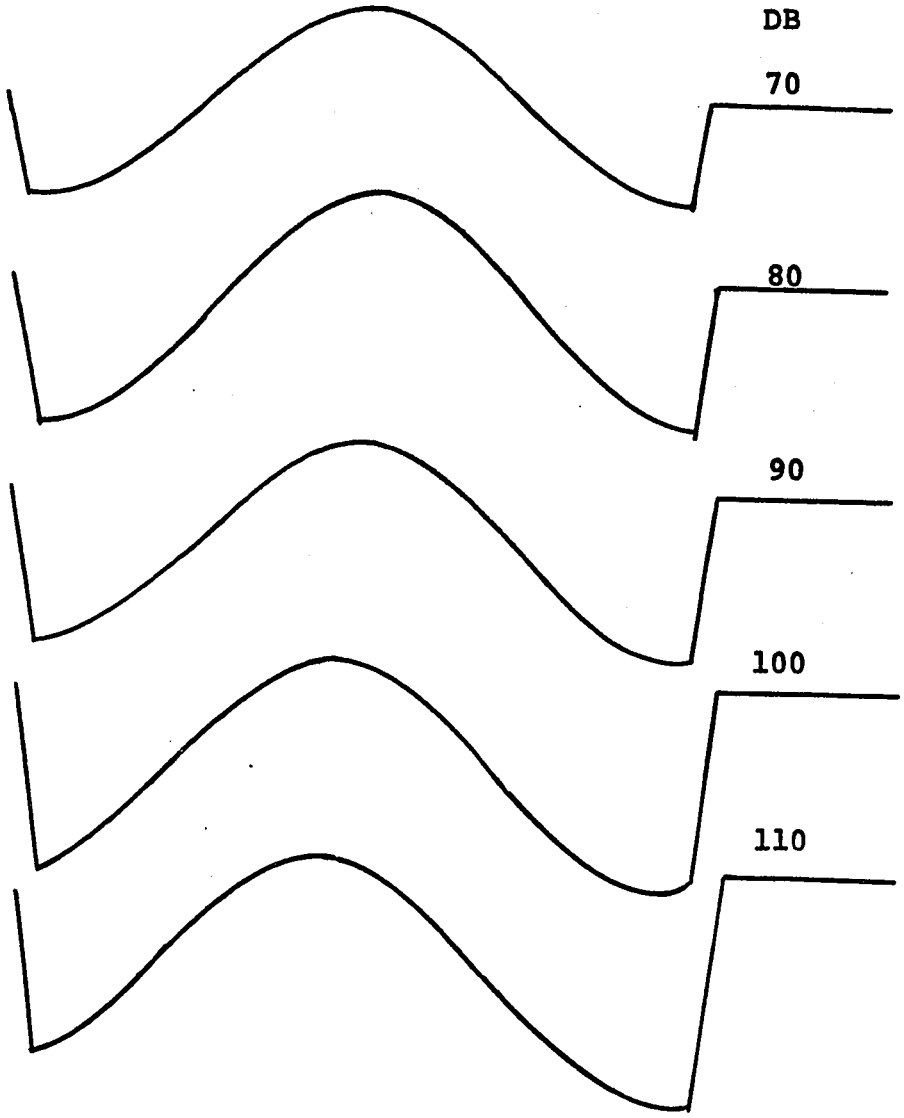

Fig.9.8b Waveforms of the filtered 'gross' cochlear potential arising from 180 HCs distributed along the cochlea. The individual HCs produce the output shown in Fig.9.5. Electrode located at 3.5 mm; attenuation 6 db/mm; 15 point linear average filter. Stimulus: 7000 Hz sinewave.

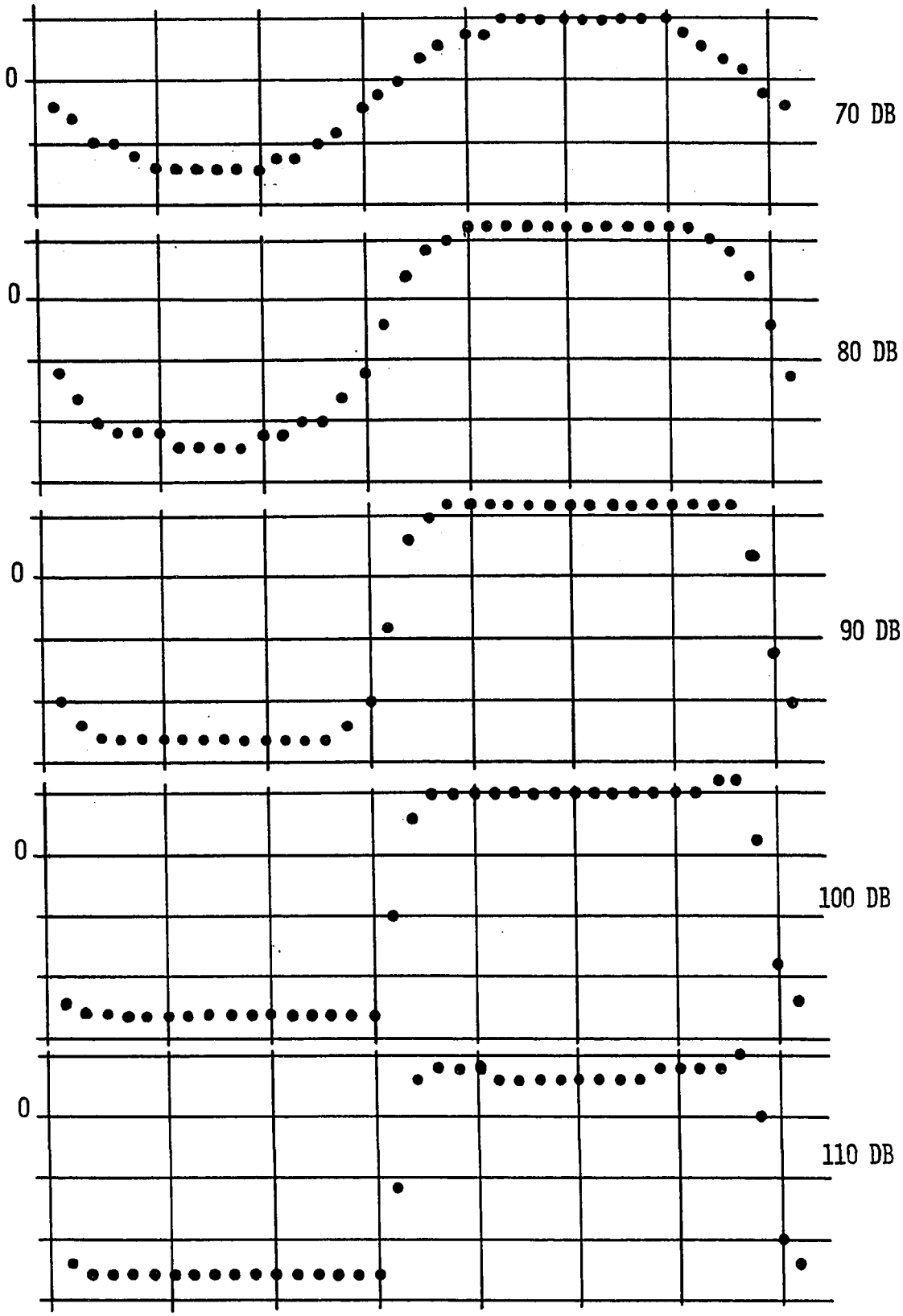

FIG.9.9 WAVEFORMS OF THE 'GROSS' COCHLEAR POTENTIAL ARISING FROM 180 HCs DISTRIBUTED ALONG THE COCHLEA. THE INDIVIDUAL HCs PRODUCE THE OUTPUT SHOWN IN FIG.9.5. ELECTRODE LOCATED AT 8.7 MM; ATTENUATION 6 DB/MM.

of distortion depending on the location of the recording electrode.

9.3. The simulation of the cochlear potentials as a function of sound pressure level

9.3.1. A simple phase cancellation mechanism

As presented in Chapter 3, the CM vs SPL functions[1] have the shapes shown in Figs.3.5 and 3.13 and furthermore, for high frequencies and Turn-1 electrodes at least, there is very little waveform distortion. Whitfield and Ross (70) have suggested that both the CM vs SPL curve shape and the lack of distortion are due to the same phase cancellation mechanism. According to their hypothesis, at high SPL levels the potential output of some haircells is maximal and the waveform is distorted. Other cells which are farther away from the region of maximal basilar membrane displacement move with lesser amplitudes. Due to the time delay involved between the mechanical displacements of the maximally and submaximally excited cells there is a phase difference between their potential output. It is supposed that the

---

[1] This relationship is commonly called the 'input-output' function in cochlear electrophysiology, but since this terminology is misleading for the system analyst the more appropriate 'CM vs SPL' function will be used.

cancellation resulting from this phase difference is sufficient to cause a decrease in the summated CM output of many cells while the SP will keep on increasing since more and more distant cells will be contributing as the SPL increases.

Since this hypothesis appears to be quite reasonable we have simulated the conditions described above with our model. The model parameters and the results are shown in Fig.9.10. It can be seen immediately that although the CM potential will reach a maximum, it will not decrease even for extremely high SPL levels. This indicates that the phase cancellation mechanism proposed by Whitfield and Ross is not sufficiently significant to produce the effects observed experimentally.

9.3.2 Modification of the transfer characteristics

An alternative hypothesis is that the individual haircell outputs decrease as the input sound intensity passes a certain limit. Suitable transfer characteristics may be obtained from the arcot function (see Section 5.1.4) in the manner shown in Fig.9.11. It is reasonable to assume that the individual haircell output must either stabilize at some value or it must go to zero as the sound pressure level increases. It is surprising to find, however, that there

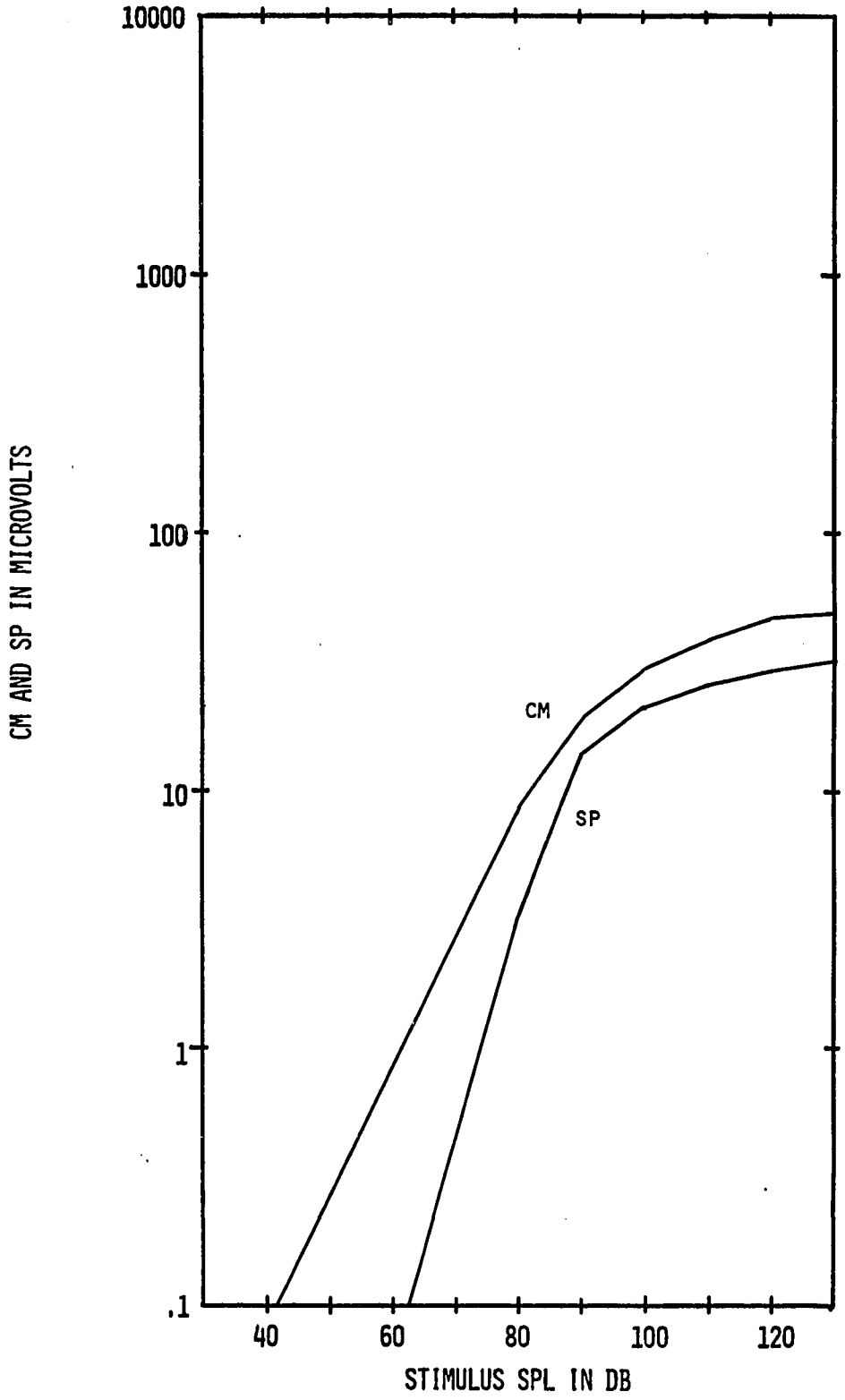

FIG.9.10 THE CM AND SP OUTPUTS OF ONE 'SEGMENT' 3.5 MM FROM THE STAPES USING THE JOHNSTONE MODEL (SECTIONS 5.14 AND 8.3.2). MODEL CONFIGURATION: IHC OPERATING POINT 60 DEGREES, OHC OPERATING POINT 130 DEGREES; ELECTRODE AT 3.5 MM; NO ATTENUATION.

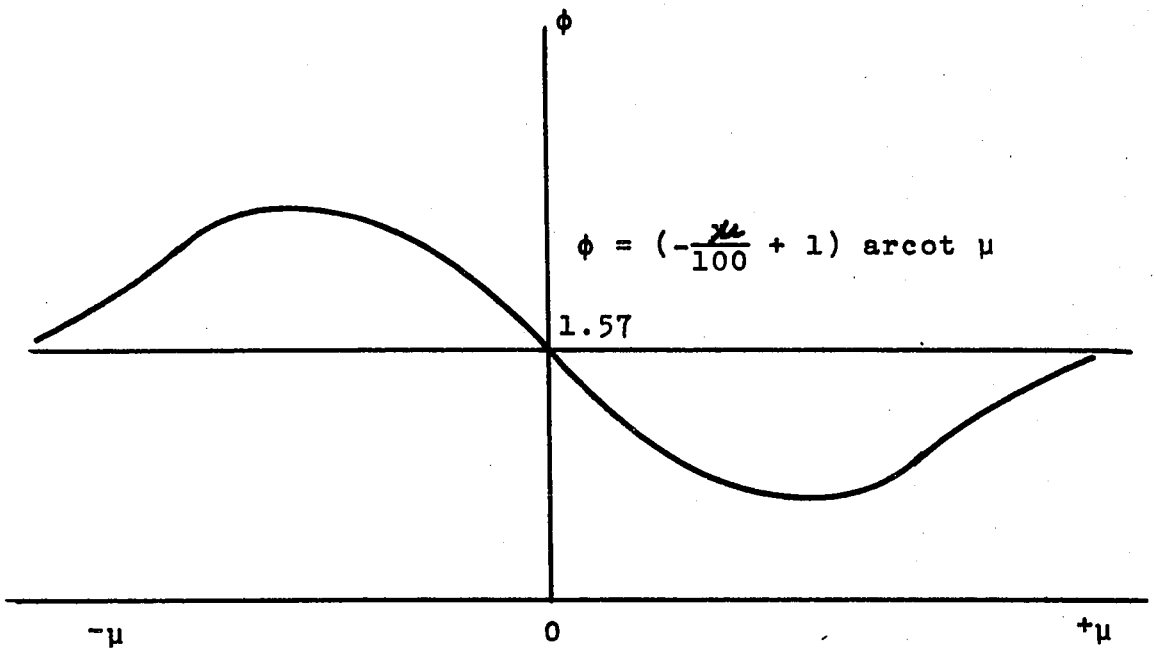

Fig.9.11 Modified 'arcot-type' transducer characteristics. The function is not plotted to scale.

is relatively little drop in either the individual haircell CM output or the gross CM potential before extreme distortion of the waveforms occurs (Figs.9.12 and 9.13). Filtering has little effect on the output of the individual haircell, but the 'gross' CM potential decreases to about 1/3 of its peak value. This decrease is accompanied, however, by a corresponding decrease in the SP which is contradictory to physiological evidence (see Fig.3.13).

9.3.3 Interference effects between out-of-phase IHC and OHC potential outputs

Since neither the simple phase cancellation mechanism nor the modified arcot transducer characteristics produces simulated cochlear potentials with the expected functional dependence on the sound pressure level, it is necessary to re-examine the assumption made earlier that the IHC and OHC models should be identical in every respect. The anatomical differences between the IHC and OHC and the observations of Bekesy (40) which suggest that the two types of haircells produce maximum CM for two different directions of bending of the hairs indicate that perhaps simulation should differentiate between the two types of cells. Considering Fig.4.3 which shows the cross-section of the organ of Corti, it is seen that the IHCs and the OHCs have different orientations. This is dynamically important, because if,

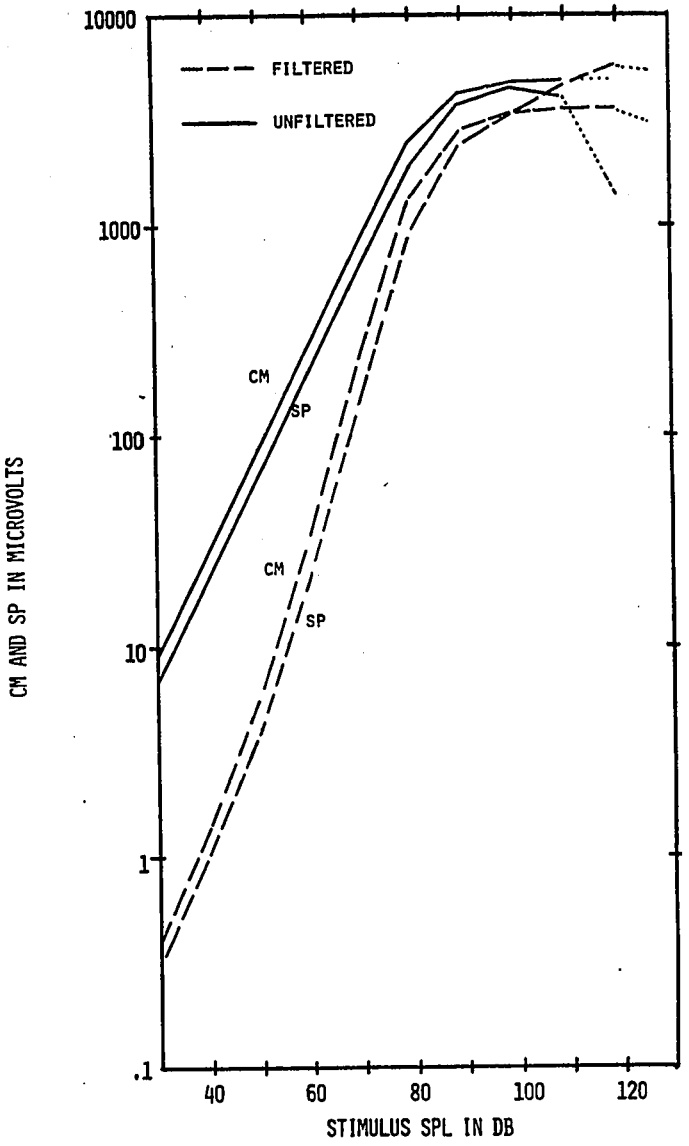

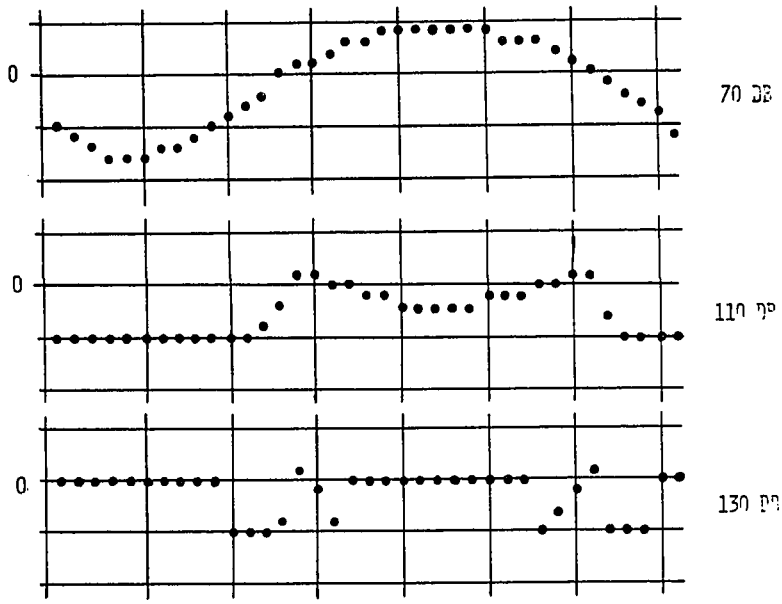

FIG.9.12 THE OUTPUT OF ONE 'SEGMENT' 3.5 MM FROM THE STAPES WITH TRANSFER CHARACTERISTICS SHOWN IN FIG.9.11. MODEL CHARACTERISTICS: ELECTRODE AT 3.5 MM; ATTENUATION 6 DB/MM; ELECTRODE 1 MM ABOVE THE BASILAR MEMBRANE;

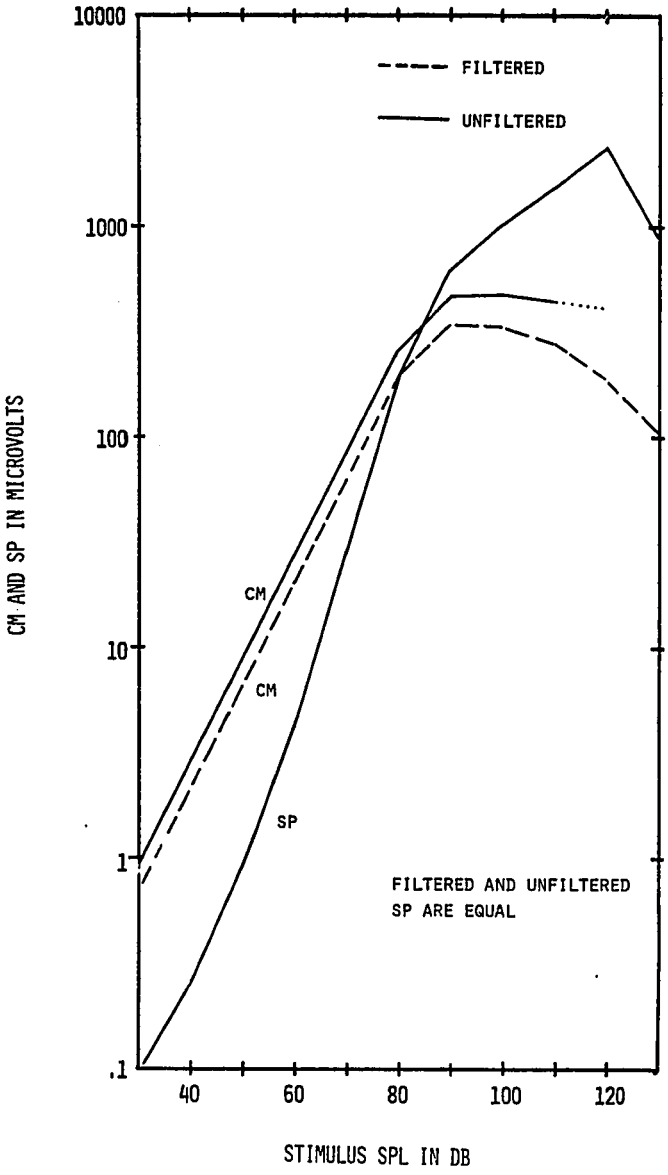

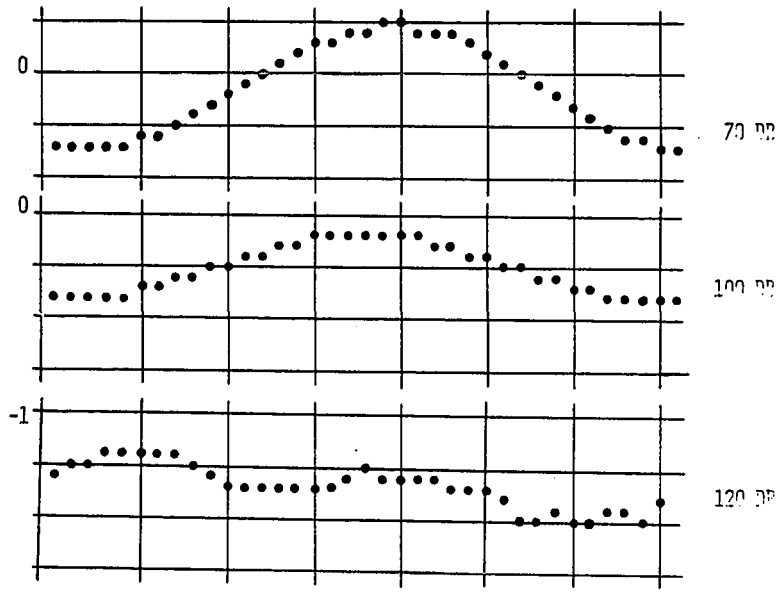

FIG.9.13 THE SIMULATED 'CROSS' POTENTIAL USING 180 'SEGMENTS' WITH TRANSFER CHARACTERISTICS SHOWN IN FIG.9.11. MODEL CHARACTERISTICS: ELECTRODE AT 3.5 MM; ATTENUATION 6 DB/MM; ELECTRODE 1 MM ABOVE THE BASILAR MEMBRANE; 15 POINT LINEAR AVERAGE FILTER.

for example, the hairs are bent towards the inner edge of the basilar membrane then the angle between the hair and the cell body center-line will increase for the IHC and decrease for the OHC. Thus, if the hair-to-cell angle is significant in determining the potential output of the cochlear transducer, the IHC and the OHC will produce signals with 180 degrees phase difference.

Even if the haircell orientation has no significance the IHC and OHC may produce out-of-phase signals. According to Bekesy (37) it is possible that the basilar membrane displacements in a plane perpendicular to the longitudinal axis of the cochlea have different directions for the parts carrying the IHCs and OHCs. Presumably in consequence the IHCs and OHCs respectively will bend the hairs in opposite directions, resulting in out-of-phase potentials.

The relative magnitudes of the potentials produced by a single IHC and OHC are also of importance. It has been demonstrated that OHCs are more susceptible to acoustically induced structural damage than the IHCs (96). It is likely that this occurs because the OHCs are subject to larger displacements than the IHCs and consequently the former reach a region of dangerous overload for smaller SPLs than the latter. The different sensitivities of the IHCs and OHCs are possibly also indicated by the observation of Engstrom and

his co-workers that at rest the hairs of the IHCs do not touch the tectorial membrane but some hairs of the OHCs do (39). Since quantitative physiological data are non-existent we conduct a number of simulation experiments to determine the effect of changes in relative OHC and IHC sensitivities on the cochlear potentials. As a result it is found that the best correspondence with cochlear potential experimental data is obtained when the OHCs are made 10-15 times more sensitive than the IHCs.

In the following computer experiments we use the simulation model discussed in Section 9.1 with appropriate modifications to represent the difference between IHCs and OHCs. In particular, we now assume that the IHC and OHC potential outputs are out of phase by 180 degrees and the IHC output reaches its maximum for 20-30 db higher sound pressure levels than the OHC. Figs.9.14a and 9.14b show the behaviour of the CM amplitude and the SP of a single haircell 'complex' at 500 Hz and 7000 Hz as a function of SPL. The curves have similar shapes, the differences reflecting the different responses of the basilar membrane, 3.5 mm from the stapes, to 500 and 7000 Hz. The response of the individual haircell is as expected: the CM potential increases, reaches a maximum and then starts to decrease but the SP never reaches a plateau. The effect of filtering is

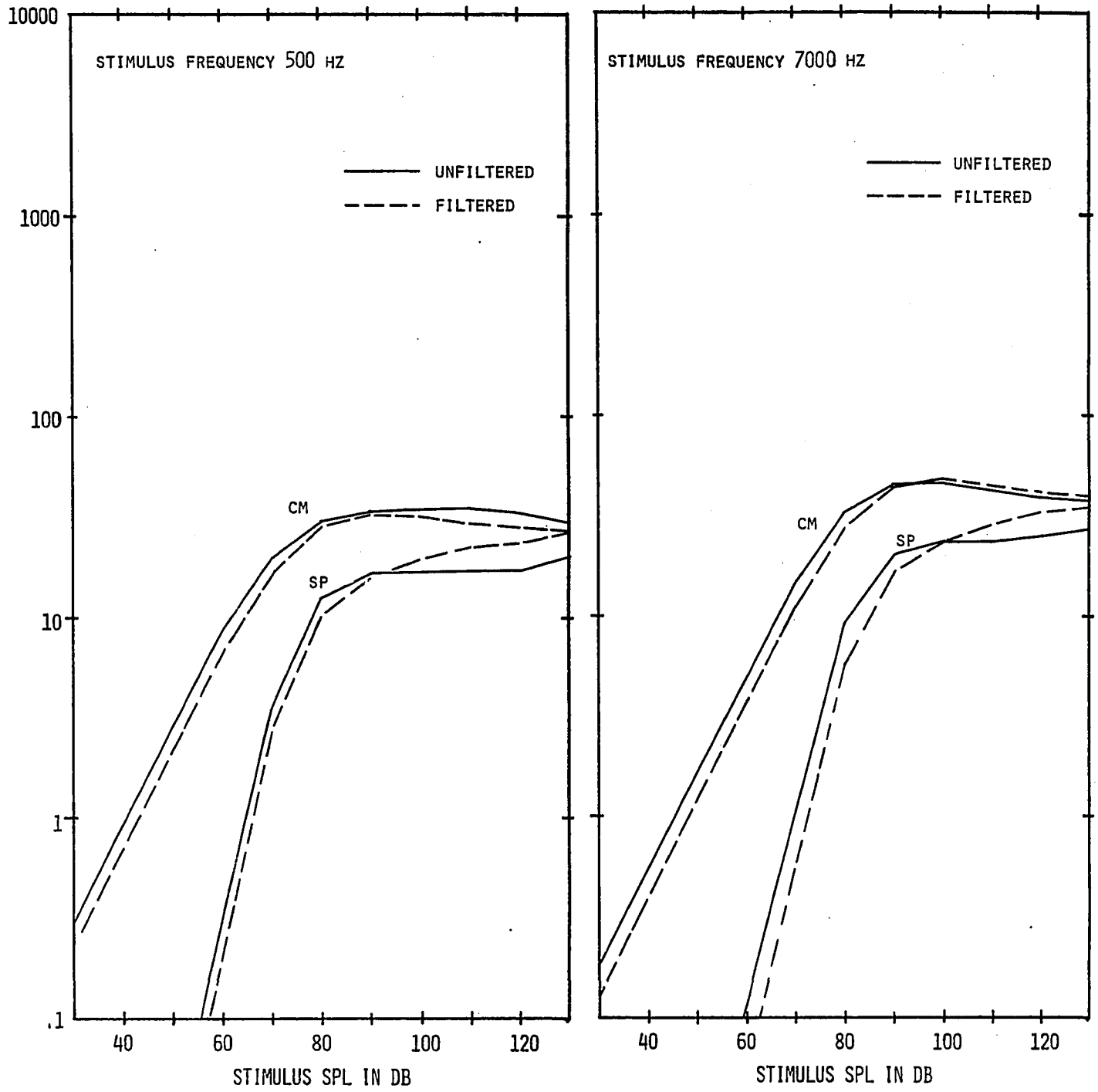

FIG.9.14 CM AND SP AS A FUNCTION OF STIMULUS SPL. MODEL CONFIGURATION: 1 'SEGMENT' AT 3.5 MM; ELECTRODE AT 3.5 MM; ATTENUATION 6 DB/MM; ELECTRODE 1 MM ABOVE THE BASILAR MEMBRANE; 15 POINT LINEAR AVERAGE FILTER.

slight up to about 90 db at which level the unfiltered output starts to become distorted. Since the individual haircell output has never been recorded experimentally no comparison of the single haircell 'complex' output and a real haircell output can be made.

It is possible, however, to compare 'gross' potentials measured experimentally and simulated dynamically by our model. In Figs.9.15-9.18 the results of the 'gross' potential simulation are shown for 100, 500, 2000 and 7000 Hz in Turns 1, 2 and 3. For 100 Hz the simulated CM outputs reach approximately the same peak level in all three turns of the cochlea, but this occurs at different sound pressure levels: Turn 3 reaches the maximum at about 90 db SPL, Turn 2 between 90 and 100 db SPL and Turn 1 at 100 db SPL. This compares favorably with experimental data obtained by Tasaki (24) for 103 Hz (see Fig.3.5). For 500 Hz no direct comparison is possible, because Tasaki's data do not include the corresponding responses but our results (Fig.9.16) seem to fall somewhere between the curves for 280 Hz and 1020 Hz on Fig.3.5. For this frequency the curves become 'flatter' and the peak amplitude smaller as we proceed from Turn 1 to Turn 3. For 2000 Hz (Fig.9.17) the results for Turn 1 and Turn 2 are comparable with Tasaki's curves for 2370 Hz. Turn 2 peak output is smaller and reached at a lower SPL

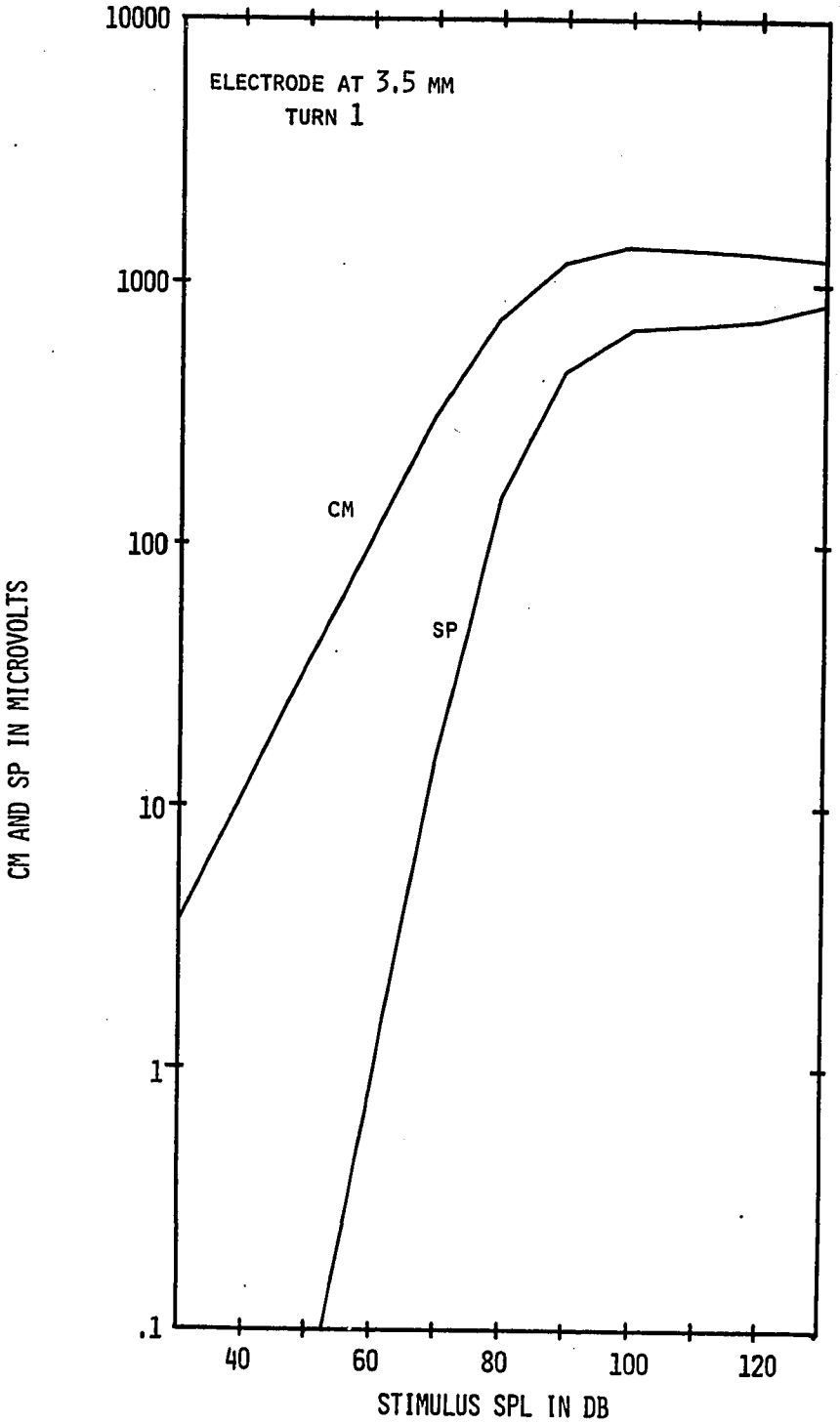

(A)

FIG.9.15 CM AND SP AS A FUNCTION OF STIMULUS SPL. MODEL CONFIGURATION 180 'SEGMENTS'; ATTENUATION 6 DB/MM; ELECTRODE 1 MM ABOVE BASILAR MEMBRANE. STIMULUS 100 HZ SINEWAVE.

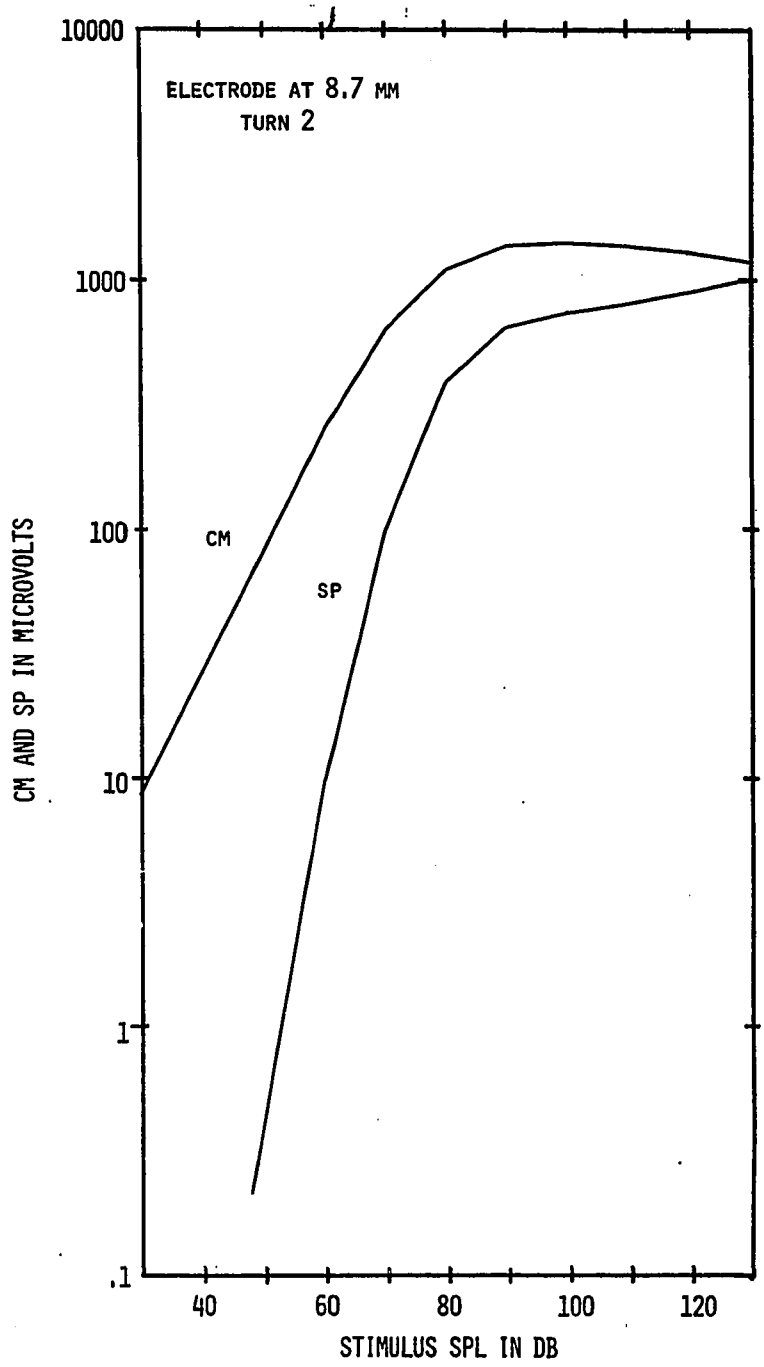
ELECTRODE AT 8.7 MM
TURN 2
10000
1000
100
10
1
.1
CM
SP
CM AND SP IN MICROVOLTS
40
60
80
100
120
STIMULUS SPL IN DB

(B)

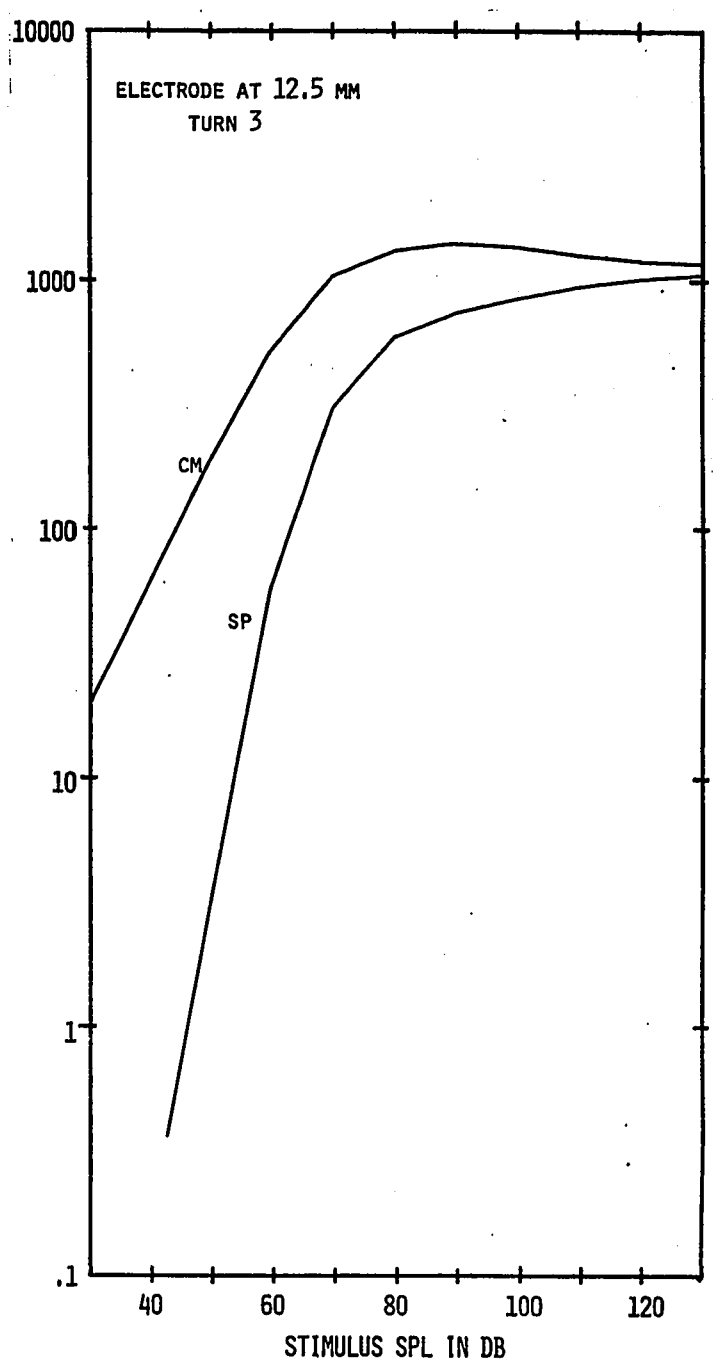
ELECTRODE AT 12.5 MM
TURN 3
10000
1000
100
10
1
.1
CM
SP
40
60
80
100
120
STIMULUS SPL IN DB

(C)

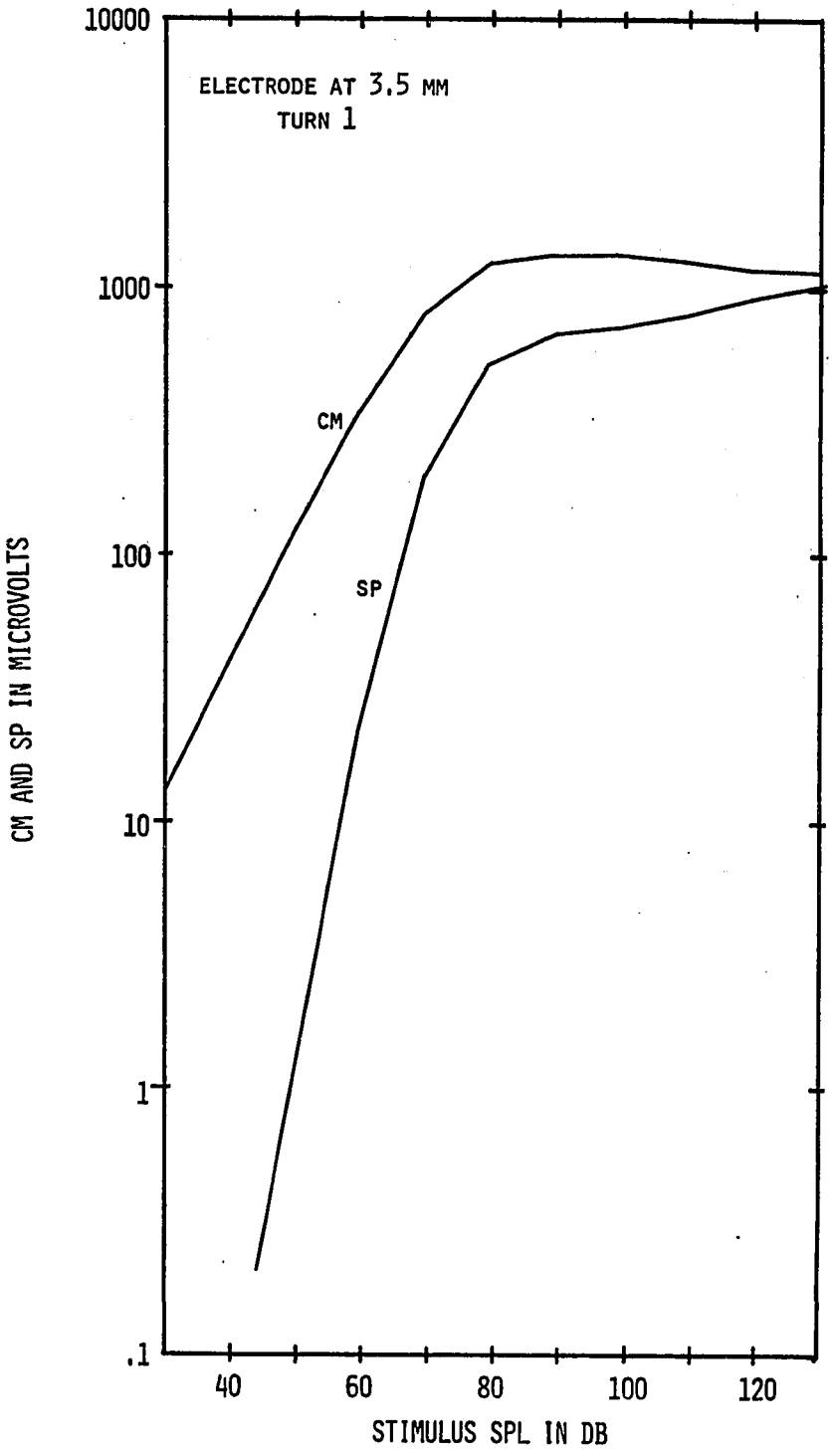

(A)

FIG. 9.16 CM AND SP AS A FUNCTION OF STIMULUS SPL. MODEL CONFIGURATION 180 'SEGMENTS'; ATTENUATION 6 DB/MM; ELECTRODE 1 MM ABOVE BASILAR MEMBRANE. STIMULUS 500 HZ SINEWAVE.

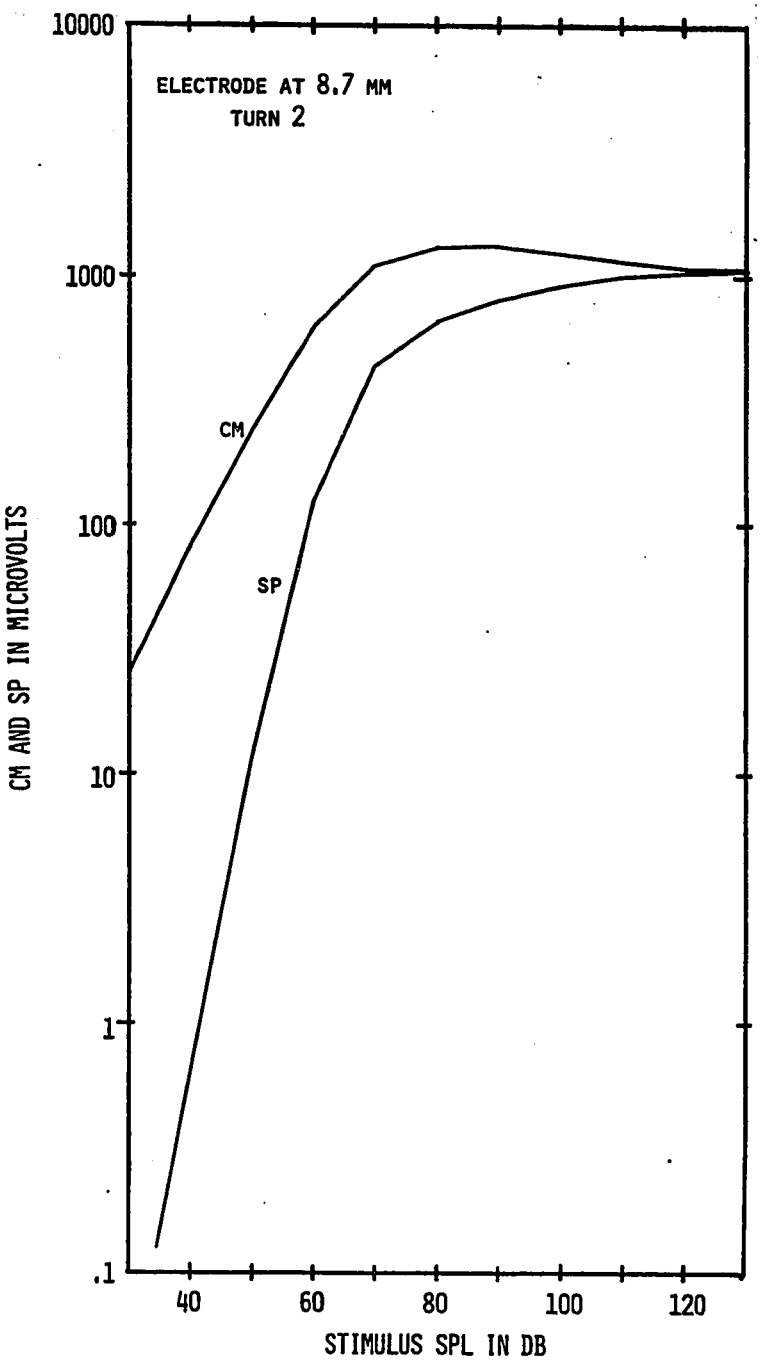
ELECTRODE AT 8.7 MM
TURN 2
10000
1000
100
10
1
.1
CM
SP
CM AND SP IN MICROVOLTS
40
60
80
100
120
STIMULUS SPL IN DB

(B)

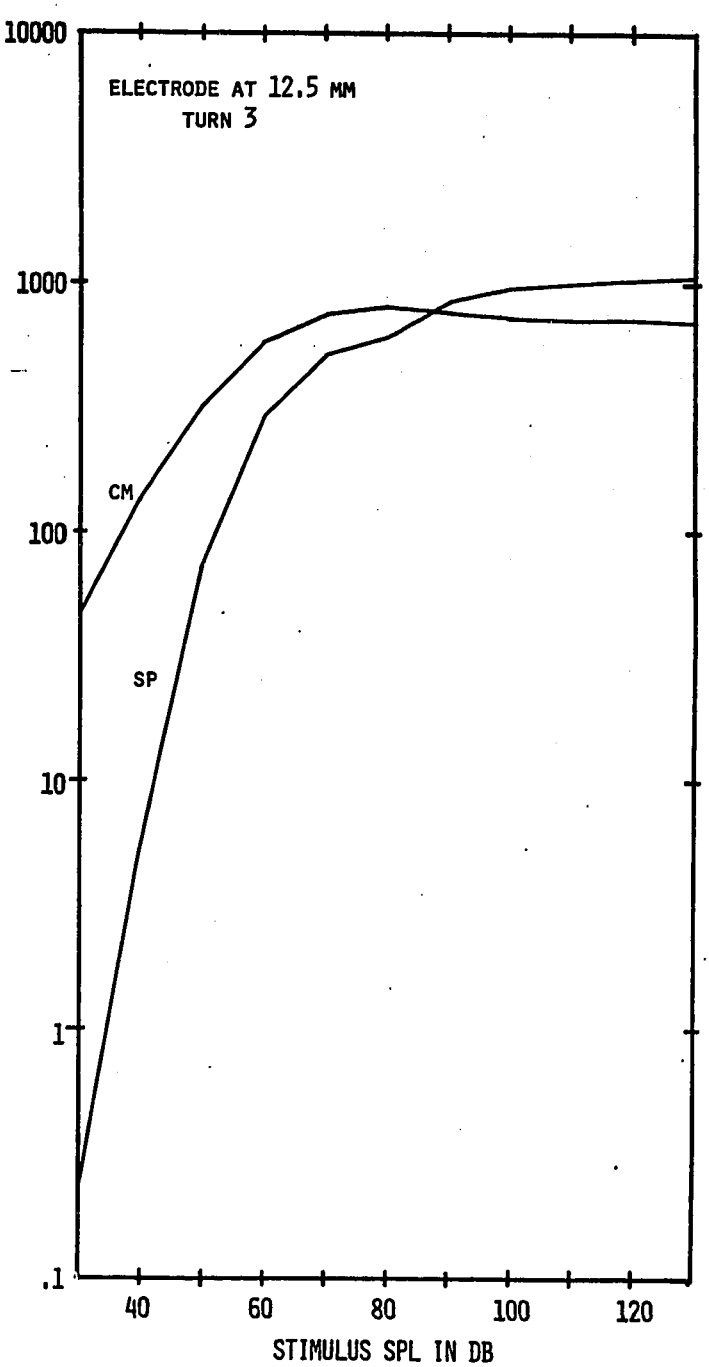
ELECTRODE AT 12.5 MM
TURN 3
10000
1000
100
10
1
.1
CM
SP
40
60
80
100
120
STIMULUS SPL IN DB

(C)

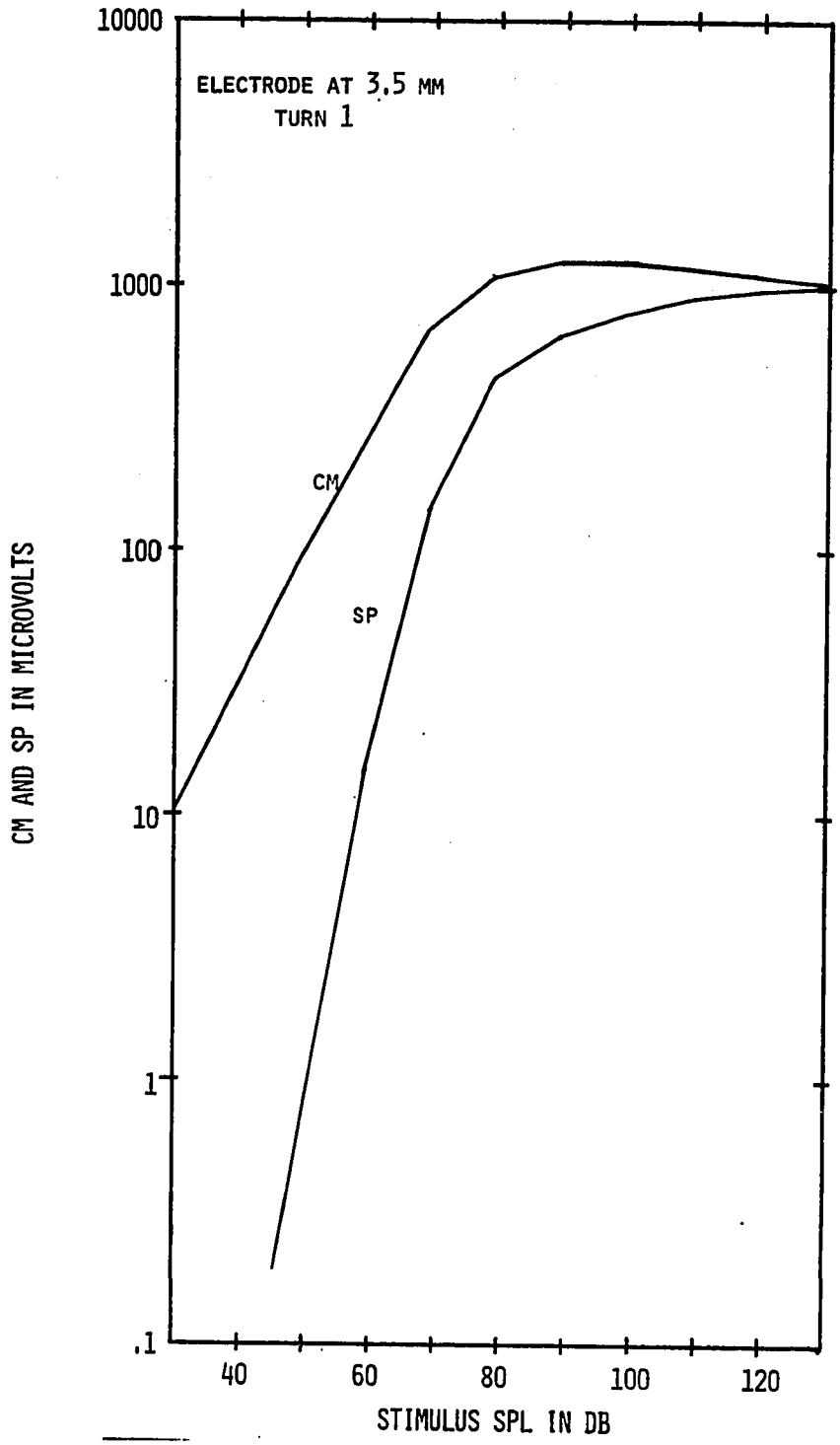

(A)

FIG. 9.17 CM AND SP AS A FUNCTION OF STIMULUS SPL. MODEL CONFIGURATION 180 'SEGMENTS'; ATTENUATION 6 DB/MM. ELECTRODE 1 MM ABOVE BASILAR MEMBRANE. STIMULUS 2000 HZ SINEWAVE.

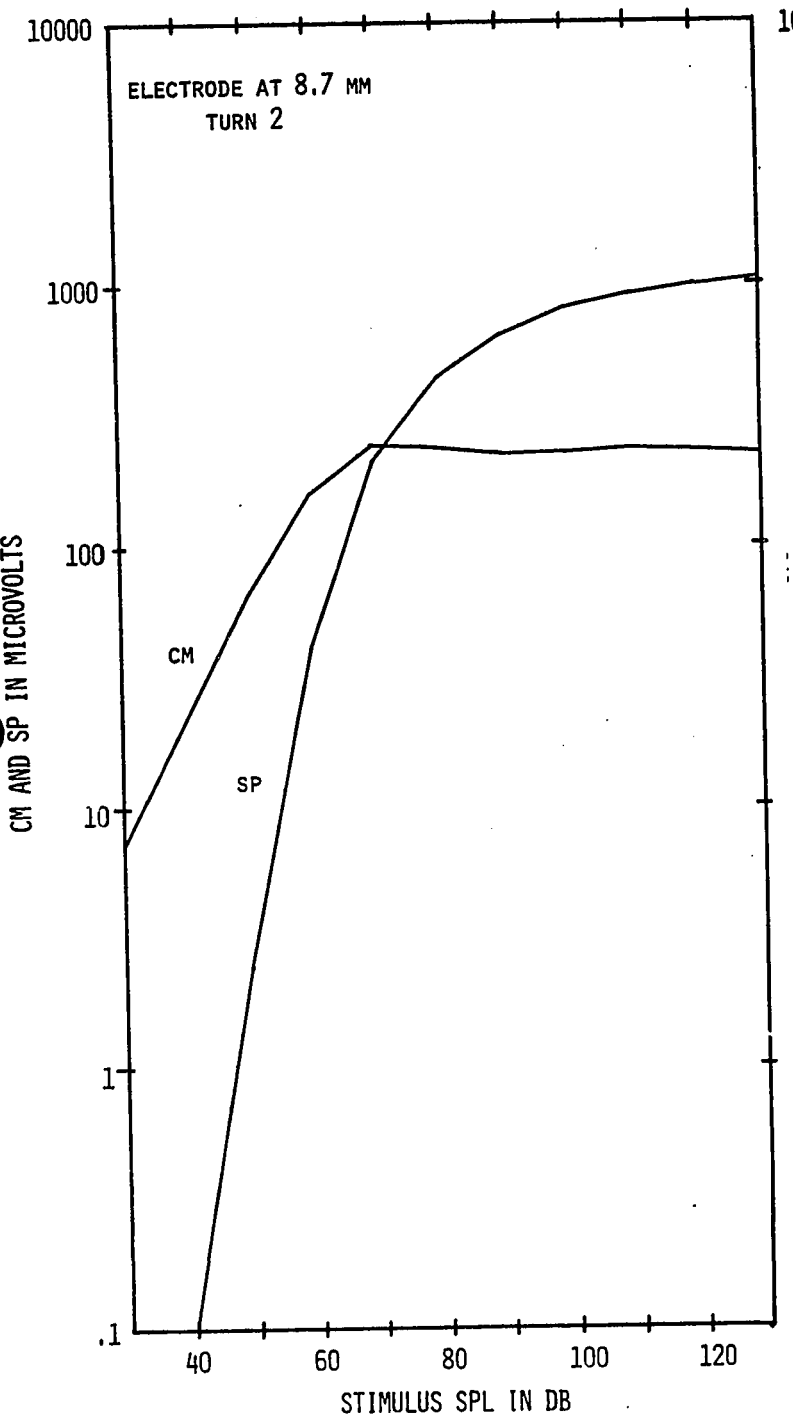
10000
1000
100
10
1
.1
ELECTRODE AT 8.7 MM
TURN 2
CM
SP
CM AND SP IN MICROVOLTS
40
60
80
100
120
STIMULUS SPL IN DB

(B)

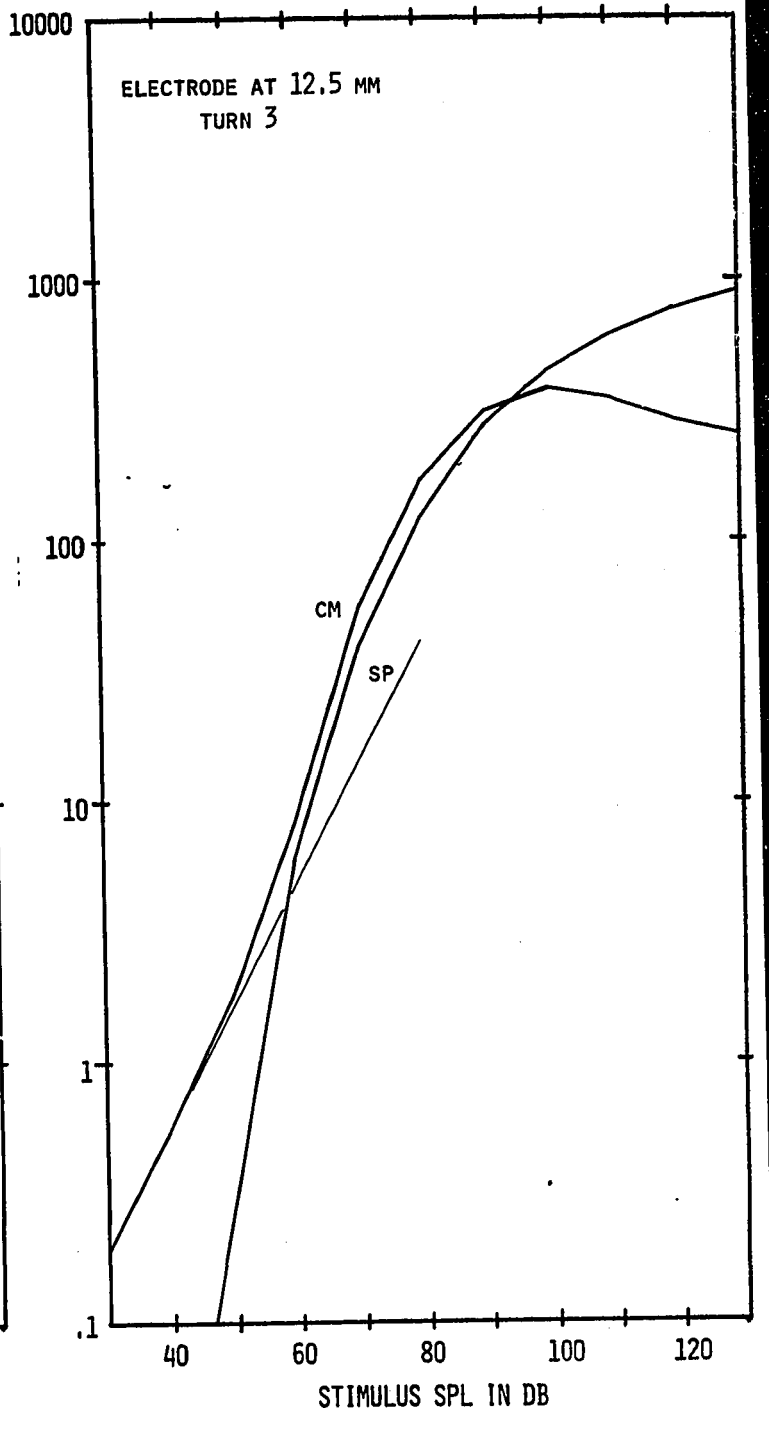
10000
1000
100
10
1
.1
ELECTRODE AT 12.5 MM
TURN 3
CM
SP
40
60
80
100
120
STIMULUS SPL IN DB

(C)

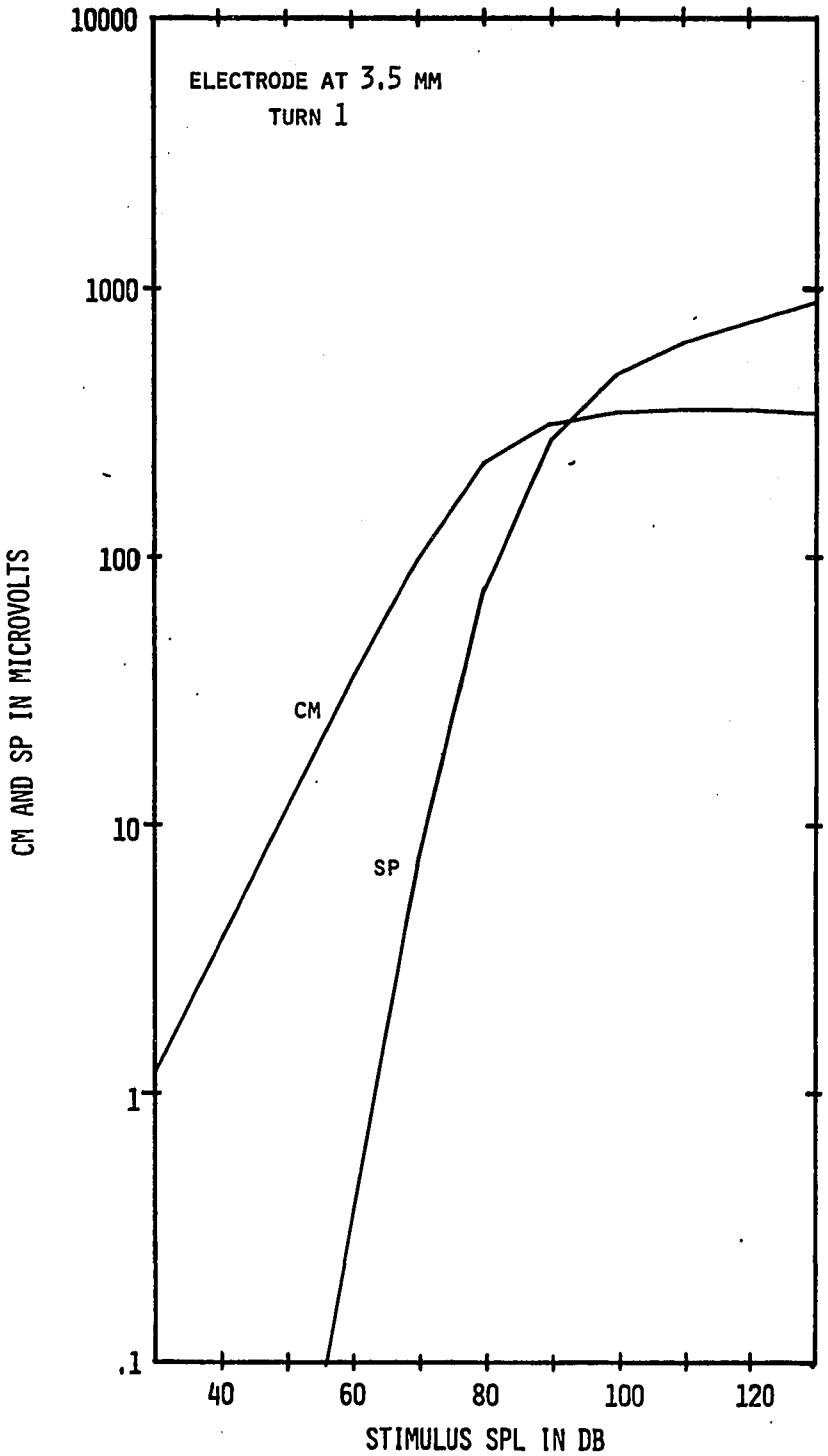

(A)

FIG. 9.18 CM AND SP AS A FUNCTION OF STIMULUS SPL. MODEL CONFIGURATION 180 'SEGMENTS'; ATTENUATION 6 DB/MM; ELECTRODE 1 MM ABOVE BASILAR MEMBRANE. STIMULUS 7000 HZ SINEWAVE.

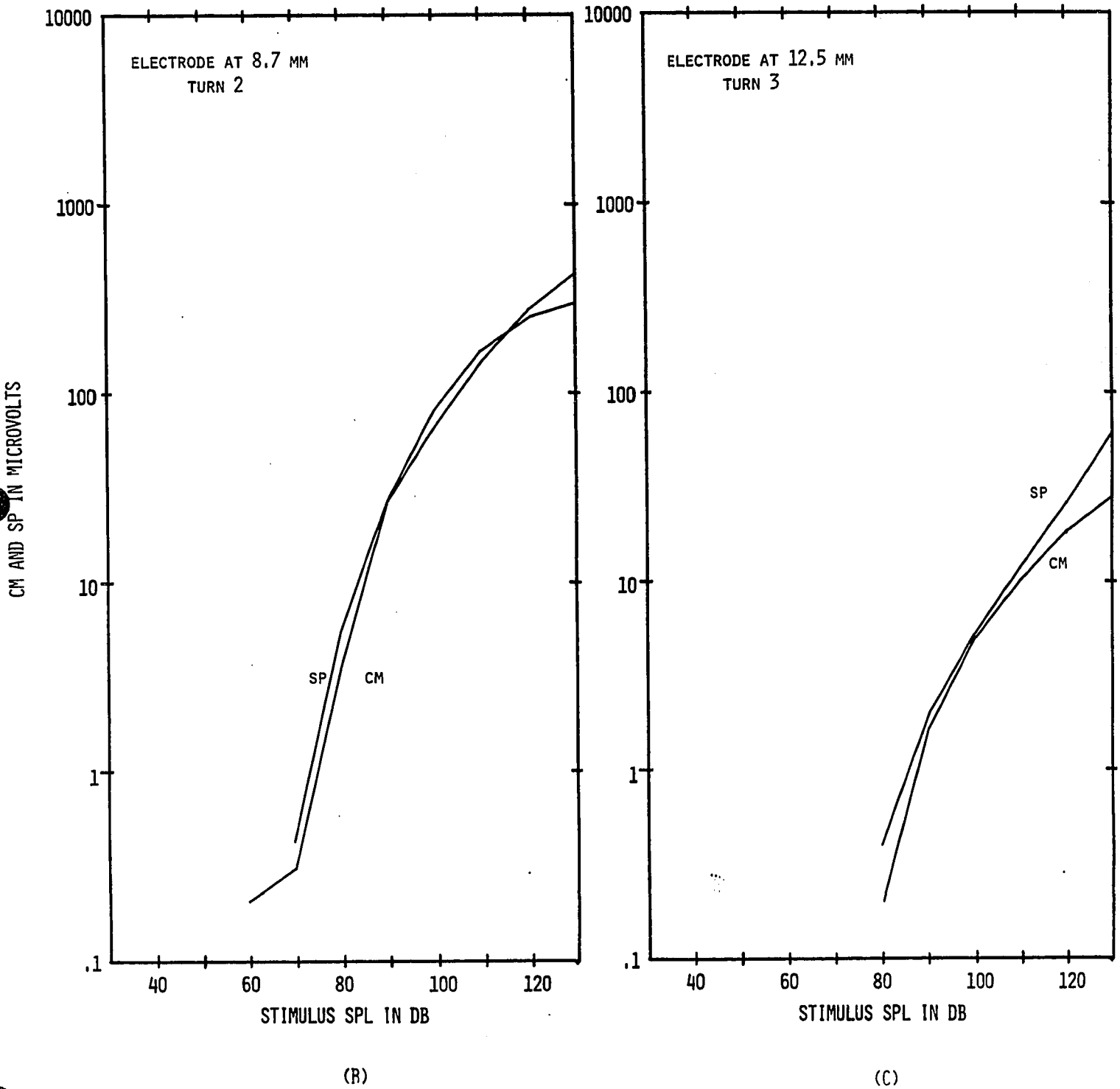
ELECTRODE AT 8.7 MM
TURN 2
10000
1000
100
10
1
.1
SP
CM
40
60
80
100
120
STIMULUS SPL IN DB
CM AND SP IN MICROVOLTS
(R)
ELECTRODE AT 12.5 MM
TURN 3
10000
1000
100
10
1
.1
SP
CM
40
60
80
100
120
STIMULUS SPL IN DB
(C)

than Turn 1 peak output. The Turn 3 CM vs SPL plot (Fig.9.17c) shows some unexpected characteristics. At low levels the slope of the curve is the same as for Turn 1 and Turn 2, but between 50 and 60 db SPL the CM response becomes a non-linear function of the sound pressure level. Furthermore, the peak amplitude of the CM is larger than in Turn 2. Comparison of the curve for 1980 Hz in Fig.3.5 with Fig.9.17c shows that for this electrode location and frequency the simulated CM does not correspond to the experimental observations (see also Section 9.4 and Fig.9.22).

Fig.9.18 shows the simulated CM response for 7000 Hz. In Turn 1 the response is similar to that observed experimentally up to about 90-100 SPL, but at higher levels only slight decrease of the CM is observable on the model while the experimentally observed decrease is more significant. It should not be forgotten, however, that for 120 and 130 db SPL there is usually permanent damage to the ear, although this necessarily is not taken into account in the simulation. Both Turn-2 and Turn-3 responses for 7000 Hz show anomalous behaviour similar to that observed for 2000 Hz in Turn 3 (see also Section 9.4 and Fig.9.24).

The behaviour of the summating potential produced by the model agrees well with the experimental data of Konishi and Yasuno (Fig.3.12) for frequencies over 2000 Hz in Turn 1.

Comparing the simulation results for Turn 1 at 7000 Hz with Fig.3.13 we also see good agreement: the SP keeps increasing although the CM reaches a maximum and decreases. Unfortunately there are no sufficiently detailed experimental data for the other turns, but judging from Figs.6.23-6.26 it can be expected that the SP will be positive in Turn 1 for frequencies below 1000 Hz, in Turn 2 for frequencies above 1000 Hz and in Turn 3 for both low and high frequencies with the exception of the 200-500 Hz region. This positive SP will not be generated by the simulation because as we will show in Chapter 10 the SP positivity is a result of the resistance distribution in the cochlea. This resistance distribution at present cannot be defined in sufficient detail and accuracy to permit modelling (see Section 8.2.3).

9.4. The simulation of the cochlear potentials as a function of frequency

The model used in the simulation of the cochlear potentials as a function of frequency is the same as the model used in Section 9.3.3. In order to compare the experimental results of Chapter 6 with the data generated by the model, this simulation produces the CM amplitude, the CM phase and the SP as a function of frequency at 60 and 80 db SPL in Turns 1, 2 and 3. The results are plotted in Figs.9.19-9.24.

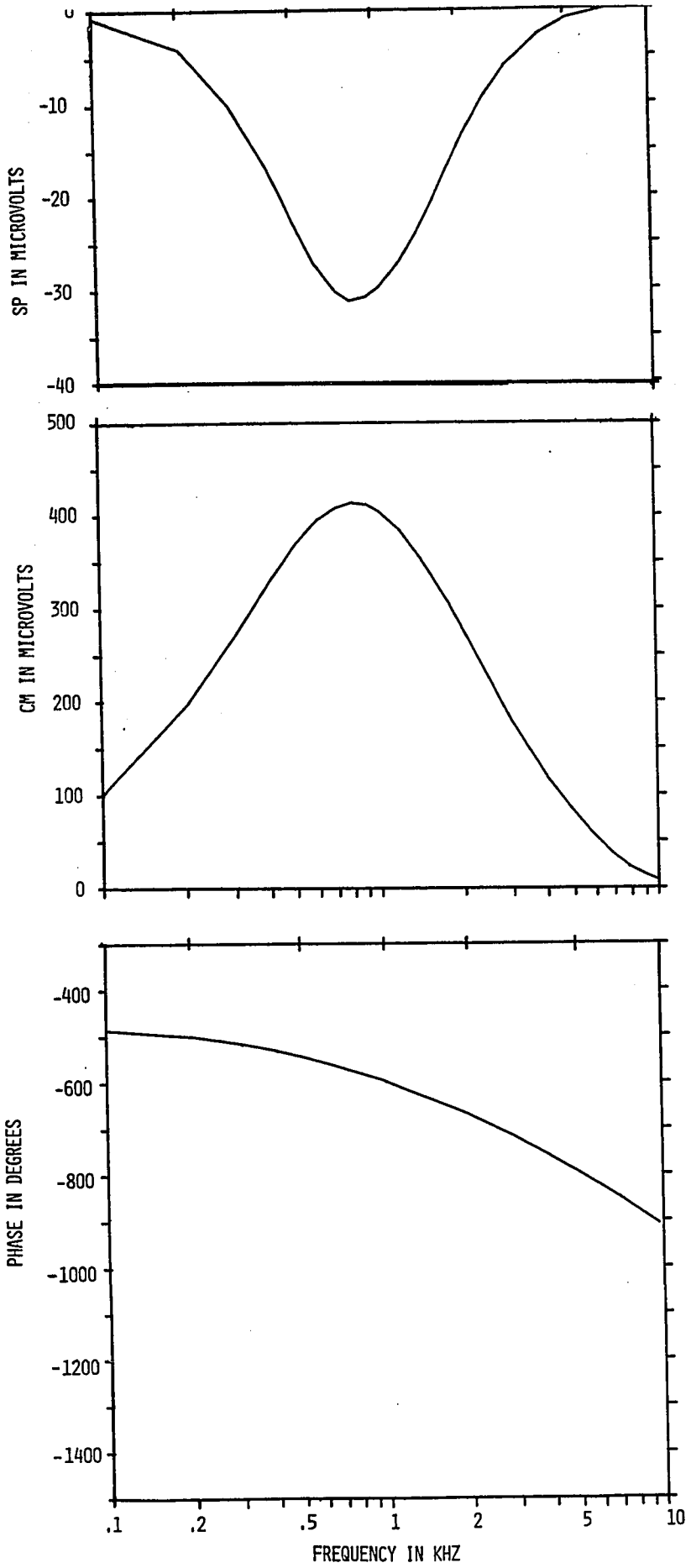

FIG.9.19 SP, CM AMPLITUDE AND CM PHASE AS A FUNCTION OF FREQUENCY IN TURN 1 AT 60 DB SPL. MODEL CONFIGURATION: 180 'SEGMENTS'; ATTENUATION 6 DB/MM; ELECTRODE 1 MM ABOVE BASILAR MEMBRANE.

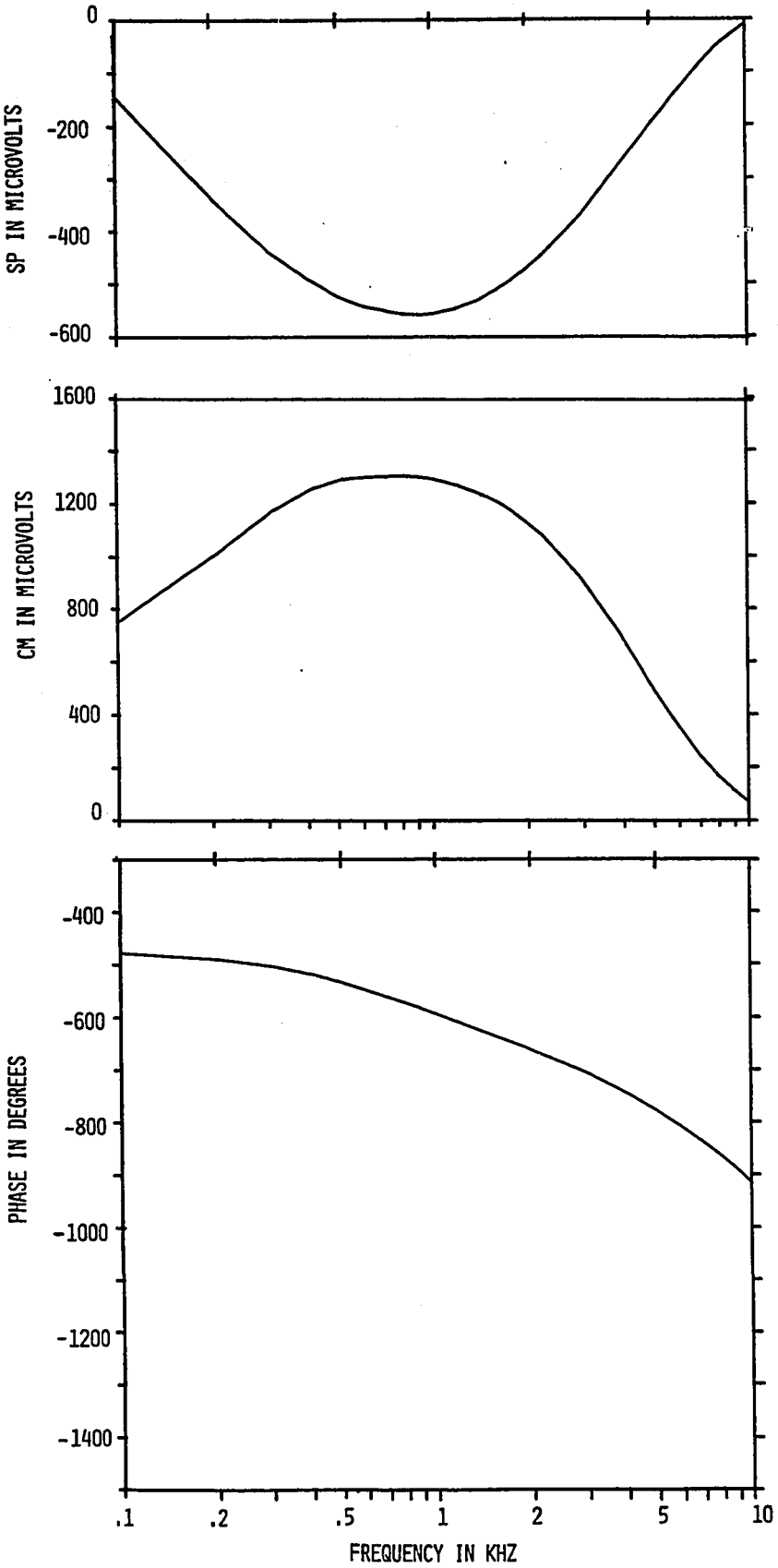

FIG.9.20 SP, CM AMPLITUDE AND CM PHASE AS A FUNCTION OF FREQUENCY IN TURN 1 AT 80 DB SPL. MODEL CONFIGURATION: 180 'SEGMENTS'; ATTENUATION 6 DB/MM; ELECTRODE 1 MM ABOVE BASILAR MEMBRANE.

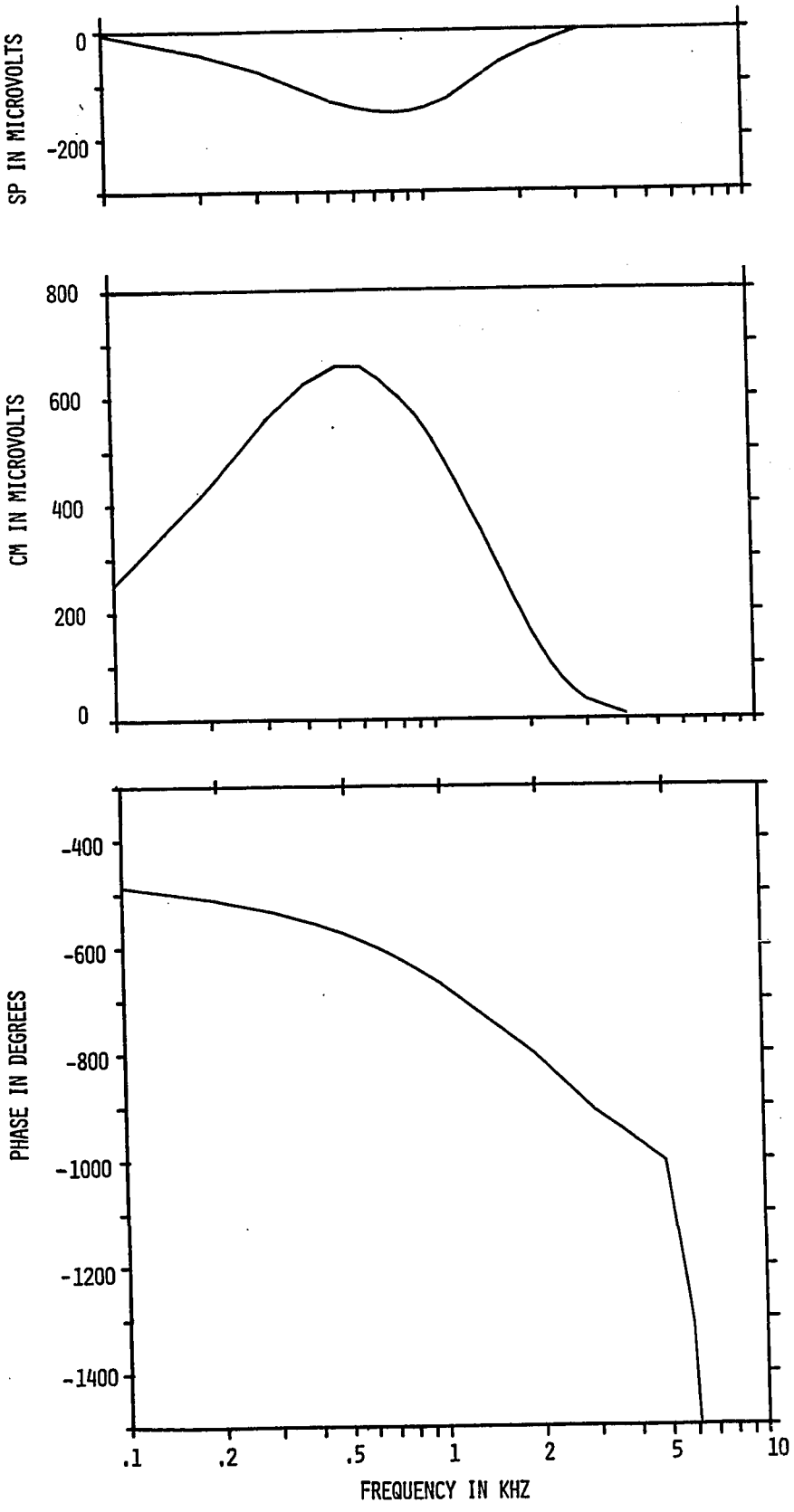

FIG.9.21 SP, CM AMPLITUDE AND CM PHASE AS A FUNCTION OF FREQUENCY IN TURN 2 AT 60 DB SPL. MODEL CONFIGURATION: 180 'SEGMENTS'; ATTENUATION 6 DB/MM; ELECTRODE 1 MM ABOVE BASILAR MEMBRANE.

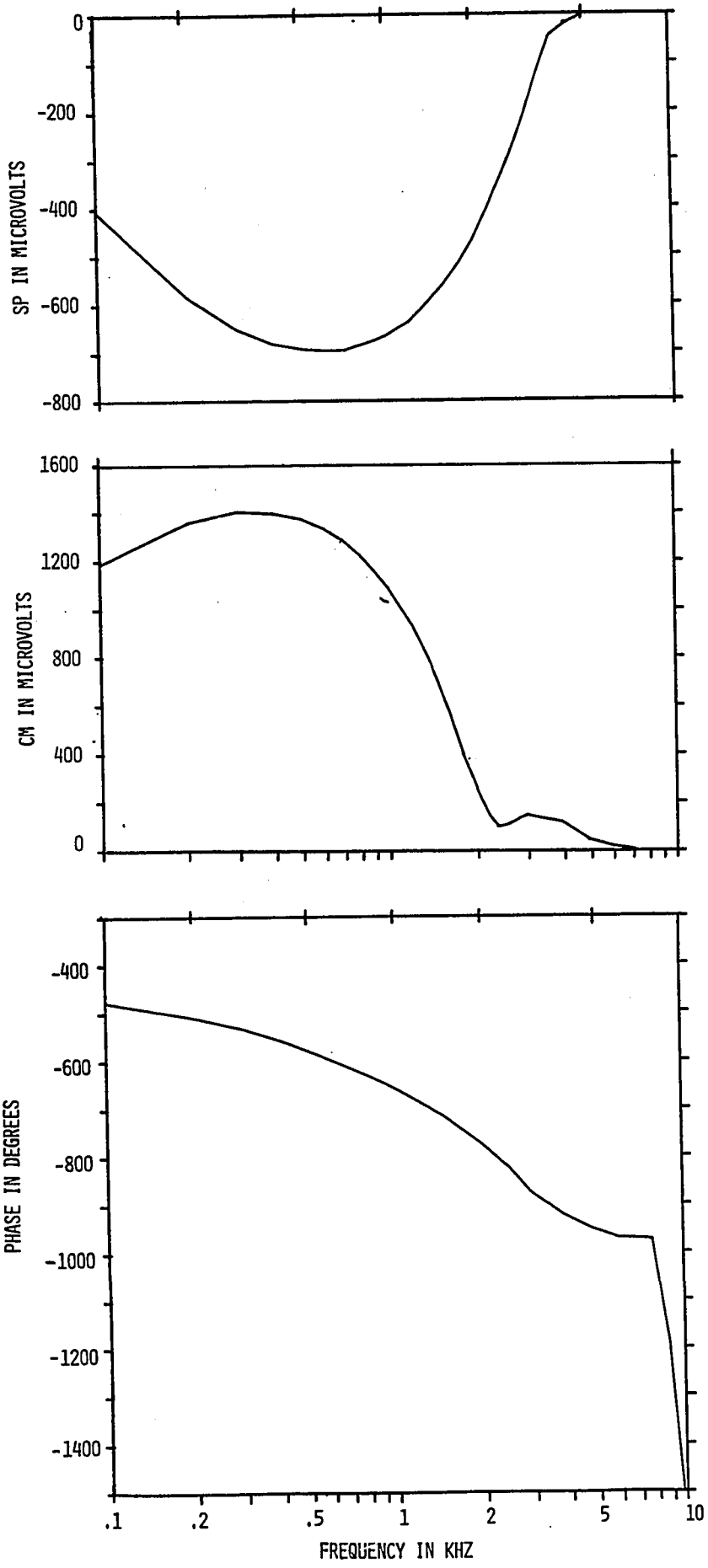

FIG.9.22 SP, CM AMPLITUDE AND CM PHASE AS A FUNCTION OF FREQUENCY IN TURN 2 AT 80 DB SPL. MODEL CONFIGURATION: 180 'SEGMENTS'; ATTENUATION 6 DB/MM; ELECTRODE 1 MM ABOVE BASILAR MEMBRANE.

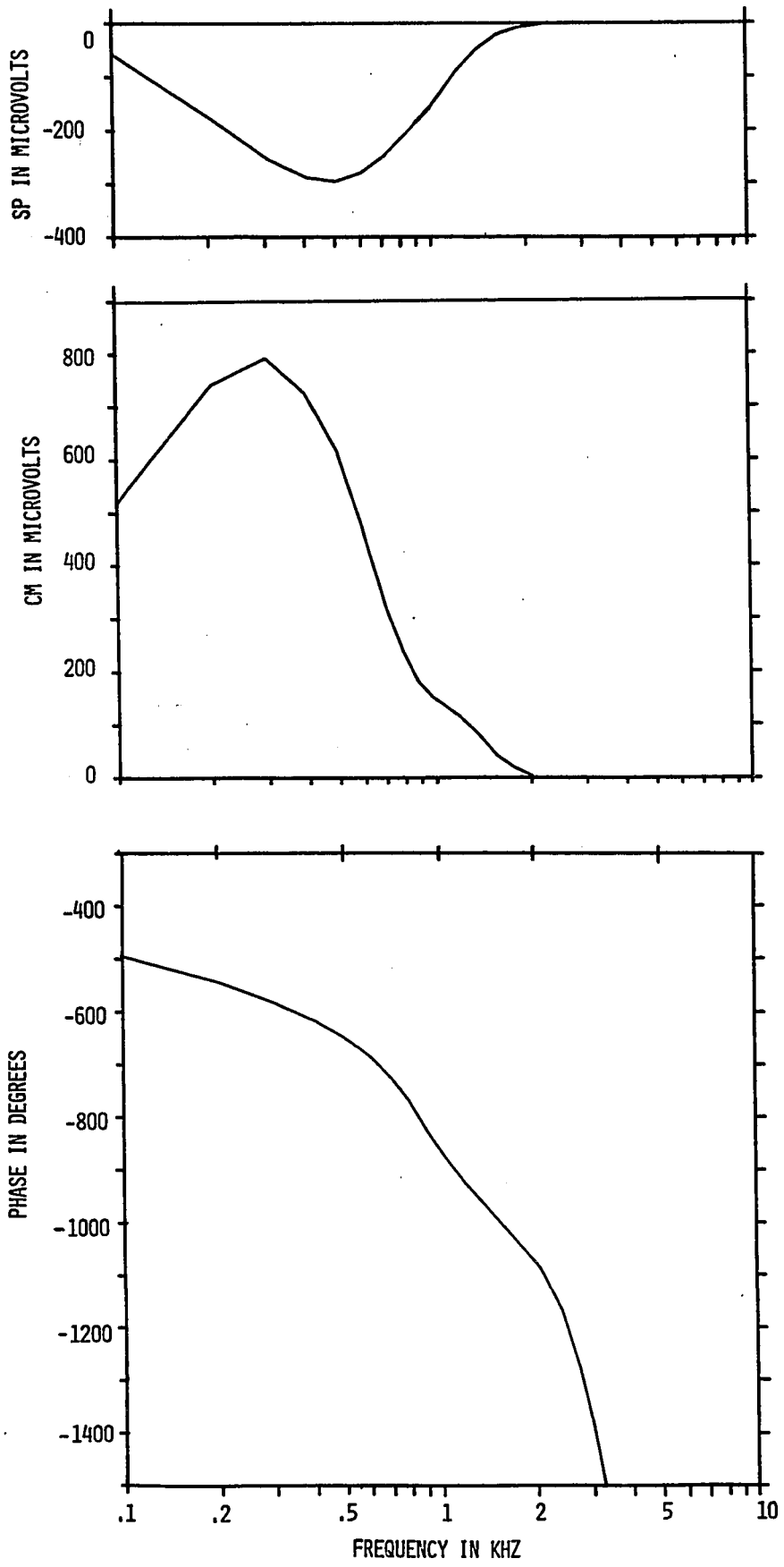

FIG.9.23 SP, CM AMPLITUDE AND CM PHASE AS A FUNCTION OF FREQUENCY IN TURN 3 AT 60 DB SPL. MODEL CONFIGURATION: 180 'SEGMENTS'; ATTENUATION 6 DB/MM; ELECTRODE 1 MM ABOVE BASILAR MEMBRANE.

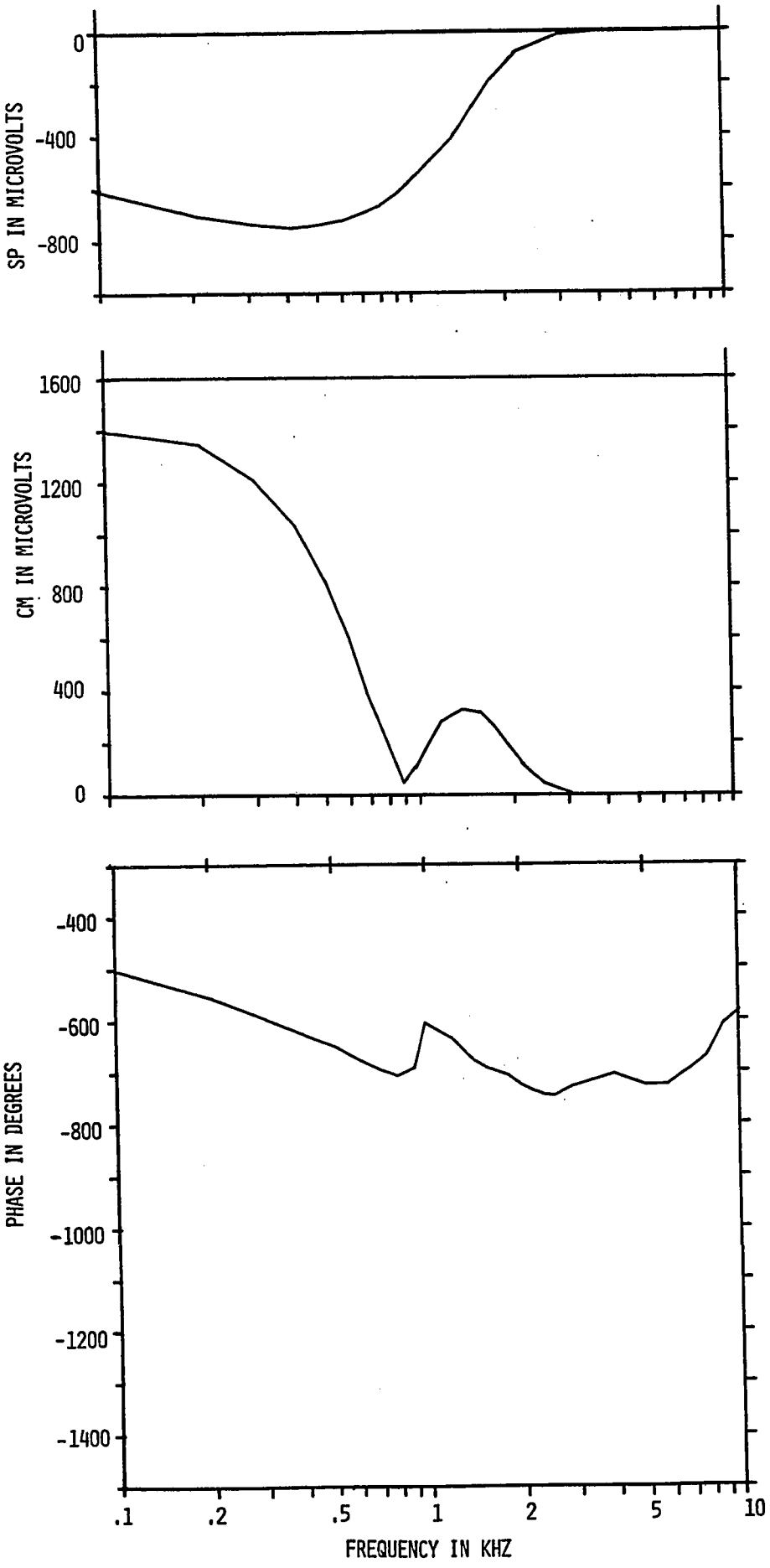

FIG.9.24 SP, CM AMPLITUDE AND CM PHASE AS A FUNCTION OF FREQUENCY IN TURN 3 AT 80 DB SPL. MODEL CONFIGURATION: 180 'SEGMENTS'; ATTENUATION 6 DB/MM; ELECTRODE 1 MM ABOVE BASILAR MEMBRANE.

The simulated CM amplitude data agree very well with the experimental data presented in Section 6.4.1. The CM amplitude 'peaks' in Turn 1 at 800-900 Hz, in Turn 2 at 500-600 Hz and in Turn 3 at approximately 300 Hz. These results are in agreement with the average frequency data presented in Fig.6.14 corresponding to the average peak CM amplitudes. Furthermore, the frequency at which the CM amplitude peak appears decreases as the SPL increases (compare Figs.9.19 with 9.20, 9.21 with 9.22 and 9.23 with 9.24,respectively) and this is in agreement with data presented in Figs.6.23 to 6.26.

Although the simulation results are not plotted in a normalized fashion, it can easily be seen that as the input sound intensity increases the CM amplitude curves become wider, indicating a relative icrease in the contribution of distant haircells to the total potential. This broadening effect was also observed experimentally as the results presented in Figs.6.9-6.12 show. These figures also indicate that at the same SPL the CM amplitude curves become progressively narrower from Turn 1 to Turn 3. A comparison of Figs.9.19, 9.21 and 9.23 shows that this indeed is the case for the simulated CM amplitude curves. It is interesting that the Turn-2 and Turn-3 CM amplitude responses exhibit anomalous behaviour in the 2000-3000 Hz region; it is

probably the same effect which produced the curve shown in Figs.9.17c, 9.18b and 9.18c (see Section 10.2).

The simulated CM phase responses are also in close agreement with our experimental results as comparison of the phase curves of Figs.9.19, 9.21 and 9.23 with the average experimental phase curves of Fig.6.18 shows. The Turn-1 phase response curve is relatively flat showing the effect of many interfering cochlear potential generators but Turn 2 and 3 show progressively steeper phase delay curves. Also, both the experimental and the model phase curves show a decrease in phase delay as the sound intensity increases (see Figs.6.15-6.17 and compare Figs.9.19 with 9.20, 9.21 with 9.22, 9.23 with 9.24 respectively). The irregular behaviour of the Turn-3 phase at 80 db SPL indicates that some unwanted interference effects develop in the simulation. These effects are discussed in detail in Chapter 10.

The experimentally observed and the simulated SP are not in as close agreement as the CM potential amplitude and phase. This is at least partially due to the fact that, as we mentioned in Section 9.3.3, the cochlear impedance distribution greatly effects the sign of the SP and this distribution is inadequately described. If the sign of the SP is disregarded and the shape of the curves is compared we see that for Turn 2 and 3 there is considerable agreement between

experimental data (Figs.6.24 and 6.26) and simulation results (Figs.9.21 and 9.23).

9.5. The effect of change of the value of the potential attenuating factor on the simulated cochlear potentials

The cochlear potential attenuation as a function of the relative distance between an electrode and a haircell is given by Eq.8.7. Now given our ignorance of physical parameters, it is important to show that the value of the attenuation per unit distance (A) does not affect the results of the simulation to a great extent. Using exactly the same models as previously, but changing the value of A to 0.7079 (3 db/mm attenuation) from 0.5 (6 db/mm attenuation) the CM and SP are simulated as a function of sound pressure level (Fig.9.25). As expected the curves corresponding to 3 db/mm attenuation larger potential values than the curves for 6 db/mm attenuation (see Figs.9.14b and 9.18a) but the shapes of the curves are almost identical.

In Fig.9.26 the CM amplitude and phase and the SP are plotted as a function of frequency for 3 db/mm attenuation. Apart from the general increase in amplitude the CM and the SP curves are similar to the corresponding curves of Fig.9.19. The CM amplitude curve, however, is somewhat narrower for the smaller attenuation, reflecting stronger interference between

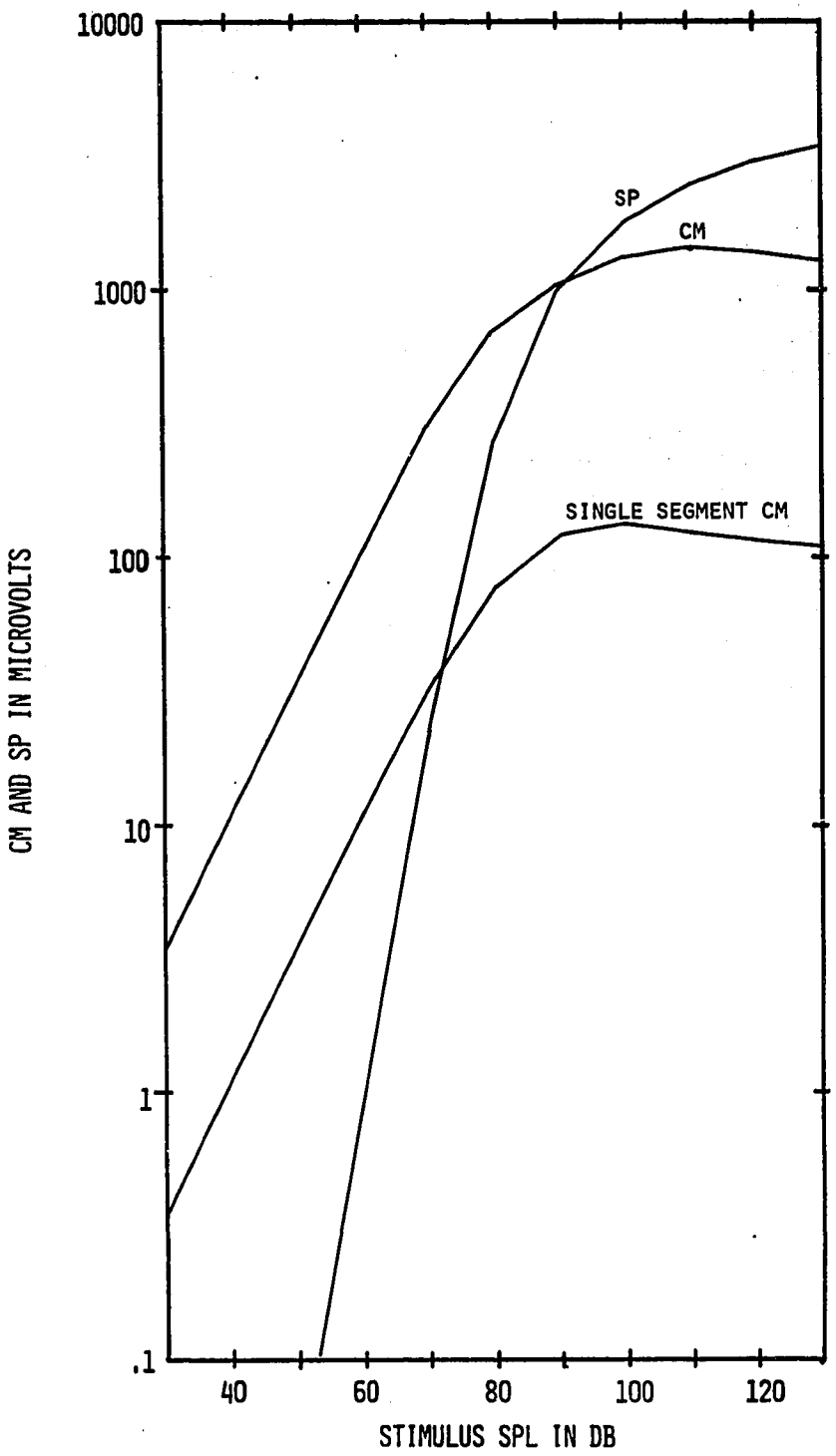

FIG.9.25 CM AND SP AS A FUNCTION OF STIMULUS SPL. MODEL CONFIGURATION: 1 'SEGMENT' AT 3.5 MM OR 180 'SEGMENTS'; ATTENUATION 3 DB/MM; ELECTRODE 1 MM ABOVE BASILAR MEMBRANE. STIMULUS: 7000 HZ SINEWAVE.

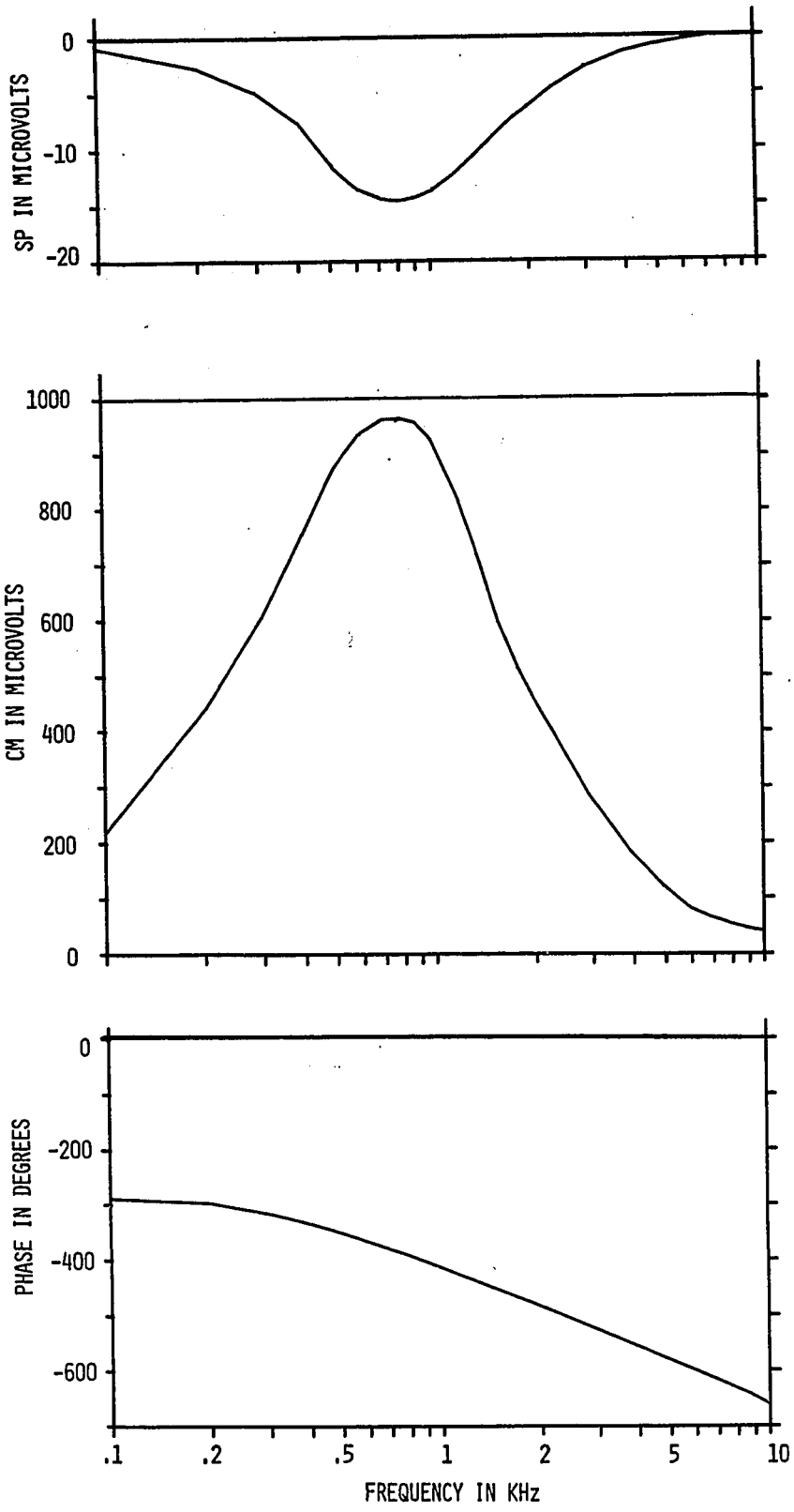

FIG.9.26 SP, CM AMPLITUDE AND CM PHASE AS A FUNCTION OF FREQUENCY IN TURN 1 AT 60 DB SPL. MODEL CONFIGURATION: 180 'SEGMENTS'; ELECTRODE AT 3.5 MM; ATTENUATION 3 DB/MM; ELECTRODE 1 MM ABOVE BASILAR MEMBRANE. STIMULUS: 7000 HZ SINEWAVE.

distant points along the cochlea for 3 db/mm than for 6 db/mm attenuation. This increased interference is also noticable on the phase curve which shows decreased phase delay for 3 db/mm attenuation.

It is perhaps significant that waveforms are also relatively insensitive to changes of the potential attenuating factor. In Figs.9.6 and 9.7 the waveforms for A = 0.5 and A = 1 are shown and the differences between the two sets appear to be slight.

9.6. CM augmentation produced by simulated OCB stimulation

Electrical stimulation of the crossed component of the olivo-cochlear bundle (OCB) reduces auditory nerve responses (AP) to acoustic stimuli and concurrently enhances the amplitude of the cochlear microphonic (CM) potential (29,30,31). The experimental observations are summarized by Desmedt (30): "The OCB activation (also) paradoxially potentiates the cochlear potential (CM), but the change amounted at most to +4-equivalent-db increase in sound energy. This increase in receptor potential, while important for understanding the synaptic mechanism of the inner ear, is ignored by the central nervous system, since acoustic signals are simultaneously suppressed in the auditory nerve." The augmentation of the CM potential has been also observed in

experiments where the AP was depressed by ototoxic drugs (streptomycin) and there has been no OCB stimulation (97).

Let us assume now on the basis of the evidence of Fex (32) that the effect of the OCB is inhibitive on the haircell and recall that the CM potential is considered to be the generator potential giving rise to the AP. The strong phase cancellation effects observed on the simulation model suggest that perhaps inhibition of the haircell activity and the corresponding decrease in AP is not reflected in a decrease of the 'gross' CM. To investigate this possibility we have 'inhibited' segments of the cochlea by inactivating the corresponding haircell models and simulating the CM and SP as a function of SPL for a Turn-1 electrode (Fig.9.27). To allow comparison with published experimental observations the db changes are shown for 70 and 90 db SPL respectively in Fig.9.28. The results show that even massive 'inhibition' of the cochlear generators will not result in a decrease but in an enhancement of the CM. This enhancement is due to the elimination of some of the interference between the potentials generated by the individual haircells and consequently not only the extent, but also the location of the 'inhibition' is significant. The inhibition of a relatively small segment may result in a decrease, while the elimination of 3 complete turns of the cochlea results in an increase of the CM (see 'B' and 'G' in Fig.9.28). It is also interesting to note

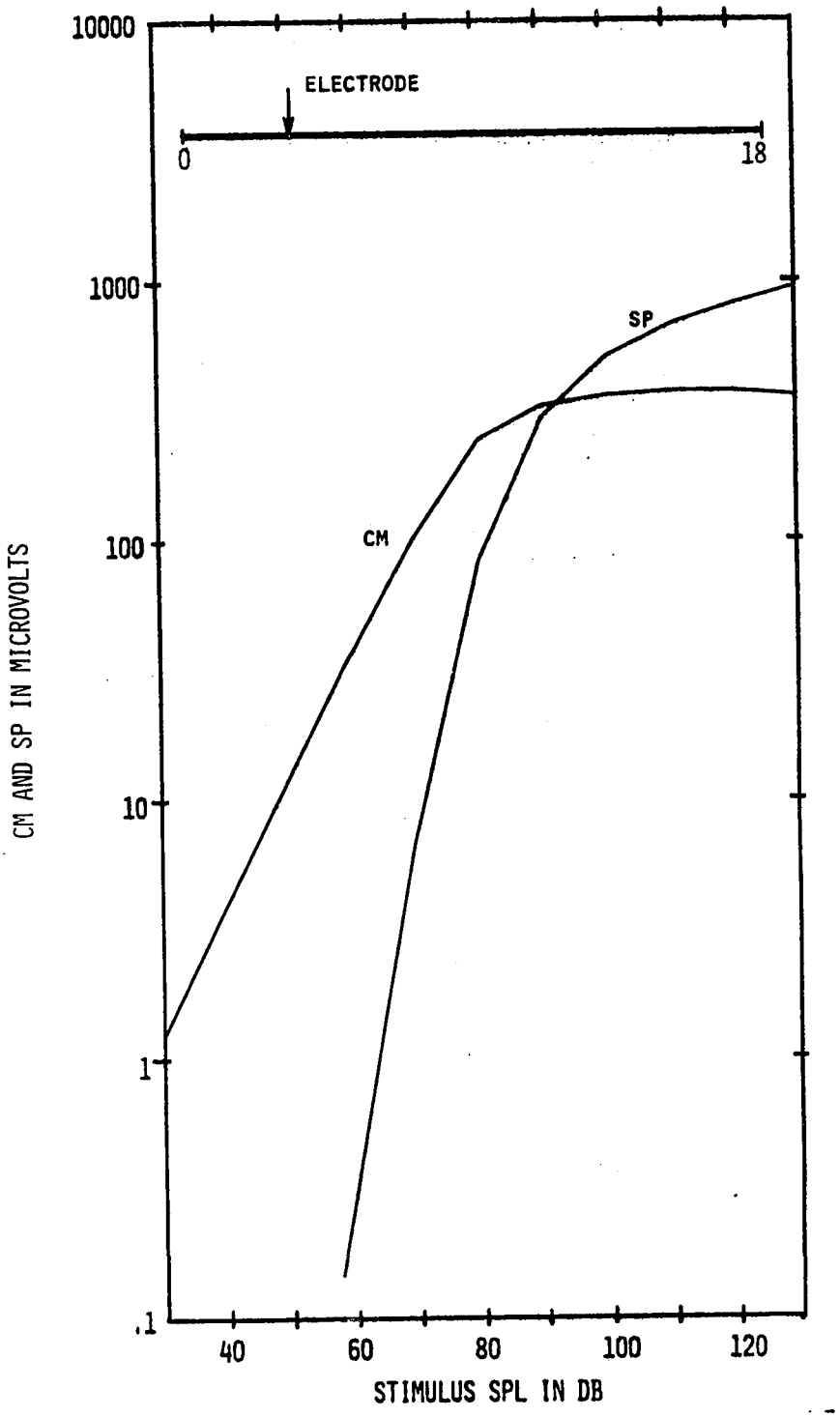

(A)

FIG.9.27 CM AND SP AS A FUNCTION OF STIMULUS SPL. THE LENGTH OF THE COCHLEA IS SHOWN AS A HORIZONTAL LINE (0 - 18 MM). THE HEAVIER LINE INDICATES THE ACTIVE AND THE THINNER LINE THE INACTIVE PART OF THE ORGAN OF CORTI ALONG THE BASILAR MEMBRANE. MODEL CONFIGURATION: 10 'SEGMENTS'/MM (ACTIVE PART); ELECTRODE AT 3.5 MM; ATTENUATION 6 DB/MM; ELECTRODE 1 MM ABOVE BASILAR MEMBRANE. STIMULUS: 7000 HZ SINEWAVE.

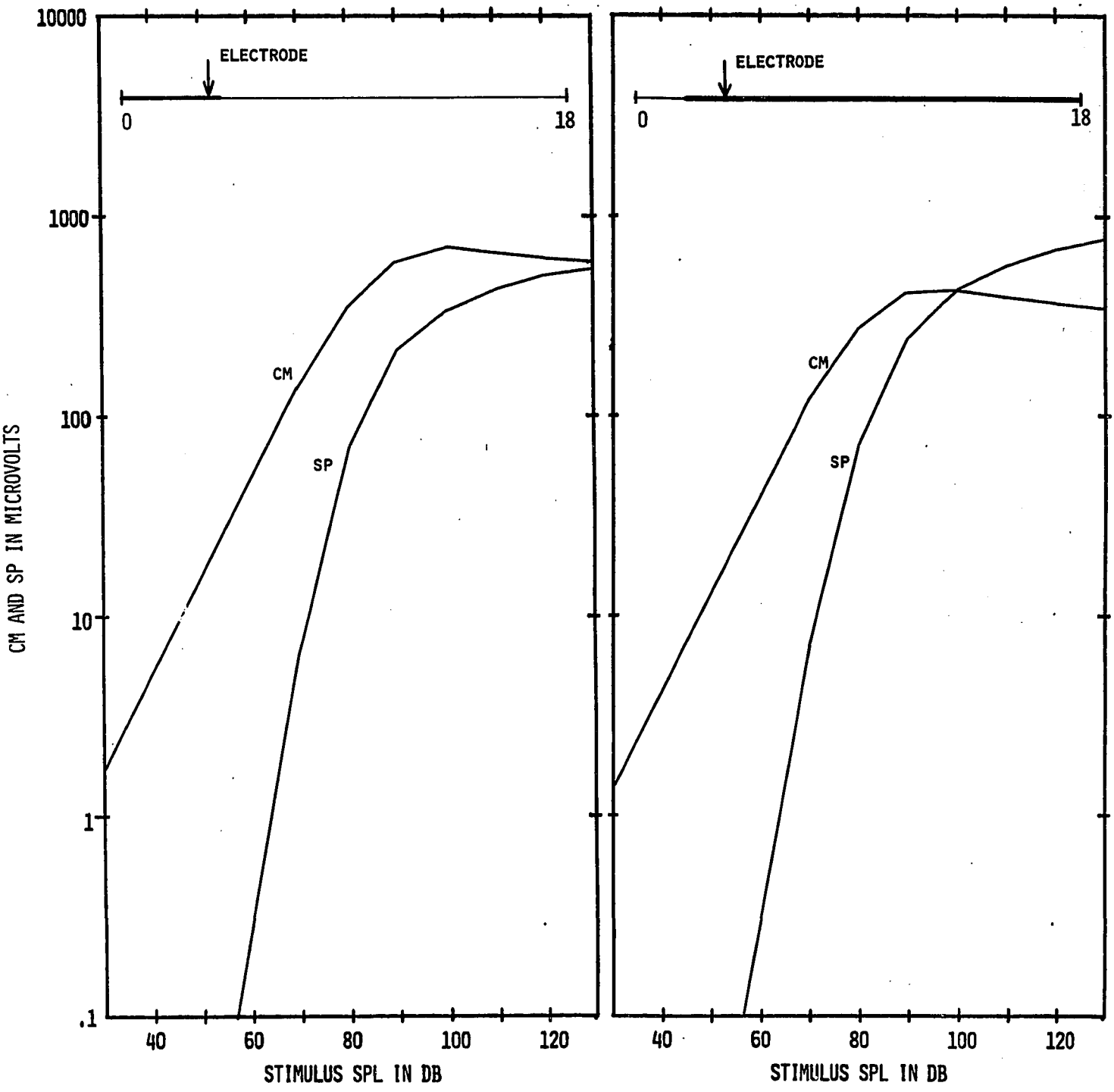
10000
1000
100
10
1
.1
CM AND SP IN MICROVOLTS
ELECTRODE
0
18
CM
SP
40
60
80
100
120
STIMULUS SPL IN DB
(B)
ELECTRODE
0
18
CM
SP
40
60
80
100
120
STIMULUS SPL IN DB
(C)

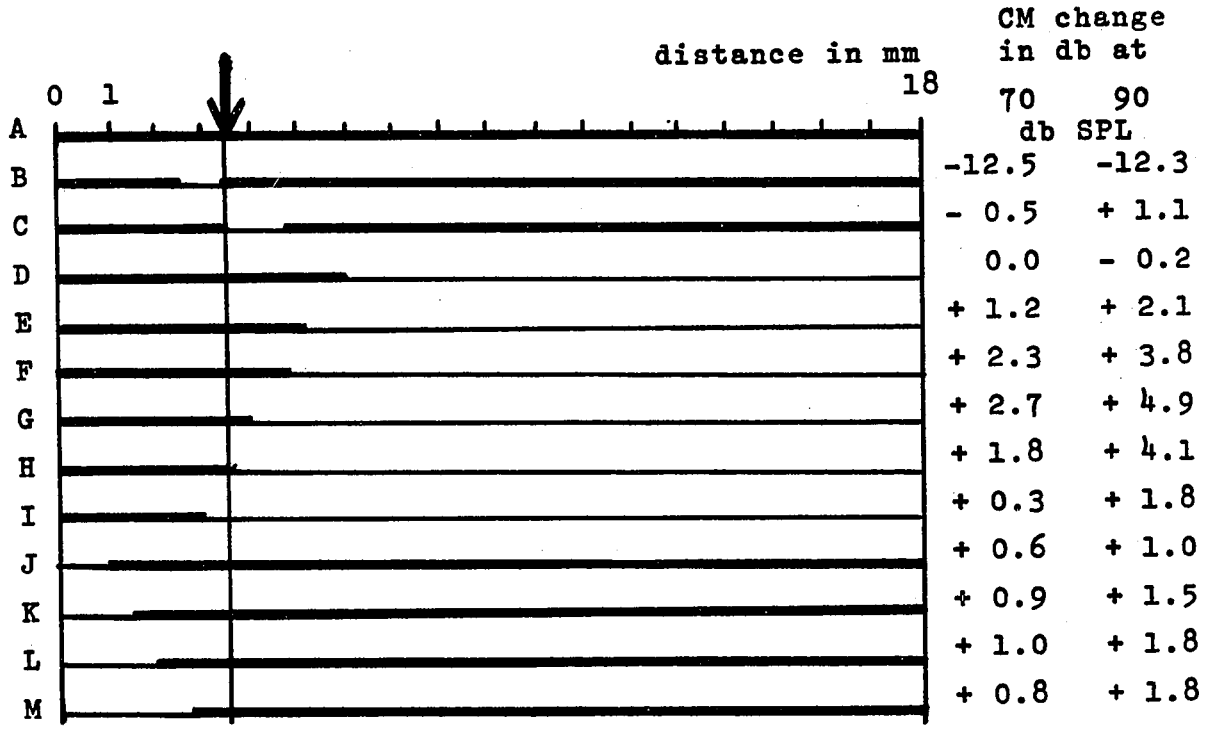

Fig.9.28 The solid lines represent the active and the thin lines the inhibited parts of the cochlea. The arrow shows the relative location of the electrode and the numbers on the right show the CM change (in db).

that whether the inhibited part of the cochlea is apical or basal to the electrode the augmentation of the CM is possible and furthermore the changes are approximately equal to the change observed experimentally (up to +4 db SPL).

The results summarized in Fig.9.28 suggest that the experimental observations indicating CM increase and AP decrease due to OCB stimulation do not present a paradox, but are explicable in terms of the inhibition of haircell activity and phase cancellation effects between individual haircell generators.

CHAPTER 10

DISCUSSION OF RESULTS

In this final chapter the work covered in this thesis is summarized. Some aspects of the experimental work and the simulation which deserve further consideration are discussed in detail and plans for future developments are indicated.

10.1. On the measurement of the cochlear potentials

Using improved techniques and instrumentation we are able to measure the cochlear potentials with reasonable accuracy. The results are believed to be more reliable and complete than other published data. The greater reliability is achieved because of the greater attention given to the control of the acoustic stimulus to the ear; specifically we have been able to keep the sound intensity constant at the input of the auditory system by measuring the sound pressure level in front of the eardrum, and have shown quantitatively that no indirect methods suffice. The results are more complete because for the first time, the simultaneous measurement of the CM potential amplitude, the CM potential phase and the SP has been successfully accomplished. Furthermore, the measurements have been carried out over a wide frequency range at several sound pressure levels.

The plots of the amplitude of the cochlear microphonic potential as a function of frequency resemble the basilar membrane displacement (tuning) curves and may appropriately be named the electrical tuning curves of the cochlea. These curves confirm some earlier observations regarding the behaviour of the basilar membrane. First, the frequency at which the electrical tuning curves reach their peak value changes as predicted by the mechanical transfer characteristics of the middle ear and the basilar membrane. Secondly, as the sound intensity increases the CM amplitude responses reflect the experimentally observed shift towards the lower frequencies of the vibration pattern of the basilar membrane.

The phase of the cochlear microphonic potential mirrors the travelling wave characteristics of the basilar membrane. Changes in intensity result in a slight decrease in phase delay, in agreement with direct basilar membrane observations and CM amplitude measurements.

Both the amplitude response and the phase response curves of the cochlear microphonic potential show the effects of electrical interference between the individual microscopic cochlear transducers. The electrical tuning curves become narrower from Turn 1 to Turn 3, approaching the shape of the mechanical tuning curve at the location of the electrode in Turn 3. The relatively slow increase of the measured phase

delay in the first turn is also due to interference effects. Evidence for this is given in Fig.10.1 which shows the CM phase shift measured in Turn 1 of a normal cochlea and in a cochlea in which the haircells located between the electrode and the stapes were damaged by neomycin. The damaged cochlea, with some of the interfering potential generators destroyed, shows much larger phase delays at high frequencies than the normal cochlea.

The measurement of the SP as a function of frequency also has produced interesting results. The SP shows much greater variability than the CM in time and between experimental animals, but it is possible nevertheless to confirm previously reported features of the SP behaviour. In some aspects our results are different, however, because we have utilized the differential recording technique. The use of differential electrodes eliminates the effect of remote and 'common-mode' potentials in the measured SP and therefore our Turn-2 and Turn-3 SP curves go to zero at high frequencies.

The significance of well balanced electrodes can be seen in Fig.10.2 where cochlear potential responses are shown with balanced differential electrodes (no response), with scala-vestibuli electrode grounded (CM with 'SP^-') and with scala-tympani electrode grounded (CM with 'SP^+'). Thus, the

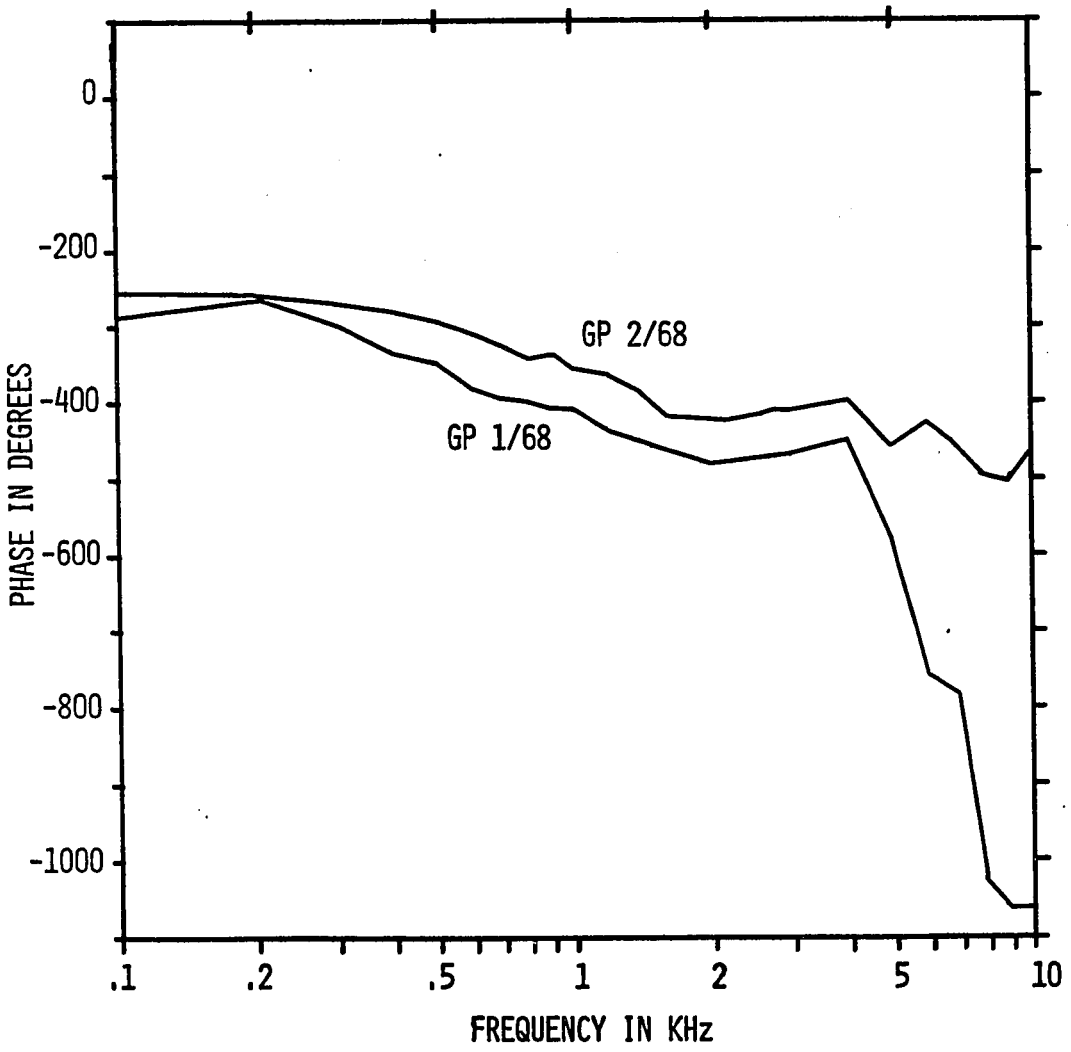

FIG.10.1 CM PHASE RESPONSE CHANGES DUE TO DESTROYED HAIRCELLS IN THE FIRST 3 - 4 MILLIMETERS OF THE COCHLEA. DAMAGED COCHLEA: GP 1/68; NORMAL COCHLEA: GP 2/68.

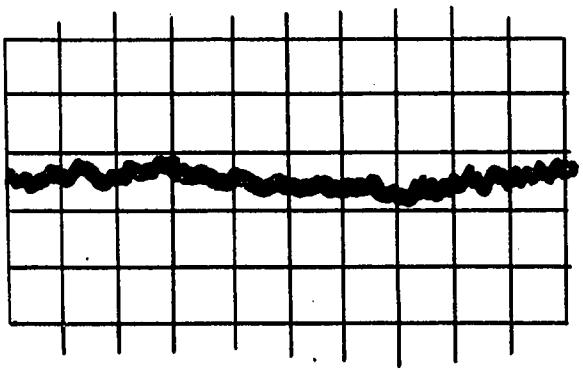

(A)

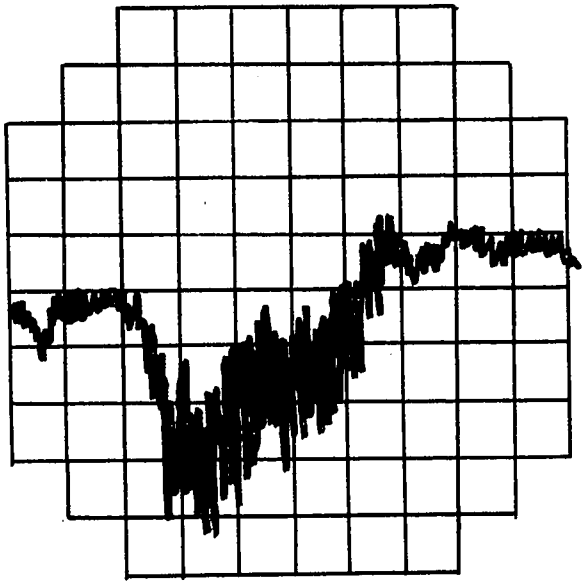

(B)

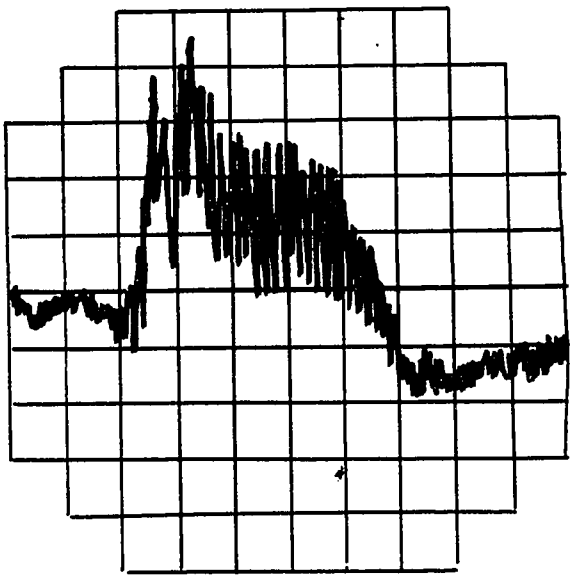

(C)

FIG.10.2 COCHLEAR POTENTIAL RESPONSES WITH (A) BALANCED DIFFERENTIAL ELECTRODES, (B) SCALA-VESTIBULI ELECTRODE GROUNDED AND (C) SCALA-TYMPANI ELECTRODE GROUNDED. TRACED FROM FILM.

results of those SP observations reported in the literature which were not made with differential electrodes must be appraised with care.

Perhaps the most interesting feature of our SP results is that the SP curves are negative for those frequencies which generate the largest CM values in the turn in which the electrodes is located, and positive for frequencies which generate the largest CM values in other turns. In explanation of related observations Bekesy has suggested (68,83) that it is quite possible that differences in relative size of the ac and dc components of the cochlear potentials measured at various points along the cochlea are due to the differences in conducting paths between the site of the potential generation and the location of the recording electrodes. On the basis of our model simulation studies we suspect that the SP vs frequency characteristics described in the previous paragraph are also due to the impedance distribution in the cochlea.

In an attempt to prove this we now consider a simplified picture of the cochlear impedances, which obviously form a bridge circuit (Fig.10.3). In order to find the value of the voltage V_{12} the numerical values of the various resistances must be known. Direct data are not available, but it is possible to estimate the resistance values using results of

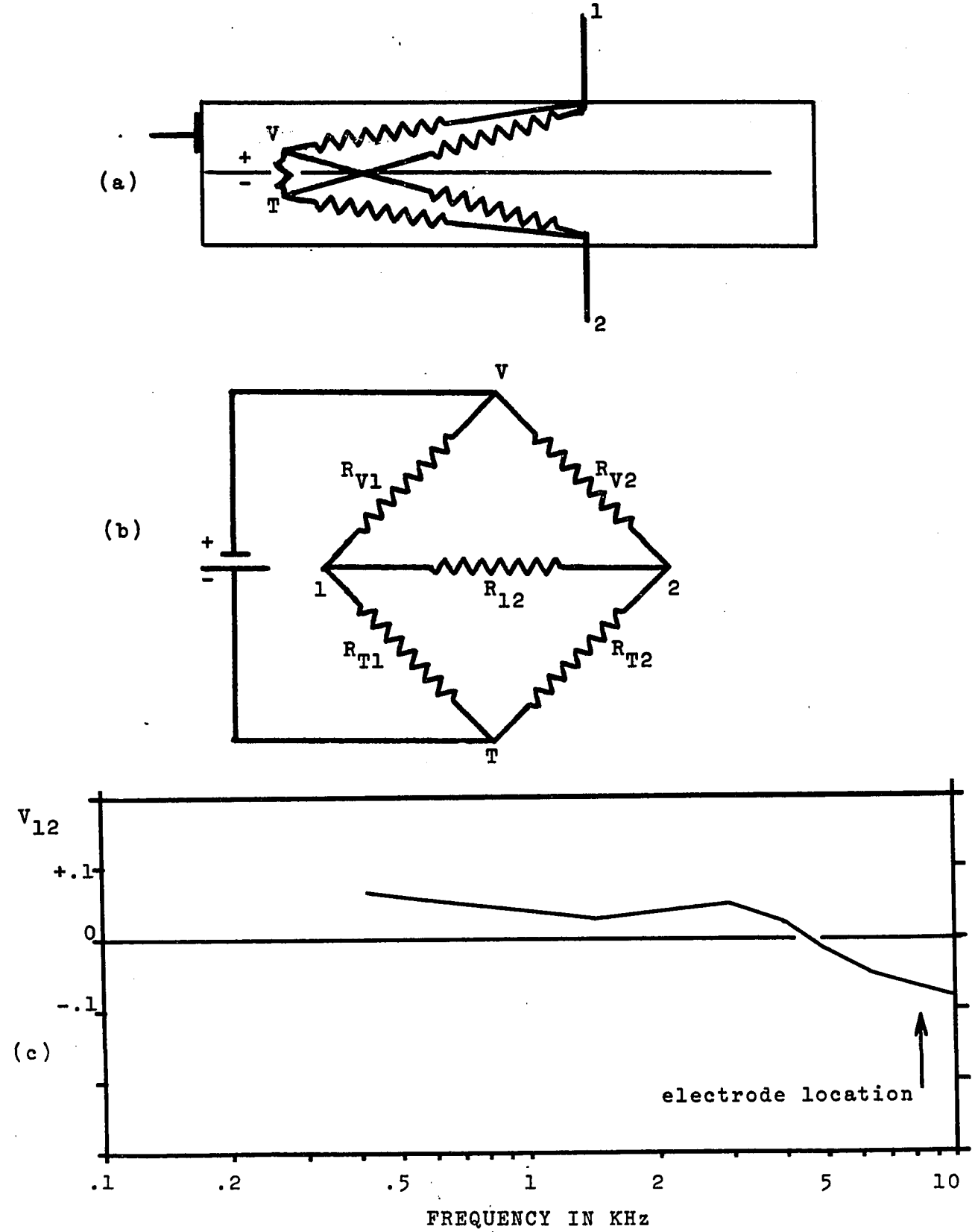

Fig.10.3 A simplified arrangement of the cochlear impedances.

Bekesy (83) who measured R_{12} and $R = R_{V1} + R_{T2}$ experimentally. The distribution of resistances along the cochlea will depend on the ratio of cross section areas of the scala vestibuli and the scala tympani. We utilize the relevant data of Fernandez (90) and calculate R_{V1} and R_{T2} from R. Since $R_{V2} = R_{V1} + R_{12}$ and $R_{T1} = R_{T2} + R_{12}$ the numerical values of all resistances are known and V_{12} can be determined. Fig.10.3c shows the value of V_{12} for a source of 1 V located at various points along the cochlea in succession, with the 'electrode' located 3 mm from the stapes. A comparison of Figs.6.22 and 10.3c shows that the curves are similar, indicating that SP polarity is indeed a function of the conducting path between the potential source and the recording electrode.

Similar measurements of V_{12} were made with an 'electrode position' of 12 mm. Unfortunately, for such an arrangement the calculated resistance values are very close and thus a small change in any of the bridge arms would change V_{12} from negative to positive and vice-versa. Consequently, with the calculated resistance values, positive and negative V_{12} values were obtained seemingly at random.

Although present instrumentation is satisfactory for the measurement of the 'gross' cochlear potentials the data

processing phase of the experiments needs further improvement. Due to present manual methods the measurements cannot be completed fast enough and this often results in incomplete data from a preparation since the animal dies. Furthermore, the evaluation of the data is so time consuming that it takes approximately three working days to process one complete experiment. It is essential, therefore, to fully automate the measurement of the cochlear potentials. This work is already in progress with the collaboration of the author in the OTL Research Laboratories where the experimental work presented was carried out. A LINC-8 computer has been installed and the necessary special equipment is at present being built. With the help of automated instrumentation we will be able to investigate further the behaviour of the cochlear potentials and also to start new experiments suggested by our model simulation work.

10.2. On the modelling and simulation of cochlear potentials

The primary purpose of the simulation of the cochlear potentials is to help in evaluating and understanding physiological phenomena. There are a number of physiological hypotheses regarding the operation of the ear which at present cannot be proved or disproved by direct experimental evidence. As this work shows, modelling and simulation may help in deciding between plausible alternative theories.

One of the significant results arising from simulation of the cochlear potentials is that we can show that non-linear haircell transducer functions are compatible with physiological observations. Furthermore, analysis and reformulation of the resistance-modulation theory of cochlear potential generation indicates that certain linearity assumptions are restrictive and unnecessary. Thus, it is possible to satisfy existing hypotheses with new mechanical-to-electrical conversion laws which are physically plausible and perhaps desirable, while being in agreement with physiological observations.

Equally as important as transducer non-linearity considerations is the possibility that the measured 'gross' cochlear potentials are not necessarily representative of the behaviour of the individual potential generator. We show by simulation that a number of physiological observations can be explained in terms of interference effects between the individual haircell generators distributed along the basilar membrane. It is satisfying to find that experimental results are directly reproducible by a simulation model based on the concept of haircell generator potential interference. These experimental results are: the behaviour of the electrical tuning curves of the cochlea as a function of location and sound pressure level; the measured amplitude and phase delay

characteristics of the cochlear microphonic potential, and the experimentally observed linearity of the 'gross' CM potential.

At the beginning of this work it was also believed that a simple interference mechanism could account for the behaviour of the cochlear potentials (CM decrease, SP increase) at very high sound pressure levels, but this was not to be the case. Instead, in order to account for such physiological behaviour we have found it necessary to investigate the differences in orientation and sensitivity between IHCs and OHCs. In particular, we assume on the basis of physiological and anatomical considerations that the IHCs are less sensitive to mechanical stimulation than the OHCs and that the ac output of the two types of haircells is 180 degrees out of phase. The models constructed on the basis of such assumptions are satisfactory, although the simulated CM potential decrease at high SPLs is smaller than the decrease observed experimentally. This, however, is probably due to temporary or permanent damage to the haircells rather than being an inherent property of the modelled processes.

To prove physiologically that the IHCs and OHCs produce potentials which are 180 degrees out of phase we propose a simple, albeit tedious, series of experiments. Guinea pigs are to be injected with neomycin or some other ototoxic drug

and after a period of two to three weeks the CM phase response of each ear is determined, followed by the preparation of the cochleas for microscopic examination. The ototoxic drugs cause varying degrees of haircell damage and a number of the damaged cochleas will show almost complete OHC destruction while the IHCs will appear normal. Comparing the previously recorded phase responses of normal cochleas a 180 degree phase shift should be observable. The author has already started this experimental series.

The assumption that the IHCs and OHCs have different sensitivity gives rise to an interesting speculation. Since presumably both haircell and nerve are 'noisy', then at low sound intensity it is possibly advantageous for the CNS to take a 'majority vote' in order to decide whether or not a true stimulus exists at a point on the basilar membrane. Accordingly, there are three high sensitivity cells (OHCs) and if the majority of these cells produce neural discharge then the stimulus is said to exist. As the intensity increases the OHCs saturate, but the signal-to-noise ratio improves simultaneously and the CNS can rely on the single, low sensitivity transducers (IHCs).

Our next significant result is that we can show with the help of the developed simulation models that the 'paradoxical' CM augmentation and AP reduction which are due to OCB stimulation

are a natural result of known cochlear processes. By selectively suppressing the cochlear potential generators of our model we can demonstrate that fewer active haircells may result in increased CM potential due to lessened interference between potential sources. If fewer haircells produce generator potentials because of the inhibitory action of the OCB efferents, then of course, fewer nerve fibers can fire and a decrease of the AP will be observed. The importance of these results is that we can now propose that inhibition, a physiologically common mechanism, combined with the cochlear interference effect satisfactorily explains the dual effect of CM augmentation and AP depression accompanying OCB stimulation. In contrast, previous hypotheses regarding this phenomenon are complicated and necessarily depend on assumptions yet unproved.

Some known ototoxic drugs acting on the haircells have also been observed to produce CM augmentation accompanied by AP depression. Therefore, it is suggested that results of experiments in which drugs were injected or chemicals were perfused through the cochlea be re-examined and the effect of the cochlear potential interference be taken into account.

Although the simulation of the cochlear potentials as a function of SPL, frequency and electrode location generally produced results which were compatible with physiological

observations some anomalous responses were also found. Such anomalies resulted only, however, when high frequency responses were simulated in Turns 2 or 3 at high sound pressure levels. Therefore, it is concluded that the primary reason for such physiologically incompatible responses is the cochlear 'segment'size chosen in Section 9.1. In Turn 2 and, especially in Turn 3, for high frequencies the basilar membrane displacement pseudo-travelling wave is small in amplitude and has small wavelength. Thus, the phase shift over a segment is not negligible and consequently at high SPLs some unforseen interference effects develop between segments. It is also suspected that the cochlear potential distribution model is insufficient and the simulated Turn-2 and Turn-3 high frequency responses originate partially in Turn 1. Further improvement, however, must await detailed cochlear impedance distribution data.

10.3. Conclusion

Summarizing the work covered by this thesis, the following major results are claimed:

(i) Experiments which were designed to establish the relations between the acoustic input to the ear and the cochlear potentials have yielded results not previously available:

the simultaneous measurement of the cochlear microphonic potential (CM) amplitude, the CM phase and the summating potential (SP) amplitude has been accomplished for the first time;

improved accuracy and reliability of cochlear measurements have been achieved by ensuring constancy of the auditory input stimulus;

functional relationships between the cochlear potentials and the stimulus parameters could be established because of the wide frequency and intensity ranges covered by the experiments.

(ii) The modelling and simulation of the cochlear potentials have been accomplished. It is shown that:

the 'gross' cochlear potential is a weighted sum of the output of the microscopic cochlear potential generators;

the cochlear transducer function is probably non-linear;

the 'paradoxical' combination of CM augmentation and action potential (AP) depression are results of cochlear generator (haircell) inhibition and microscopic cochlear potential interaction;

results obtained by simulation of the cochlear potentials are compatible with experimental observations.

(iii) A model of the mechano-acoustical system of the guinea-pig ear has been derived in terms of state variables and a scaling and optimization scheme is proposed for the economical solution by computer of the state equations.

APPENDIX 1

For the bulla open case the coefficients are determined by

$$A_o = \frac{\gamma\{(\alpha - d)^2 + \beta^2\} + 4d(\gamma - d)(\alpha - d)}{\{(\alpha - d)^2 + \beta^2\}^3 (\gamma - d)^2}$$

$$B_o = \frac{d^2\{(\alpha - d)^2 + \beta^2\} + 4d(\gamma - d)(\alpha - d)}{\{(\alpha - d)^2 + \beta^2\}^3 (\gamma - d)^2}$$

$$C_o = \frac{-\gamma}{\{(\alpha - \gamma)^2 + \beta^2\}^2 (d - \gamma)^2}$$

$$D_{o0} = \alpha D_{o1} - (\alpha^2 - \beta^2)D_{o2} + (\alpha^3 - 3\alpha\beta^2)D_{o3} + 0.5(F_{o1} + F_{o2})$$

$$D_{o1} = 2\alpha D_{o2} - 3(\alpha^2 - \beta^2)D_{o3} + 0.5(F_{o3} + F_{o4})$$

$$D_{o2} = 3\alpha D_{o3} - j\frac{F_{o3} - F_{o4}}{4\beta}$$

$$D_{o3} = \frac{\beta(F_{o3} + F_{o4}) + j(F_{o1} - F_{o2})}{4\beta^3}$$

where

$$r_1 = -\alpha + j\beta$$

$$r_2 = -\alpha - j\beta$$

and

$$F_{o1} = \frac{r_1}{(r_1 + d)^2 (r_2 + \gamma)}$$

$$F_{o2} = \frac{r_2}{(r_2 + d)^2 (r_2 + \gamma)}$$

$$F_{o3} = \frac{\gamma(r_1 + d) - 2r_1(r_1 + \gamma)}{(r_1 + d)^3 (r_2 + \gamma)^2}$$

$$F_{o4} = \frac{\gamma(r_2 + d) - 2r_2(r_2 + \gamma)}{(r_2 + d)^3 (r_2 + \gamma)^2}$$

For the <u>bulla closed</u> case the coefficients are determined by

$$A_c = (1/g) \times Im(G_1)$$

$$B_c = Rl(G_1) + (f/g) \times Im(G_1)$$

$$C_c = \frac{-\gamma}{\{(\alpha - \gamma)^2 + \beta^2\}^2 \{(f - \gamma)^2 + g^2\}}$$

$$D_{c0} = \alpha D_{c1} - (\alpha^2 - \beta^2)D_{c2} + (\alpha^3 - 3\alpha\beta^2)D_{c3} + 0.5(F_{c1} + F_{c2})$$

$$D_{c1} = 2\alpha D_{c2} - 3(\alpha^2 - \beta^2)D_{c3} + 0.5(F_{c3} + F_{c4})$$

$$D_{c2} = 3\alpha D_{c3} - j\frac{F_{c3} - F_{c4}}{4\beta}$$

$$D_{c3} = -\frac{\beta(F_{c3} + F_{c4}) + j(F_{c1} - F_{c2})}{4\beta^3}$$

where

$$r_1 = -\alpha + j\beta$$

$$r_2 = -\alpha - j\beta$$

$$p = -f + jg$$

and

$$G_1 = \frac{p}{(p + \gamma)\{(p + \alpha)^2 + \beta^2\}^2}$$

$$F_{c1} = \frac{r_1}{\{(r_1 + f)^2 + g^2\}(r_1 + \gamma)}$$

$$F_{c2} = \frac{r_2}{\{(r_2 + f)^2 + g^2\}(r_2 + \gamma)}$$

$$F_{c3} = \frac{\gamma\{(r_1 + f)^2 + g^2\} - 2r_1(r_1 + \gamma)(r_1 + f)}{\{(r_1 + f)^2 + g^2\}^2 (r_1 + \gamma)^2}$$

$$F_{c4} = \frac{\gamma\{(r_2 + f)^2 + g^2 - 2r_2(r_2 + \gamma)(r_2 + f)}{\{(r_2 + f)^2 + g^2\}^2 (r_2 + \gamma)^2}$$

REFERENCES

1. Flynn, W.E., and D.N. Elliott: Role of the pinna in hearing, J. Acoust. Soc. Am. 38:104-105 (1965).

2. Wiener, F.M., and D.A. Ross: The pressure distribution in the auditory canal in a progressive field, J. Acoust. Soc. Am. 18:401-408 (1946).

3. Guinan, J.J., Jr., and W.T. Peake: Middle-ear characteristics of anesthetized cats, J. Acoust. Soc. Am. 41:1237-1261 (1967).

4. von Bekesy, G.: Experiments in Hearing, edited by E.G. Wever, pp. 95-104, McGraw-Hill Book Co., New York, 1960.

5. Burns, W.: The peripheral mechanism of hearing: the response of the ear to normal and to intense sound, The Advancement of Science 68:1-18 (1960).

6. Davis, H., R.W. Benson, W.P. Covell, C. Fernandez, R. Goldstein, Y. Katsuki, J-P. Legouix, D.R. McAuliffe, and I. Tasaki: Acoustic trauma in the guinea pig, J. Acoust. Soc. Am. 25:1180-1189 (1953).

7. Wever, E.G., and M. Lawrence: Physiological Acoustics, Princeton University Press, Princeton, N.J., 1954.

8. Barany, E.: A contribution to the physiology of bone conduction, Acta Otolaryngol. Suppl. 26 (1938).

9. Simmons, F.B., and D.L. Beatty: A theory of middle ear muscle function of moderate sound levels, Science 138:590-592 (1960).

10. Simmons, F.B.: Perceptual theories of middle ear muscle function, Ann. Otol. Rhinol. Laryngol. 73:724-740 (1964).

11. Davis, H.: Biophysics and physiology of the inner ear, Physiol. Rev. 37:1-49 (1957).

12. von Bekesy, G.: On the elasticity of the cochlear partition, J. Acoust. Soc. Am. 20:227-241 (1948).

13. von Bekesy, G.: Paradoxical direction of wave travel along the cochlear partition, J. Acoust. Soc. Am. 27:155-161 (1955).

14. von Bekesy, G.: The variation of phase along the basilar membrane with sinusoidal vibrations, J. Acoust. Soc. Am. 19:452-460 (1947).

15. von Bekesy, G.: Experiments in Hearing, edited by E.G. Wever, pp. 404-429, McGraw-Hill Book Co., New York, 1960.

16. von Bekesy, G.: On the resonance curve and the decay period at various points on the cochlear partition, J. Acoust. Soc. Am. 21:245-254 (1949).

17. Johnstone, B.M., and A.J.F. Boyle: Basilar membrane vibration examined with the Mossbauer technique, Science 158:389-390 (1967).

18. Lawrence, M.: Dynamic ranges of the guinea-pig cochlear transducer, Cold Spring Harbour Symp. Qual. Biol. 30:159: 167 (1965).

19. Flanagan, J.L.: Models for approximating basilar membrane displacement, Bell System Tech. J. 39:1163-1192 (1960).

20. von Bekesy, G.: Experiments in Hearing, edited by E.G. Wever, pp. 500-510, McGraw-Hill Book Co., New York, 1960.

21. Laszlo, C.A.: A model-oriented study of the cochlear microphonic response in the auditory system, Master's Thesis, McGill University, Montreal, 1966.

22. Schmidt, R.S., and C. Fernandez: Labyrinthine dc potentials in representative vertebrates, J. Cellular Comp. Physiol. 59:311-322 (1962).

23. Moscovitch, D.: Personal Communication.

24. Tasaki, I., H. Davis, J-P Legouix: The space-time pattern of the cochlear microphonics (guinea pig) as recorded by differential electrodes, J. Acoust. Soc. Am. 24:502-519 (1952).

25. von Bekesy, G.: Microphonics produced by touching the cochlear partition with a vibrating electrode, J. Acoust. Soc. Am. 23:29-35 (1951).

26. Zwislocki, J.: Office of Naval Research Symposium Report No. ACR-1, pp. 182-190 (1955).

27. Tonndorf, J.: Localization of aural harmonics along the basilar membrane of guinea pigs, J. Acoust. Soc. Am. 30:938-943 (1958).

28. Tasaki, I., and C. Fernandez: Modification of cochlear microphonics and action potentials by KCl solution and by direct currents, J. Neurophysiol. 15:497-512 (1952).

29. Fex, J.: Augmentation of cochlear microphonics by stimulation of efferent fibers to the cochlea, Acta Otolaryngol. 50:540-541 (1959).

30. Desmedt, J.E.: Auditory-evoked potentials from cochlea to cortex as influenced by activation of the efferent olivo-cochlear bundle, J. Acoust. Soc. Am. 34:1478-1496 (1962).

31. Sohmer, H.: The effect of contralateral olivo-cochlear bundle stimulation on the cochlear potentials evoked by acoustic stimuli of various frequencies and intensities, Acta Otolaryngol. 60:59-70 (1965).

32. Fex, J.: Efferent inhibition in the cochlea related to hair-cell dc activity: Study of postsynaptic activity of crossed olivocochlear fibres in the cat, J. Acoust. Soc. Am. 41:666-675 (1967).

33. Davis, H., C. Fernandez, and D.R. McAuliffe: The excitatory process in the cochlea, Proc. Natl. Acad. Sci. U.S. 36:580-587 (1950).

34. Davis, H., B.H. Deatherage, D.H. Eldredge, and C.A. Smith: Summating potentials of the cochlea, Am. J. Physiol. 195:251-261 (1958).

35. Konishi, T., and T. Yasuno: Summating potentials of the cochlea in the guinea pig, J. Acoust. Soc. Am. 35:1448-1452 (1963).

36. Davis, H.: Peripheral coding of auditory information, Sensory Communications, edited by W.A. Rosenblith, pp. 119-141, M.I.T. Press, 1961.

37. von Bekesy, G.: Description of some mechanical properties of the organ of Corti, J. Acoust. Soc. Am. 25:770-785 (1953).

38. Hawkins, J.E., Jr.: Cytoarchitectural basis of the guinea-pig cochlear transducer, Cold Spring Harbor Symp. Quant. Biol. 30:147-157 (1965).

39. Engstrom, H., H.W. Ades, and J.E. Hawkins, Jr.: Structure and functions of the sensory hairs of the inner ear, J. Acoust. Soc. Am. 34:1356-1363 (1962).

40. von Bekesy, G.: Shearing microphonics produced by vibrations near the inner and outer hair cells, J. Acoust. Soc. Am. 25:786-790 (1953).

41. Davis, H.: Some principles of sensory receptor action, Physiol. Rev. 41:391-416 (1961).

42. Corti, A.: Recherches sur l'organe de l'ouie des mammifères, Z. wiss. Zool. 3:109-169 (1851).

43. Hensen, V.: Zur Morphologie der Schnecke des Menschen und der Säugetiere, Z. wiss. Zool. 13:481-512 (1863)

44. Retzius, G.: Zur Entwicklung der Zellen des Ganglion spirale acustici und zur Endigungsweise der Gehörnerven bei den Säugetieren, Biol. Untersuch. Neue Folge 6:52-57 (1894).

45. Held, H.: Die Cochlea der Säuger und der Vögel, ihre Entwicklung und ihr Bau, Handbuch der Normalen und Pathologischen Physiologie, edited by A. Bethe, Vol. II, pp. 467-526, J. Springer, Berlin, 1926.

46. Duvall, A.J., A. Flock, and J. Wersall: The ultra-structure of the sensory hairs and associated organelles of the cochlear inner hair cell, with reference to directional sensitivity, J. Cellular Biol. 29Ñ497-506 (1966).

47. Engstrom, H.: Electron micrographic studies of the receptor cells of the organ of Corti, Neural Mechanisms of the Auditory and Vestibular Systems, edited by G.L. Rasmussen and W. Windle, pp.48-64, C.C. Thomas, Springfield, Ill., 1960.

48. Engstrom, H., and J. Wersall: The ultrastructural organization of the organ of Corti and the vestibular sensory epithelia, Exptl. Cell Res. 5:460 (1958).

49. Engstrom, H., H.W. Ades, and A. Andersson: Structural Pattern of the Organ of Corti, Almqvist and Wiksell/ Gebers Forlag AB, Stockholm, 1966.

50. Flock, A., R. Kimura, P.G. Lundquist, and J. Wersall: Morphological basis of directional sensitivity of the outer hair cells in the organ of Corti, J. Acoust. Soc. Am. 34:1351-1355 (1962).

51. Wersall, J., A. Flock, and P.G. Lundquist: Structural basis for directional sensitivity in cochlear and vestibular sensory receptors, Cold Spring Harbor Symp. Quant. Biol. 30:115-132 (1965).

52. Iurato, S., et al: Submicroscopic Structure of the Inner ear, Pergamon Press, Toronto, 1967.

53. Schuknecht, H.F.: Neuroanatomical correlates of auditory sensitivity and pitch discrimination in the cat, Neural Mechanisms of the Auditory and Vestibular Systems, edited by G.L. Rasmussed and W.F. Windle, pp. 76-90, C.C. Thomas, Springfield, Ill., 1960.

54. Kolmer, W.: Gehororgan, Handbuch der microskoposchen Anatomie des Menschen, edited by W. von Mollendorf, vol 3, p.250, Springer-Verlag, Berlin, 1927.

55. Iurato, S.: Submicroscopic structure of the membraneous labyrinth. 2. The epithelium of Corti's Organ, Z. Zellforsch. u. mikroskop. Anat. 53:259 (1961).

56. Mygind, S.H.: Functional mechanism of the labyrinthine epithelium- I, Arch. Otolaryngol. 82:452-461 (1965).

57. Mygind, S.H.: Functional mechanism of the labyrinthine epithelium- II, Arch. Otolaryngol. 82:579-590 (1965).

58. Mygind, S.H.: Functional mechanism of the labyrinthine epithelium-III, Arch. Otolaryngol. 82:3-8 (1966).

59. von Bekesy, G.: Pressure and shearing forces as stimuli of labyrinthine epithelium, Arch. Otolaryngol. 84:122-130 (1966).

60. Naftalin, L.: The distribution of acoustic energy within the cochlea, Life Sci. 5:1345-1348 (1966).

61. Wei, L.Y.: A new theory of nerve conduction, IEEE Spectrum 3:123-127 (1966).

62. Davis, H.: A model for transducer action in the cochlea, Cold Spring Harbor Symp. Quant. Biol. 30:181-190 (1965).

63. Tasaki, I: Afferent impulses in auditory nerve fibers and the mechanism of impulse initiation in the cochlea, Neural Mechanisms of the Auditory and Vestibular Systems, edited by G.L. Rasmussen and W.F. Windle, pp. 40-47, C.C. Thomas, Springfield, Ill., 1960.

64. Johnstone, J.R., and B.M. Johnstone: Origin of summating potential, J. Acoust. Soc. Am. 40:1405-1419 (1966).

65. Johnstone, B.M., J.R. Johnstone, and I.D. Pugsley: Membrane resistance in endolymphatic walls of the first turn of the guinea-pig cochlea, J. Acoust. Soc. Am. 40:1398-1404 (1966).

66. Schwartz, M.: Information Transmission, Modulation and Noise, pp. 213-214, McGraw-Hill Book Co., New York, 1959.

67. von Bekesy, G.: Gross localization of the place of origin of the cochlear microphonics, J. Acoust. Soc. Am. 24:399-409 (1952).

68. von Bekesy, G.: Comments on the measurement of the relative size of dc potentials and microphonics in the cochlea, J. Acoust. Soc. Am. 34:124 (1962).

69. Simmons, F.B., and D.L. Beatty: The significance of round-window recorded cochlear potentials in hearing, Ann. Otol. Rhinol. Laryngol. 71:767-801 (1962).

70. Whitfield, I.C., and H.F. Ross: Cochlear-microphonic and summating potentials and the outputs of individual hair-cell generators, J. Acoust. Soc. Am. 38:126-131 (1965).

71. Pestalloza, G., and H. Davis: Electric responses of the guinea-pig ear to high audio frequencies, Am. J. Physiol. 185:595-600 (1956).

72. Teas, D.C., S.P. Diamond, H. Davis: Electrophysiologic response to acoustic transients. I. Cochlear microphonics, J. Acoust. Soc. Am. 31:1574 (1959).

73. Teas, D.C., D.H. Eldredge, and H. Davis: Cochlear responses to acoustic transients, An interpretation of whole-nerve action potentials, J. Acoust. Soc. Am. 34:1438-1459 (1962).

74. Laszlo, C.A., and R.P. Gannon: A precision time measuring technique for biomedical use, Proc. 18th Ann. Conf. Eng. Med. Biol. 7:215 (1965).

75. Möller, A.R.: Transfer function of the middle ear, J. Acoust. Soc. Am. 35:1526-1534 (1963).

76. Zwislocki, J.: Analysis of the middle-ear function. Part II: Guinea-pig ear, J. Acoust. Soc. Am. 35: 1034-1040 (1963).

77. Flanagan, J.L.: Computational model for basilar membrane displacement, J. Acoust. Soc. Am. 34:1370-1376 (1962).

78. Flanagan, J.L: Models for approximating basilar membrane displacement. Part II, Bell System Tech. J. 41:959-1009 (1962).

79. Flanagan, J.L., and C.M. Bird: Minimum phase responses for the basilar membrane, J. Acoust. Soc. Am. 34:114-118 (1962).

80. DeRusso, P.M., R.J. Roy, and C.M. Close: State Variables for Engineers, p. 326, John Wiley and Sons, Inc., New York, 1965.

81. Liou, M.L.: A novel method of evaluating transient response, Proc. IEEE 54:20-23 (1966).

82. Matsuoka, K., T. Konishi, and F. Nakamura: Electric impedance of the cochlea and its significance for evaluating cochlear microphonics, Acta. Otolaryngol. 47:326-335 (1957).

83. von Bekesy, G.: The coarse pattern of the electrical resistance in the cochlea of the guinea pig (Electroanatomy of the cochlea), J. Acoust. Soc. Am. 23:18-28 (1951).

84. Misrahy, G.A., K.M. Hildreth, E.W. Shinabarger, and W.J. Gannon, Electrical properties of wall of endolymphatic space of the cochlea (guinea pig), Am. J. Physiol. 194: 396-402 (1958).

85. Mizukoshi, O., T. Konishi, and F. Nakamura: Physico-chemical process in the hair cells of organ of Corti, Ann. Otol. Rhinol. Laryngol. 66:106-126 (1957).

86. Engebretson, A.M., and D.H. Eldredge: An analysis of interference in the cochlea, J. Acoust. Soc., Am. 41:1578 (1967).

87. von Bekesy, G.: D-C potentials and energy balance of the cochlear partition, J. Acoust. Soc. Am. 22:576-582 (1950).

88. Weiss, T.F.: A model for firing patterns of auditory nerve fibers, M.I.T. Tech. Report 418, 1964.

89. Hirsch, I.J.: The Measurement of Hearing, pp. 195-199, McGraw-Hill Book Co., New York, 1952.

90. Fernandez, D.: Dimensions of the cochlea (guinea-pig), J. Acoust. Soc. Am. 24:519-523 (1952).

91. Cooley, J.W., and F.A. Dodge: Digital computer solutions for excitation and propagation of the nerve impulse, Biophysical J. 6:583-599 (1966).

92. Spoendlin, H.: The Organization of the Cochlear Receptor, S. Karger, New York, 1966.

93. Ruch, T.C., and J.F. Fulton: Medical Physiology and Biophysics, p.48, 19th edition, Saunders, Phila., 1960.

94. Stauffer, W.M., J.C. Dill, and R.W. Stacey: Real-time numerical filtering of physiological signals, IEEE Trans. BioMed. Eng. BME-12:195-197 (1965).

95. Davis, H: Mechanisms of excitation of auditory nerve impulses, Neural Mechanisms of the Auditory and Vestibular System, edited by G.L. Rasmussen and W.F. Windle, pp. 21-39, C.C. Thomas, Springfield, Ill., 1960.

96. Paparella, M.M., and W. Melnick: Stimulation deafness, Sensorineural Hearing Process and Disorders, edited by A.B. Graham, pp. 427-443, Little, Brown and Co., Boston, 1967.

97. Feinmesser, M., and H. Sohmer: Influence of streptomycin and dihydrostreptomycin on the cochlear potentials of the guinea pig, Ann. Otol. Rhinol. Laryngol. 74:48-58 (1965).